FACTORS CONTROLLING ROOT GROWTH IN HETEROGENEOUS SUBSTRATES: PHYSICAL STRUCTURE AND ROOT BEHAVIOUR

A thesis submitted for the degree of Doctor of Philosophy (PhD)

by

Caroline Upton

School of Science, Engineering and Technology
Abertay University

September, 2016

FACTORS CONTROLLING ROOT GROWTH

IN HETEROGENEOUS SUBSTRATES:

PHYSICAL STRUCTURES AND ROOT BEHAVIOUR

A thesis submitted in partial fulfilment of the requirements of Abertay University for the award of PhD

by

Caroline Upton

Abertay University

August 2016

Declaration

I hereby declare that this thesis has been composed by myself and that it has not been accepted in any previous application for a degree. The work, of which it is a record, is my own, unless otherwise stated. All verbatims have been distinguished by quotation marks and sources of information specifically acknowledged by means of references.

Caroline Upton

Acknowledgements

This project was funded by the University of Abertay and the James Hutton Institute. Both institutions provided the financial support, equipment and assistance necessary for this project. I would like to thank my supervisors; Wilfred Otten, Lionel Dupuy, Sonja Schmidt and Tracy Valentine for the guidance that they have provided during my research. Together they have trained me and taught me so many things, about science and life in general. I will always have fond memories of the time that we worked together.

I would also like to thank the following people; Tim George and Craig Simpson, my thesis committee who always encouraged me to keep going, Susan Mitchell, who helped me find my way around the laboratory, Kirsty Binnie, who helped to train me in a number of laboratory techniques, Katherine Preedy, who provided statistics support and Fabien Roussot, who helped to develop my Python Scripts for this project. I made many friends along the way who were always there to keep me smiling; CJ, Jackie, Jaleh, Amanda, David, Dimitris, Fiona and Sonia and Emma - thank you for making the past few years a joyous adventure!

Finally, I want to thank the people who have been there for me behind the scenes; Nicky and Richard, my mum and dad who somehow always had faith in me. Jonathan and Catherine, my brother and sister who have always been around for much needed cinema nights! Helen and Aesha, my two best friends...who would have thought we'd all end up achieving so much?

And finally, to my two favourite people in the world...Big Alex and Little Alex, who have always provided me with cups of tea, plenty of cuddles, crazy hikes and a never ending supply of love and support. Thanks for putting up with me during the writing of this thesis. This is for you.

Abstract

Roots are essential for nutrient uptake and anchorage for the plant, however there is published evidence to suggest that the physical structure of soil has a strong influence on their abilities to grow and develop healthily. Observing roots in 3-dimensions, *in situ* and non-destructively is important for understanding the complex nature of the physical root/soil relationship, however roots are notoriously difficult to observe due to the opaque nature of soil. This problem can be partially negated by using techniques such as X-ray micro-computed tomography, but is an expensive and time-consuming technique. Furthermore, soil is a growth medium prone to spatial and temporal variation in terms of water, nutrient availability, and microbial populations, making it difficult to observe the effects of soil physical structure alone.

The development of transparent soil (**TS**) by Downie et al. (2012) has brought about a new era in the study of root/soil interactions. **TS** is a growth medium with the transparency of agar and some of the physical heterogeneity of soil. **TS** has particles and pores, so roots can explore it in much the same way as they would soil, however the water and nutrient levels can be better controlled and microbial influences are less of an issue, due to the semi-sterile conditions that transparent soil cores are kept under. Downie et al (2012) used **TS** to study root growth of small *Arabidopsis thaliana* roots and also imaged *Psuedomonas fluorescens* colonising lettuce seedling roots.

This project scaled the **TS** system up in order to image larger root systems of *Hordeum vulgare* (barley) seedlings under different physical conditions. Comparisons of barley roots growing in soil and **TS** were made, and it was found that roots grew longer in natural soil than in **TS**. The **TS** was then sieved into different particle size ranges and it was found that barley roots grew more successfully in the smaller particles (850-1250 μm) than the larger particles (>1676 μm). Vertically stratified split pots, containing large particles down one side and small particles down the other were also used and non-destructively imaged at 24-hour intervals. It was found that the presence of the large particles had an inhibitory effect on root growth across the entire root system, including the roots that were growing in the smaller particles. Finally a device was designed which allowed the application of compression to the **TS** system. It was found that root growth decreased proportionally with the level of pressure that was applied to the **TS** cores.

Manipulation of **TS** structure and the development of techniques to quantitatively record root growth and physical soil conditions from 3-D images has enabled us to measure root growth in barley roots under different physical conditions. The results showed that root growth is heavily influenced by particle size, pore structure and soil strength. Root/soil contact was consistently observed as an important soil property for root growth across experiments.

Table of Contents

List of Figures

List of Tables

List of Abbreviations

ABS	Acrylonitrile Butadiene Styrene
ANOVA	Analysis of Variance
CLSM	Confocal laser scanning microscopy
CT	Computed Tomography
DEZ	Distal elongation zone#
GFP	Green fluorescence protein
GSA	Gravitropic set-point angle
HGMF	High gradient magnetic field
KOH	Potassium hydroxide
MRI	Magnetic Resonance Imaging
MS	Murashige & Skoog
OPT	Optical projection tomography
PIG	Postmitotic isodiametric growth
QC	Quiescent centre
RAM	Root apical meristem
REML	Restricted Maximum Likelihood

RI	Refractive index
ROI	Region of interest
RSA	Root system architecture
SEM	Scanning electron microscopy
SL	Split pot-large
SS	Split pot-small
TS	Transparent soil
µCT	Micro computed tomography

1 Introduction

As the global population continues to increase, alongside land degradation due to climate change and intensive crop production, the necessity for efficient crop growth has never been greater (Lambin et al., 2013). The green revolution occurred approximately half a century ago, during which a global effort was made to develop high-yielding cereal grain varieties, expand and improve irrigation infrastructure, and widely distribute artificial fertilisers and pesticides to farmers (Matassa et al., 2015). These measures improved global crop production through increased shoot biomass and grain yield (Den Herder et al., 2010), however the use of artificial fertilisers alone has had enormous negative consequences for the environment, both in terms of nitrogen run-off into global water supplies, and the energy required in order to fuel the Haber-Bosch process (Matassa et al., 2015).

Research into effective farm management practices and high-yielding cereal grains continues today, however plant roots have more recently also been brought into sharper focus within the scientific community, as an un-tapped research area that could lead to higher crop yields under ever-increasingly challenging conditions for agriculture (Den Herder et al., 2010). Soil structure is of particular importance when considering the factors that contribute to the health of plants, because it wields great influence over how and where root systems are able to access water and nutrients (Prochnow and Cantarella, 2015), both of which are limiting factors to crop yield. Plants are sessile organisms; therefore the immediate surrounding environment has a direct influence on their growth and development (Alizadeh et al., 2015). Wherever a plant is located, its roots must be able to elongate, branch and adapt to the local soil conditions (Prochnow and Cantarella, 2015). Relatively little is known about how roots are influenced by their immediate environments, when compared with what is known about

'above-ground' parts of plants (Gregory, 2008), due to the opacity of soil and difficulties in directly observing root behaviour (Downie et al., 2012).

Barley is important for global food production. In 2015/2016, corn was the crop which produced the most yield (5.43 metric t/ha), followed by wheat (3.27 t/ha), rice (4.43 t/ha) and barley (2.96 t/ha) (USDA, 2016). It is also important within the UK, with a gradual increase in barley production being observed from 2011 (5,494 thousand tonnes) through to 2015 (7,281 tonnes), almost 50% of the recorded wheat production (DEFRA, 2015). Barley is one of the oldest crops used by farmers, being of historical as well as current importance and as such, efforts were made to domesticate cultivars that were high-yielding, particularly six-rowed barley varieties (Pourkheirandish and Komatsuda, 2007). Since 1982, at least 88% of the improvement in barley yield is attributable to genetic improvement, with little evidence that changes in agronomy have improved yields. This is not the case in other crops such as maize, whereby genetic improvement and agronomy practices have contributed equally to increased yield (Mackay et al., 2011). Therefore, there are still agronomical improvements to be made which can further improve barley yields.

Modern 3-Dimensional (3D) imaging technologies such as X-ray micro computed tomography (µCT) and optical projection tomography (OPT) allow non-destructive imaging of roots *in situ*, in physically heterogeneous substrates, thus helping us to understand the physical relationship that exists between roots and soil (Downie et al., 2015). Much work has already been carried out using µCT, which has helped scientists to quantify important factors in root elongation such as root/soil contact (Schmidt et al., 2012). All imaging techniques have their own advantages and limitations, however when used appropriately there is the potential to

combine them in order to learn more about the intricate physical relationship that exists between roots and soil (Downie et al., 2015).

The purpose of this project was to understand the physical conditions that influence barley root elongation in **TS**. The recently developed **TS** growth medium (Downie et al., 2012) has undergone extensive development and been used, in combination with novel 3-D image analysis techniques, to ascertain important physical parameters that influence root elongation in barley seedlings, such as particle and pore size, water content, soil strength and root/soil contact.

1.1 Soil and substrates for root growth

1.1.1 What is soil?

Soil is a physically heterogeneous substrate, composed of solid, liquid and gaseous phases. The physical structure of soil is dynamic and roots have the ability to influence changes in all three phases of soils (Letey, 1985). Knowledge of the subtle physical interactions that occur between root systems and soil is currently limited by soil's opacity and physical complexity. Soil differs spatially and temporally, with biological and chemical components changing regularly, thus affecting its physical structure (Hinsinger et al., 2009).

The solid particle component of soil is made from the weathering of different kinds of rocks, by mechanical, chemical and biological processes (Wilson, 2004). The type of soil that results from this process will depend on the rocks from which the particles came. Solid particles of soil fall into 3 types; sand, silt and clay, with sand being the largest particles and clay being the smallest. All soils are composed of a combination of these three particle types (Figure 1-1), and the relative proportions of each will affect other properties of the soil such as water conductivity and air availability (Hajnos et al., 2006). Nutrient availability is also affected by the relative amounts of these particles, as the particles bind to nutrients in different ways, largely due to their complicated 3-D structures.

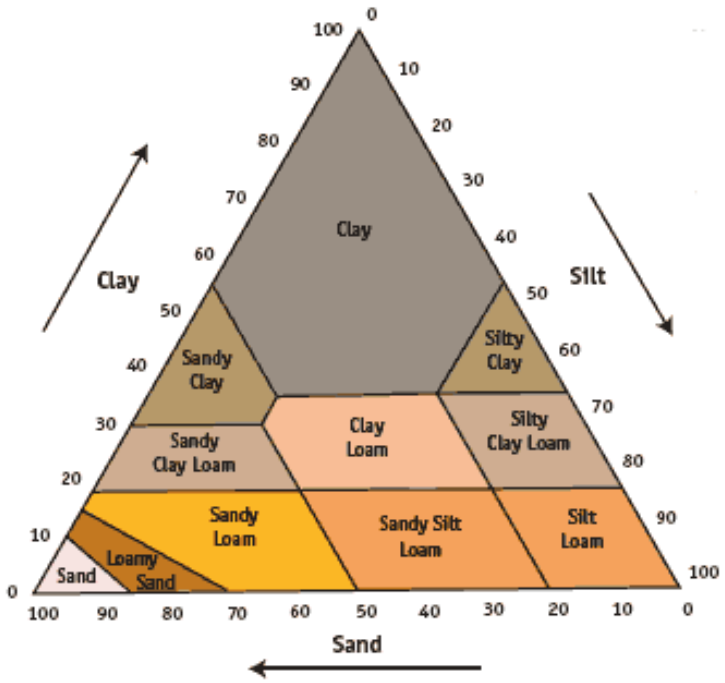

Figure 1-1: Soil texture triangle showing the relative percentages of particle types present within each type of soil, image taken from The Scottish Government (2005)

Soil water is constantly changing, both spatially and temporally (Western et al., 1999). Soils containing higher proportions of clay are generally wetter than those that contain higher proportions of sand, due to the larger pores in sandy soils, and the ability of water to drain through sand quickly (Rodriguez-Iturbe et al., 1999). For loamy soils, which are in between these two extremes and commonly used to grow crops, water content has a significant effect on soil strength. Dryer soils are harder and stronger, holding any available water more strongly and transmitting nutrients less readily (Passioura, 2002).

Soil carbon, another important component in soil structure, originates from plants, animals and micro-organisms, (Bronick and Lal, 2004) and is also variable depending on the soil type, with clay soils containing the highest levels of carbon, and sandy soils containing the lowest. Soil organic carbon is important in the formation of soil aggregates, which help to form the structure of soils, allowing the formation of pores of various sizes necessary for root growth

whilst being able to maintain a good water holding capacity. Soil organic carbon also helps to form a stable soil top soil layer, more resistant to erosion (Rillig et al., 1999).

1.1.2 Other substrates for root growth

The opacity and physical heterogeneity of soil has traditionally made it challenging for researchers to observe root growth *in situ*, therefore alternative growth mediums have been developed for observing root growth. Specially designed filter papers can be used for germinating and growing seeds (Fisher Scientific, 2011). Such filter papers will generally be strengthened, so that they maintain their structure whilst wet. This allows the seed and growing roots to have constant access to a water supply, whilst having the paper to grow against. They can be manufactured in different colours, which may be useful for imaging applications, as coloured filter paper allows automated image analysis software to easily distinguish between the roots and the paper. They also have a breathable structure, allowing exchange of gases, but contain very small pores which roots usually cannot penetrate (Fisher Scientific, 2011). Therefore, the roots remain on one side of the filter paper at all times, which is where the camera would be positioned, should imaging techniques be used.

Phytagel™ is made from a bacterial substrate, known as glucuronic acid, and is a substitute for agar (Sigma Aldrich, 2016). It creates a gel, which is clear and high-strength. The advantage of it being clear and colourless is that microbial contamination can easily be detected, however vitrification has been cited as a problem in Phytagel™ (Sigma Aldrich, 2016). To address this, other gel-based mediums have been developed, such as Agargel™, which is a blend of agar and Phytagel™ (Sigma Aldrich, 2016). Gel-based mediums have been used to study root growth since the early 1990s (Zacarias and Reid, 1992, Volkmar), however it has

been suggested that anoxia may be a problem in gel-based growth mediums, due to the lack of air-filled pores (Wiengweera et al., 1997).

Ballotini is a growth medium that is made up of glass beads, which are round in shape and can be manufactured in a variety of different sizes (Potters-Ballotini Co. Ltd., 2004-2011). The seed can be planted within the ballotini, which can then be submerged in nutrient growth solution (Mozafar, 1991). This allows the roots to receive water and nutrients, but maintain contact with solid particles. Ballotini has been used to study root system architecture and mechanical impedance (Wilson and Robards, 1979).

TS (Downie et al., 2012, Downie, 2013) is made from the pre-cursor, Nafion®, which begins as translucent pellets, ≤4 mm in diameter. It is ground down inside a cryo-mill to create a variety of particles in both shape and size (Downie et al., 2012, Downie, 2013). It is then treated with a variety of different acids and water, and then it is coated in media, which is adsorbed onto the surfaces of the particles. It is stored inside the media of choice, but is drained for the purposes of root growth, so that liquid media remains on the surface of the particles, but there is still a network of air-filled pores, through which roots can grow. Seeds are sown inside **TS** using the same methods as would be used if sowing in natural soil. After the specified incubation period, the **TS** is saturated in an optically-matching solution (Figure 1-2), which makes the particles transparent, so that only the roots are visible (Downie et al., 2012, Downie, 2013). This is how imaging is carried out. A detailed description of the preparation of transparent soil is provided in section 2.4.1.2.2.

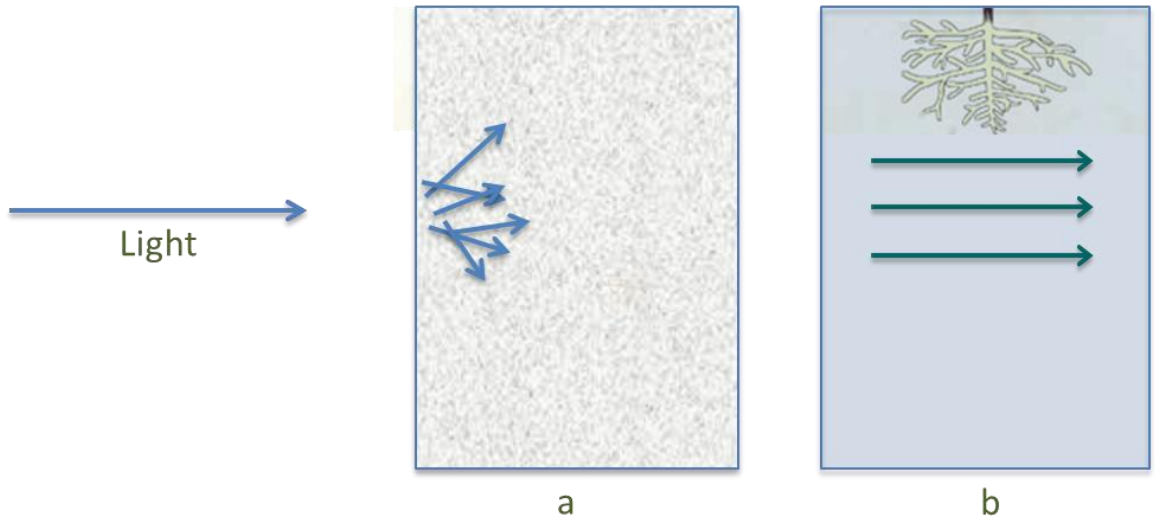

Figure 1-2: A diagram of two TS samples. a shows TS particles without an optically matching solution whereby particles are translucent and light is absorbed. b shows TS particles with an optically matching solution whereby particles are transparent and light can travel straight through the sample to show the roots.

1.2 Mechanisms of root elongation

The root tip is a particularly important region, because it is where cell division, elongation and differentiation take place. These processes are essential, as the root grows and explores its immediate surroundings. Within root tips, specialised zones are present, which are responsible for different processes involved in root elongation. These zones are the root cap, the meristem, the transition zone, the elongation zone and the maturation zone (Ubeda-Tomás et al., 2012) (Figure 1-3).

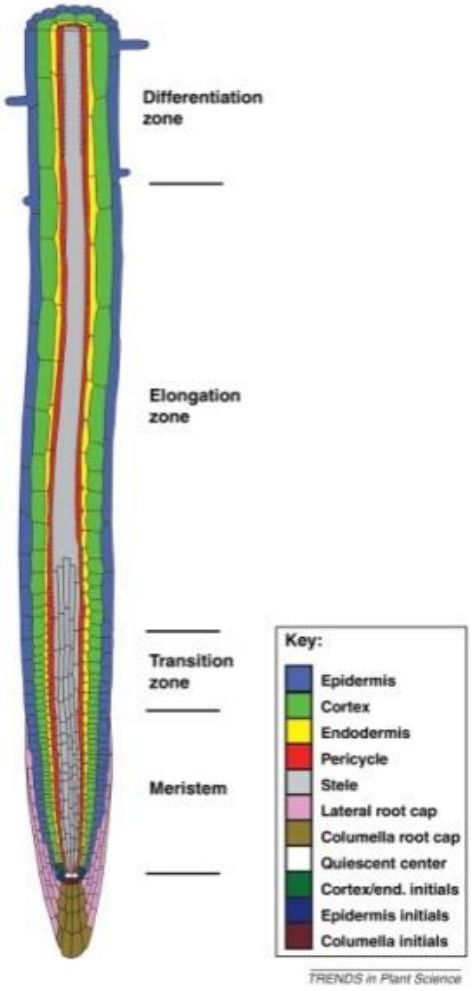

Figure 1-3: Specialised zones of the root tip in the model plant *Arabidopsis thaliana* – taken from Ubeda-Tomás et al. (2012)

The root cap is the first point of contact with soil during exploration of new areas and responds to external stimuli such as gravity, touch and nutrient and water availability (Sievers et al., 1996). It is an important, largely universal feature of plant roots and is responsible for protecting the meristem, reducing friction whilst exploring the soil and generating the rhizosphere surrounding the root (Hawes et al., 2002).

The direction of growth by the root is thought to be heavily influenced by the root cap's responses to external stimuli, which is in turn influenced by the genetically pre-determined architecture of the plant's roots (Falik et al., 2005). The root cap is also capable of altering its environment by manufacturing the rhizosphere surrounding the root, mainly through the release of exudates and border cells (Hawes et al., 2002). Root exudates are released by the root cap and contain mucilage and various chemical compounds involved in plant defence, including allelochemicals which are able to influence other organisms, including other plants, insects and microbes (Walker et al., 2003). It has also been suggested that mucilage plays a role in forming a rhizosphere sheath, which assists in the lubrication of soil thus making root elongation easier (Iijima et al., 2003), maintaining root-soil contact (Schmidt et al., 2012, Read et al., 1999) and increasing the water-holding capacity of the soil immediately surrounding the root (Young, 1995).

The root apical meristem (RAM) is the region of the root tip involved with cell division. Much research on the RAM has been carried out, using the model A. thaliana, due to its simple and consistent cellular structure (Scheres et al., 1996). With regards to cereals, much of what is known about the root tip has been discovered through observation of rice or maize (Coudert et al., 2010). The RAM is important for providing the cells necessary for growth in the elongation zone, proximal to the meristem, and so has also been referred to as the stem cell

region of the root apex (Sablowski, 2004). The quiescent centre (QC) is a region in the apical meristem whereby cells divide rapidly during very early root growth, but then slow down, with division in this zone occurring rarely or never after the seedling stage. The function of the QC in the RAM is to maintain the surrounding stem cells of the meristem (Sablowski, 2004), by providing signals to adjacent meristem cells that stop them from differentiating (Van den Berg et al., 1997). It has been shown using laser ablation that if the QC is damaged for any reason, other cells in the surrounding region, specifically the stele region, are able to change their fate in order to re-establish the QC rapidly, thus suggesting its importance in meristem maintenance (Van den Berg et al., 1997).

Initial cells in the meristem are ordered in a predictable fashion, dividing to create columns of cells that run parallel to the length of the root (Meyerowitz, 1997). These initials remain stationary relative to the QC, while the cells that are produced from their divisions contribute to the body of the root, differentiating to form specified tissues, depending on their positions (Scheres et al., 1996). Using histological techniques, scanning and transmission electron microscopy, Dolan et al. (1993) defined three important zones of cells in the meristem of A. thaliana, which are the initials required for growth of the different root tissues. These zones are named as follows; the protoderm - composed of the initials of the root cap and epidermis, the periderm - composed of the mostly mitotically inactive quiescent centre, and finally the plerome – composed of the cells responsible for the growth of the stele. The initials of the cortex and endodermis are positioned on either side of the quiescent centre (Figure 1-3; Dolan et al. (1993)).

The transition zone (Ubeda-Tomás et al., 2012) has also been referred to at times as the distal elongation zone (DEZ) (Ishikawa and Evans, 1995), or the postmitotic isodiametric growth

(PIG) zone (Baluška et al., 1996). It is a small region where division and elongation of cells occurs simultaneously, thereby allowing the plant to control how many cells enter the elongation zone (Ubeda-Tomás et al., 2012). Although overlooked for some time, it is now recognised as an important, specialised region in its own right with regards to root elongation. It is responsive to many different hormones, and capable of differential growth of cells on each side of the root, thus dictating changes in the direction of the root tip (Baluška et al., 2010). Curvature of roots during growth occurs due to differential elongation of cells in the transition zone, in response to sensory perception of stimuli such as touch or gravity by the root cap (Barlow, 2006). In the case of gravitropism, differential expression of the phytohormone auxin causes cells in the lower region of the root to slow elongation of cells down, thus producing downward curvature (Baluška et al., 2010, Mullen et al., 1998).

By the time cells reach the elongation zone, division has completely ceased. It is situated proximal to the transition zone and is where elongation of the daughter cells produced by the meristem occurs. In order for this to happen, turgor pressure builds up inside the cells (Pritchard, 1994), and the cytoskeleton and cell walls increase in size and strengthen, while still retaining the flexibility required for further expansion (Gregory, 2008). The cell wall plays a critical role in this process, ensuring that the cell takes the correct size and shape. This process is also highly dependent on tight control of ion and water uptake by the cells, and can be easily influenced by low temperatures and high soil strength (Dolan and Davies, 2004).

The maturation zone is the region of the RAM whereby cell differentiation takes place. For example, it is in this region that trichoblasts differentiate and begin to develop root hairs (Gregory, 2008). Once the cells have reached this zone, elongation has ceased.

1.3 How root growth is affected by different external stimuli

It has long been known that plants are able to respond to a variety of different external stimuli, with a constant exchange of information occurring between the plant and its environment (Darwin and Darwin, 1880). With regards to root growth and development, responses to physical stimuli such as gravity, touch, water availability, aeration, temperature and sunlight; chemical stimuli such as nutrients and metals; and biological stimuli such as microbes and parasitic weeds, have all been observed and are known to influence one another (Gregory, 2008). These responses are essential functions of the RAM, both in resource identification and uptake, as well as protection against undesirable environmental conditions. This project is primarily concerned with physical interactions that occur between roots and their external environment; therefore this review will focus on the physical stimuli of gravity, touch, water and aeration.

The idea that roots respond to gravity was first published by Darwin and Darwin (1880) and is broadly defined as the tendency for an organism to grow or move in a particular direction in response to gravity. It was hypothesised that perception of gravity occurred in the root cap, and that a mechanism of some sort enabled the roots to respond to this so that a downward growth pattern could occur. In 1928, both Cholodny and Went independently proposed that differential transport of auxin resulted in the root's growth response to gravity, and its downward growth pattern (Went and Thimann, 1937). This theory has since been supported and further refined by molecular and genetic techniques that have accumulated evidence over time, showing that uneven distribution of auxin in the root tip is responsible for differential growth, and the gravitropic response shown by roots (Rigas et al., 2013).

Gravity perception occurs in specialised columella cells in the root cap, known as statocytes (Iversen and Larsen, 1973). It is inside these cells that starch-filled amyloplasts sediment to the bottom region of the cell, thus enabling the root to perceive gravity and initiate the gravitropic response (Boonsirichai et al., 2003). This idea was tested using a high gradient magnetic field (HGMF) that simulated a gravity vector (Kuznetsov and Hasenstein, 1996). Amyloplasts sedimented in the direction of the magnetic field, thus enabling the artificial manipulation of root elongation direction. Root tips which did not contain amyloplasts, did not respond to HGMF, thus adding weight to the argument that amyloplasts are important for gravitropism (Kuznetsov and Hasenstein, 1996).

It has been argued that plant organs do not simply grow towards the 'ideal' 0° (positive gravitropism, as seen in roots) or 180° (negative gravitropism, as seen in shoots), nor are they required to (Digby and Firn, 1995). In fact, root systems in particular show wide variation in their gravitropic responses. The concept of the gravitropic set-point angle (GSA) was formulated, and was defined as an angle from the gravity vector that a root would aim for, in order to reach a stable gravitropic position (Firn and Digby, 1997). The GSA is likely to be influenced by different interacting external stimuli and the developmental stage of the plant itself as well as its genotype (Firn and Digby, 1997).

Thigmotropism, the tendency of roots to response to touch, is another physical stimulus that is important in determining RSA. This was demonstrated by Massa and Gilroy (2003), who grew A. thaliana roots in gel and placed a glass barrier in the direction of growth. The root cap remained in a vertical orientation, in direct contact with the barrier, whilst the elongation zone changed direction and grew parallel to the obstruction, whilst not touching the barrier (Massa and Gilroy, 2003).

Hydrotropism, the tendency of plants to respond to water, is of great importance due to the essential function of the root tip to locate water in soil, and avoid drought stress (Takahashi, 1997). It has been shown by removing the root cap of maize plants that hydro-sensing is dependent on an in-tact root cap (Takahashi and Scott, 1993). Traditionally, it has been suggested that deep-rooting may be beneficial for plants that are in a dry top-soil environment, thereby prompting research into how fast root elongation rates can be achieved in particularly dry soil conditions (Monteith and Greenwood, 1986). Roots often show positive hydrotropism, however due to the difficulties involved in analysing hydrotropic responses of plants grown in soil, and separating these responses from the influence of gravity, research in this area is challenging. *A. thaliana* mutants (nhr mutant) were developed that showed no hydrotropic response (Eapen et al., 2003, Jaffe et al., 1985). When these were grown on a water potential gradient, the roots showed a gravitropic response with less affinity to high moisture areas than the wild type, which showed less of a gravitropic response than the mutants and tended to grow towards regions where there was more water (Eapen et al., 2003).

Although research has suggested that roots actively seek to locate water sources, water-logging is also an enormous problem in agriculture, with much of the literature focusing on the agricultural impact of water-logging (Gales, 1983). Water-logging reduces the amount of available O_2 in the soil and induces hypoxia in roots (Mustroph and Albrecht, 2003). For this reason, a balance of adequate water content whilst maintaining drainage and aeration in soil is essential (Biemelt et al., 1998).

1.3.1 Undesirable physical soil conditions inhibit root growth

High soil bulk density has been shown consistently to inhibit root elongation. Research into the influence of compaction and high soil bulk density on shoot growth has yielded conflicting results in the literature, however the basic effects on root growth are remarkably consistent with a reduced elongation rate and a thicker diameter of roots just proximal to the root tip being observed in many plant species, barley included (Bengough et al., 2005, Goodman and Ennos, 1999, Wilson et al., 1977). When soil mechanical impedance (i.e. the amount of force required for roots to push soil particles aside during elongation) is >2 MPa, it has been commonly observed that root elongation is reduced by approximately 50% (Bengough et al., 2011, Goss, 1977, Wilson et al., 1977). The cellular responses of barley to soil compaction have been debated over time in the literature (Gregory, 2008). In early research it was found that when subjected to mechanical impedance, the stele increased in diameter by as much as 22%, 0.5 cm from the root apex, and the number of cells was 9% less than the control, 200 µm from the apex (Wilson et al., 1977). The thickness of the cortex increased along the entire length of the root when subjected to mechanical impedance and this was due to both an increase in the number of cells present, as well as an increase in cell diameter due to turgor (Wilson et al., 1977). In more recent studies, it was suggested that the thickness of roots under compaction increases not because of increased cell numbers, or in stele diameter; rather it was due to higher solute concentrations in the cortex, resulting in increased turgor, and therefore cell diameter, specifically in this region (Atwell et al., 1989).

Soil mechanical impedance and water stress both have important roles to play in the physical relationship between roots and soil (Bengough et al., 2011). Typically, root elongation is halved at penetrometer resistances of > 0.8 -2 MPa, and in matric potentials that are drier

than -0.5 MPa (Bengough et al., 2011). Drier soil increases soil strength, as well as reducing the amount of available water that roots can access, so both factors have an inhibitory effect on root elongation rate, but differences do exist between different plant species (Schmidt et al., 2013). Approximately 60% of soils recently surveyed in Scotland had penetration resistances of > 2 MPa, with water potentials of between -0.01 MPa and -0.2 MPa, indicating that mechanical impedance is likely to be of great importance in Scottish fields (Bengough et al., 2011). This was supported by a further study, indicating that mechanical impedance and specifically soil pore volume was of great importance for barley roots to be able to elongate, with pore sizes of 60 μm – 300 μm accounting for 65.7 % of the variation seen in root elongation rates (Valentine et al., 2012b).

1.3.2 Interactions between roots and other growth substrates

It has been suggested that root system architecture analysis can be performed by placing a seed on filter paper in-between two Perspex plates and automatically scanning the roots as they grow (Adu et al., 2014), whilst using semi-automated software such as SmartRoot (Lobet et al., 2011). This method has been shown to be useful for high throughput phenotyping studies (Adu et al., 2014), however due to the lack of physical heterogeneity of the filter paper and Perspex surfaces, the effects of soil conditions on roots cannot be replicated, and any root system architecture that is observed is due to genetic mechanisms (Adu et al., 2014). This is the same for other homogeneous substrates, such as Phytagel™ (Sigma Aldrich, 2016), which lack the physical complexity associated with soil, and therefore are limited as growth substrates to observe root growth as a function of soil physical properties (Bengough et al., 2004).

The use of ballotini beads is another option for researchers, and created a more realistic heterogeneous environment for roots to grow in, due to the porous structure that is created by the particles (Bengough and Mullins, 1990). Root growth in ballotini beads was shown to be of considerable relevance to soils, with root growth decreasing when extrernal pressure was applied to ballotini cells, in much the same way as would be expected in compacted soils (Bengough and Mullins, 1990). However, the in situ imaging of root growth in ballotini had similar challenges to that of root growth in soil, due to ballotini beads not being fully transparent. Therefore, it was possible to image samples that were positioned in a 2-D set-up, for example inside ballotini cells (Bengough and Mullins, 1990), but it was not possible to image larger 3-D samples using light-based imaging techniques.

TS was later developed (Downie et al., 2012), which was similar to ballotini, in that the roots could grow around particles, through a porous system, however it had the advantage that it was possible to make the particles transparent, by adding a solution to it, whose refractive index matched that of the particles (Section 2.4.2.2.4). This system was used to observe root growth in several different plant species. When a comparison was made between 2-week-old *Nicotiana benthamiana* (Tobacco) roots grown in phytagel, sandy loam soil, sand and **TS**, it was found that those grown in soil, sand and **TS** had a higher biomass and far more lateral branching than those grown in phytagel (Downie et al., 2012). The mean root diameter was also significantly lower in phytagel than it was in soil and sand, and significantly higher in those grown in **TS**. The primary roots of plants grown in phytagel and **TS** were longer than those grown in soil and sand (Downie et al., 2012). It should be noted that *N. benthamiana* is a dicotyledon, which has a single root with many laterals branching from it, as opposed to monocotyledonous roots, which have multiple roots very early on, with laterals branching

from them slightly later. Therefore there is a possibility that monocotyledons may grow differently in **TS** compared to dicotyledons (Materechera et al., 1991).

1.4 Studying roots in soil

When observing the root-soil relationship, several root traits and soil characteristics can be measured. With specific regards to roots, researchers are often interested in measuring the responses of roots to specific stimuli, such as gravitropism, thigmotropism, hydrotropism etc.; or mechanical stresses such as cell turgor pressure in response to compaction (Clark et al., 2003). One way of measuring phenotypic traits and root responses is through analysis of the RSA which may include root number, length, angle, trajectory, diameter, mass, surface area, number of branches, distribution of branches, and the presence of root hairs (Smith and De Smet, 2012). Much RSA research has been focused on *A. thaliana*, however the RSA of cereal crops differs greatly, having more primary roots that are significantly larger, early on in seedling development. Table 1-1 provides an overview of the methods that are available for root phenotyping, and a selection of the methods which are directly relevant to this project are described in further detail below.

Root phenotyping method	Growth medium	Description of method
X-ray computed tomography	Soil and TS	Non-destructive imaging of root systems in 3-D. Small samples required, usually grown in pots. A number of 2-D projections are taken of the specimen from different angles and then reconstructed into a 3-D image.
Rhizoponics	Liquid media	A combination of rhizotrons and hydroponics. Samples are grown inside a nylon fabric core, supported by a metal frame, which is completely immersed in liquid media. Useful for direct visual access to root systems.
Clear pot	Soil or TS	Cores are transparent and filled with growth medium. Roots are grown in the growth medium and then imaged non-destructively, using light-based techniques such as OPT. If soil is used, roots can only be imaged if they are growing close to the edge of the pot.
Rhizoslides	Paper-based	A central layer of plexi glass, surrounded by a layer on each side of moist germination paper, which are turn covered with a transparent cover so that roots do not dry out. Embryonic roots grow in-between plexi-glass and paper layers, whereas crown roots grow in-between paper layer and transparent cover.

Root phenotyping method	Growth medium	Description of method
Shovelomics	Soil	Manual excavation of large numbers of plants. Root are separated from shoots and washed. Then roots are placed on a phenotyping board and imaged. Quantitative imaging techniques are used to analyse RSA traits.
Soil coring	Soil	A tractor-mounted, hydraulic corer can be used to drive sampling tubes into the ground and remove sections of roots sytems. Can be removed from cores and washed for quantification, or can be imaged using X-ray µCT.
Rhizolysimeters	Soil	Underground corridors which contain deep soil cores, for direct observation of how roots grow underground.
Minirhizotrons	Soil	Transparent observation tubes directly in the ground. Images can be taken of the growing roots automatically to obtain time-lapse data.

Table 1-1: An overview of root phenotyping methods for quantifying RSA. Based on Paez-Garcia et al. (2015).

When measuring root traits, it has been common procedure to extract the entire root system from the soil and wash the roots. Root washing can be done using a sieve, or dry removal of soil from roots can be carried out using a fine brush. Roots that are to be used later on for further analysis should be stored in 50% ethanol at room temperature in order to preserve their state at the time of extraction (Böhm, 1979). Once roots have been washed, it is possible to take measurements such as root number, length, mass, number of branches, distribution of branches and the presence of root hairs. Despite being used extensively, root extraction is destructive and makes the subsequent analysis of undisturbed soil structure impossible (Mooney et al., 2012).

Rhizotrons and minirhizotrons were an important step in the repeated observation of roots growing undisturbed in soil, and have been used by researchers for a number of years (Pierret et al., 2003, Phillips et al., 2000). Rhizotrons and mini-rhizotrons are available in a variety of forms, and can be artificially constructed in the laboratory, or installed directly into the field (Johnson et al., 2001). The basic features of a rhizotron is a device such as a tube or shallow box, with a transparent panel at least on one side, and a device for image acquisition which allows *in-situ*, real time observation of roots (Kuchenbuch and Ingram, 2002, Huck and Taylor, 1982). The transparent areas have to be covered when not undergoing observation, so that the roots do not show phototropic responses, and the soil volumes in mini-rhizotrons have to be shallow so that the roots can be seen, therefore often forcing them to grow in a 2-D plane. It is recommended that rhizotrons installed directly into the ground should be left for 6-12 months before beginning any experimentation, so that the roots and soil surrounding them are allowed sufficient time to equilibrate first (Johnson et al., 2001). Despite earlier research

suggesting that destructive sampling remained the most accurate way of observing roots grown in the top 0-10 cm soil layer (Heeraman and Juma, 1993), the rhizotron method has shown itself in many other studies to be a valuable tool for observing roots directly in their soil environment in real-time (Pierret et al., 2003), and allows researchers to carry out controlled, replicated experiments (Huck and Taylor, 1982).

Soil properties have a direct influence on the RSA of many plants (Smucker, 1993, Bengough and Mullins, 1990) and measurements of soil properties can be carried out using a variety of techniques. Soil strength is an indication of the mechanical resistance that roots must overcome, in order for elongation to occur (Bengough and Mullins, 1990). It is measured using a penetrometer; a metal probe which can vary in diameter and length, with a cylindrical cone at the end. The amount of force required to push this probe through the soil is divided by its cross-sectional area, and provides an indication of the strength of the soil. A problem with this method is that the probe does not behave in the same way as roots whilst penetrating the soil. Roots are able to change their trajectory as well as produce border cells and mucilage which reduce the amount of resistance that they have to overcome in order to penetrate the soil further (Bengough and Mullins, 1991), whereas penetrometers are unable to do this, therefore possibly overestimating the amount of force required by roots to penetrate soil. Although penetrometer readings may not fully mimic root behaviour, they can offer a value which indicates the relative strength of a soil sample (To and Kay, 2005).

When measuring particle size distribution, methods such as sedimentation and laser diffraction (Ryżak and Bieganowski, 2011) have both been used. Pore size distribution in soils has traditionally been measured using a method known as mercury intrusion porosimetry (Lawrence, 1978), or very commonly tension tables. Pore and particle size distribution along

with many other soil properties such as connectivity of pores, particle displacement, pore geometry, soil anisotropy and water movement can also be routinely carried out using imaging techniques which have advanced greatly in recent years (Downie et al., 2015). Caution has been recommended however, particularly during image processing in complex 3-D data sets, which have the potential to be open to researcher subjectivity (Baveye et al., 2010).

In looser soils with a low bulk density, root tips are able to explore larger pores, and may be able to elongate with relative ease (Valentine et al., 2012b). In soils of a high bulk density, where particles are closer together and the number and volume of air-filled pores decreases, roots must expend energy in order to push aside particles and create pores that are large enough for them to penetrate (Groenevelt et al., 1984). The ideal soil structure allows root/soil contact to be maintained (Schmidt et al., 2012), without it being so strong or compacted that root growth is impeded (Arvidsson, 1999, Bengough and Mullins, 1990).

1.5 Imaging roots in soil and growth substrates

Traditional methods involving the extraction of roots from the soil make analysis of soil structure problematic (Gregory et al., 2003). Researchers have therefore employed numerous methods in order to study undisturbed root growth. Some techniques involve using transparent growth mediums such as Phytagel (Jain et al., 2009), others involve using rhizotrons (Mathieu et al., 2015), or µCT, which allows non-destructive imaging of roots inside natural soil (Mooney et al., 2012). Each technique has advantages and limitations, and is suitable for different purposes (Downie et al., 2015).

Soil physical properties should ideally be analysed in conjunction with RSA measurements and then applied to predictive models if a functional understanding of the physical root-soil relationship is to be achieved (Hinsinger et al., 2009). As described previously, traditional methods of analysing soil structure and root position within that structure are often destructive, (Kuchenbuch and Ingram, 2002). Therefore, the raw data cannot be re-examined later on and time-lapse information cannot be obtained. Imaging techniques allow detailed, undisturbed data acquisition of root systems *in situ* within their surrounding physical environment, potentially over time. Imaging techniques can be categorised into one of two categories; 2-D and 3-D, with both having been used to answer specific questions about root interactions with soil (Pierret et al., 2003). There are also countless image analysis tools now available to researchers such as RooTrak (Mairhofer et al., 2012) and SmartRoot (Lobet et al., 2011), which aim to remove observer bias as much as possible so that quantitative data can be obtained from images of root systems.

1.5.1 Understanding roots in 2-D

2-D imaging techniques using cameras or scanners, such as the technique developed by Adu et al. (2014) have been described earlier, and are useful for large-scale, 2-D phenotyping studies. 2-D optical microscopy enabled early research into root soil interactions, with Barley (1962) using it to observe the response of *Zea mays* roots to physical stress. He found that roots were able to continue elongation without interruption after they were compressed, albeit at a slower rate, and that this rate decreased as the physical pressure on the roots increased (Barley, 1962). Microscopy of soil thin-sections was used to develop the first quantitative imaging methods analysing root-soil contact (Van Noordwijk et al., 1993) where it was found that deeper roots had a lower percentage of contact than shallower roots, and roots in macropores had a lower degree of contact than those in small pores. Resin-impregnated thin sections of soil were also used to describe the tendency for roots to be found within close distance (<5 mm) of macropores (Stewart et al., 1999). Despite the ability of 2-D microscopy to provide high resolution, spatial information about cross-sections of roots in relation to the surrounding soil structure, creating thin sections is a time-consuming and destructive process, so it is not possible to obtain time-lapse information about root growth. The same is true for scanning electron microscopy (SEM), which provided detailed images of the rhizosphere and demonstrated the rhizosheath in high resolution for the first time (Watt et al., 1994).

1.5.2 Understanding roots in 3-D

The information that can be obtained from 2-D systems is limited, because roots by nature are 3-D structures. Therefore it is uncertain as to whether root growth observed in 2-D is a true representation of root growth (Downie et al., 2015). This has prompted the development

of more sophisticated 3-D imaging techniques, which not only provide information pertaining to root growth, but can also shed greater light on the complicated interactions that occur between roots and the surrounding soil.

Prior to µCT becoming available, the thin section technique was an equivalent method, which allowed researchers to image roots within soil systems. This required impregnating soil samples with a resin, before slicing samples into thin sections (Moran et al., 2000). This technique allowed researchers to better understand how surrounding soil structure influenced the way that plant roots grew. It also produced a permanent record of the roots within the soil structure that could be referred to at a later time. A problem with the technique is that it is laborious and time-consuming (Pierret et al., 2003), and ultimately destructive to the plant, preventing real-time analysis of undisturbed root growth.

Another method which was used for the first time in 1960 and is still used in various ways today is the rhizotron (Rogers, 1969). Rhizotrons are tubes, often (but not always) transparent, which are filled with natural soil. They are usually wrapped in something that blocks light, so that the plant roots within them behave as would be expected from roots growing in the dark; the roots are only exposed to light during observation or imaging. This technique has been used to observe the growth of roots when exposed to different water potentials (Kuchenbuch and Ingram, 2002) and different soil bulk densities (Kuchenbuch and Ingram, 2004). An advantage of the rhizotron is that it provides a more natural environment for roots to grow in whilst being contained enough for the researcher to observe the roots within. It is important to note that the roots can only be observed if they are close to the edge of the rhizotron. The best images are those taken of roots which are growing against the inner surface of the rhizotron tube, which may make it difficult to attribute any observed effects on

root growth to soil structure alone. Furthermore, the narrow rhizotron tubes force roots to grow within particular dimensions, so root systems may appear denser inside rhizotrons than they would in natural soil (Pierret et al., 2003).

Neutron Computed Tomography takes multiple 2-D projections of a sample, which are then reconstructed to produce a 3-D image, allowing the external and internal structures of it to be observed. It relies on the attenuation values of neutrons and has been used as a technique to study single roots and their water uptake, demonstrating clear water content gradients in the rhizosphere (Tumlinson et al., 2008). Imaging water is a strength of neutron radiography, due to the large difference that usually exists between the water content of roots (70-95%) and field soil (5-30%), thus enabling the reconstruction of highly detailed images of roots in soil (Menon et al., 2007).

X-ray µCT works according to the same principle as neutron computed tomography, taking many 2-D projections of a sample and then combining them to create a 3-D reconstruction. It uses electron attenuation instead of neutron attenuation and has been used to image 2-D thin slice sections, as well as 3-D soil rhizotrons and cores of various sizes and dimensions (Pierret et al., 2003). The advantage of using µCT for horizontal thin sections is the high resolutions that can be achieved and increased contrast, enabling easier quantification of roots within the soil profile. However the greatest advantage of µCT imaging is its ability to produce detailed 3-D data of entire root systems, within the undisturbed soil structure (Mooney et al., 2012). Despite having both advantages and limitations, µCT is a valuable tool to non-destructively observe the entire root-soil relationship over time in opaque mediums, and as technology and root segmentation software improves, it has the potential to become a high-throughput, quantitative technique (Flavel et al., 2012). µCT has been used to observe

a number of different soil parameters and their effects on root growth. Root system and soil metrics that can be measured using µCT are summarised in Table 1-2

Component of sample being measured	Metric	Reference
Root	Root length	Heeraman et al. (1997)
Root	Root diameter	Heeraman et al. (1997)
Root	Root angle	Tracy et al. (2012)
Root	Branching pattern	Stuppy et al. (2003)
Root	Spatial distribution	Perret et al. (2007)
Root	Convex hull volume	Tracy et al. (2012)
Root	Root system width	Mairhofer et al. (2012)
Root	Centroid	Mairhofer et al. (2012)
Soil	Pore size distribution	Pierret et al. (2002)
Soil	Hydraulics	Cheng et al. (2012)
Soil	Connectivity	Tracy et al. (2012)
Soil	Porosity	Mooney (2002)
Soil	Macro/ microporosity	Mooney (2002)
Soil	Root/ soil contact	Schmidt et al. (2012)

Table 1-2: Root and soil metrics that can be taken using µCT

Whilst problems such as speed of scanning, resolution and computer power have all been improved substantially over time, there is still difficulty associated with obtaining sufficient contrast between soil and roots for perfect segmentation to be possible because the attenuation values of soil water and roots are similar (Mooney et al., 2012). Therefore a

certain degree of manual image processing is usually required, so it is essential that researchers are aware of the potential for subjectivity and that they try to design image analysis methods that are as reliable and reproducible as possible (Baveye et al., 2010).

1.5.3 TS and 3-D imaging techniques as new tools for observing roots in soil

TS is a root growth medium that provides the transparency of agar with the heterogeneity of soil. Combined with 3-D imaging techniques such as μCT, OPT and confocal laser scanning microscopy (CLSM), it can provide a powerful tool for the study of root/soil interactions (Downie, 2013). Some of the early work on **TS** was carried out using small dicotyledonous seedlings, such as *A. thaliana* or *N. benthamiana* in small cylindrical containers, approximately 1 cm x 1 cm for *A. thaliana and* 2.5 (diameter) x 7 cm (depth) in dimension for *N. benthamiana* (Downie et al., 2012). For the same study, OPT was used to gain an image of the entire root system and CLSM was used to observe GFP labelled *Escherichia coli* 0157:H7 cells and colonies on the surface of *Latuca sativa* (lettuce) roots. **TS** has a number of advantages and limitations, which are discussed in greater detail throughout this thesis, in particular Chapter 2 whereby significant method development was performed so that **TS** could be used to image larger, more complicated root system architectures.

1.6 Aims of this project

The development of **TS** was a great achievement, opening up a number of possibilities for researchers who wish to understand root growth, as affected by the physical structure of soil. However, no work has yet been carried out to understand how monocotyledonous root growth of cereals occurs in this growth medium.

The first aim of this thesis is to describe the development of the **TS** system, from a growth substrate only suitable for imaging very small, simple, dicotyledonous samples (1 x 1 cm cuvette-size), to one which can be used to image larger monocotyledonous barley root seedlings (3 x 5 cm specimen pot size). This will require developing methods for the following aspects of imaging roots in **TS**:

- Cleaning and handling larger quantities of **TS**;
- Sowing and incubating barley seedlings inside **TS**;
- Imaging the seedlings *in situ,* using μCT and optical projection tomography;
- Analysing complex 3-D images of the root systems physically interacting with **TS**.

By establishing these methods it will be possible to better understand if or how root growth in natural soil is similar or different to that seen in **TS**. Once these similarities and differences are established it will be possible to explore how **TS** can be manipulated in different ways so that root growth in different physical conditions can be observed.

Ways in which the **TS** will be manipulated during this project will be as follows:

- Sieving **TS** into different particle size ranges, so that the roots are forced to explore different pore size ranges. This will aim to better understand how roots explore pores of different size ranges and how root growth is affected by different **TS** pore size ranges;
- Creating vertically stratified 'split pots', which contain **TS** of different particle size ranges on each side of the pot. These pots will be imaged at specified, equally distributed time points, so that root development can be observed over time. This research will aim to understand whether root growth is autonomous (i.e. determined by the immediate environment surrounding individual root tips) or governed by communication across the whole plant;
- Creating a compact soil strength apparatus, which can be used with **TS** to create strength within the system. Seedlings will be sown in **TS** and then placed under mechanical pressure using this apparatus during the incubation period and imaging. This will aim to understand how the **TS** system behaves when placed under mechanical pressure and how roots grown in compacted **TS** relate to those that are grown in compacted natural soil.

Measurements of the physical properties of **TS** will be assessed using the 3-D images obtained during this project and compared with root measurements, to understand how particular physical soil characteristics affect barley root characteristics. This will further develop our understanding of physical root/soil interactions and the effects that are observed on roots due to factors that can only be observed within heterogeneous growth substrates, including pore size, soil structure and soil compaction.

2 Developing techniques to image and quantify the root system architecture of barley seedlings grown in heterogeneous substrates

2.1 Introduction

Imaging techniques have been used in plant research to analyse physical properties of leaves and stems to detect early signs of disease (Chaerle and Van Der Straeten, 2001). Imaging techniques have also been used to understand nutrient and oil distribution in seeds that are germinating (Lombi et al., 2011, Neuberger et al., 2008). Imaging of roots has been less common, largely due to the opacity of soil making it a challenge to obtain images of undisturbed roots (Downie et al., 2012). Traditionally, researchers have had to extract roots in order to take images of them which is destructive and makes analysis of root system architecture impossible (Taylor et al., 1991). Roots could only be observed non-destructively if they grew inside a transparent container, or if they were imaged using a technique that was able to penetrate opaque objects.

In 2012, a new growth medium was developed by Downie et al. (2012), known as transparent soil (**TS**) which was used to observe fluorescent *Escherichia coli* colonising lettuce roots. This growth medium has a physically heterogeneous structure, can be used in the same way as natural soil and can be imaged using optical projection tomography (OPT); a method which is similar to μCT, however uses light instead of radiation to obtain images. In order to image roots in TS using OPT, the TS core has to be saturated with a solution such as percoll or

sorbitol, whose refractive index matches that of the TS particles. This causes the particles to appear invisible, thus allowing the observation of the roots within (Figure 1-2).

With very small samples **TS** has been shown to work well as a root growth medium and it was found that roots grown inside **TS** were more similar to sand than to Phytagel (Downie et al., 2012). Unfortunately with larger samples, air bubbles become a challenge in TS, because there are pores within the **TS** volume that do not flood. These pores contain air, whose refractive index does not match that of the particles and the solution. Therefore air bubbles can obscure the roots from view, and the more there are, the more noise is created within the resulting images (Figure 2-1).

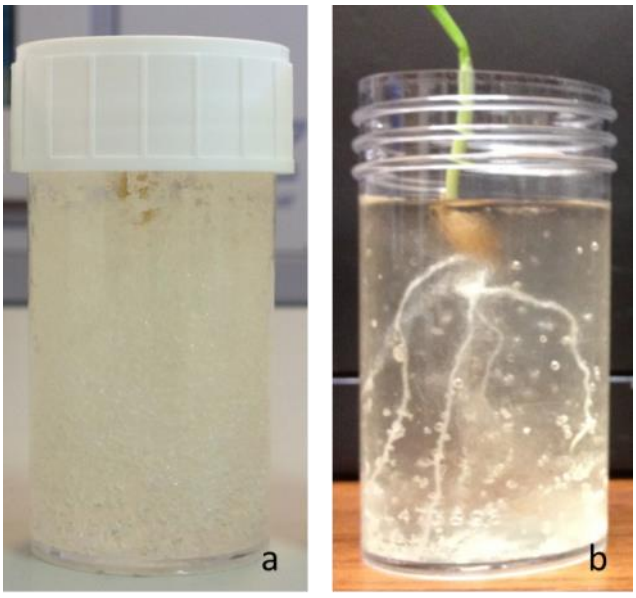

Figure 2-1: Barley seedling in a TS core before flooding with sorbitol (a) and after flooding with 15% sorbitol (b), when particles become transparent but air bubbles remain

Despite current limitations with the **TS** system, OPT relies on light instead of radiation and can be built on-site for a fraction of the cost of µCT. It allows the observation of roots *in situ* and obtains high quality 3-D images. It also requires little specialist training, making OPT a more viable option for some researchers who may not have access to µCT facilities.

Whilst **TS** shows promise as a new growth medium for understanding root system architecture under different growth conditions, it is still in its infancy, having only been used to image very small, immature *A. thaliana* , *L. sativa* and *N. benthamiana* roots (grown inside 1 x 1 cm cuvettes), and multiple challenges are associated with its further development. These challenges include, but are not limited to:

- Scaling the system up so that it can be used to grow and image larger monocotyledenous samples (3 x 5 cm specimen pots);
- Improving the OPT system further, so that it can obtain more detailed images. In particular, a method for removing air bubbles from the **TS** system should be developed so that clearer images can be obtained using OPT;
- Developing an image analysis technique to analyse 3-D images of complicated monocotyledenous root systems.

Such challenges must be addressed if **TS** is going to become a viable option for developing our understanding of root system architecture as it is affected by physically heterogeneous growth mediums. A large component of this chapter has been to develop **TS** further by addressing these issues, so that it can be used to enhance our understanding of monocotyledonous root growth.

2.2 Aims

The aim of the project was to test the effects of root physical parameters on root performance utilising **TS**. In order to achieve this several technical difficulties needed to be overcome. When broken down into components, the main aims were as follows:

- To select suitable barley cultivars with contrasting root phenotypes, fast elongation rates and high germination rates.
- To develop the **TS** system, and scale up the processing technique, so that larger quantities of TS could be cleaned; making it suitable for use with larger barley roots.
- To develop the OPT system by improving refractive index matching and removing dense air bubbles which collect in **TS** pores during sample saturation. This would make the system suitable for use with larger barley roots.
- To develop a standardised image analysis method for the large 3-D data sets that are produced using μCT and OPT techniques.

2.3 Experimental outline

Developing the methods and techniques for large-scale use of **TS** was constantly ongoing and formed a significant component of this thesis, which is why all of them have been brought together in this chapter. Each chapter in this thesis involved method development, and therefore all of the experiments that are described throughout this thesis are referred to within this chapter. Table 2-1 contains chapter numbers in this thesis, codes for the experiments which are described in this chapter and a brief description of the main experiments that were involved in each chapter, in order to assist the reader whilst navigating their way through the thesis.

Chapter number	Experiment code	Experiment description
Chapter 3	E.i	An experiment to compare barley root growth in soil vs **TS**.
	E.ii	An experiment to find a replacement barley cultivar for B83.
	E.iii	An experiment to create a diagnostic atlas of different types of noise created during OPT imaging.
	E.iv	An experiment to compare barley root growth in **TS** sieved to three different particle size ranges; ○ 850-1250 µm - **S** ○ 1250 – 1676 µm - **M** ○ >1676 µm - **L**
Chapter 4	E.v	A time point experiment to test barley root growth in three different **TS** core set-ups; ○ 850-1250 µm - **S** ○ >1676 µm - **L** ○ Split pots (vertically stratified **TS** cores, containing 50% 850-1250 µm and 50% >1676 µm) – **SS**/**SL**

Chapter number	Experiment code	Experiment description
Chapter 5	Evi	An experiment to improve the refractive index matching of **TS** and sorbitol.
	E.vii	An experiment to observe root growth in **TS** under three different levels of compaction; ○ No compression - **N** ○ Medium compression - **M** ○ High compression - **H**

Table 2-1: Outline of the main experiments described in this thesis

2.4 Methods

2.4.1 Experimental setup

Previous published experiments involved using **TS** mainly as a growth medium for small (grown inside 1 x 1 cm cuvette) dicotyledonous seedlings (Downie et al., 2012). For this project, scaling up the **TS** setup was necessary in order for it to be suitable for use with large monocotyledonous barley seedlings. During early experimental development, barley varieties that were expected to show specific phenotypic traits were chosen and prepared carefully during the project. Core preparation was carried out in order to ensure that the structure of the **TS** had specific physical traits that changed the way that the seedling roots grew. A new piece of equipment was also designed later on in the project, which was able to apply pressure to the **TS** in order to simulate the effect of soil strength.

2.4.1.1 Seedling selection

For E.i, barley varieties were chosen using data previously obtained by Valentine et al. (2012a) during experiments that had taken various measurements of young barley plants that were grown on gel plates. The two varieties Troon and B83, were chosen because they showed a significant difference in root angle, with Troon having a large standard deviation of rooting angle, indicating a greater root spread. The aim was to have one phenotype (B83) that would show immediate vertical descent during initial root elongation, and another phenotype (Troon) that would show a more lateral spread of the roots before the gravitropic response occurred. Whilst phenotypic differences were seen during E.i between the two cultivars, B83 roots were much shorter than Troon roots (Section 3.5.1) so it was difficult to compare other phenotypic traits, such as verticality and curvature. Therefore E.ii was designed with the aim of testing cultivars to find one that was a more suitable comparator for Troon.

In experiment E.ii, barley varieties were selected from the same data as before (Valentine et al., 2012a) if they had a similar average root length to Troon, but a different average root angle. Based on this criteria, seven varieties were selected for further assessment; Waggon, Derkado, Chime, Bowman, Optic, Westminster and Troon. Five seeds of each variety were sown randomly in soil packed at 1.1 $g.cm^{-3}$, 20% gravimetric water content and each was assigned an ID number from 1 – 35. The cores were randomised and positioned in an incubator, in the manner depicted in Figure 2-2. The cores remained there for 72 hours, after which the seedlings were extracted in the same order as they were sown and placed in individual sterile specimen pots, containing 50% ethanol for preservation.

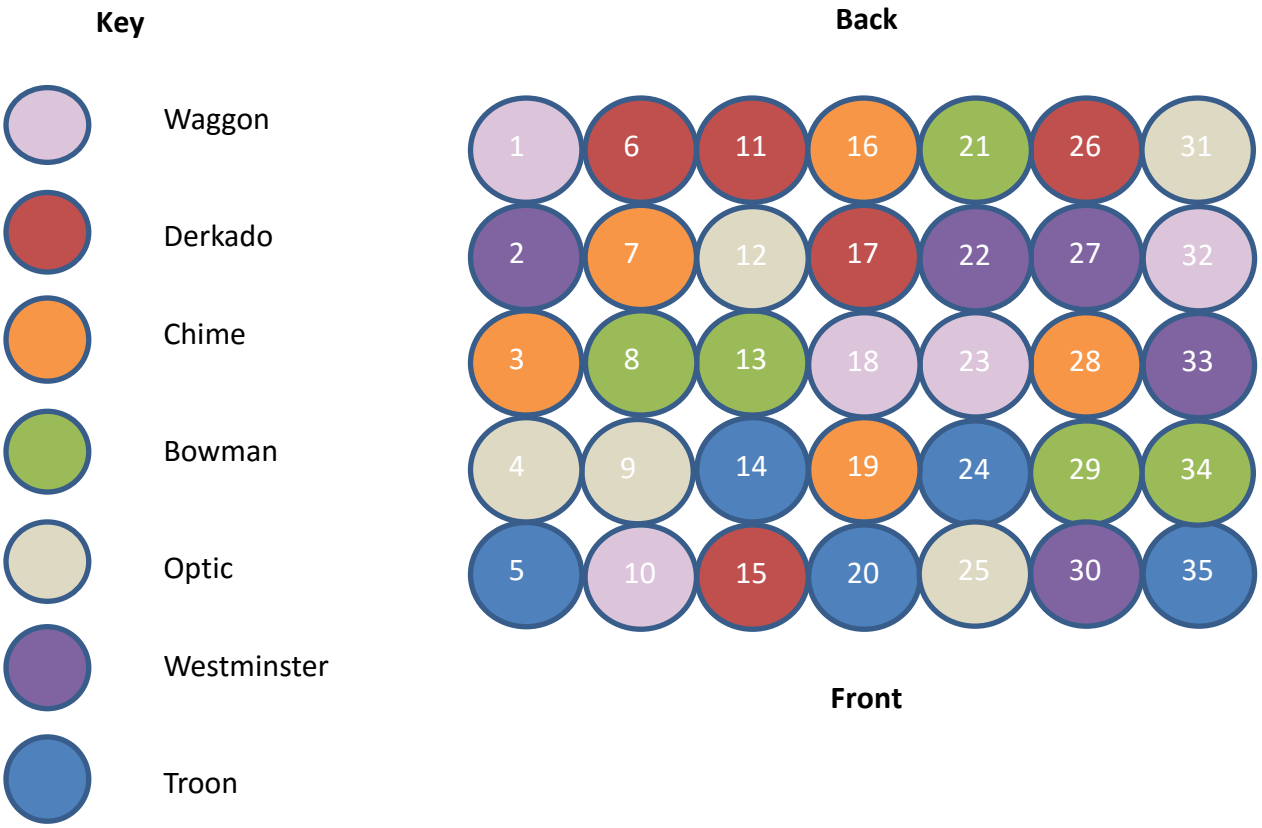

Figure 2-2: The positions of seedlings inside the incubator and the order in which they were sown and extracted (1st – 35th).

The seedlings were scanned using an Epson flatbed scanner (Epson Expression 10000XL) at the James Hutton Institute, set to professional mode and a resolution of 1200 dpi. The number of roots was recorded and the length of the longest root of each seedling was measured using a polygonal line, manually drawn on the images (Figure 2-28) in the open source software, ImageJ (Schneider et al., 2012). Figure 2-3 shows the average lengths (mm) of the longest roots of each variety. In descending order, Derkado, Westminster and Chime were the three varieties closest in length to Troon.

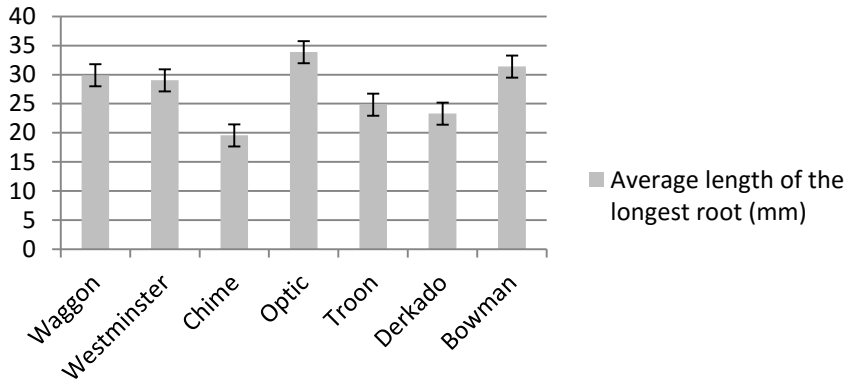

Figure 2-3: Average length (mm) of the longest roots of 7 different barley varieties after 72 hours of growth. Standard error bars shown.

Figure 2-4 shows the average number of roots for each variety. In descending order, Westminster, Bowman and Optic were closest to Troon in the number of visible roots present.

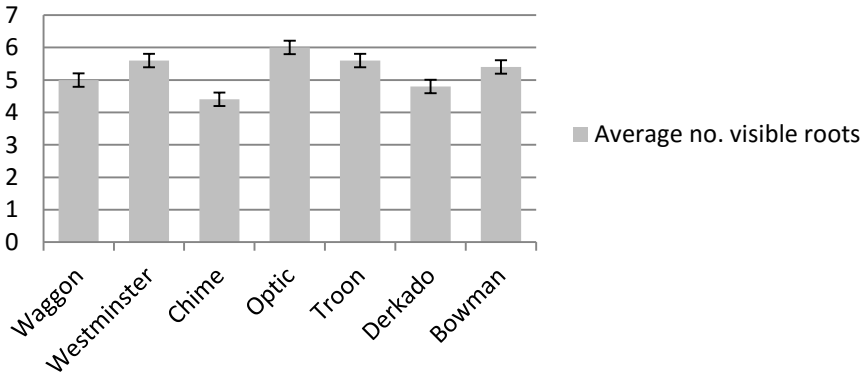

Figure 2-4: Average number of visible roots observed in seven different barley varieties after 72 hours of growth. Standard error bars shown.

The Westminster variety was the most similar to Troon when considering both the number of visible roots and length of the longest root after 72 hours of growth, however previous data (Valentine et al., 2012a) had detected a difference in root angle when these varieties were grown in 2-D gel systems. Therefore, this was chosen as a suitable comparison to Troon for subsequent experimentation involving multiple cultivars.

Golden Promise was also selected as a cultivar for further experimentation, as this variety is often used for transgenic work. Whilst no transgenic barley varieties were developed during this project, it may be the case that fluorescent lines are developed in the future so that cell-scale root elongation can be studied and better understood. Therefore, acquiring some root growth data for this cultivar may be useful.

E.iv (Chapter 3) failed to detect significant differences between Troon, Westminster and Golden Promise with regards to root properties such as root verticality and curvature. Therefore, it was decided that for experiments E.v (Chapter 4) and E.vii (Chapter 5) it would be better to focus solely on the treatment, as opposed to differences between cultivars. At this point, Westminster was used on its own and Troon and Golden Promise were no longer included in experiments.

2.4.1.2 Seedling preparation

2.4.1.2.1 Pre-germination and seed-sowing protocol

The pre-germination protocol for all barley seedlings used in this project involved soaking seeds for 24 hours at room temperature in distilled H_2O and then sterilising by soaking for 15 minutes in 2% Calcium Hypochlorite. The seeds were rinsed thoroughly and then placed in

between two layers of damp filter paper, inside a petri dish which was then wrapped in tin foil. Seeds were incubated at 15°C for 72 hours.

Seedlings were selected for sowing based on the lengths of their roots which were between 5 and 10 mm. Sowing was done in a laminar flow cabinet which had been cleaned with 75% ethanol, to ensure that the conditions were as sterile as possible. A small pocket was made approximately 1 cm deep at the surface of the soil. Forceps which had been surface sterilised with 75% ethanol and then rinsed in sterile distilled H_2O were used to transfer the seedlings from the filter paper to the pocket in the surface of the soil. The seedling was then covered with soil or **TS** using a spatula that had been surface sterilised ethanol and rinsed with distilled H_2O.

Incubator settings were chosen based on the typical conditions that barley seedlings might encounter in a Scottish spring time. The incubator's temperature was set at 15°C and an L.E.D light board (http://www.fastlight.co.uk/acatalog/LED_Grow_Boards.html) placed above the seedlings in the incubator was plugged into a timer, ensuring that the seedlings received 16 hours of light followed by 8 hours of darkness each day. For E.v (Chapter 4), seedlings were removed each day for one hour, during the incubator's light phase, for the purpose of µCT imaging. Figure 2-5 shows the process involved in sowing barley seedling in **TS**.

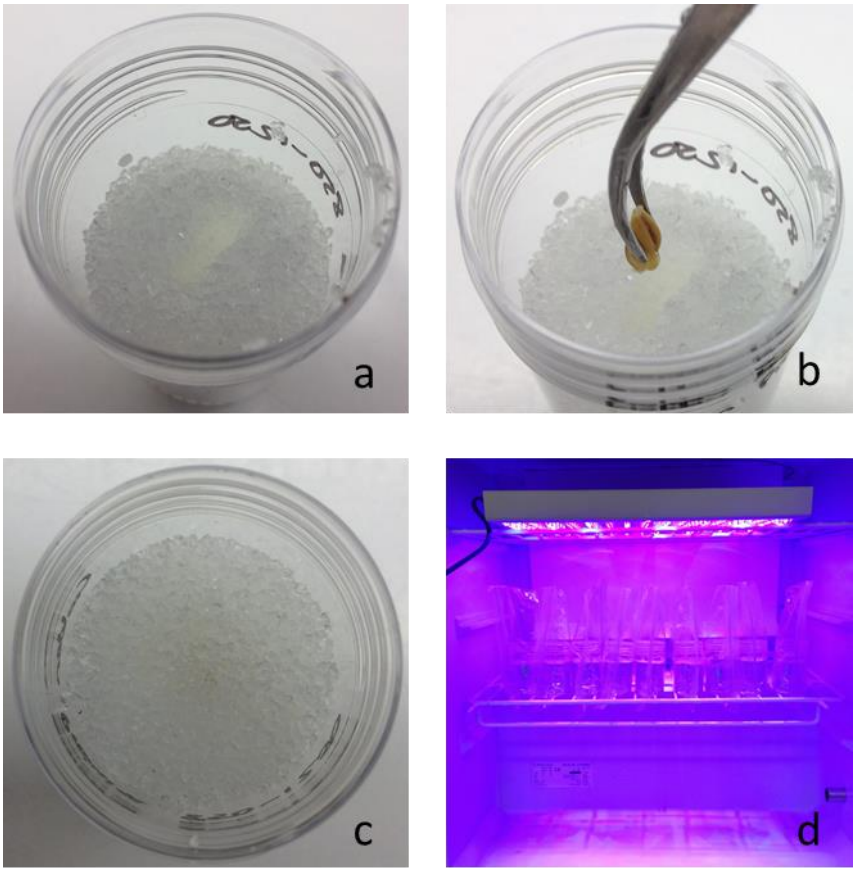

Figure 2-5: Photographs showing the process involved in sowing barley seedlings in TS. Images show; a small pocket in the top pf the TS volume (a), sowing the pre-germinated seed using forceps (b), the seed covered by the TS (c), TS cores inside the incubator with the L.E.D light plate switched on (d)

2.4.1.2.2 Soil and TS preparation

For the experiments involving soil cores, soil was taken from Mid-Pilmore Mylnefield Farm, Invergowrie, DD25EL (geo coordinates: 56° 27' 22.2" N 3° 5' 34.1" W) and sieved to <2 mm. Samples were taken from the soil, weighed and placed in an oven at 105°C to obtain dry weights. The dry mass was used to calculate total soil moisture, which was then made up to 20%. The soil was then shaken, sealed within a plastic bag (<500 g in each bag) and left to equilibrate for 24 hours at room temperature. Soil cores were packed at a dry bulk density of 1.1 g cm^{-3}. After packing, cores were sealed in individual plastic bags to reduce moisture loss and left in an incubator set to 15°C until seeds were ready for sowing.

For all of the experiments in this project, it was essential that the **TS** could be cleaned and prepared for re-use in as little time as possible (Downie et al., 2012) because the volume of **TS** that was available was limited and needed for repeats. In order for **TS** to be suitable for barley experiments, the cleaning process had to be scaled up and made quicker. The initial protocol detailed by Downie (2013) was suitable for cleaning small amounts of **TS** (<5 g), however when the same protocol was applied to large volumes of **TS** (>200 g), it was inefficient, taking up to 2 weeks to clean the particles. Therefore, the protocol was revised and a column system was introduced, which sped up the process greatly. The initial protocol described by Downie et al. (2012) for cleaning **TS** is included in Appendix A.

Nafion pellets of 4 mm diameter were crushed to particle sizes of >350 µm using a cryo-mill (6850, SPEX SamplePrep, UK) in order to have enough **TS** particles for all experiments during this project. After crushing the first time there were enough particles and all were treated using the procedure described below.

15%KOH/ 35%DMSO/ 50% distilled water was added to the particles in order to replace F with K^+ ions (Figure 2-6), swell the particles and hydrolyse the nafion particles. They were then placed in a water bath at 80°C for 5 hours which assisted in breaking the chemical bonds in order for hydrolysis to occur. The KOH/DMSO/H_2O was rinsed off and the particles were submerged in distilled H_2O and left at room temperature for 30 minutes before being rinsed again, which helped to remove any remaining traces of the un-reacted KOH. The distilled water was removed and 15% nitric acid was added to the particles which were then left at room temperature for one hour. This was rinsed off and then nitric acid was added again and left at room temperature overnight. This part of the cleaning process added H^+ ions to the particles, thus converting them to the acid form and giving the particles cation exchange

properties, enabling them to exchange nutrients with plant roots. Adding nitric acid also helped to remove any remaining organic matter from the particles which may have accumulated if the particles had already been used for plant growth.

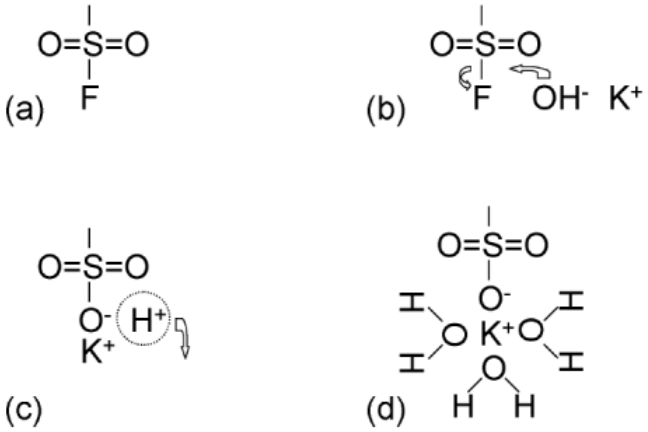

Figure 2-6: The mechanism of Nafion precursor hydrolysis (a) to the K+ cation form of Nafion (d) according to the method described in the Du Pont patent (Grot, 1973) – Image from Elliot et al. (2001)

The next day, the nitric acid was removed and 1M sulphuric acid was added to the particles. The particles were placed in a water bath at 65°C in order to achieve full swelling of the particles and clean them thoroughly. The sulphuric acid was rinsed off, replaced with distilled H_2O and placed in the water bath again at 65°C for one hour. The particles were then rinsed, submerged in 3% hydrogen peroxide and placed in a water bath at 65°C for one hour again. Hydrogen peroxide is an aggressive oxidiser which removed any remaining organic particles and cleaned them thoroughly. The **TS** particles were then rinsed with distilled H_2O and loaded into a column, which is shown in Figure 2-7. A beaker holding full strength Murashige & Skoog (MS) Media at pH5.5 (approximately 20x the volume of **TS** being washed) was placed on a shelf at a higher level than the column. A rubber tube led from the beaker to the column and a syringe was used to create negative pressure so that the MS media would start to drip out of the beaker, through the tube, into the column containing the **TS** particles. The level of MS media in the column was always above that of the **TS** particles, so they were fully submerged

at all times. The MS media would titrate the particles and the acid waste would drip out through the bottom of the column, into a beaker. The advantage of this method is that the particles can be left overnight to titrate, but often this is unnecessary as the particles titrate within 1 – 2 hours, depending on the volume of **TS** particles inside the column. This was a vast improvement compared with the previous method, which took much longer to process much smaller quantities of **TS**. The waste dripping out of the bottom of the column was tested by placing a strip of indicator paper underneath the flow. Once the pH was at 5.5, the particles were removed from the column. They were then rinsed with distilled H_2O and placed in a beaker of ½ MS media. Particles were then autoclaved and remained saturated in ½ MS media until they were used to prepare cores.

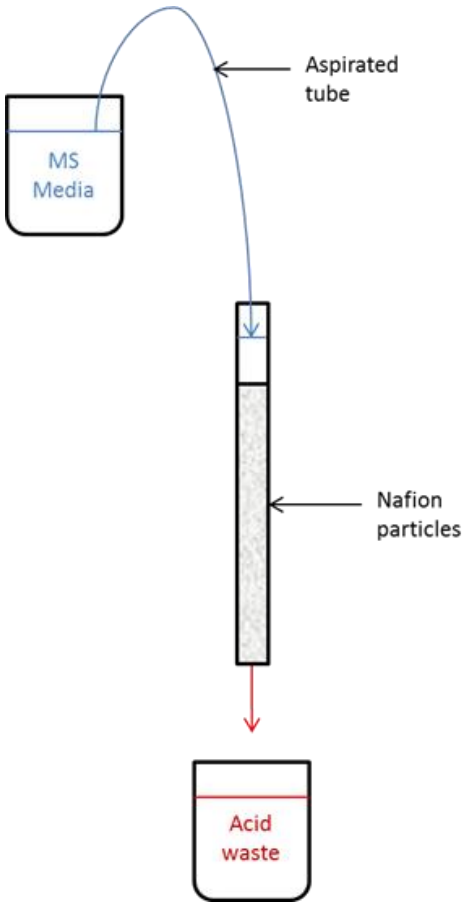

Figure 2-7: The column method developed in order to maximise the efficiency of the titration stage during the processing of Nafion for use as transparent soil

The initial protocol (Downie, 2013) stated that **TS** particles should be transferred into the core under sterile conditions and then a syringe used to remove excess fluid from the core. This method was used initially, however caused difficulties in standardising the amount of fluid that was inside the cores at the time of sowing the seeds. Therefore, for E.v and E.vii the **TS** was returned to the column system and allowed to drain using gravity so that the particles were free from excess fluid prior to loading into incubation chambers. A small amount coating the particles, remained adsorbed to the particles' surfaces. This made it easier to weigh out precise amounts of **TS** and standardise the **TS** plant growth conditions.

2.4.1.3 Soil and TS core preparation

For E.i and E.ii, sandy-loam soil from Mid- Pilmore field, The James Hutton Institute, Dundee, UK was used. Soil cores were prepared using Acrylonitrile Butadiene Styrene (ABS) plumbers pipe obtained from Graham's plumbers, Dundee (http://www.grahamplumbersmerchant.co.uk/) of 5 cm internal diameter, cut to the length of 5 cm, providing a total internal volume of 98.17 cm^3. Fabric mesh cut to 10cm x 10 cm was obtained from Dunhelm Mill (luxury plain voile; http://www.dunelm.com/product/white-sheer-elegance-voile-panel-1000006194?searchTerm=luxury+plain+voile) and secured to the bottom of the tubing using an elastic band in order to hold the soil in place.

TS was packed into transparent specimen pots of 5 cm (length) x 5 cm (diameter), giving a total volume of 98.17 cm^3 during E.i (Chapter 3) so that two seedlings could be grown in each core, however for E.iv and E.v only one barley seed was sown in each core, so smaller specimen pots (http://www.medfor.co.uk/product/707/110/clear-ps-jar-with-white-pe-screw-cap/709bbca2f05a03b04aadf9542e0d975b) were used in order to reduce the noise caused by air bubbles surrounding the sample during OPT imaging. The smaller pots had

dimensions of 5 cm (height) x 3.2 cm (diameter), giving a total volume of 40.21 cm^3. For E.vii these specimen pots were changed for transparent acrylic cast tubing which is strong, lightweight and has up to 92% light transmission, which is higher than that of glass. The acrylic cast tubes (Plastock, object ID: TR03A.040.030I.CLR) were open at both ends and had dimensions of 6 cm (length) x 3.4 cm (internal diameter), giving a total volume of 48.25 cm^3, although the **TS** was only packed to a height of 5 cm, giving a total volume of 45.4 cm^3. The **TS** samples were packed to a bulk density of 0.67 $g.cm^{-3}$ and a gravimetric moisture content of 0.18 – 0.3$g.g^{-1}$ Fabric mesh (luxury plain voile http://www.dunelm.com/product/white-sheer-elegance-voile-panel-1000006194?searchTerm=luxury+plain+voile) was secured to the bottom of the tubing with an elastic band in order to hold the particles within the core, whilst still allowing gases and liquids to be exchanged more easily. This was particularly useful when the particles had to be saturated with an optically matching solution such as sorbitol for the purposes of OPT imaging.

2.4.1.3.1 Separating particle size ranges and preparing split pot cores

In E.i (Chapter 3), the **TS** particle sizes were mixed and ranged between 500 and 4000 µm in diameter. In order to manipulate the physical structure of **TS** for E.iv and E.v, the **TS** was dried and then sieved into different particle size ranges; <500 µm, 500-850 µm, 850-1250 µm, 1250-1676 µm and >1676 µm. The **TS** was then cleaned again, according to the aforementioned protocol (Section 2.4.1.2.2) and used in **TS** cores.

For the E.v (Chapter 4), the cores were split vertically with a different particle size on each side of the core. Figure 2-8 summarises this process.

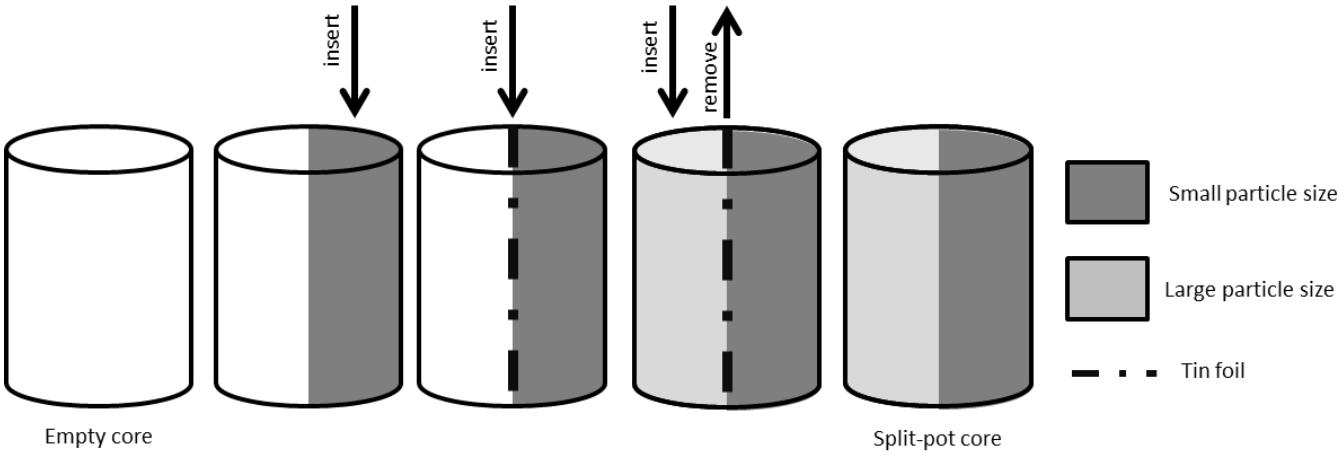

Figure 2-8: Schematic diagram demonstrating the process involved in forming a split pot TS core

The specimen pot being used to make up the core was tilted on its side and **TS** from one particle size was transferred into the core using a surface-sterilised spatula, until it filled 50% of the core. Then a strip of tin foil spanning the diameter of the core was placed on the **TS** and this was used to separate the **TS** already inside the core from the **TS** of a different particle size that was then inserted. After the second particle size had been inserted, the tin foil was gently removed, so that only the particles remained inside the core, however there was a clearly defined boundary between the two different particle sizes, as is demonstrated in Figure 2-9.

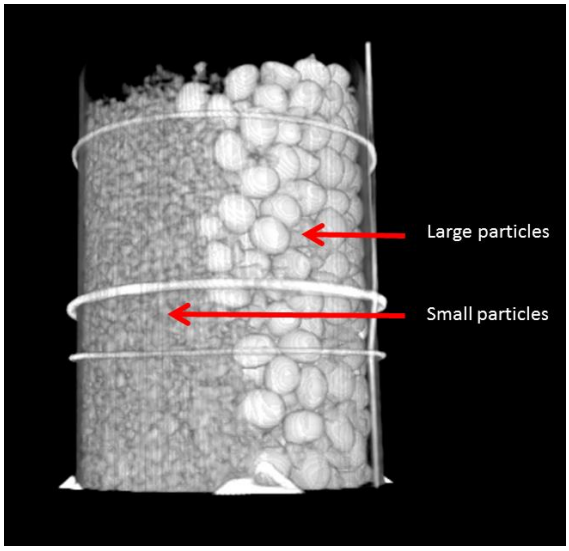

Figure 2-9: A 3-D µCT image showing the particle structure within the split pot cores (voxel resolution, 51µm)

TS cores were wrapped in tin foil, up to the top of the **TS** volume, so that the seedlings would be in the dark during growth. Cling film was stretched across the top of the cores to minimise contamination and holes were pierced in it, to allow for gaseous exchange. All **TS** cores were then kept in individual sealed transparent bags whilst incubating, again to minimise contamination.

2.4.1.4 Development of soil strength apparatus

Penetrometer measurements were taken at the James Hutton Institute and it was found that **TS** has very little mechanical strength. Therefore, in order to create strength between particles and to test root growth in a strong soil equivalent medium, a novel apparatus was developed for E.vii which is shown in Figure 2-10. A 20 cm long aluminium construction rail (Thorlabs, object ID: XE25L900/M) was used with a mounting base (Thorlabs, object ID: BA2/M) and a right angle bracket (Thorlabs, object ID: AB90E/M). The bracket and base were fixed to the construction rail with steel screws and washers. The **TS** core was constructed using acrylic cast transparent tubing, 34 mm in diameter and a mesh material was secured at the bottom with an elastic band. A round, opaque, acrylic disc, 3 mm thick and 32 mm in

diameter, with a round hole in the middle of 5 mm diameter was placed on top of the **TS** volume inside the core. A compression spring with an outside diameter of 30.937 mm, a free length of 31.750 mm and a rate of 18.47 N/mm was then placed on top of the acrylic disc (Lee Spring, object ID: LC125N0M). The free horizontal end of the right angle bracket rested on top of the spring which was then compressed manually and fixed in place to the construction rail with a steel screw and washer. The distance that the spring was compressed by was measured with a ruler and this along with the rate was used to calculate the level of compression that had been applied to the **TS** core.

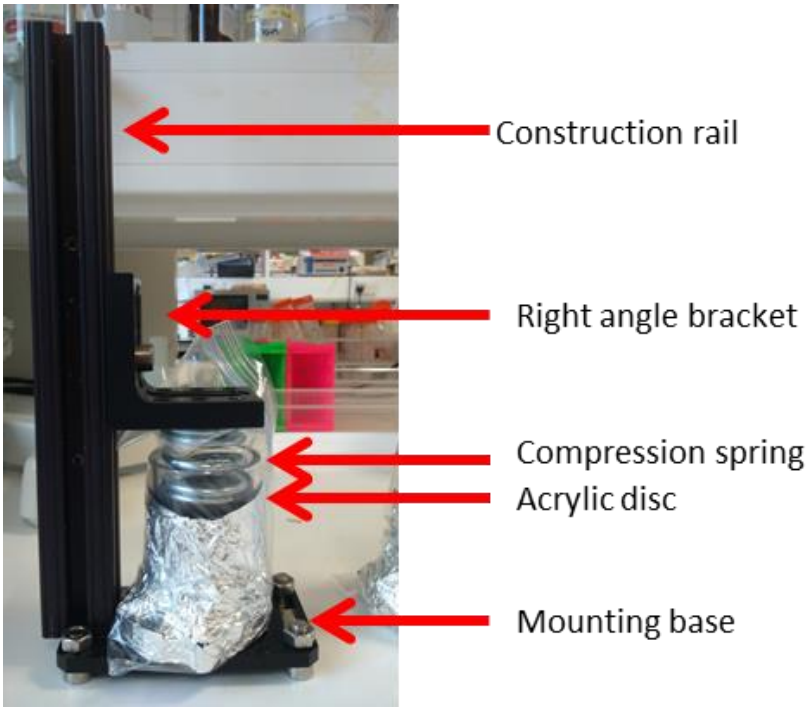

Figure 2-10: A labelled photograph of the soil strength apparatus

2.4.2 Imaging techniques

µCT was used in E.i, E.iv, E.v and E.vii however a novel technique for 3-D imaging of roots known as optical projection tomography (OPT), which was used in the Downie et al. (2012) study for imaging lettuce seedlings, was also developed further for imaging larger scale monocotyledonous roots. OPT was used in E.iii, E.iv, E.v, E.vi and E.vii. Both OPT and µCT have advantages and disadvantages depending on the questions that the researcher is trying to answer, and both have a place in better understanding root growth in heterogeneous substrates. Flatbed imaging of extracted samples was also used in E.i, E.iv, E.v and E.vii after 3-D imaging *in situ* so that a 2-D comparison was available. The applications for the three imaging techniques are briefly described in Table 2-2 and protocols for all three imaging techniques are described in detail throughout this section.

	X-ray Micro CT (µCT)	Optical Projection Tomography (OPT)	Flatbed Scanner
Transmission source	X-ray radiation	Light	Light
Sample size (length x diameter)	5 cm x 5 cm	5 cm x 5 cm	N/A
Resolution	<100 µm	<100 µm	1200 dpi
Type of medium	Soil and TS	TS	Soil and TS (after extraction)
2-D or 3-D	3-D	3-D	2-D
Imaging Applications	Overall structure of root systems in soil and TS cores. Soil and TS soil structure. Air/water/particle distribution in soil and TS cores. Time lapse imaging of root growth.	Visualisation and analysis of root system architecture of barley seedlings. Detection of fluorescence.	'Control' images to check the data obtained using 3-D techniques.

Table 2-2: The applications for the three imaging techniques used in this thesis

2.4.2.1 µCT Imaging Protocol

Seedlings were pre-germinated and incubated for a specified amount of time according to the experiment in question. Following the incubation period, seedlings were removed from the incubator and placed in the HMX 225 X-ray µCT scanner (Nikon, 2016) at Level 5 Kydd Building, Abertay University, Bell Street, Dundee, DD1 1HG, where scanning was immediately carried out. The sample was rotated on its stage about a central axis whilst radiation was fired at it

from the front. The radiation was absorbed by the sample, and absorption varied depending on the density of the substance that it was hitting. The level to which the radiation was absorbed was measured by a detector behind the sample and converted into grey-scale values, also known as attenuation values. These attenuation values (one for each pixel) were converted into 2-D images which were then reconstructed into 3-D data using Metris software CT Pro v2.0, which makes use of a filtered back-projection algorithm in order to create the x, y and z planes that make cross-sectional viewing of 3-D images possible after reconstruction (Figure 2-11).

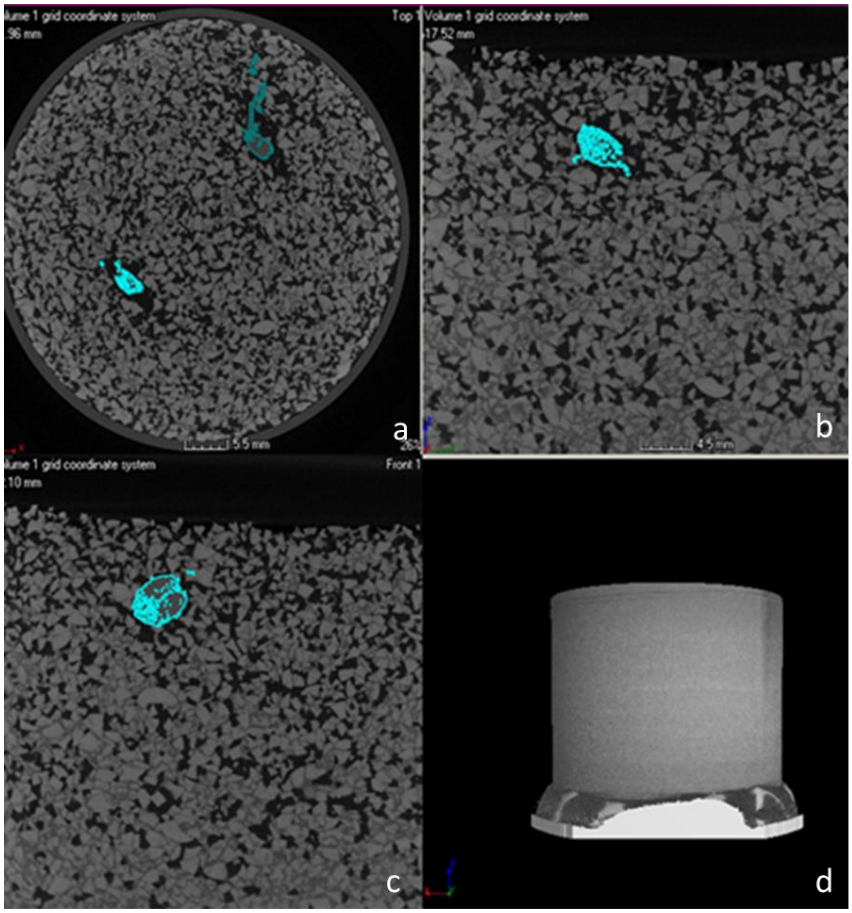

Figure 2-11: The layout of a 3-D image of a TS core in VG StudioMax2.2. a shows the core in the z plane, b shows the core in the y plane, c shows the core in the x plane and d shows the full reconstruction in 3-D. The seedling ROI detected by the region grower is highlighted in blue in the different planes.

The settings used for all µCT scans are listed in Table 2-3 and were chosen because they allowed the radiation to penetrate the entire object and capture the most detail possible within the least amount of time. Scans took approximately 1 hour so a maximum of 6 plants could be imaged in one day. This was always taken into account when preparing cores and planning replicates.

Settings	kV= 95, uA=80
X ray filter material	Aluminium
X-ray filter thickness	0.25 mm
Minimise Ring Artefacts	No
Projections	2500
Frames Per Projection	2
Reconstruction Quality	100
Beam Hardening Preset	0
Noise Reduction Preset	1

Table 2-3: Settings that were used for nafion and soil cores that underwent µCT scanning

The resolution of the images for E.i was 29 x 29 x 29 µm but was adjusted as the project continued, as it was found that barley roots and **TS** particles could still be detected at resolutions of 51 x 51 x 51 µm, which was the resolution used for E.iv, E.v and E.vii. By decreasing the resolution in this manner, the image analysis could be carried out faster, thus improving the speed of acquiring data, without compromising the detail necessary for the analysis being carried out on them. Examples of different scans are shown in Figure 2-12, whereby the seeds, particles, pores and roots are clearly distinct from one another, despite the decrease in resolution.

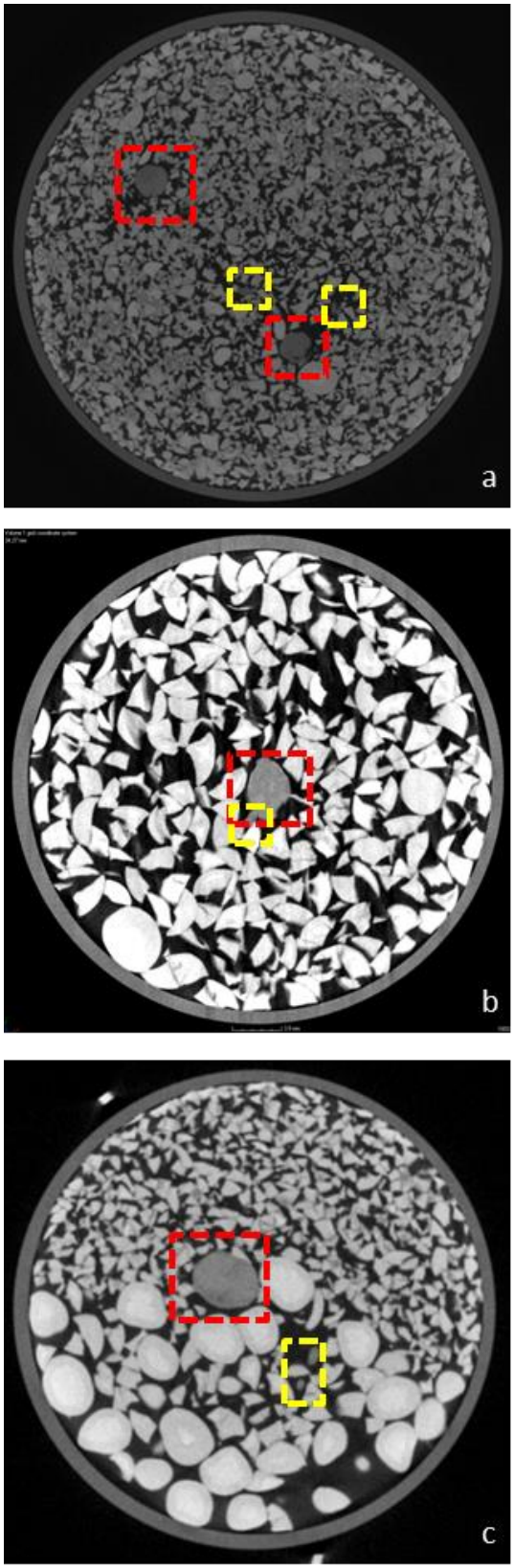

Figure 2-12: Cross-sectional images of TS cores taken at resolutions of 29 x 29 x 29 µm (a), 34 x 34 x 34 µm (b) and 51 x 51 x 51 µm (c). The seed is shown inside the red box and examples of roots are shown in yellow boxes.

2.4.2.2 OPT imaging

OPT imaging has many potential benefits for observing root growth in 3-D, including the ease with which it can be built and the relative inexpensiveness of the equipment when compared with a µCT scanner. The OPT equipment for this project was built on site at the James Hutton Institute by Lionel Dupuy and consists of a light box, stage for the sample with a rotating stepper motor, stereo microscope (Leica MZ 16 FA) and camera (Leica DFC 350 FX). An image of the OPT setup is shown in Figure 2-13.

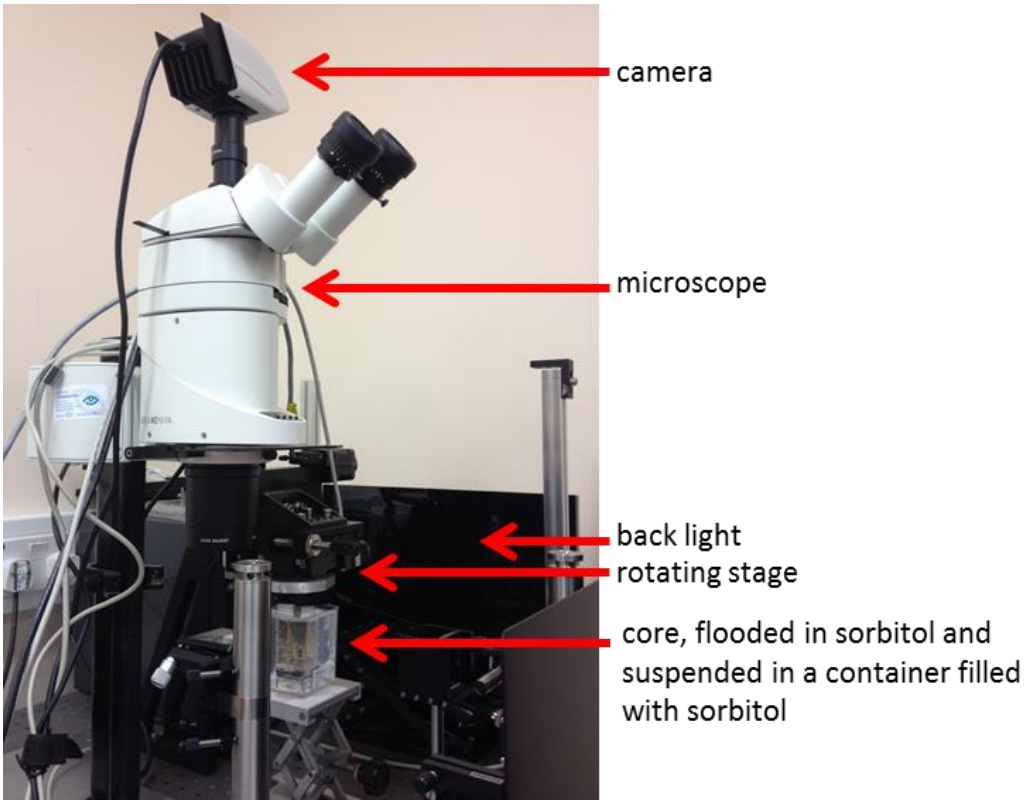

Figure 2-13: A photograph of the custom-built optical projection tomography microscope built by Lionel Dupuy at the James Hutton Institute

2.4.2.2.1 OPT imaging protocol

After incubation, seedling samples were flooded with sorbitol solution (Section 2.4.2.2.4). The sorbitol raised the RI of water to match that of Nafion (1.34). Matching the RI of the particles with sorbitol causes light to travel straight through the particles rather than bouncing off or

being absorbed by them. This causes them to appear completely transparent, with just the roots and any air bubbles present between particles being visible (Figure 2-1).

The top of the sample was suspended from the stage into a container containing more sorbitol, the same concentration as that which was being used to flood the particles inside the core. A camera was positioned in front of the sample and a white backlight was behind it so that the roots in the core were illuminated. Software built in-house allowed the control of imaging parameters, such as the number of projections per degree, exposure and gain. As the stage rotated, 360 2-D projections were taken of the sample, one at each angle. The 2-D images were reconstructed to produce 3-D data using the Iradon function in Matlab (The MathWorks, Inc.).

2.4.2.2.2 Improving OPT imaging of large-scale barley seedlings

Testing was required in order to ensure that the best parameters were chosen. Clear 2-D projections were needed in order to obtain the best 3-D images after reconstruction. Several adjustable parameters which could influence the quality of images were identified including; core alignment, camera alignment, immersing the object in sorbitol during imaging and calibration using the sample itself before imaging.

E.iii was a small experiment designed to assess the varying parameters of OPT imaging. A **TS** core containing two cocktail sticks was flooded with 15% sorbitol and placed in the OPT setup. Each of the parameters listed previously was adjusted individually so that they were purposely inadequate and different types of noise were produced depending on the parameter that had been adjusted. This enabled the development of a diagnostic atlas, useful for identifying types of noise in reconstructions and the parameter that was causing it. Figure 2-14 shows an example of the 2-D projections obtained during this experiment, a 2-D cross-

section of the 3-D reconstruction whereby different types of noise can be seen and the resulting 3-D image.

In Figure 2-14 the left-hand figure on row a shows a 2-D projection of the core, which was purposely misaligned. 360 of these projections, taken 1° apart were used to create a 3-D image, which is shown in the right-hand figure on row a. The cocktail sticks can be seen clearly, as can the air bubbles that were not removed during flooding. The central image on row a is a cross-section through the 3-D image. This image shows the two cocktail sticks clearly as the two large white regions almost in the centre and a ring artefact connecting the two large regions is also seen. Ring artefacts were commonly seen in instances whereby the core was not aligned correctly.

Row b shows equivalent images to row a, however the camera was purposely misaligned, rather than the core. When the camera was not aligned correctly, the ring artefacts were much more extreme. The cocktail sticks were reconstructed as two large rings in the middle of the image (centre b). The 3-D image (right b) as a result did not show two clearly defined cocktail sticks. Camera alignment was found to be one of the most important parameters, with misalignment causing levels of noise that would render the image useless for data acquisition.

In row c, the image was taken without submerging the core in a pot of sorbitol. The 2-D projections immediately lost definition (left c) and whilst there were no ring artefacts in the centre of the core (centre c), the boundaries of the two cocktail sticks were not as clearly defined and when shown in 3-D (right c) the image was noisier, especially towards the edge of the core.

Row d shows the core when calibrated using the sample itself before imaging. For calibration, four 2-D projections were taken, 90° apart from each other and were projected onto each other. If they were aligned perfectly, the setup was deemed to be calibrated. If they were misaligned, the setup was not calibrated correctly and this produced inferior images. In this instance, the stage was moved to the left or the right and new calibration images were taken. This process was repeated until the superimposed calibration images were perfectly aligned, after which imaging began. Normally, calibration had been carried out using a screw which was suspended from the stage, however in this experiment it was tested whether the sample itself could be used to calibrate the setup. The resulting images in row d show that there were no ring artefacts (centre) and although the 3-D image was noisier at the bottom of the sample, this was only at the edges of the core, not in the centre where the cocktail sticks were positioned.

E.iii showed that alignment of the core and the camera were essential in order for suitable raw images to be obtained. Suspending the core from the stage into a pot of sorbitol was important in order to improve the definition of the cocktail sticks and calibrating the position of the stage using the core itself was also a way in which the resulting images could be improved. From this experiment it was also clear that roots growing close to the edge of the pot had to be treated carefully during the image analysis process, as noise could occur particularly in this region.

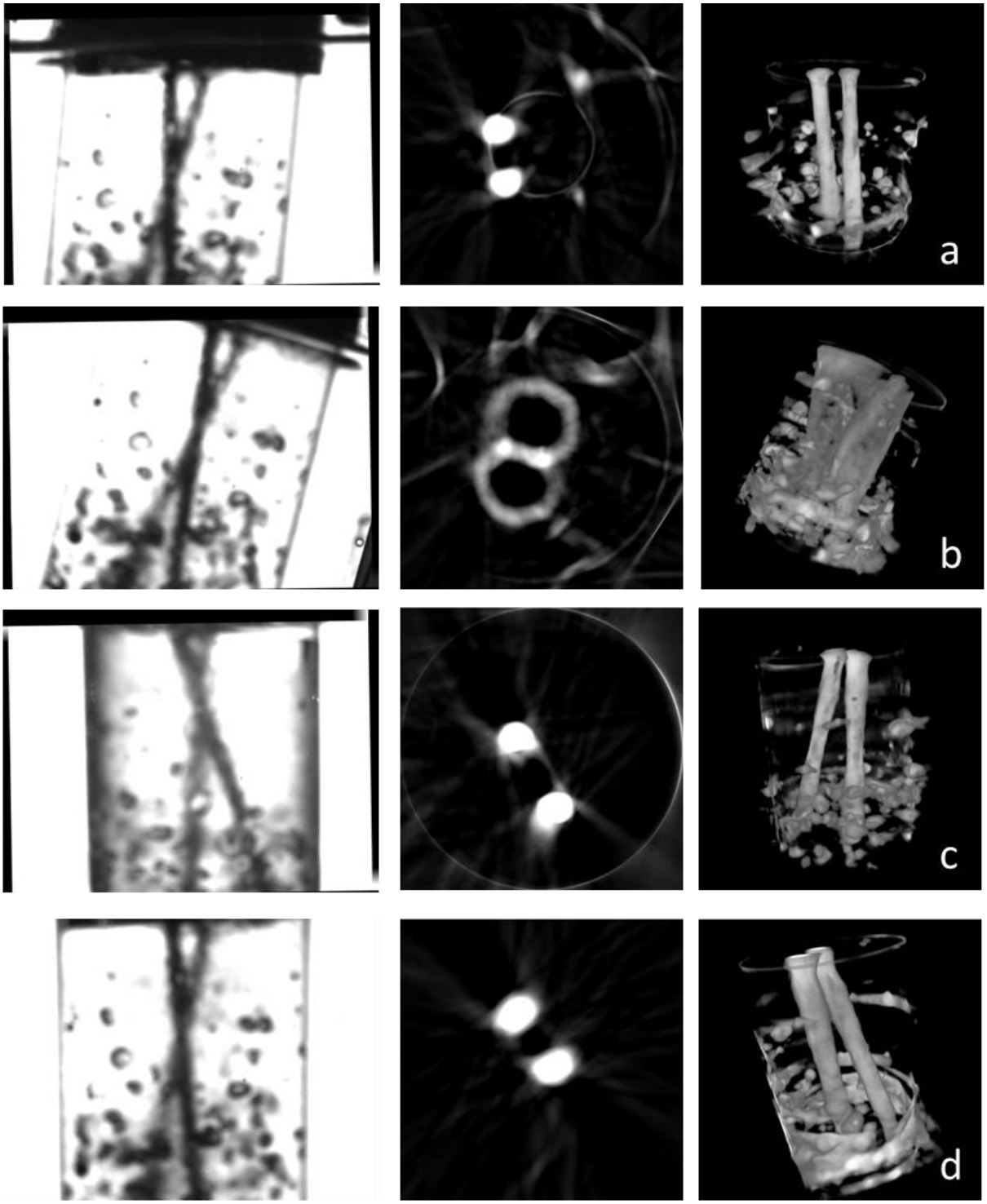

Figure 2-14: Diagnostic atlas of OPT noise using cocktail sticks in TS(resolution, 41μm). Images of a 2-D projection (1st column), a cross-section of the 3-D reconstruction (2nd column) and a full 3-D reconstruction (3rd column) of cocktail sticks flooded with 15% sorbitol and then imaged using OPT. Different parameters tested were core alignment (a), camera alignment (b), removing additional pot of sorbitol that the core was suspended in (c) and calibrating camera using the sample before imaging (d)

2.4.2.2.3 Selecting suitable TS particle sizes for OPT imaging

TS particles were dried, sieved into 5 particle size ranges and cleaned as described in sections 2.4.1.3.1 and 2.4.1.2.2. The particle size ranges were <500 µm, 500-850 µm, 850-1250 µm, 1250-1676 µm and >1676 µm. Two cores of each particle size range were prepared so that there were 10 cores in total. One Westminster seed and one Golden Promise seed was sown in separate cores of each particle size range. They were then incubated for 72 hours and flooded with 15% sorbitol. They were each imaged using the OPT setup, extracted from the **TS** core and preserved in 50% ethanol. The particle size ranges <500 µm and 500-850 µm were too small for producing images of roots using OPT (Figure 2-15). This was mainly because as the particle size reduces, so too do the pore sizes. As a consequence during flooding with optical matching solution, the air bubbles were difficult to remove. This resulted in too many air bubbles being present in the cores during imaging, which obscured the seedlings, and produced inadequate images. This was not as much of a problem in the particle size ranges 850-1250 µm, 1250-1676 µm and >1676 µm, whereby fewer, larger air bubbles were present. These were easier to remove, simply by gently inserting a needle into the pore and gently coaxing the air bubble out. Despite attempting a number of ways to remove air bubbles (including suction, pressure and changing the speed of flooding), a satisfactory automated method of removing tiny air bubbles from the smallest particle size ranges was not successfully developed during this project, so the three larger particle size ranges were used for further experimentation during this project.

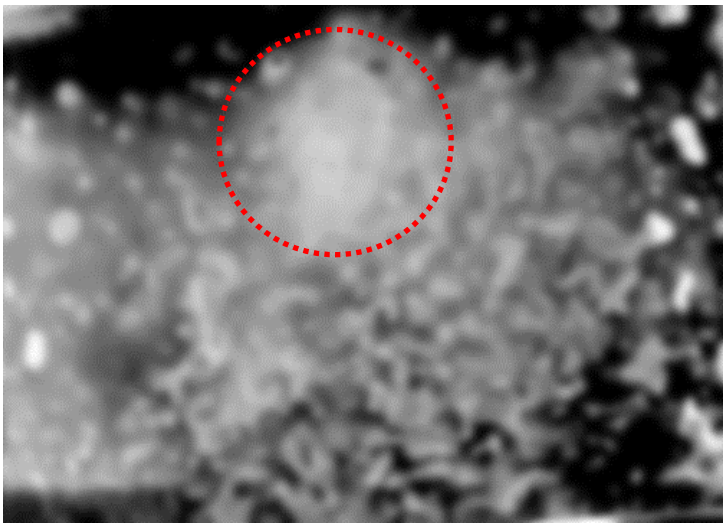

Figure 2-15: An image of a Golden Promise seedling inside a core containing the TS particle size range <500 µm. The high density of small air bubbles surrounding the seedling has obscured the seed (red circle) and the roots

2.4.2.2.4 Refractive index matching for different particle sizes

The refractive index of dry nafion is 1.34, close to that of water which is 1.33. Whilst this is a close match, the **TS** particles do not appear completely transparent in water and instead have a slightly cloudy appearance, which hinders the ability of the OPT camera to take high quality images. In order for good images to be obtained, the refractive indexes of **TS** and water needed to be as close to each other as possible. For E.i, E.iii, E.iv and E.v 15% sorbitol was used based on Downie (2013). The sorbitol raised the refractive index of the solution, so that the **TS** particles were completely transparent when flooded with the solution, as seen in Figure 2-16. Prior to E.vii the refractive index matching was reassessed on **TS** particles that had gone through the cleaning process, and also on **TS** particles of different size ranges to ensure optimal matching for this experiment.

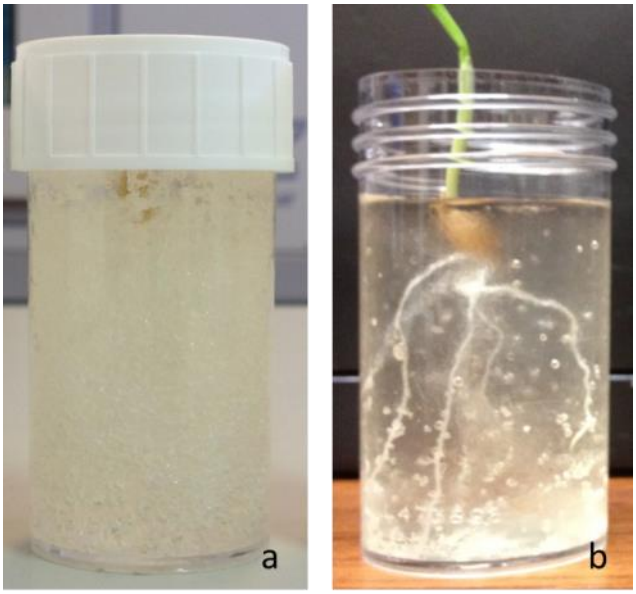

Figure 2-16: Barley seedling in a TS core before flooding with sorbitol (a) and after flooding with 15% sorbitol (b), when particles become transparent

In order to check that the sorbitol concentration was correct for all **TS** particle size ranges, E.vi was designed which involved **TS** particles in the size ranges of 850-1250 µm and >1676 µm. 18 **TS** cores were set up in total, nine containing the smaller particle size range (**S**) and nine containing the larger particle size range (**L**). They were then submerged with different concentrations of sorbitol, (11% - 19%, increasing by increments of 1% each time). These cores were placed in the OPT setup and a laser was shone through them. Without a **TS** core in the way, the light from the laser was concentrated in a thin line. Figure 2-17 shows an example of this line (a), as well as example images obtained using the following protocol. Before placing a core in the OPT, a control image was taken of the laser line with no **TS** sample in front of it (a). Each core was then placed in the OPT in turn, directly in the path of the laser. This caused the laser light to spread as it was refracted and absorbed by the **TS** particles in its path, so the light behind the core was no longer a thin line, but a wider line with scatter around it (b). An image of this spread was taken and imported into Fiji (Schindelin et al., 2012) in 32-bit colour .bmp format along with the control image. Both images had a Gaussian filter of 2 pixels applied to them in order to remove noise in the images. The control was subtracted

from the image of the laser light that had travelled through the core using the image calculator plugin so that only the spread of green light surrounding the line was left behind (c). The number of green pixels present in the image was then measured in Fiji (Schindelin et al., 2012), recorded and converted into a percentage of the total number of pixels contained within the image. Ideally, if the refractive index matching was perfect, there would be no scatter at all and the percentage of green pixels present in the resulting image would be 0. The image that contained the lowest percentage of green pixels was an image of the core that had scattered the laser the least, and was therefore the one whose refractive index was best matched.

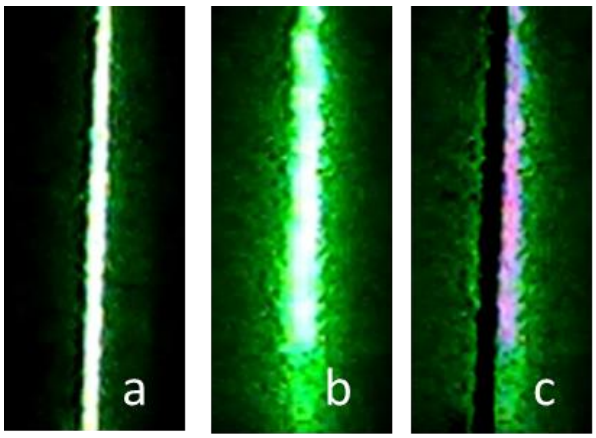

Figure 2-17: Example images obtained during refractive index matching of 850-1250 µm TS particles flooded in 10% sorbitol. Image a is the control image with no TS sample in the OPT machine. Image b is the same laser line which has been scattered by the presence of a TS sample. Image c is image a subtracted from image b, so that only the scatter surrounding the line remains.

This process was repeated for all sorbitol concentrations in both **TS** particle sizes 10 times and the results are shown in Figure 2-18. In this figure it can be seen that the most appropriate concentration of sorbitol is dependent on the particle size range of **TS**. The >1676 µm cores had the lowest percentage of green pixels at a sorbitol concentration of 12%, indicating that this was the best concentration for achieving transparency of this particle size range. For the 850-1250 µm particles, the lowest percentage was seen at 16%.

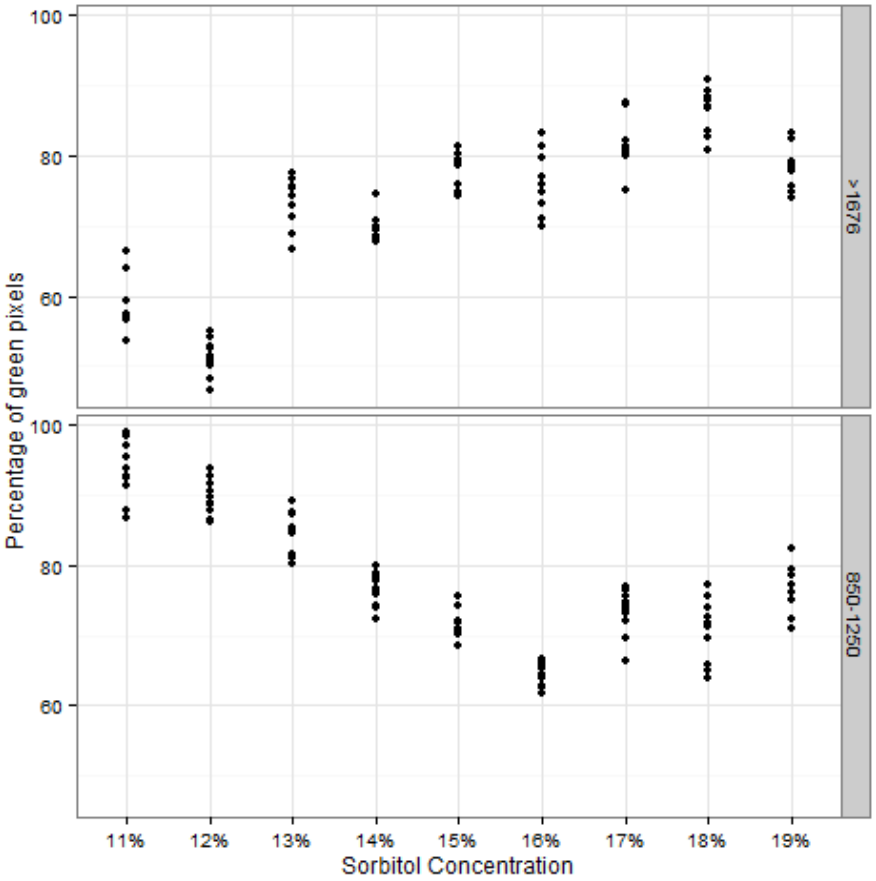

Figure 2-18: The percentage of green pixels recorded in images of TS cores flooded with different percentages of sorbitol solution. Top shows data for cores containing >1676 µm particles, bottom shows data for cores containing 850-1250 µm particles.

The best sorbitol concentration may be due to the cleaning process involved in producing **TS** that is ready for use as a growth medium. Each particle is coated in MS media, and if there is a higher number of particles in the core, such as is the case for the 850-1250 µm size range,

there are more layers of MS media for the light to penetrate. Collectively, this may result in a change in the refractive index of the **TS**, which the sorbitol concentration then has to account for. Therefore, it can be concluded that the particle size range, the size of the sample and the type of media used may have an effect on the RI of **TS** and therefore should be tested before each experiment where a new setup for the **TS** system is being applied. Following the results of E.vi, a sorbitol concentration of 16% was used for cores containing the 850-1250 µm **TS** particle size range in E.vii.

2.4.2.3 Flatbed Imaging

After 3-D imaging, all seedlings were extracted from the soil/**TS** cores, washed with water and placed in a petri dish lid containing water and a scale bar for calibration purposes. The water in the petri dish allowed the roots to spread out from one another, so that they could be easily isolated from each other during image analysis. The scale bar was a strip of transparent tape with mm and cm markings stuck to the petri dish lid so that a manual calibration of the resolution could be done using Fiji (Schindelin et al., 2012). The seedlings were scanned using the Epson flatbed scanner (Epson Expression 10000XL) at the James Hutton Institute, set to professional mode and a resolution of 1200 dpi which was high enough to detect root hairs. Colour scans were taken and saved in .tiff format. Seedlings were then removed from the petri dish lid and stored in specimen pots (http://www.medfor.co.uk/product/707/110/clear-ps-jar-with-white-pe-screw-cap/709bbca2f05a03b04aadf9542e0d975b), in 50% ethanol.

2.4.3 Image analysis

This section describes the protocols that were developed for analysing images of barley roots obtained using µCT, OPT and flatbed scanning. Protocols that were developed for analysing soil and **TS** structure from 3-D µCT images are also detailed below.

2.4.3.1 µCT image analysis of roots

Images of cores that were taken in the HMX 225 X-ray µCT scanner and reconstructed using the computer software CT Pro v2.0 were then imported into VG StudioMax2.2 (Volume Graphics, 2013) in 16-bit unsigned format so that the images were small enough for the computer to handle but were still detailed enough for analysis.

2.4.3.1.1 Image processing, segmentation and skeletonisation

During importation of the images into VGStudioMax2.2 the handles of the histogram were adjusted so that images were between -0.010591 and 0.076726. This removed noise and reduced the complexity of the image. It also enhanced the contrast of the images so that different components within the core were clearly distinct from one another. Once imported into VG StudioMax, the core was shown as stacks of images in the x, y and z planes in different windows, alongside a window containing the 3-D reconstruction (Figure 2-11)

The region grower tool available in VG StudioMax was used to segment the seedling from the soil/**TS** volume. Region grower is a semi-automated tool which allows the researcher to manually choose a starting point pertaining to the region of interest (ROI), from which it detects and extracts all other voxels that are connected to that initial point and within a calculated, specific range of greyscale values. The seed was located and selected as an initial starting point for the ROI and the region grower tool detected voxels that were connected to that point and within an acceptable range of greyscale values, resulting in the seed and roots being included within the ROI (Figure 2-11). The tolerance level of the region grower affects how likely a connected voxel of different greyscale values is to be included in the ROI, so a low tolerance value (e.g. 100) will include only the voxels that are close to the initial starting point and of a very similar greyscale value. A high tolerance value (e.g. 20000) will include

more voxels that are further away from the starting point as well as greyscale values that are different from the initial seed point. Therefore the tolerance level of the region grower had to be selected carefully during root segmentation as it was important to include the entire root system without including areas close by such as pores and particles. For soil scans the tolerance level was set to 500-600 in order to segment the seedling from the surrounding volume. For **TS** scans, a tolerance level of 650-750 was used. The tolerance levels were different for soil and **TS** because the range of greyscale values within the images were different due to their different attenuation values.

It was often necessary to add sections to the ROI detected by the region grower because it didn't detect all of the root system from the initial point. This was done by choosing additional points on the root system close to the ROI boundary, running the region grower again and adding the new ROI to the previous one so that the entire root system was gradually included. Once the entire root system had been incorporated into the ROI, any obvious outliers (e.g. pores or particles next to the root system) were manually removed by highlighting that specific region of the ROI, setting the tolerance level in the region grower to 50000 and then subtracting it from the ROI. The erode/dilate function in VGStudioMax was then used to open the root system by a voxel radius of +2 in order to remove holes in the ROI and then close it by a voxel radius of -1 in order to remove any remaining small outliers. The segmented seedling was then dilated by a voxel radius of +1.

All voxels within the ROI were changed to opaque and all voxels outside the ROI were changed to transparent, so that the root system appeared white and the soil volume, core and other background components appeared completely black. The z plane stack was then exported as .bmp images.

The binary .bmp stacks were imported into Fiji (Schindelin et al., 2012) and the process>binary>fill holes function was applied to the stack, so that all holes were removed. The process>binary>skeletonise function was then applied to the images so that the roots were skeletonised. The fill holes and skeletonise functions were applied a second time, to make sure that the root system was completely skeletonised. This process is depicted in Figure 2-19.

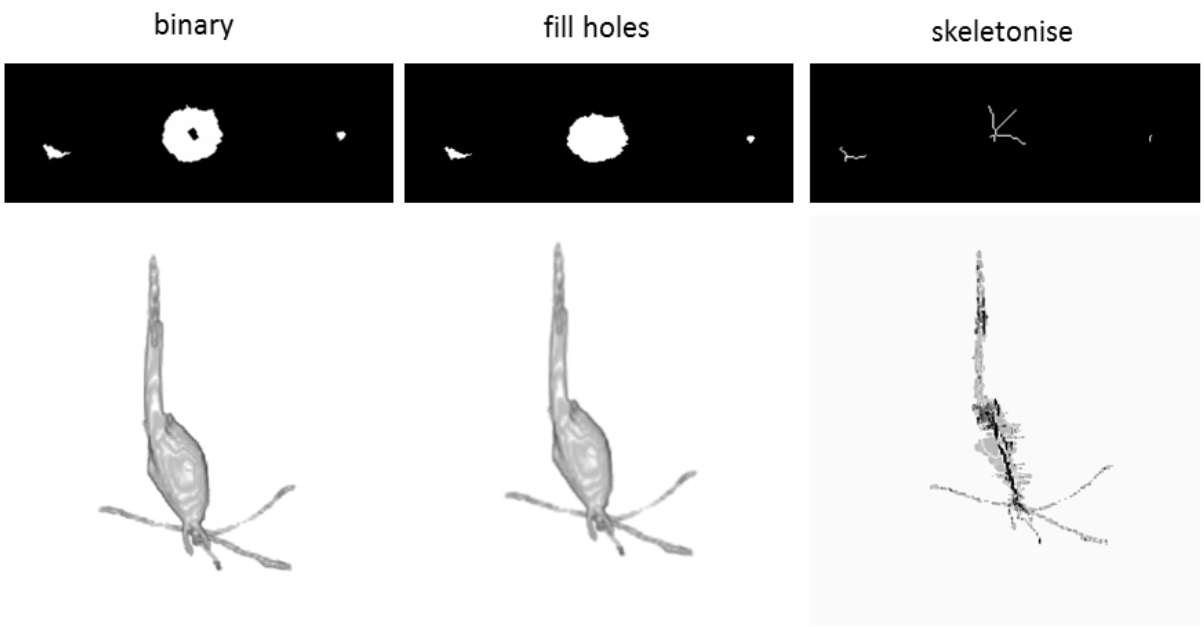

Figure 2-19: Example images depicting the image processing method. Top row shows the same image mid-way through the z-stack, as binary image (left), after filling holes (centre) and after skeletonising (right). Bottom row shows the reconstructed 3-D images of the same stack after these processes have been applied to the images in the z-stack (resolution, 41µm).

2.4.3.1.2 Aligning stacks taken during a time series

During E.v (Chapter 4), a µCT scan was taken of each core at 24 hour intervals. This produced 5 separate 3-D images of the same core. In order for the growth of individual roots to be measured correctly, they each had to be identified, assigned an ID and then the next 3-D image taken 24 hours later had to be aligned correctly so that the same I.D.s were assigned to the same roots. This was performed after the image processing stage in VGStudioMax 2.2. Greyscale z-stacks of the core showing the particles, pores and seedling were exported in

.bmp format as well as the binary images, described in section 2.4.3.1.1. They were then imported into Fiji (Schindelin et al., 2012) and the first image taken at 0 hours was used as the baseline to which all subsequent images were aligned. The second stack was compared to the first and aligned using a particle at the edge of the core that was easily identifiable.

The Plugins>Transform>TransformJ>TransformJ Rotate function was opened and the z-angle (degrees) was adjusted appropriately until the images appeared to be aligned. The process was then repeated with the z-stack's corresponding binary image, so that the binary images could also be aligned correctly. The roots were then assigned individual I.D.s and the protocol described in section 2.4.3.1.1 was then applied in order to achieve skeletonisation of the root systems. An example of the unaligned greyscale images, aligned greyscale images and corresponding binary images are shown in Figure 2-20.

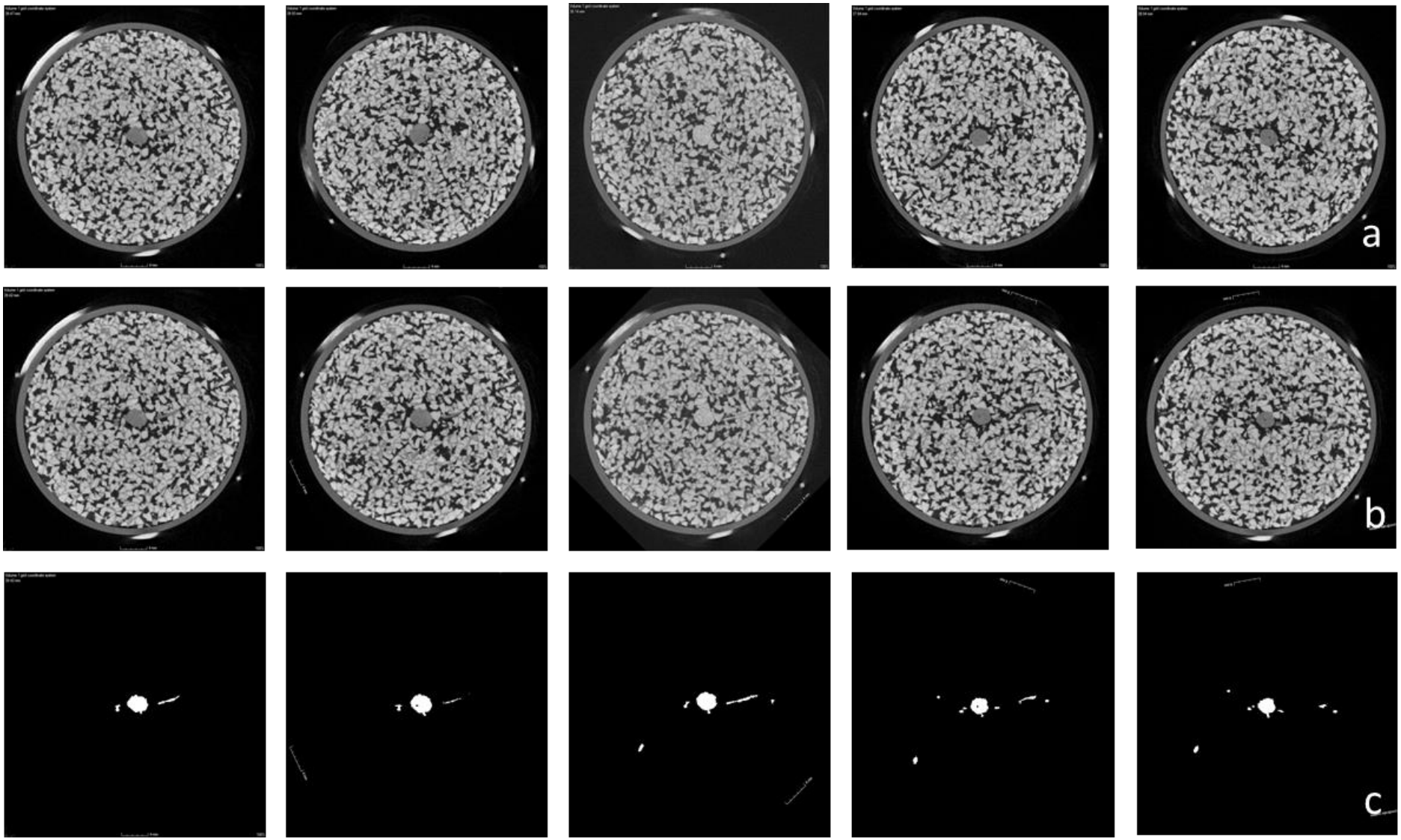

Figure 2-20: Examples of the same image in a stack not aligned at the different time points (row a), aligned at the different time points (row b) and the aligned segmented images (row c). Resolution, 51 µm.

2.4.3.1.3 Image analysis

After µCT images of the seedlings were processed by segmentation and skeletonisation, the point at which the first root began to diverge from the seed was identified in the stack and this x,y,z co-ordinate was chosen as the first one from which all the roots were measured. Each root was measured individually, but the single coordinate was used as the starting point or seed point for each root. To achieve this the seed point was selected using Ctrl+T in Fiji (Schindelin et al., 2012) which recorded the co-ordinate in the ROI manager. The next point in the sequences was selected by scrolling 10 slices (0.27 mm – 0.51 mm, depending on the image resolution) down in the skeletonised z-stack, locating the same root and choosing a central pixel. Ctrl+T recorded this x,y,z co-ordinate again and this process was repeated until the tip of the root was reached and a list of x,y,z co-ordinates was present in the ROI manager which was saved as a .txt file. Each root was measured in exactly the same way returning to the seed point at the start of each root to produce an individual .txt file containing the co-ordinates of each. The .txt lists were entered into a custom-written Python file (Appendix B). This file was run in Python version 2.7.3. and returned an image showing the root system with each root represented in a different colour (Figure 2-21).

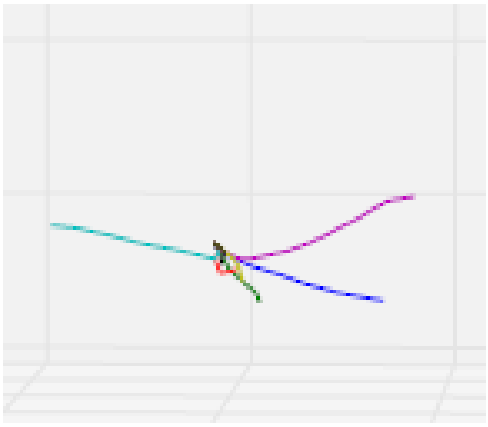

Figure 2-21: The image output from the custom-written Python file after entering the co-ordinates of the root system belonging to the same seedling shown in Figure 2.17. Individual roots are represented in different colours.

The output includes the length of each root, as well as its verticality and curvature measurements at each co-ordinate along the list for each root. Curvature was obtained by fitting a circle to each co-ordinate and calculating the radius of that circle. Curvature is then defined as:

$$curvature = \frac{1}{radius}$$

Verticality was calculated by obtaining the angle between the vertical vector (0°) and the line between two consecutive co-ordinates. Figure 2-22 shows visual representations of curvature and verticality measurements.

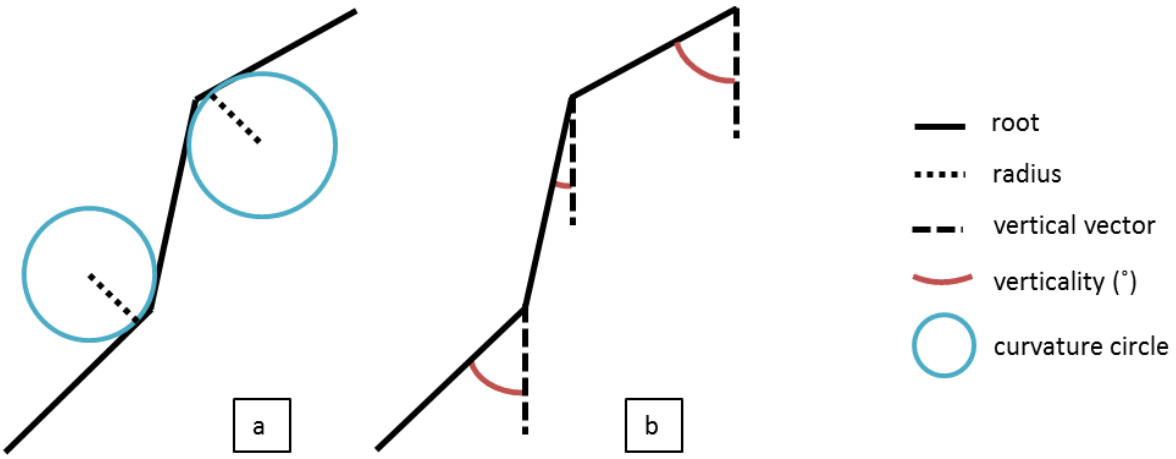

Figure 2-22: Visual representations of how the custom written Python programme measures curvature (a) and verticality (b)

Convex hull and root system width measurements were calculated automatically by importing the .bmp z-stack of segmented binary images (before skeletonisation) into the Tools>Measurement function of the computer programme RooTrak (Mairhofer et al., 2012) and entering the resolution of the images manually. Figure 2-23 shows examples of convex hull and root system width measurements. The convex hull volume is measured by identifying the outermost points of the sample in question and creating a box whose boundaries are defined by these points. The root system width is the measurement between the two outer-most points of the sample.

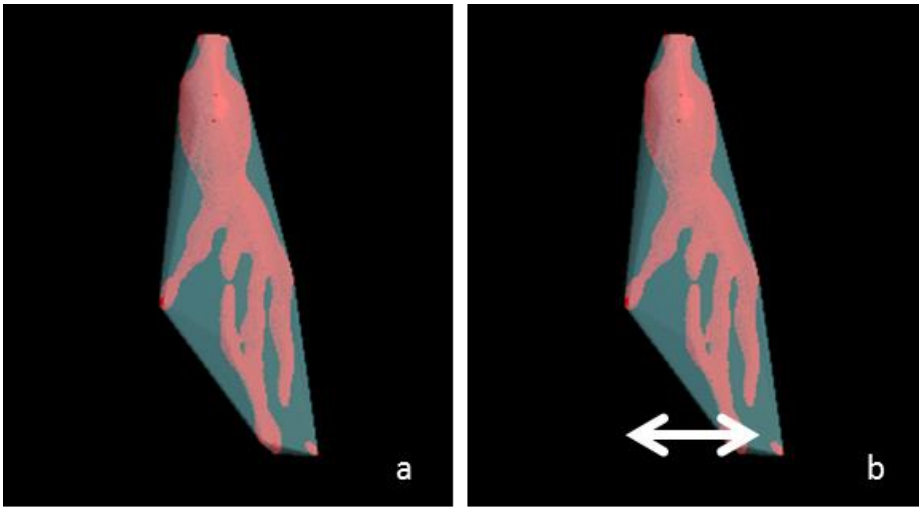

Figure 2-23: Examples of convex hull volume (a) of a seedling and root system width (b, white arrow) of the same seedling as measured by RooTrak (Mairhofer et al., 2012). Resolution, 41µm.

In summary, the process of analysing µCT images of roots for this project involved the following steps; reconstruction, segmentation, skeletonisation, extraction of co-ordinates and data entry into the Python programme. This work flow is visualised in Figure 2-24.

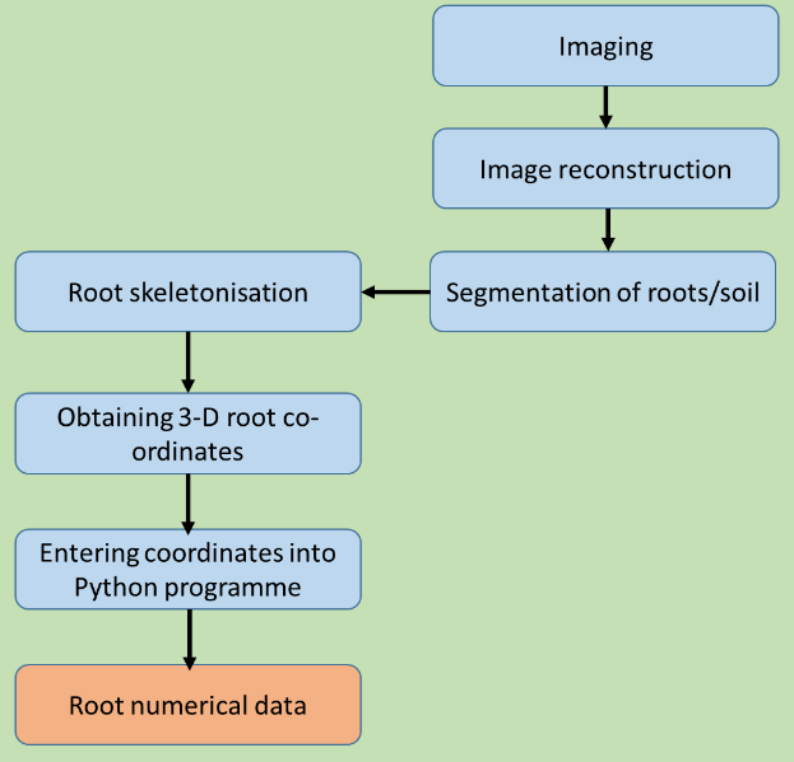

Figure 2-24: Workflow involved in analysing 3-D images of roots

2.4.3.1.4 Statistical analysis

All statistical analysis was carried out in Genstat 16th edition (Payne et al., 2011) and RStudio (RStudio RStudio Team, 2015). Figures were made using the ggplot2 package in RStudio (Wickham, 2009) and Microsoft Excel (2010).

Three types of measurements were taken from the 3-D µCT images of roots; individual root co-ordinate measurements (e.g. curvature and verticality), individual root measurements (e.g. length, average curvature of a root, total curvature of a root, average verticality of a root) and root system measurements (e.g. convex hull volume, root system width, average

length of roots in a seedling, average curvature of roots in a seedling, average verticality of roots in a seedling).

Summary statistics of all variables were carried out using the statistical programming software, RStudio. After initial inspection of the raw data, subsets were created in order to gain a deeper understanding of the data when separated according to the factors being tested. The exact subsets made for each dataset are specified in the associated chapters. The Shapiro-Wilk test (Royston, 1982) available in the stats package of RStudio was performed on each variable in all data sets in order to determine whether the data followed a normal distribution or whether transformation was required. A p-value of <0.05 was used as the threshold at which the dataset was judged to require transformation. A Box-Cox test (Box and Cox, 1964) was carried out using the MASS package in R Studio for all data requiring transformation, in order to determine the log value necessary to transform each variable. If the λ value resulting from the Box-Cox test was a decimal number, the value was rounded up or down to the nearest integer for the purposes of log transformation.

To test for differences between roots grown in different growth mediums, Restricted Maximum Likelihood (REML) tests were carried out on datasets using Genstat 16th edition (Payne et al., 2011). REML analysis allowed the inclusion of fixed effects (treatments being applied) and random effects such as the root I.D., seedling I.D. and the rep number into the model, therefore allowing roots and root co-ordinates to be treated as individual n-values. p-values of <0.05 were judged to be statistically significant.

For whole root system measurements, such as convex hull volume and root system width, ANOVA tests were carried out in Genstat 16th Edition, taking into account random effects from the treatments being applied to the samples. p-values of <0.05 were judged to be significant.

2.4.3.2 µCT image analysis of soil

Image analysis of soil using µCT is challenging due to its water content and organic matter. Roots are also mostly water, so their attenuation values are very similar. Various analysis methods for µCT images of soil exist (Baveye et al., 2010); analysis of **TS** using µCT has never been done before, so it was important that the method was developed carefully. **TS** has an advantage over soil in that the particles, pores and water are clearly distinct from one another in µCT images, whereas it is more difficult to separate them from one another in natural soil samples (Figure 2-25). The method for analysing **TS** structure evolved over the duration of the project between experiments and this process is outlined in the following section.

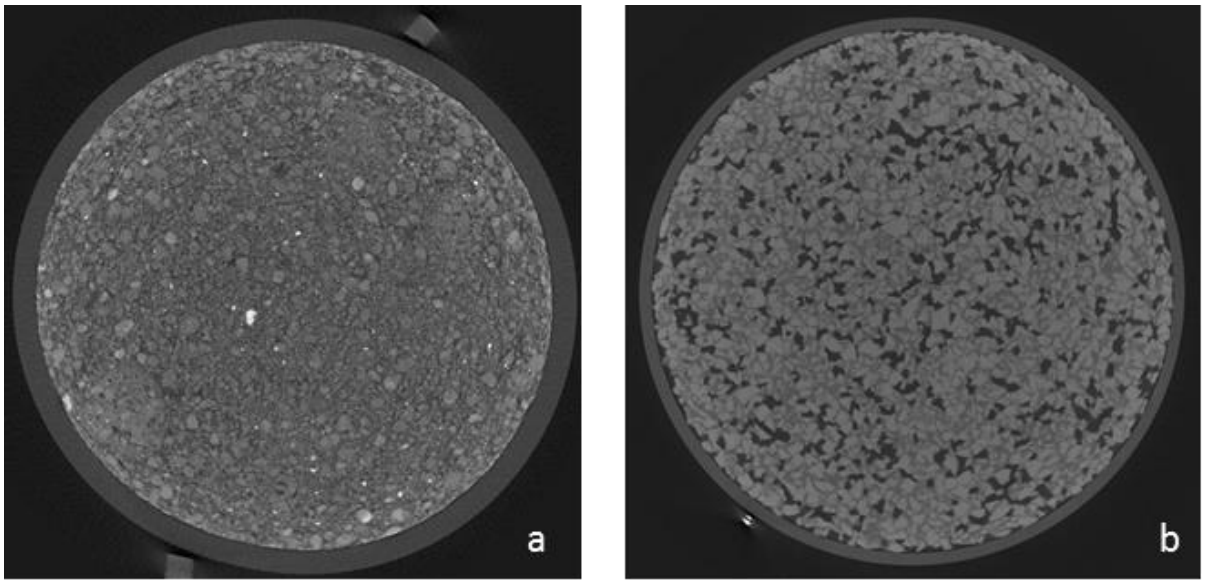

Figure 2-25: Cross-sectional µCT images of soil cores. Image a is a core filled with soil, image b is a core filled with TS. Resolution, 29µm.

2.4.3.2.1 Image processing and analysis

For each experiment it was possible to apply the same protocol to all images, with minor parameter changes being necessary due to slightly different numbers of greyscale values between cores. Pixel and voxel (3-D equivalent of pixel) colours are derived from greyscale values which are between 0 (black) and 255 (white). A range of greyscale values exist between

these two extremes and the numbers of pixels of particular greyscale values in an image is found by producing a histogram. Histograms are useful because the attenuation levels, and therefore the greyscale values can differ between different components within the object being imaged. Therefore, each peak in a histogram can potentially represent a specific component of a sample and these components can be easily separated from one another using thresholding techniques. Greyscale value peaks of pixels are relatively well defined in **TS** volumes, with particles, water and air being distinguishable from one another, as opposed to soil volumes whereby the peaks are often not distinct, making particle, water and air difficult to separate from one another (Figure 2-26).

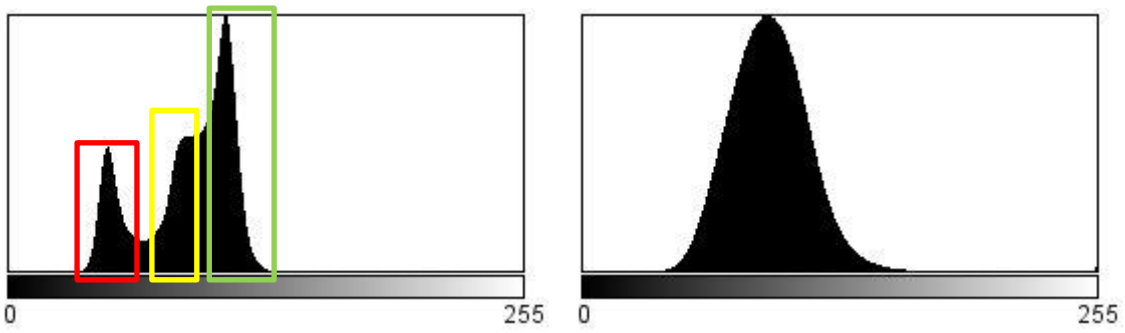

Figure 2-26: Example soil and TS ROI histograms of images obtained using X-ray µCT. The TS volume histogram (left) has discernible peaks, the red representing air-filled pores, the yellow representing water and the green representing particles. The soil volume histogram (right) has no clear peaks, making it difficult to estimate values for air, water and particles.

For E.i, images were imported into VG StudioMax2.2 in 16-bit unsigned format and a median filter of 3 voxels was applied to both soil and **TS** volumes in order to remove noise from the images, whilst retaining the edges of the individual particles. A clearly visible soil or **TS** particle was then selected manually and the region grower tool was used to detect the rest of the soil volume, with the tolerance level set to 4000-8000 for soil and 3000 for **TS**. Whilst this seemed to separate particles from their surroundings reasonably well and produced strong data for root/soil contact analysis (Section 3.5.2), the method was not standardised or repeatable enough to be used for accurate analysis of particle/water/air content. E.iv later showed that

differences did occur between treatments and therefore, the distribution of particles/water and air within **TS** cores had to be researched in greater detail. This led to further development of the method for the split pot experiment (Chapter 4).

For E.v, the greyscale z-stacks of the reconstructions carried out in VG StudioMax2.2 were exported as a series of .bmp files. The distribution of particles, air and water was analysed by importing the .bmp z-stacks into Fiji (Schindelin et al., 2012) and then extracting a series of cubes of 5.1 mm^3 at adjacent depths down the **TS** profile. The Autocontrast tool in Fiji (Schindelin et al., 2012) was used to enhance the contrast between particles and pores, after which a median filter of 2 pixels was applied throughout the image stack. The number of black pixels resulting from the Li thresholding method was used to obtain the volume of air-filled pores throughout each stack. The number of white pixels resulting from the Intermodes thresholding method provided the volume of particles in each stack. These auto thresholding systems were chosen based on visual assessment of the resulting segmented images after applying them, and were deemed by the author to be the most appropriate for segmenting air, particles and water in TS. The particle and pore volumes were subtracted from the total cube volume in order to obtain a value for the water content. For the soil strength experiment (Chapter 5), an even simpler way of thresholding the **TS** images was found. The reconstruction was imported into VGStudioMax 2.2 as described earlier. A median filter of 3 voxels was applied and then global thresholds were performed in VGStudioMax 2.2. The values 0 – 25000 segmented air from the images, 25000 – 32000 segmented the water and 32000-50000 segmented the particles. These three segmented stacks were each saved as separate ROIs. The seedling ROI, which had already been segmented using the method described in section 2.4.3.1, was subtracted from all three soil ROIs so that none of the seedlings were present in

the soil analysis images. The three z-stacks of particles, air and water were all exported as .bmp z-stacks with the ROI in question fully opaque (white) and everything else in the image fully transparent (black).

The TS property measurements total porosity and connectivity were obtained for all µCT images. For total porosity and connectivity analysis during earlier experiments (Chapter 3), greyscale **TS** .bmp z-stacks of were imported into Fiji (Schindelin et al., 2012). A 3-D block, measuring 10.2 mm^3 and devoid of roots was extracted from the volume by manually selecting a region, specifying its dimensions using the Edit>Selection>Specify function and duplicating the stack. The images were thresholded using Indicator Kriging (Houston et al., 2013a). This software used Gaussian Mixture Model/Expectation-Maximization (GMM/EM) thresholding, which "is a binomial mixture method, particularly robust against anomalous features such as population spikes or noise" (private correspondence, Houston, 2013).

Connectivity (the percentage of pores that are connected in a single sample) and porosity (the percentage of the image made up of air spaces) measurements of all **TS** 3-D samples were taken using the thresholded images of particles. (Houston et al., 2013a).

2.4.3.2.2 Root/soil contact analysis

Root/soil contact measurements were carried out on all µCT images using VGStudioMax2.2. The method used was similar to that published by Schmidt et al. (2013), with adjustments made to the parameters due to the different physical nature of **TS** cores when compared with natural soil. Once the root system and **TS** volume had been segmented from one another, the surface determination tool, also available in VGStudioMax2.2 was used. For surface determination the root system ROI was used as the starting contour, the option to remove particles and small voids was selected and the search distance was limited to one voxel. A

new ROI was created using the surface determination and this was subtracted from the **TS** ROI. The **TS** ROI was then dilated by 1 voxel in order to create an overlap between the root system and adjacent **TS** particles. The surface area of the root system and the surface area of the root regions directly in contact with the particles was then recorded in order to calculate root/soil contact as a percentage:

$$\textbf{Root/soil } \boldsymbol{contact} \ (\%) = \frac{Surface\ area\ of\ root\ regions\ in\ contact\ with\ surrounding\ particles\ (mm^2)}{Surface\ area\ of\ roots\ (mm^2)}$$

2.4.3.2.3 Statistical analysis

For all ANOVA and REML tests, a P value of <0.05 was treated as significant. In Chapter 3, differences between soil and **TS** variables such as porosity and connectivity were tested for using ANOVA tests in the statistical programming software, R. The rep number and treatment were treated as variables.

In Chapter 4, **TS** measurements were sorted into data subsets according to the treatment, the day of imaging, and depth along the **TS** profile. Summary statistics were then produced using RStudio. REML analysis was then conducted on the entire dataset using Genstat 16th edition. The rep number, the day of observation and the depth along the **TS** profile were included in the model as random variables. Particle size range was included as a fixed variable. REML analysis was performed on subsets according to the day of imaging with the week and depth along the **TS** profile being included as random variables and the particle size distribution being included as a fixed variable. REML analysis was carried out on the depth subsets, during which the day of observation was included as a random variable and the particle size distribution was included as a fixed variable.

In Chapter 4, **TS** subsets were also created according to the age of the root at the time of imaging, so that the soil measurements could be directly compared with measured root variables. REML analysis was carried out on **TS** variables within these subsets, with rep number and depth being included as random variables and particle size distribution being included as the fixed variable.

In Chapter 5, data were imported into RStudio and summary statistics were carried out on **TS** measurements according to the level of pressure (none, mid and high) that had been applied to the core. REML analysis was performed using Genstat 16th Edition with rep number being treated as a fixed effect and pressure level being treated as a random effect.

To test for relationships between soil and root variables in all experiments, the statistical dependence of the transformed root measurement data and the soil/**TS** data was measured using the Pearson correlation coefficient in the statistical software programme, R. In Chapter 5, the Pearson correlation coefficient was also used to test for a relationship between the pressure applied to TS cores and root measurement data. For correlation tests, a value of > 0.7 or < -0.7 was treated as significant.

2.4.3.3 OPT image analysis of roots

Although OPT images are obtained with light and therefore look very different to µCT images, the basic image analysis technique (reconstruction, segmentation, skeletonisation, extracting co-ordinates and entering them into the custom-written Python programme) that was developed for µCT images could also be applied to OPT images. Figure 2-27 shows a summary of this process for both µCT images and OPT images. The detailed OPT image analysis method is described in the following section.

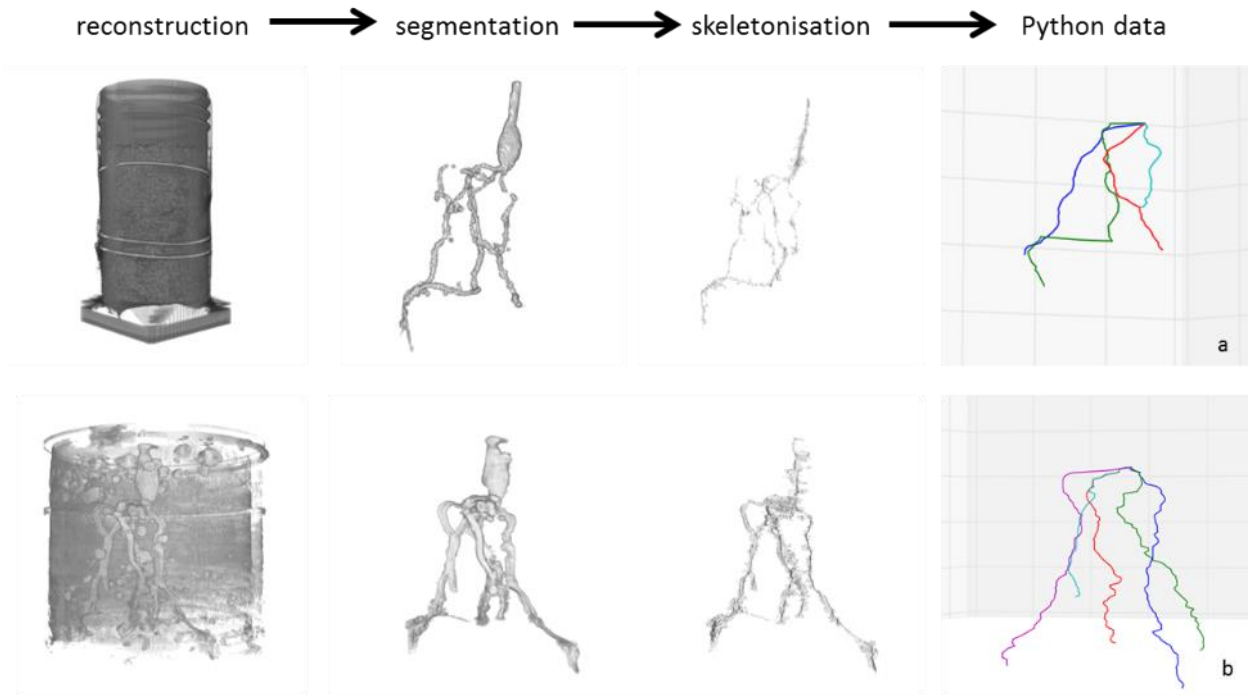

Figure 2-27: The main processes involved in obtaining data from 3-D images of barley root systems. Row a shows data from µCT imaging (resolution, 51µm), row b shows data from OPT imaging (resolution, 41µm).

2.4.3.3.1 Image processing, segmentation and skeletonisation

OPT reconstructions were imported into Fiji (Schindelin et al., 2012) as a z-stack of .bmp images in 8-bit greyscale format. Stacks were cropped in order to remove much of the surrounding volume whilst still retaining all roots. Image contrast was increased automatically using the Image>Adjust>Brightness/Contrast function in Fiji (Schindelin et al., 2012). The image stack was then imported into the 3D Viewer plugin in Fiji with a resampling factor of 5. Regions that were clearly noise (e.g. pot walls, bubbles) were manually selected using

freehand drawings and removed using the right click>Fill Selection option. Filling an area in the 3-D viewer also fills the same area in the z-stack, allowing the precise removal of noise. This method was found to be more successful at removing noise than any automatic thresholding technique or segmentation software, such as RooTrak (Mairhofer et al., 2012) that were tested.

Skeletonisation was performed in the same way as previously described in Section 2.4.3.1.1.

2.4.3.3.2 Image analysis

Image analysis of OPT images was performed in the same way as previously described in Section 2.4.3.1.3.

2.4.3.3.3 Statistical analysis

Statistical analysis of roots obtained from OPT images was performed in the same way as previously described in Section 2.4.3.1.4.

2.4.3.4 Flatbed image analysis of roots

Flatbed images were taken of all seedlings after 3-D imaging had been performed so that a 2-D, photographic comparison was available. The method is described below in greater detail.

2.4.3.4.1 Image analysis

Images were imported into Fiji (Schindelin et al., 2012), and the scale was set manually by drawing a straight line 10 mm long on the scale bar present in the image and setting the known distance as 10 mm in the Analyse>Set scale function in Fiji. The number of roots was recorded, and a polygonal line was drawn along the axis of each root (Figure 2-28). The Analyse>Measure function in Fiji was then used to measure the exact length of the polygonal line.

Figure 2-28: An example of a flatbed image with a scale bar on the left and a polygonal line manually drawn over one of the roots

2.4.3.4.2 Statistical analysis

Statistical analysis of root lengths obtained from flatbed images was performed in the same way as previously described in Section 2.4.3.1.4.

2.5 Discussion and summaries

Developing the **TS** system for use with barley presented a multitude of challenges, some of which were addressed during this project and some that still require further work. In this section the results of this chapter, according to the aims listed in section 2.2, are presented and discussed in further detail.

2.5.1 Selecting suitable barley cultivars

The first aim of this chapter was to select suitable barley cultivars which could be used to study monocotyledonous root growth. Barley was selected due to its agricultural importance in Scotland and many regions elsewhere in the world (Ullrich, 2010). Contrasting phenotypes were necessary in order to understand whether the differences that have been observed in 2-D systems such as gel plates and filter paper are also applicable in 3-D systems such as **TS**. These differences include measurements such as length and root angle. Verticality (the number of degrees the root deviates from 0°) was used as a measure of the root angle and the method also allowed measurement of curvature, which provides an understanding of the tortuosity of a root's path.

For E.i, data from roots grown on 2-D gel plates was used in order to select the barley cultivars, B83 and Troon (Valentine et al., 2012a). It was concluded that B83 was unsuitable for observing in **TS**, due to its very short root length after 96 hours of growth (Section 3.5.1). The roots were too short to gain an accurate understanding of curvature and verticality. Furthermore the B83 roots were already short in **TS** without any additional stress, such as undesirable pore space or increased soil strength. Troon in contrast grew well in the **TS** medium and so it was important to find a cultivar that grew to similar lengths as Troon within

a short period of time so that information about the behaviour of roots, not just their lengths, could be acquired easily.

E.ii was again based on data from Valentine et al., which indicated that there were cultivars that grew to a similar length as Troon on gel plates but showed differences in their root angles (Valentine et al., 2012a). Several varieties were selected and tested during this experiment, which involved taking 2-D images of extracted roots following the growth period of 3 days. 3-D images could have been captured, however this would have been more time-consuming and the information may have been unnecessary. It was already known that these varieties behaved differently in a 2-D growth medium; it was merely necessary to ascertain whether they grew to the same lengths as Troon in a 3-D growth medium. The Westminster variety that was chosen grew to similar lengths as Troon inside soil, whilst showing different root angles in the 2-D gel plates. This variety grew well inside the **TS** and had a high germination rate.

2.5.2 Developing the TS system for use with barley roots

There are multiple advantages and limitations to the TS system. Some of the advantages are:

- It offers the transparency of agar whilst being a porous system, thus reducing possible anoxic effects;
- It makes 3-D imaging of roots in a porous medium using relatively inexpensive equipment possible;
- Different nutrient media can be loaded onto the particles allowing nutrient manipulation;
- Particles can be dyed for use with fluorescent imaging techniques;

- The processing method allows **TS** particles to be recycled repeatedly. The processing method also removes fluorescent dyes from particles if it has been applied.

Limitations of **TS** as a growth medium include:

- Difficulties in removing air bubbles between particles once they have been submerged in an optically-matching solution;
- The current optically-matching solutions not being conducive to plant growth. Sorbitol induces an osmotic shock to roots (Bustos et al., 2008) and Percoll, another optically-matching solution, induces a pH shock;
- Time-lapse experiments are currently not possible using a light-based imaging technique as roots cannot be saturated in either optically-matching solution for extended periods of time without negative effects on root-growth being observed.

Despite the challenges associated with **TS**, it can be concluded that the advantages of the technique outweigh the limitations and is therefore suitable for answering specific questions pertaining to plant growth. Therefore, it was developed further from the original Downie et al. (2012) paper in order to be used on large monocotyledonous barley roots as well as small dicotyledonous roots.

In the original protocol for processing **TS** for use as a growth medium, the titration process involved taking the particle stock, which had already been washed and soaked in a number of different chemicals, and shaking it in MS media for 30 minutes at 30°C, replacing the nutrient solution and then shaking it again. This step was followed until the **TS** reached a neutral pH (Downie et al., 2012). Whilst this method may have been appropriate for processing very small quantities of TS (20 - 50 mL in 2 – 3 hours), it was found to be too time-consuming when

working with larger volumes of TS (> 400 mL in 2 weeks). Therefore, it was necessary to find a quicker way of completing the titration process very early on in the project. This was achieved using the column method described in section 2.4.1.2.2. Using a column set-up reduced the time needed for titrating large quantities of **TS** from 4 - 5 days to 1 – 2 hours and could be done on the bench at room temperature. Another advantage of this method is that the flow of the media through the column can be adjusted by the researcher, as the amount of time that the particles are submerged in the media does not matter. What is most important is that the full quantity of 20 x the **TS** volume flows through the particles. It should be kept in mind that the particles should not be submerged in nutrient solution any longer than 24 hours at room temperature, as the possibility of contamination may increase. However, as long as the particles have had the full volume of fresh media run through them within 24 hours and are rinsed and autoclaved immediately afterwards, contamination should not occur. It should also be noted that equipment must be cleaned thoroughly as soon as the particles are removed from the set-up in order to avoid contamination of the beakers, column and tubing.

Another significant development in the **TS** protocol concerns the amount of time that **TS** particles must be saturated in media when it is being used and recycled intensively. During an experiment that observed root growth in different particle size ranges of **TS** (Chapter 3), a decline in the average root length was observed each week, regardless of the particle size range being used (Figure 2-29). Initially, it was difficult to say why this may be the case. Up until that point, **TS** had been used and recycled without these effects being observed, however this was the first time that **TS** had been used and recycled within the time frame of one week repeatedly for 5 weeks.

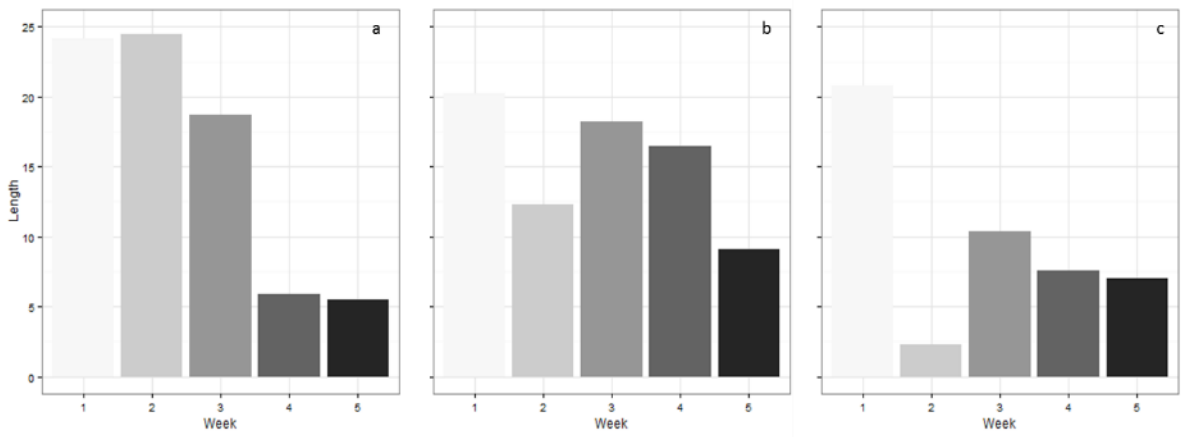

Figure 2-29: The average decrease in root length over time each week for each TS particle size range. Figure a is of the small (850 – 1250 µm) range, figure b is of the medium (1250 – 1676 µm) range, figure c is of the large (>1676 µm) range.

One possible explanation for this phenomenon could be gradual nutrient depletion over time, however in the experiment described above, particles were treated the same way each week, being given at least 24 hours of saturation time inside MS media. 24 hours of particle saturation inside MS media is adequate for particles that have never been used before, so there is no reason to suspect that nutrient availability was a problem in this experiment. Water availability was also not a problem, due to the particles being saturated in MS media that had been made up using distilled water. The most plausible explanation for the pattern observed is that Nafion particles contain a network of micropores, which are known to swell and decrease with the addition/removal of liquids (Divisek et al., 1998). It is possible that during **TS** processing, some of the acid used to clean the **TS** remained within the swollen micropores. Without adequate resting time in media between repeats, the acid content of the particles could increase over time and leach out of the particles during the incubation time, thus causing a pH shock to roots and inhibiting root elongation (Marschner, 1991).

It was found that by increasing the amount of time that the particles were saturated in MS media, this effect could be removed. Following the information obtained from this experiment, **TS** particles were titrated in MS media, rinsed thoroughly with distilled H_2O and then saturated and autoclaved in ½ strength MS media for one week before being used for sowing. The **TS** particles were stored in ½ MS media, as this reduced gradual discolouration to the particles over time. A decrease in length between repeats was no longer seen after this change in the protocol was made.

2.5.3 Developing the OPT system for use with barley roots

Scaling up the OPT system to take adequate images of large barley seedling root system samples was a particularly challenging aspect of this project. This was partly because of the increased size of the samples and partly due to the number of parameters that were manually controlled by the OPT set-up. Image quality could be affected by the slightest displacement of the camera, incorrect focussing, or a slightly incorrect sorbitol concentration, so all parameters had to be adjusted over the course of the project and carefully controlled once the correct settings had been found. The same problems were not experienced during use of the µCT scanner, as once the correct settings had been established, the same parameters could be controlled with each scan just by loading a saved profile into the computer that ran the machine. Manual control over a machinery set-up such as the OPT can be beneficial to an individual who has extensive experience in using it, however this took time to acquire and therefore, some of the initial images taken during the beginning of the project were not as high quality as those that were taken at the end of the project once all of the parameters had been optimised and standardised. Nevertheless, the images that were acquired were all useful in developing the method further and many were suitable for analysis. The various

advantages and disadvantages of the different imaging techniques used during this project are described in greater detail during the following section.

2.5.3.1 Advantages and disadvantages of 3-D imaging techniques

The advantages and limitations of µCT imaging for better understanding roots and soil have been thoroughly addressed in the literature due to the method having been available to researchers for approximately 35 years (Flavel et al., 2012, Gregory et al., 2003, Anderson and Hopmans, 1994). The advantages that are often listed are the high resolution of <0.5 µm possible with µCT imaging (Tracy et al., 2010), the ability to take non-invasive time-lapse images (Dhondt et al., 2010), the detailed analysis of soil samples (Taina et al., 2008) and the measurement of root/soil interactions, such as physical contact (Schmidt et al., 2012). Perhaps one of the greatest advantages of µCT imaging is the potential to use it for phenotyping roots in natural soil in ever-increasing detail (Zhu et al., 2011), thus increasing our knowledge of how different plant cultivars are affected by the physical processes acting upon them.

One major disadvantage of µCT which is often overlooked in the literature is the amount it costs in both time and money to acquire images (Zhu et al., 2011). µCT scanners can cost anywhere between £65,000 and £650,000 depending on the model and accompanying analysis software that is bought with it (Ache, 2015). The amount of time necessary to train someone in using a µCT scanner is also an important consideration. It is often the case that researchers who want µCT scans but do not have on-site facilities are forced to outsource these services to other institutions.

Another disadvantage of µCT imaging is the current limitations on sample size in order to acquire images at the high resolutions necessary for observing roots inside soil (Helliwell et

al., 2013). Local tomography, which involves imaging a sub-region of a large core at extremely high resolution offers a possible solution to this problem (Carminati et al., 2009). This may be a suitable method for understanding activities at the root tip, however would be an inappropriate method for observing root exploration throughout a soil volume over time. Imaging small samples is highly time-consuming, with fewer than 10 scans per day usually being possible, making it difficult to perform high-throughput imaging and replicated experiments of root/soil interactions using µCT (Gregory et al., 2009). This time-frame is improving with times of as little as 4 minutes and 10 seconds per scan of resolution 68.23 µm voxel size for 30 x 26 mm sample sizes being described in the literature (Flavel et al., 2012).

Another possible disadvantage is the effect of repeated X-ray exposure on plant roots during time-lapse experiments, the effects of which are currently undetermined (Mooney et al., 2012). This has been questioned in the literature by several researchers, with the general consensus being that in optimised µCT systems the radiation doses are not high enough to have a significant effect on root growth (Flavel et al., 2012, Gregory et al., 2009, Jenneson et al., 2003). However this may depend on the frequency of exposure and the age of the plant when imaging takes place.

Although constructing an OPT set-up is also expensive, it is not as expensive as a µCT scanner. To buy all of the equipment necessary, the full cost would be approximately £35,000, which would include 1200 g of transparent soil. The set-up could be constructed at even cheaper cost if components such as the microscope and light box were bought second-hand. Theoretically, the same set up for observing root system architecture could be achieved with a good quality camera, a light box and a rotating base for the sample to be positioned on. Perhaps the greatest difficulty would be the knowledge and expertise necessary to build the

equipment and write the computer software necessary to control the different imaging parameters and reconstruct the images.

Another benefit is the very high resolutions that can be achieved using OPT and the potential to use fluorescence technology, as long as the correct microscope with filters is present on the OPT set-up. These advantages were outlined in by Downie et al. (2012), whereby they observed GFP labelled E.coli cells and colonies on the surface of lettuce roots. This was done using confocal laser scanning microscopy (CLSM), however could be theoretically done using OPT as well, as fluorescence can be used and high resolutions are possible. Further development of fluorescent barley lines will enable researchers to use fluorescence as an additional segmentation tool, thus improving downstream processing of 3-D images in **TS** and enhancing our understanding of how monocotyledonous root systems explore soil.

A great difficulty with the OPT imaging technique and **TS** is the requirement to saturate **TS** in an optically matching solution in order to take images. Whilst this works well on very small samples, it is more difficult to achieve **TS** volumes free of air bubbles when the samples are larger. The air bubbles cause difficulties because they block the path of light to the root, reducing the image quality. This is partly negated by the fact that the sample rotates 360° during imaging, so if the root is blocked by an air bubble at one angle, it can be viewed from another angle. At very small particle sizes (<500 µm), the density of air bubbles is too great and the roots can no longer be imaged to a high enough quality. This is an area in which **TS** should be developed further through experimentation.

The OPT and **TS** set-up also needs further development so that time-lapse work can be carried out. Currently, this is not possible due to the problems associated with exposing roots to sorbitol or Percoll. Also, even if the optically matching solutions were suitable for plant growth

and the roots could be saturated permanently, the risk of hypoxia would still be a problem. The ideal scenario would be to construct a system that can be saturated and drained easily, so that roots could grow freely through air and water-filled pores and then be saturated in an optically-matching solution that is conducive to plant growth just for the duration of imaging, which takes approximately 4 minutes.

Perhaps the greatest advantage of all 3-D imaging techniques is the ability to take extremely detailed images that act as a permanent record of the sample at that particular time. This allows the researcher to go back and analyse the data in greater detail as image analysis techniques are developed (Rahman et al., 2009). Furthermore, imaging allows researchers to share information and communicate their findings in a visual manner, thus enabling them to demonstrate exactly what is happening to samples as they are undergoing various treatments. This is an important, often overlooked benefit of using imaging techniques in scientific fields, which is applicable to all imaging techniques.

2.5.4 Developing a standardised image analysis method for different techniques

Developing image analysis techniques for 3-D root/soil images is always challenging due to the similar attenuation values of roots and surrounding soil often resulting in overlap during segmentation (Mooney et al., 2012) . So far there has been no common consensus on the best method to use, however multiple researchers have called for rigorous methods to be developed in order to reduce subjectivity during image analysis of roots and soils and allow cross-comparison of different studies (Helliwell et al., 2013, Baveye et al., 2010). The problem with this is that the image analysis technique often needs to be developed based on the type of scanner and software being used, the type of soil and plant being tested and the types of

questions that the researcher is attempting to answer. The basic image analysis protocol (Section 2.4.3.1) that was developed early on during this project may be suitable for standardising root length, convex hull and root system width measurements; however the specific parameters used may only be suitable for barley roots in **TS** cores.

2.5.4.1 Standardising 3-D image analysis techniques

Developing a basic method of segmentation, skeletonisation and extraction of co-ordinates that could be applied to both µCT and OPT images was a great step forward in this project because it allowed image analysis standardisation and the ability to compare between the different imaging techniques. Specific parameters were adjusted as the author gained experience, particularly in using OPT, however the basic method was always the same. The skeletonisation step was particularly important, as it defined a standardised point from which all measurements from the same plant would be taken. This may have resulted in measurements such as root length being slightly over-estimated compared to conventional measurements using 2-D methods, however it avoided taking a subjective decision of where measurements were to begin from.

In all experiments multiple imaging techniques were used which differed slightly in the results that were obtained, however they followed the same patterns, indicating that the differences observed between treatments were real. This is demonstrated in Figure 2-30, which shows the results of root length data from Chapter 5 for the same roots imaged using µCT, OPT and flatbed techniques under three different pressure treatments. Differences between exact values obtained using different imaging methods are unsurpising, however the fact that they all recorded the roots under no pressure as the longest, followed by those under medium pressure, followed by those under high pressure as the shortest is promising.

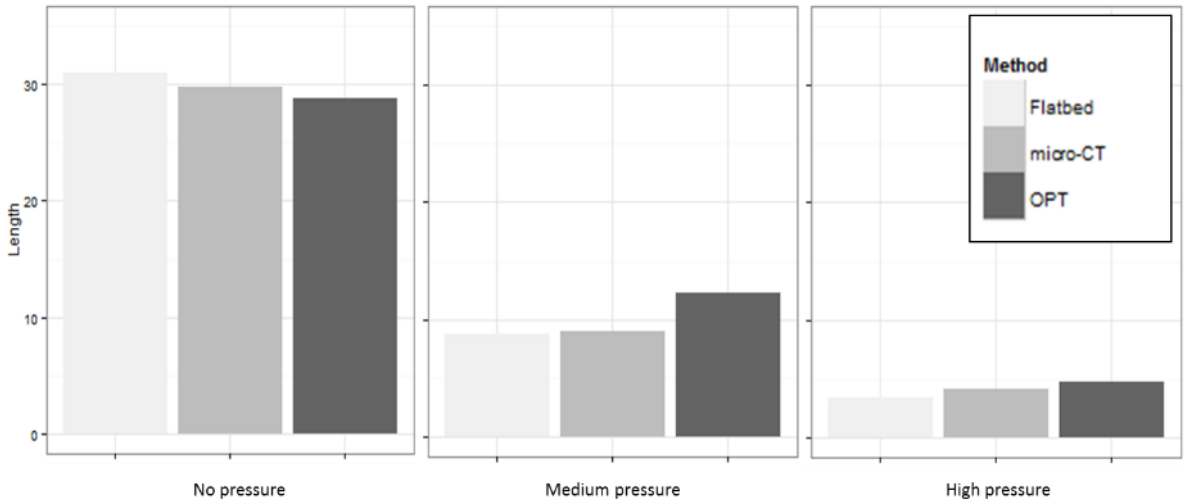

Figure 2-30: Average length of roots under no pressure (left), medium pressure (middle) and high pressure (right) treatments, as recorded using three different imaging techniques.

2.6 Conclusions

This project was successful in selecting suitable barley cultivars for experiments which involved comparing root growth in soil and **TS**, root growth in different particle sizes of **TS**, root growth in split pot treatments over time, and root growth under different pressure treatments. Differences in root growth between Troon and Westminster were not observed in different particle sizes of **TS**, so Westminster became the cultivar which was focused on the most because it had a strong germination rate and grew well in the **TS** medium.

This project was also successful in developing **TS** and OPT for use with barley roots. Scaling up the processing technique by introducing a column system helped to clean **TS** particles quicker, allowing them to be re-used multiple times during experiments. It is important that **TS** is given at least a week to equilibrate in nutrient media before being used for preparing samples. The challenges associated with saturating particles in sorbitol and removing the air bubbles which resulted was extremely difficult and to date, a satisfactory method has still not been developed for removing very small air bubbles in the smallest particle size range (<500 μm) of **TS**.

Developing a diagnostic atlas to identify the causes of different kinds of noise caused by specific OPT imaging parameters was of great benefit to this project as it enabled easier identification of noise so that the correct parameter could be adjusted quickly and the best possible images could be obtained (Figure 2-14). The most important parameters to consider when using **TS** in the OPT set-up is the camera alignment and the sorbitol concentration which must be perfectly matched to the sample in order to achieve the best images. Refractive index matching is recommended every time a new nutrient media is applied to **TS** particles as this

may slightly alter its refractive index. The refractive index can also change with different **TS** particle size ranges, so this must always be tested before using the technique to acquire data.

Developing a standardised image analysis technique was a great leap forward for this project and is recommended for use in future research. The method of segmentation, skeletonisation and extraction of co-ordinates to obtain root measurements of individual roots within the same root system provides a framework for analysing 3-D images of roots in a way that can used by all researchers, thus allowing comparison of different data sets. The use of REML statistical analysis also enabled us to treat individual roots from the same plants as separate n-values.

3 Barley root growth in soil and transparent soil

3.1 Introduction

Root growth can vary considerably between different plants, cultivars and growth mediums. For all roots the immediate point of contact with the external environment occurs between the root apex and epidermis, and the rhizosphere. This interaction causes variations in root growth due to the biological, chemical and physical composition of the rhizosphere and the complex relationship that exists between the rhizosphere and the root system. The physical structure of a root growth medium is particularly important, as this has a strong influence on root growth, which further influences the physical structure of soil in a constant, self-perpetuating cycle (Bronick and Lal, 2004). This is considered in the following chapter, which investigates how root growth of barley root seedlings differs between soil and the recently developed growth medium, transparent soil (**TS**).

3.1.1 Root growth

Root growth is thought to be largely governed by events that occur at the root tip (in particular the root cap) and its relationship with the rhizosphere (Hawes et al., 2002). Most of what is known about the root tip and the way it elongates has been discovered through studies of the model plant organism, *Arabidopsis thaliana*, a dicotyledonous plant which grows rapidly with a single primary root at germination and a simple cellular structure. It has a different structure to barley, a larger monocotyledonous plant with a more complex cellular structure and multiple primary roots which emerge at germination (Hochholdinger and Zimmermann, 2008).

The tissue organisation of root tips is universal and well-documented. These tissues can be split into 5 main sections, each with different functions and cellular organisations. These tissues from most distal to most proximal are shown in Figure 1-3 and are known as the root cap, the meristem, the transition zone, the elongation zone and the maturation zone (Ubeda-Tomás et al., 2012). Mechanisms of root elongation are described in detail in section 1.2.

The root cap protects the meristem, reduces friction, generates the rhizosphere surrounding the root (Hawes et al., 2002), and provides the cells necessary for growth in the elongation zone. The transition zone is where differential cell growth occurs (Baluška et al., 2010), which dictates changes in the direction of root elongation. The elongation zone is where elongation of the cells produced by the meristem occurs (Dolan and Davies, 2004). The maturation zone is where cell differentiation takes place (Ubeda-Tomás et al., 2012).

3.1.2 The relationship between soil structure and root growth

Soil structure has an enormous impact on root growth because plants are sessile, so can only respond directly to the region of soil surrounding the root tip (Esmon et al., 2005). Physical factors such as compaction and bulk density have been heavily researched (Bengough et al., 2005, Tracy et al., 2012), as compaction has long been considered to be of great concern to global agriculture (Batey, 2009). A mild level of compaction increases root/soil contact, so can increase yield in some cereal crops such as wheat and barley (Bouwman and Arts, 2000). If soil compaction is too high, the size of soil pores is reduced, causing mechanical impedance to roots and a decrease in crop yield (Arvidsson and Håkansson, 2014). When a root tip encounters a soil pore under these circumstances, it has to generate cell turgor in order to increase its diameter and internal pressure, overcoming the pressure of the soil particles

surrounding it and allowing it to push them out of the way so that it can enter the pore (Bengough and Mullins, 1990).

The basic effects of compaction on root growth are remarkably consistent between species with a reduced number of roots, reduced elongation rate and a thicker diameter just proximal to the root tip being observed in many plant species, barley included (Bengough et al., 2005, Goodman and Ennos, 1999, Wilson et al., 1977). When mechanical impedance is >2 MPa, it has been commonly observed that root elongation is reduced by approximately 50% (Bengough et al., 2011, Goss, 1977, Wilson et al., 1977). The variety of barley is also known to have an impact on the ability of roots to elongate (Masle, 1992), although there is a paucity of information with regards to what causes some barley varieties to exhibit root elongation traits that are more successful than others.

Water potential is also an important factor dictating root growth, as dryer soils increase soil strength, making it more difficult for roots to penetrate them (Whiteley and Dexter, 1982). Shoot growth generally stops when soil water potential is around -0.8 MPa, whereas root growth can continue until water potentials of -1.6 MPa, which is beneficial to plants who need to halt shoot growth in order to use limited resources to explore the soil environment for water (Sharp, 2002). Water potentials in Scottish agricultural soils can range from -0.01 MPa to -0.2 MPa and those that have more negative water potentials have greater soil strengths, thus limiting the ability of roots to explore them (Bengough et al., 2011).

3.1.3 Root growth in natural soil and TS

There is significant variation in the way that roots grow in different soils, and there is also variation in how roots grow in **TS** when compared with natural soil. The only published description of this is in the original Downie et al. (2012) paper. During the development of **TS**,

they found that *A.thaliana* plants that had been grown in **TS** for two weeks had a long primary root, which was similar to Phytagel-grown roots but much longer than soil or sand-grown roots. Lateral root length and numbers of **TS** roots were similar to soil and sand lateral roots but much higher than Phytagel roots (Downie et al., 2012). Lateral root density was highest in soil, then sand, then **TS**, then Phytagel (Downie et al., 2012). Overall it was found that root growth in **TS** was more similar to that seen in sand, than what was seen in soil or Phytagel. It demonstrated that **TS** is closer to mimicking soil properties than Phytagel and as a growth medium, was more suitable for studying root system architecture than Phytagel (Downie et al., 2012).

Monocotyledonous plants have root systems that grow differently to dicotyledonous plants (Hochholdinger and Zimmermann, 2008) and currently there is no information on root growth of monocotyledonous plants in **TS** and how this compares to growth in natural soil.

3.1.4 Imaging TS samples

TS appears as a mass of translucent particles during plant growth when the pores in **TS** are filled with either nutrient solution or air. At this stage, the roots within cannot be seen. In order to observe the roots, an optically matching solution such as sorbitol or Percoll must be added to the particles (Downie et al., 2012). The refractive index of the solution matches that of the particles, thus allowing light to travel straight through them, straight to the roots. This is shown in Figure 1-2.

The **TS** system allows imaging of roots using a light-based technique, as opposed to radiation-based techniques such as x-ray µCT and Magnetic Resonance Imaging (MRI) which have commonly been used to image roots in natural soil (Downie et al., 2015). This allows the possibility to use fluorescence technology in order to observe changes in cellular processes

during root elongation in a heterogeneous medium, something which was previously not possible using artificial homogeneous growth mediums such as agar or Phytagel due to the lack of physical heterogeneity in the growth medium. Optical Projection Tomography (OPT) is one light-based technique which has been particularly useful in observing the whole root systems of small plants in **TS** (Downie et al., 2012) and Confocal Laser Scanning Microscopy (CLSM) has been used to observe the colonisation of E.coli on lettuce roots in **TS** (Downie et al., 2012); demonstrating the versatility of the growth medium.

Small dicot seedlings (grown inside a 1 x 1 cm cuvette, a single primary root) have been imaged inside the **TS** growth medium, however this project aimed to scale the **TS** system up and develop techniques for imaging larger, and more complex monocot seedling roots (grown inside a 5 x 3 cm specimen pot, 6-8 roots). This presented a range of challenges and resulted in several methodological advancements, which are detailed in Chapter 2.

3.2 Aims

The aim of this study was to better understand the way that monocotyledonous roots grow in different physical structures; mainly soil and **TS**. This led to three specific objectives which were as follows:

- To measure the length and shape of barley root systems in **TS** and soil.
- To measure the length and shape of barley root systems in different **TS** particle size ranges.
- To assess correlations between the physical attributes of the two growth mediums and the root system architecture of barley roots

3.3 Questions

Four questions were developed which formed the basis for the experimental techniques chosen, as well as the subsequent analysis and interpretation of the results. These were as follows:

1. Does **TS** produce roots which are different in length, curvature, verticality, convex hull volume and root system width to those grown in soil?
2. Are there differences between roots of different barley cultivars grown in soil and **TS** in terms of length, curvature, verticality, convex hull volume and root system width?
3. Are differences between soil and **TS** due to the physical structure of the growth medium?
4. Does **TS** particle size affect root growth, curvature, verticality, convex hull volume and root system width?

3.4 Methods

Two experiments formed the basis of this study; the first compared root elongation in soil and **TS**, the other compared root elongation in **TS** sieved to different particle size ranges. The methodology employed in both of these experiments is described in the following section.

3.4.1 Soil and transparent soil core preparation

E.i (section 2.3) was designed to observe root growth in soil and **TS**. Fourteen samples in total were prepared according to the methods described in section 2.4.1.3 measuring 5 x 5 cm (diameter x length). Soil was sieved to <2 mm and packed at a bulk density of 1.1 $g.cm^{-3}$ with a gravimetric moisture content of 0.2 $g.g^{-1}$, in order to provide a growth environment with adequate water and good physical conditions for root growth. The **TS** samples were of mixed particle size up to 1676 µm, packed to a bulk density of 0.67 $g.cm^{-3}$ and a gravimetric moisture content of 0.18 – 0.3 $g.g^{-1}$. After packing excess water was removed from the saturated **TS** using a syringe, so that particles were damp and air-filled pores were present. The exact volume of water accessible to the roots themselves was unknown due to water extraction and due to the hydrophyllic network of channels that exist within the **TS** particle structure.

E.i was conducted in blocks, with 8 cores (4 x Soil; 4 x TS) being planted in the first week and 6 cores (3 x Soil; 3 x TS) being planted in the second week. This was due to insufficient amounts of **TS** being available to plant all cores in the same week. **TS** was fully cleaned in between each week, following the **TS** processing protocol (section 2.4.1.2.2) so that the seedlings were exposed to the same conditions each week. One pre-germinated seed of each selected barley variety was sown in each soil and **TS** core. A plastic disc was placed on top of the soil volume in all cores to prevent the seed from pushing itself out of the soil volume during growth and secured with an elastic band. **TS** cores were wrapped in aluminium foil, up to the top level of

TS so that light was blocked from entering the particles in their translucent state, thus reducing any possible effects on the roots from light contamination. Both soil and **TS** cores were sealed with a transparent plastic bag in order to prevent cores from drying out during incubation.

In E.iv which observed root growth in **TS** of different particle size ranges, 45 cylindrical cores were prepared, measuring 3.2 x 4.5 cm (diameter x length). The cores were transparent specimen pots, split into 3 groups of 15, containing TS sieved to the particle size range of 850-1250 µm, 1250-1676 µm and >1676 µm respectively. The experiment was conducted in blocks, with 9 cores (3 x >1676 µm; 3 x 1250-1676 µm; 3 x 850-1250 µm) being planted each week for five weeks. This was due to insufficient amounts of **TS** being available to plant all cores in the same week. **TS** was fully cleaned in between each week, following the **TS** processing protocol (section 2.4.1.2.2) so that the seedlings were exposed to the same conditions each week. **TS** was packed into the specimen pots using the same method as described above. Each week, 3 cores (one of each particle size range) contained a single barley seedling of the variety Golden Promise, 3 cores contained a single Troon seedling and 3 contained a single Westminster seedling.

3.4.2 Seedling selection, preparation and core incubation

Seedling selection for E.i and E.iv is described in detail in section 2.4.1.1. The method used during E.i and E.vi for seedling pre-germination is described in section 2.4.1.2.1. Soil and **TS** cores were prepared according to the methods described in sections 2.4.1.2.2 and 2.4.1.3.

3.4.3 Imaging of samples

For E.i, the cores were transferred from the James Hutton Institute to Abertay University. Images were obtained by scanning the samples using the HMX 225 X-ray µCT scanner (Nikon,

2016) using the settings described in section 2.4.2.1. Images were reconstructed and analysed using the methods described in section 2.4.3.1.1. 2-D images were then taken of the seedlings using the methods described in section 2.4.2.3.

E.iv imaging was carried out using OPT (section 2.4.2.2). µCT imaging was also carried out on seedlings grown in the largest particle size of **TS** (>1676 µm), using the settings and protocol described in section 2.4.2.1. µCT imaging of other particle sizes was not possible due to limited amounts of time being available for imaging in-between repeats.

3.4.4 Image analysis

Several image analysis steps were taken and these had to be optimised for each 3-D image depending on image quality and greyscale ranges. All images were processed using specific ranges of different parameters, which are described below.

3.4.4.1 Seedling Segmentation

In µCT images, seedlings and soil/ TS were segmented according to the methods described in section 2.4.3.1.1. The resolution of the images was 34 µm.

OPT image processing was carried out according to the methods described in section 2.4.3.3.1. The resolution of the images was 41 µm (243.9 pixels per cm).

3.4.4.2 Root system architecture measurements

Root system architecture (RSA) measurements were taken for all µCT and OPT images according to the method described in section 2.4.3.1.3. Measurements included; number of roots, length, convex hull volume and root system width. Whole RSA measurements of root system width and convex hull volume were taken by importing the segmented stacks into RooTrak (Mairhofer et al., 2012) and using the automatic “measurement” tool.

3.4.4.3 Soil and transparent soil parameter estimation

To assess the particle, water and air percentage per volume of **TS** and soil, as well as connectivity and total porosity, segmentation and analysis was carried out using the method described in section 2.4.3.2.1.

3.4.4.4 Root/soil contact measurements

Root/soil contact measurements were only carried out on µCT images using VGStudioMax2.2, due to the TS particles in OPT being non-visible. The method is described in full in section 2.4.3.2.2.

3.4.4.5 Flatbed image analysis

2-D tiff images were taken using the flatbed scanner at high resolution and analysed according to the method described in section 2.4.3.4.1.

3.4.5 Statistical analysis

Statistical methods are described fully in section 2.4.3.1.4 for µCT, OPT and flatbed images of roots, and section 2.4.3.2.3 for analysis of soil µCT images. Length, number of roots, convex hull volume and roots system width measurements were analysed for all seedlings. Root/soil contact, porosity and connectivity measurements of all µCT images were also analysed.

3.5 Results

3.5.1 Differences in root system architecture between varieties of barley grown in soil and transparent soil

Across the entire experiment, 23 roots of the B83 variety grew in **TS** (2-5 roots per seedling) and 49 roots of the Troon variety grew in **TS** (6-8 roots per seedling). 27 roots of the B83 variety grew in soil (3-5 roots per seedling) and 44 roots of the Troon variety grew in soil (5-7 roots per seedling). There were differences in root system architecture (RSA) of Troon seedlings compared to B83 seedlings, examples of which are shown in Figure 3-1.

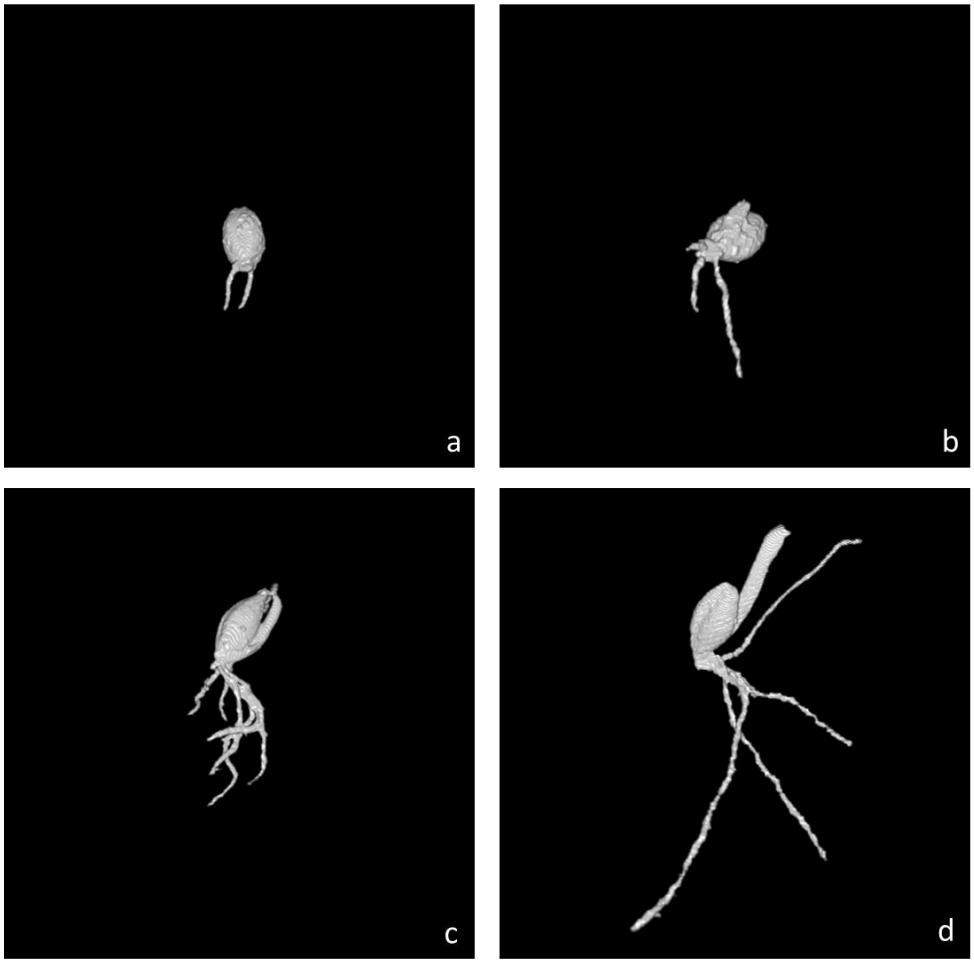

Figure 3-1: Typical examples of μCT images of B83 seedlings grown in TS (a) and soil (b), and Troon seedlings grown in TS (c) and soil (d). Resolution, 29 μm.

Figure 3-2 shows these differences in further detail. Mean averages of all roots grown during the experiment showed that Troon roots were longer (21.23 mm ± 1.48) than B83 roots (11.08 mm ± 1.097) and this was confirmed by the length measurements of the same seedlings also taken using a flatbed scanner, which provided results of 17.66 mm (± 1.46) and 10.81 mm (± 1.09) for Troon and B83, respectively. Troon root systems had a far greater convex hull volume (4153.81 mm^3 ± 771.66) than B83 root systems (547.098 mm^3 ± 184.61), indicating that they were better able to spread through the growth mediums. Troon seedling root systems were also wider (28.88 mm ± 2.08) than B83 seedlings (12.47 mm ± 0.98).

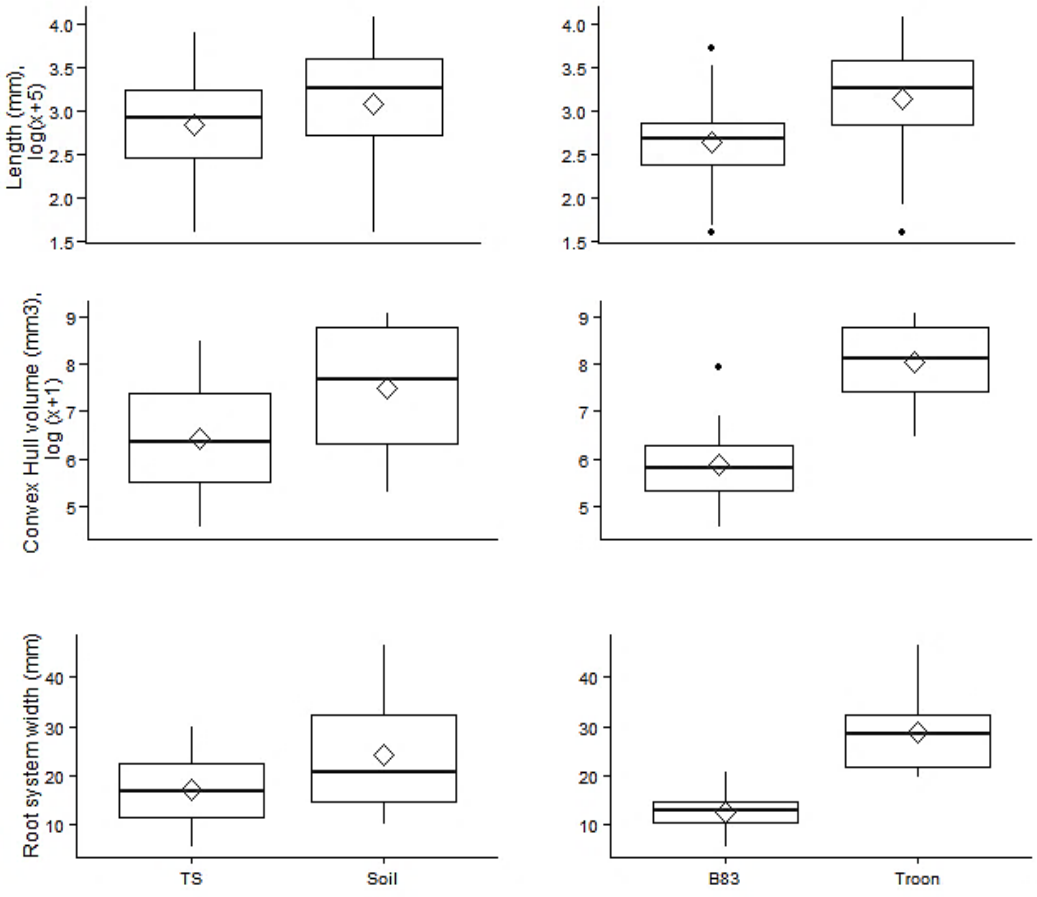

Figure 3-2: Summary boxplots of transformed variables demonstrating differences between growth medium and barley variety. ◊ Indicates the mean average.

REML analyses of the measurements taken from 3-D µCT images showed significant differences between barley cultivars in several RSA traits (Table 3-1).

Variable	Variety P value	F value
Length (mm), log(x+5)	**<0.001**	39.20
Convex Hull volume (mm^3), log (x+1)	**<0.001**	79.61
Root system width (mm)	**<0.001**	77.4

Table 3-1: Results of restricted maximum likelihood tests on transformed variables, differences between barley variety tested. Significant values highlighted in bold.

3.5.2 The relationship between root system architecture differences and soil structural differences

In the experiment comparing root system architecture (RSA) of plants grown in soil vs TS, 143 roots in total were identified and analysed. 72 were present in the TS cores and 71 in the soil cores. Figure 3-3 shows µCT images of typical root systems of seedlings grown in soil vs those grown in TS.

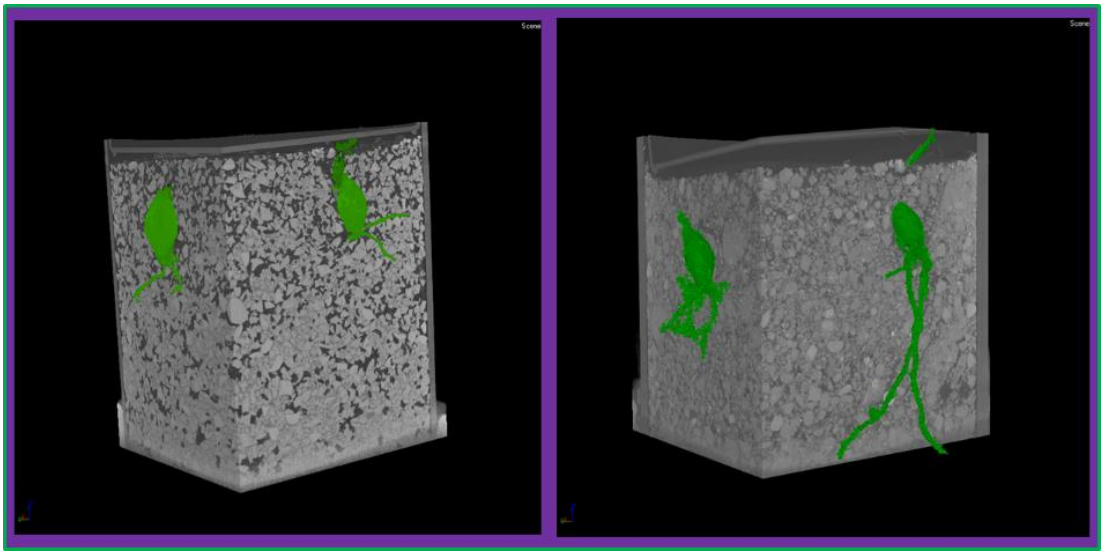

Figure 3-3: Typical µCT core sections of roots grown in TS (left) and soil (right). The seedlings and their root systems are highlighted in green (resolution, 29µm).

Figure 3-2 shows the main differences in further detail. µCT data showed that roots grown in soil were longer than those grown in **TS**, the mean values being 21.56 mm ± 1.76 and 15.10 mm ± 1.26 respectively. The convex hull volume of root systems belonging to plants grown in soil were greater (3457.38 mm^3 ± 890.03) than those grown in TS (1243.53 mm^3 ± 386.28) as was the root system width of soil root systems (24.12 mm ± 3.076) when compared with **TS** root systems (17.24 mm ± 2.09). REML analyses of transformed data showed that there were significant differences between the RSA variables of roots grown in the two different growth mediums; **TS** and soil (Table 3-3).

Table 3-2 provides further detail about the average values of different RSA variables when separated further by barley variety. It shows that regardless of variety, the roots in **TS** were consistently shorter and narrower than those grown in soil. The difference was more apparent in Troon seedlings, whose roots grew quicker and were more successful in exploring their surrounding environment than B83 roots, regardless of whether that environment was soil or **TS**. The Troon roots grown in **TS** were longer and more spread out than B83 roots grown in soil, as is also shown in the table.

	B83				Troon			
Variable	**Soil**	**TS**	**p value**	**F value**	**Soil**	**TS**	**p value**	**F value**
Root length (µCT)	14.47 ± 1.72	11.08 ± 1.097	0.007	7.17	25.68 ± 2.04	18.79 ± 1.57	0.023	7.07
Convex hull volume (mm^3)	845.12 ± 338.92	249.07 ± 56.72	0.080	3.07	6069.63 ± 1021.36	2237.9 9 ± 560.09	0.003	13.97
Root system width (mm)	14.56 ± 1.22	10.38 ± 1.099	N/A	N/A	33.68 ± 3.008	24.09 ± 1.44	0.002	9.29

Table 3-2: Average measurements of roots grown in soil and TS when separated by barley variety, with S.E.M. values included. N/A's are due to problems with statistical tests, due to small n-value.

REML analysis of transformed data showed that there were significant differences between the RSA variables of roots grown in the two different growth mediums; TS and soil (Table 3-3).

Variable	Growth medium (n = 143)	
	P value	F value
Length (mm), log(x+5)	**0.005**	12.39
Convex Hull volume (mm^3), log (x+1)	**<0.001**	18.66
Root system width (mm)	**0.001**	13.59

Table 3-3: Results of restricted maximum likelihood tests on transformed variables, differences between growth medium tested. Significant values highlighted in bold.

In summary, the length of **TS** roots was approximately 25% shorter than that of soil roots when comparing the µCT length measurements, and the width of the **TS** root system as a whole was approximately 30% narrower those that were grown in soil cores. The convex hull volumes of root systems grown in **TS** were approximately 35% of those grown in soil. When variety was also taken into account, the differences were slightly more apparent in Troon,

which grew much longer. These results showed that the root systems of Troon seedlings grown in soil were the longest and most widely spread throughout the surrounding volume, followed by Troon seedlings grown in **TS**, then B83 seedlings grown in soil and finally, B83 seedlings grown in **TS** which were the shortest and least spread out.

To assess whether soil structural variables could explain the differences seen in roots, root growth in soil and **TS**, root/soil contact, soil connectivity and soil porosity were analysed. REML analysis showed that there were significant differences in root/soil contact between root systems grown in different growth mediums. Root/soil contact was not significantly different between the two varieties of barley (Table 3-4). Mean values showed that root/soil contact was 22.03% ± 2.88 for roots grown in **TS** and 42.33% ± 4.42 for root systems grown in soil. Significant differences in total porosity and connectivity were also found between the two different growth mediums. The mean value for total porosity in **TS** was 22.86% (± 0.09) and 14.43% (± 0.08) for soil. The mean value for connectivity in **TS** was 94.86% (± 1.42) and 72.25% (± 4.44) for soil.

Variable	Growth medium		Variety	
	P value	F value	P value	F value
Root soil contact (%)	**<0.001**	16.18	0.076	3.42
Porosity (%)	**<0.001**	48.28	N/A	N/A
Connectivity (%)	**<0.001**	23.56	N/A	N/A

Table 3-4: Results of restricted maximum likelihood tests on root/soil contact, differences between growth medium and barley variety tested. Significant value(s) highlighted in bold. N/A's are present in areas that test soil differences between varieties, as there were none present.

Correlation tests and linear regressions were therefore carried out to try and ascertain whether any of the RSA variables that had shown statistically significant differences between growth mediums were dependent on root/soil contact, soil porosity or soil connectivity. When tested for a dependence on root/soil contact using Pearson's correlation coefficient, a positive correlation for all variables was found (Table 3-5), with statistically significant values of the correlation test being produced for µCT root length, convex hull volume and root system width. This indicates that a correlation between root/soil contact and root length, convex hull volume and root system width do exist, however the relationship is not linear.

Variable	Correlation		Linear regression
	P value	Estimate	R^2
Average root length (mm)	**0.01317**	0.4626796	0.1838
Convex Hull Volume (mm^3)	**0.003013**	0.540046	0.2644
Root system width (mm)	**0.005209**	0.5133516	0.2352

Table 3-5: Results of correlation and linear regression analyses on the dependence between transformed variables and root/soil contact. Significant values highlighted in bold

Statistically significant linear relationships were not found between any of the RSA variables and root/soil contact, but a positive relationship suggesting a trend between root/soil contact and root length, convex hull volume and root system width was observed (Figure 3-4).

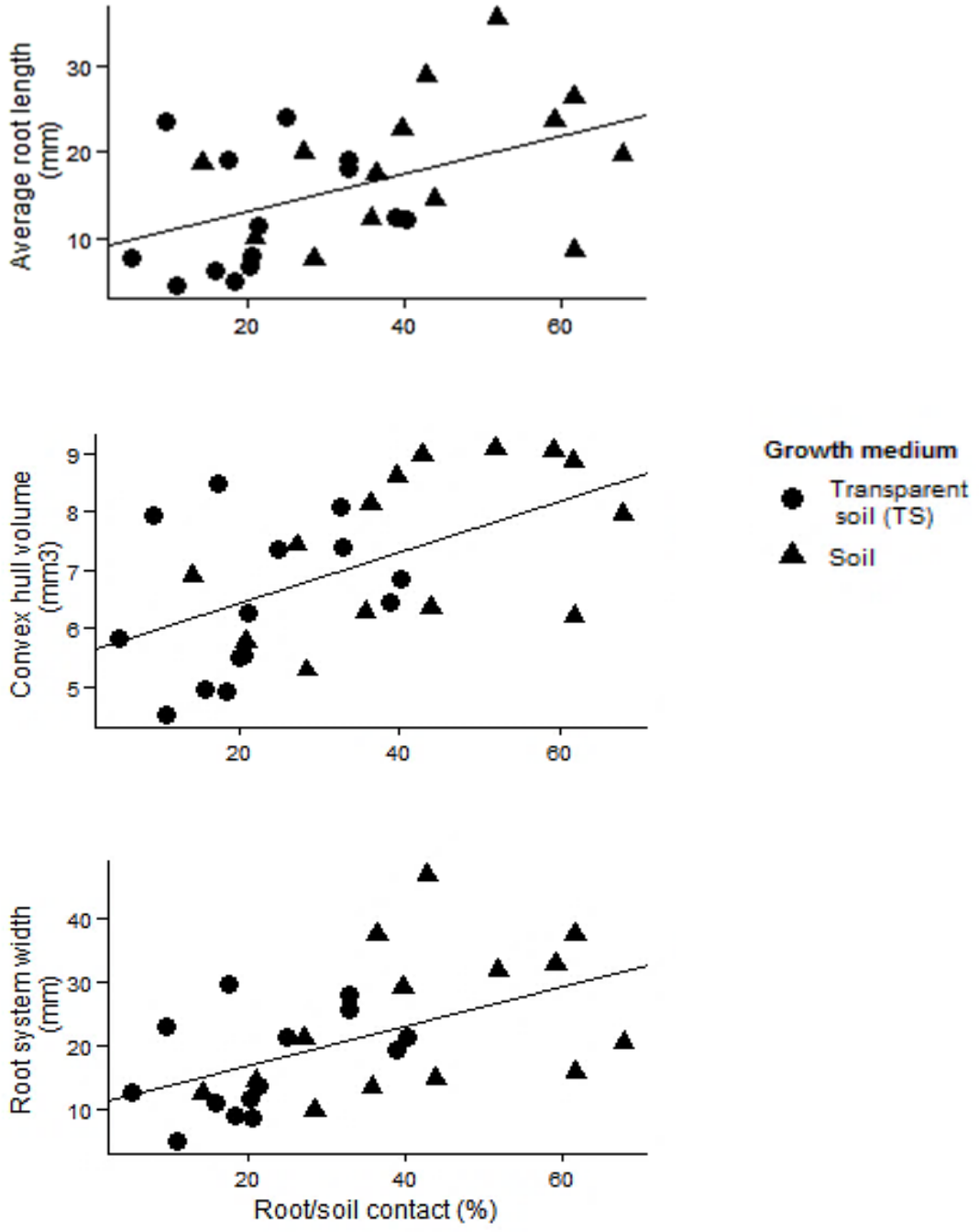

Figure 3-4: Plots showing correlation relationships between root system variables and root/soil contact

The root variables were then tested for a correlation with connectivity and porosity, which had already been shown to be statistically different depending on the growth medium in question. **TS** showed higher percentages on average for both porosity and connectivity. When the correlations were tested using Pearson's correlation coefficient, no linear relationships or significant correlations were discovered between the RSA variables and either connectivity or porosity as demonstrated in Table 3-6 and Figure 3-5.

Variable	Connectivity			Porosity		
	P value	Pearson's Estimate	R^2	P value	Pearson's Estimate	R^2
Average root length (mm)	0.1672	-0.2685	0.036	0.095	-0.322	0.069
Convex Hull Volume (mm^3)	0.4103	-0.16194	-0.0112	0.2586	-0.2209	0.0122
Root system width (mm)	0.4076	-0.16286	-0.0109	0.2247	-0.237	0.01985

Table 3-6: Results of correlation and linear regression analyses on the dependence between transformed variables and connectivity and porosity of growth mediums.

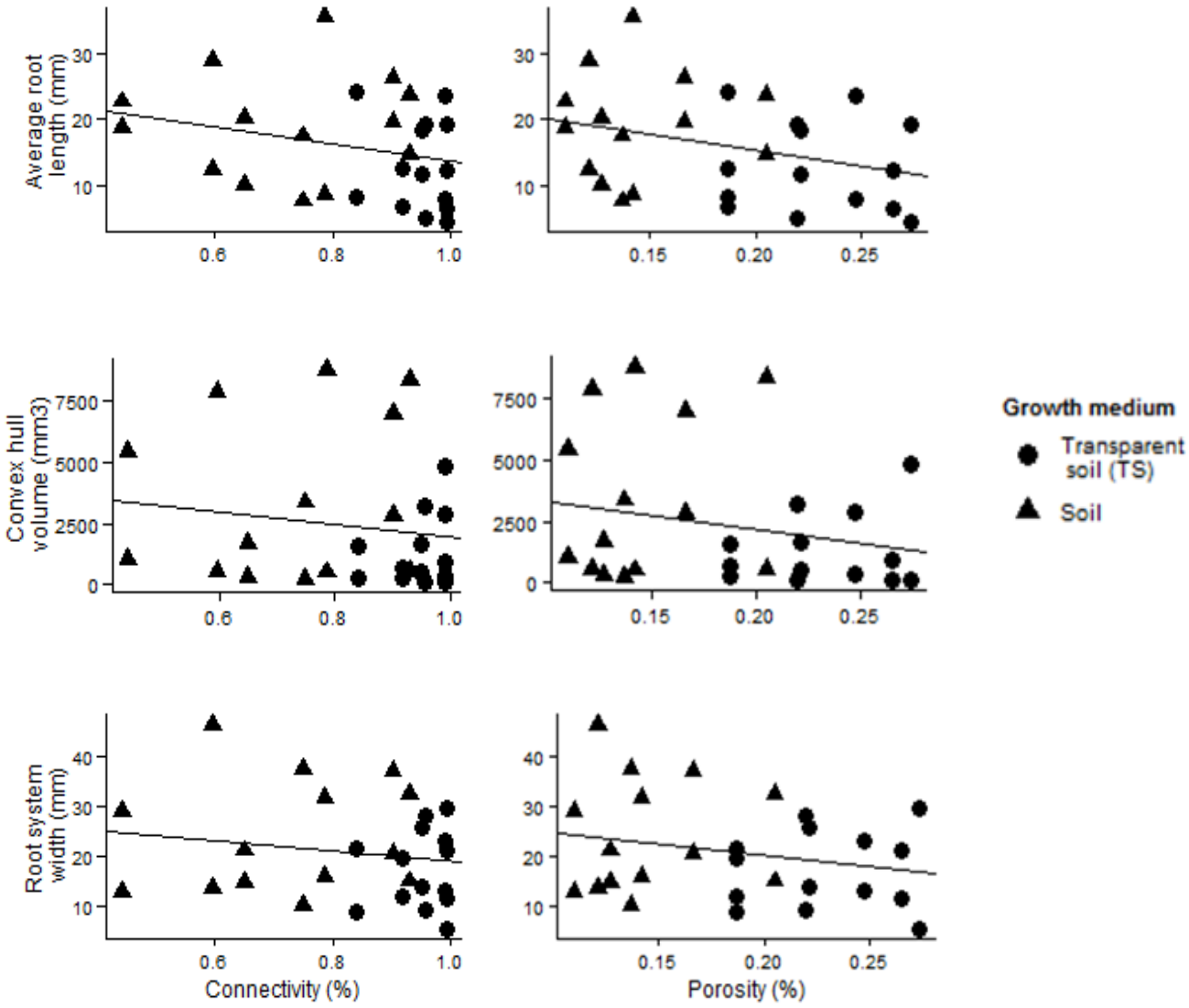

Figure 3-5: Plots showing correlation relationships between root system variables and connectivity (left) and porosity (right)

In summary, the data indicate that root length, convex hull volume and root system width are unlikely to be different as a result of connectivity or porosity of soil. Root length, convex hull volume and root system width all show correlations with root/soil contact, which suggests that root/soil contact may have an impact on the abilities of roots to grow in soil.

3.5.3 Differences in root system architecture between roots that are grown in different transparent soil particle size ranges

To understand whether root growth is affected by particle size, root systems were grown in three different particle size ranges of **TS** (E.iv). 297 roots were present in E.iv. All seedlings produced 5 – 8 roots per seed regardless of variety or particle size range, giving a total of 103 Troon roots (average 6.8 roots per seedling), 102 Westminster roots (average 6.8 roots per seedling) and 92 Golden Promise roots (average 6.1 roots per seedling). 99 roots in total were produced by seedlings growing in the 850-1250 µm (small) particle size range (average 6.6 roots per seedling), 100 were produced by seedlings growing in the 1250 – 1676 µm (medium) particle size range (average 6.7 roots per seedling) and 98 were produced by seedlings growing in the >1676 µm (large) particle size range (average 7.1 roots per seedling). The OPT method identified 175 roots out of the total 297 (59%), the flatbed method identified 258 (87%) and the µCT method identified 88 out of the 92 (96%) roots that were scanned in the µCT scanner.

Typical examples of seedlings grown in the three different treatments are shown in Figure 3-6. Figure 3-7 shows the mean values for significantly different root variables in different particle size ranges. The average length of roots using the flatbed measurement method was 11.46 mm ± 0.83 for roots grown in the small particle size range, 11.32 mm ± 0.76 for roots grown in the medium particle size range and 8.20 mm ± 0.55 for roots grown in the large particle size range. The OPT method did not result in significant differences in root length which was possibly due to a loss of information during imaging, however was almost statistically significant and the pattern of root length was the same depending on the treatments, whereby the roots grown in the small particle size range were the longest (16.58

mm ± 1.95), followed by those grown in the medium particle size range (15.75 mm ± 1.56), followed by those grown in the large particle size range which were the shortest (10.14 mm ± 1.12). Significant differences were also detected between particle size for the roots system width, with root systems grown in the small particle size range being the widest (30.71 mm ± 3.39), followed by those grown in the medium particle size range (28.83 mm ± 3.18), followed by those grown in the largest particle size range, which were the narrowest (21.63 mm ± 2.18).

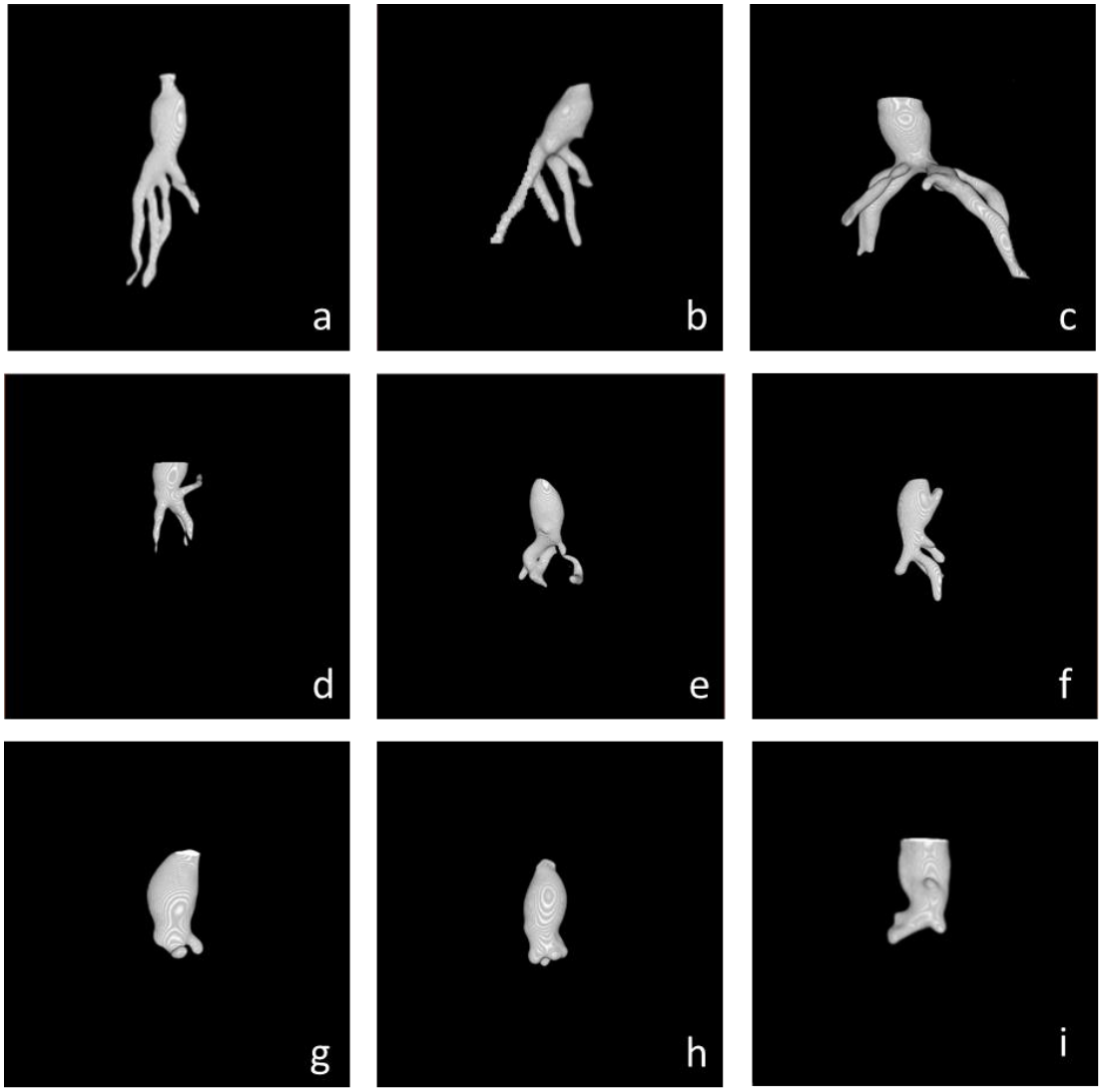

Figure 3-6: Typical example of Golden Promise (a), Troon (b) and Westminster (c) seedlings grown in the small particle size range, Golden Promise (d), Troon (e) and Westminster (f) seedlings grown in the medium particle size range, and Golden Promise (g), Troon (h) and Westminster (i) seedlins grown in the large particle size range. OPT images, resolution 41 µm.

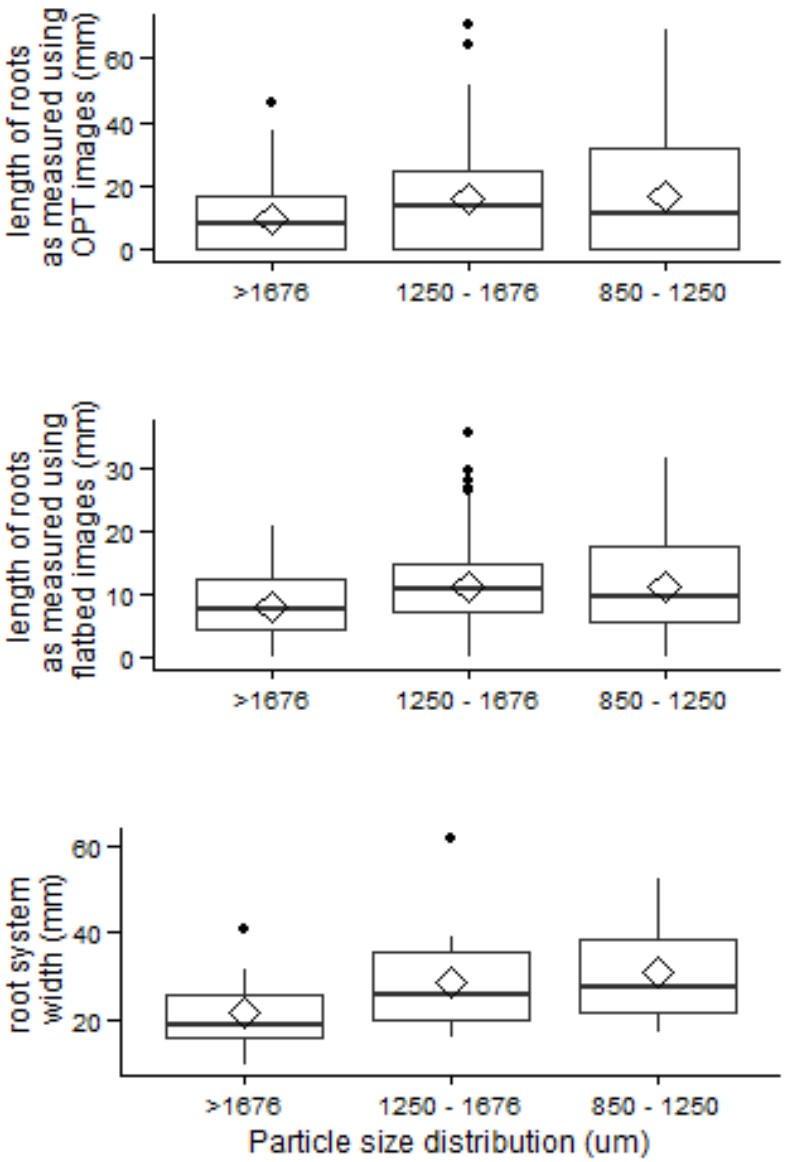

Figure 3-7: Summary boxplots of root length as measured by OPT (top), root length as measured using a flatbed scanner (middle) and root system width (bottom), demonstrating differences in root growth between TS particle size ranges (µm). ◊ Indicates the mean average.

REML analysis was carried out on the OPT measurements as well as the flatbed length measurements of roots grown in **TS**, to test for RSA differences between the roots grown in the three different particle size ranges of **TS**. The results are shown in Table 3-7.

Variable	Particle size range P value	F value
Flatbed length (mm)	**0.022**	4.26
OPT length (mm)	0.055	3.17
OPT root system width (mm)	**0.018**	4.53

Table 3-7: Results of restricted maximum likelihood tests on RSA variables, differences between transparent soil particle size ranges tested. Significant value(s) highlighted in bold.

3.5.4 Differences in root system architecture between cultivars of barley grown in Transparent Soil

The flatbed method provided a mean root length of 12.7 mm ± 0.81 for the Golden Promise variety, 8.6 mm ± 0.57 for Troon and 10.0 mm ± 0.78 for Westminster roots. The OPT method gave mean values for root length of 15.73 mm ± 1.69 for Golden Promise roots, 11.27 mm ± 1.21 for Troon and 15.20 mm ± 1.78 for Westminster roots. The µCT method gave mean values of 10.36 mm ± 0.96 for Golden Promise roots, 8.86 mm ± 0.86 for Troon roots and 10.83 mm ± 1.15 for Westminster roots, although only roots from the >1676 µm particle size range were included in these measurements.

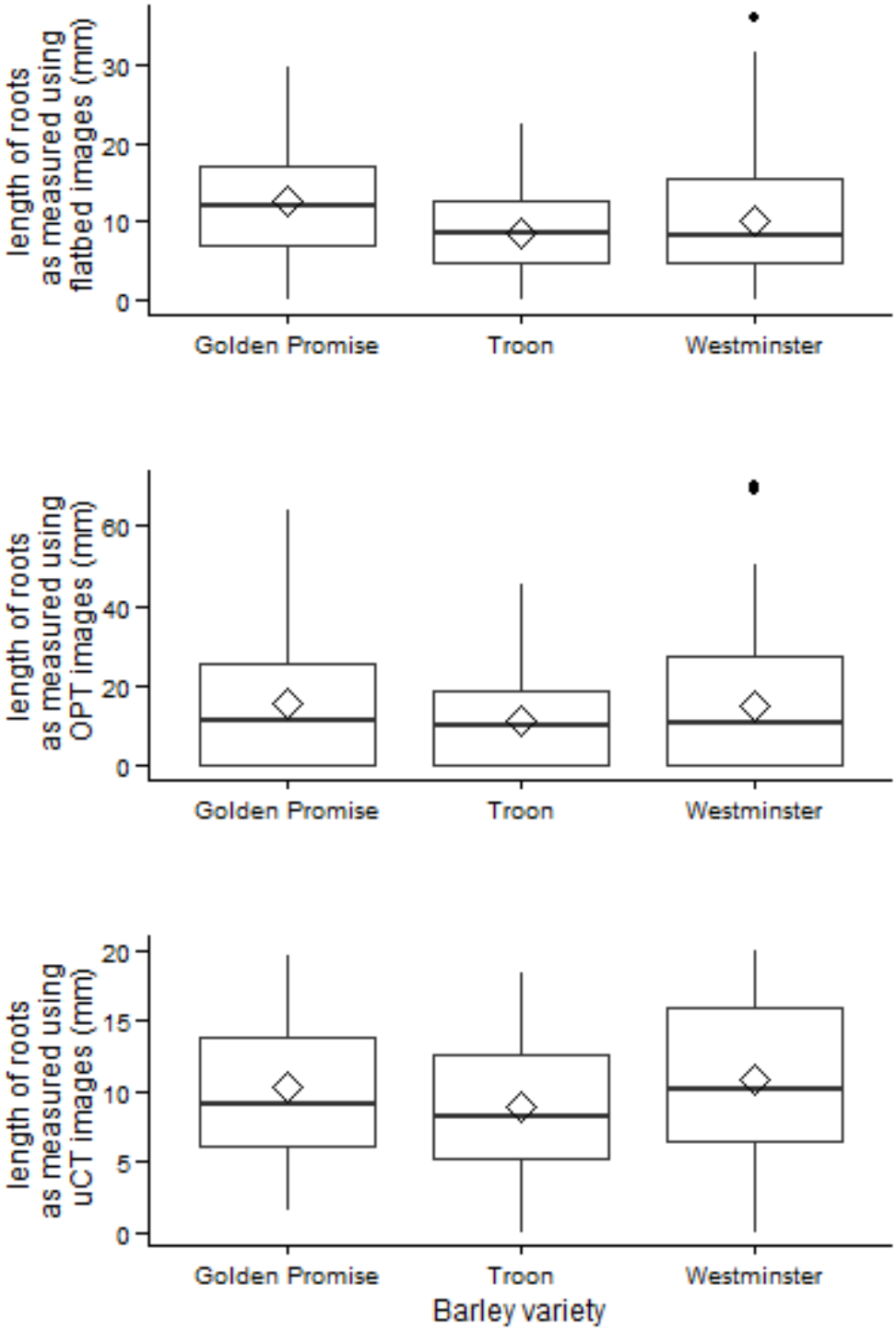

Figure 3-8: Boxplots showing the distribution of root length measurements for each barley variety as measured using flatbed images (top), OPT images (middle) and µCT images (bottom). ◊ Indicates the mean average.

REML analysis was carried out in order to analyse any difference in RSA between the three different barley varieties; Golden Promise, Troon and Westminster. The results are shown in Table 3-8.

Variable	Barley variety P value	F value
Flatbed length (mm)	**0.009**	5.33
OPT length (mm)	0.380	1.00
µCT length (mm)	0.595	0.56

Table 3-8: Results of restricted maximum likelihood tests on RSA variables, differences between barley varieties tested. Significant value(s) highlighted in bold.

The only variable that showed a significant difference between varieties was the root length as measured using the flatbed (2-D) method. The same was not true for the roots measured using the OPT method or the µCT method. The particle size range seemed to be a larger driver of differences in RSA than the variety during this study (Section 3.5.3).

3.6 Discussion

3.6.1 Discussion of methods

The method used in this chapter included entire root system measurements such as convex hull volume and root system width, giving an overall impression of how the root system as a whole is exploring the growth medium surrounding it (Tracy et al., 2012). Not only were the roots of seedlings grown in soil longer than their **TS** equivalents; their whole root systems were also more successful in exploring the soil volume, with their convex hull volumes and root system widths being consistently larger. Perhaps if **TS** roots had been given more time to grow, they would have reached similar dimensions in convex hull volume and root system width. Chapter 4 addresses these questions and analyses in greater detail whether successful root systems are wider because it is a trait of successful soil exploration, or whether it is because their roots are longer.

The soil used for this experiment was sifted and packed relatively loosely (1.1 $g.cm^3$), with 20% water content, which was distributed evenly throughout the soil volume thus it would be expected that roots in this treatment would grow to their maximum potential within the time-scale allowed, due to there being little physical stress caused by the soil (Bingham and Bengough, 2003). It can be assumed that the physical nature of natural soil, with its less-connected, less-porous network of small air spaces through which roots can explore and water can be absorbed, is more effective than **TS** at holding water in place under constant temperature conditions until it is located by a root and absorbed (Baver, 1938). As a result of less water movement in soil, nutrients are also possibly more sessile, allowing roots to locate them more easily. **TS** by contrast is made up of particles that are larger than soil, being more akin to sand particles (Downie et al., 2012). They are more jagged in their structure, due to

the cryo-milling process, and form a very highly connected, porous structure through which roots are able to elongate and grow easily, albeit at a slower rate than those that grow in natural soil. It has been shown in this chapter that the largest particle size is not optimal for root growth, which may be because of its inability to hold water in its large pores (Saxton and Rawls, 2006). A lack of water may also reduce the ability of roots to exchange ions with those that have been adsorbed on to the surface of **TS** particles, which could in turn affect their growth (Wiersum, 1962). Nevertheless, there were no significant differences in variables such as root verticality and curvature, suggesting that these remain constant for barley roots between soil and **TS**.

Troon outperformed B83 in every instance, which was to be expected from previous data from Valentine et al., which suggested that Troon roots grew longer with wider root angles than B83 did on a 2-D filter paper system (Valentine et al., 2012a). **TS** was successfully used to replicate the differences in length, but did not detect any differences in curvature or verticality, which are associated with root angle. These differences were not observed in a natural soil system either. The filter paper system forces roots to grow in a 2-D plane, which may cause them to spread out at angles that are not a true reflection of their normal growth pattern in a 3-D, physically heterogeneous growth medium (Hargreaves et al., 2009). This is an advantage of **TS** as opposed to filter paper, gel or extraction techniques, which may either have an atypical growth effect on monocotyledonous root systems or cause the root system structure to collapse entirely (in the case of extraction techniques), thus removing the ability to analyse differences in root/soil contact or porosity and connectivity of the growth medium (Mooney et al., 2012).

Missing OPT data may have contributed to the lack of differences found between barley varieties grown in E.iv. This conflicts with data obtained in E.i, which did identify differences between root systems of different barley varieties (Valentine et al., 2012a). As mentioned previously, it is known that the Valentine et al. (2012a) data was obtained using a 2-D gel plate method, which is an unrestricted growth system and thus may encourage different root growth patterns to that seen in physically heterogeneous growth mediums. The largest particle size range of **TS** resulted in the shortest roots for all three varieties and therefore the differences between them may not have been so obvious. Had µCT images of the smallest **TS** particle size been taken instead, there may have been differences found in variables such as root system width and convex hull volume.

3.6.2 Discussion of results

In the dicotyledonous organism *N. benthamiana*, it was found that roots grew longer and had a narrower diameter in **TS** than in soil (Downie et al., 2012). The results in this chapter suggest a different pattern of root growth for the monocotyledonous plant barley, whereby roots are consistently shorter in **TS** than they are in soil. Roots are known to explore soils in different ways depending on the type of plant (Goodman and Ennos, 1999) with dicotyledenous roots being able to penetrate stronger soils more successfully than monocotyledenous roots (Materechera et al., 1993). As **TS** has very little mechanical strength this is unlikely to be the reason that barley roots do not grow as easily in **TS** as dicotyledenous roots, but monocotyledenous roots do not cope with sub-optimal conditions as well as dicotyledenous roots (Materechera et al., 1991), so if there are unknown soil stressors within the **TS** system, this may explain why these results contradict those found by Downie et al. (2012).

There were differences in root growth between the two growth mediums, with roots being generally longer and wider in soil than in **TS**. There were also differences in porosity and connectivity of the growth mediums, with soil being less porous, with a less connected pore system than in **TS**. Root/soil contact was also different, with roots grown in soil experiencing a higher level of root/soil contact across the entire root system than those grown in **TS**. The physical differences between soil and **TS** are clearly visible, which makes it tempting to presume that these have a direct influence on the root growth of barley seedlings. Interestingly, the differences seen in RSA did not strongly correlate with a single specific physical property of the growth mediums. It may be that the physical properties of soil/**TS** analysed in this experiment, combined with the barley genotype contributed in varying degrees to the resulting root growth (Bronick and Lal, 2004). There may also be a more complicated mechanism at play, whereby the physical structure of the growth medium influences other abiotic variables in the system, such as water and nutrient availability, which then results in the differences observed between the growth mediums (Letey, 1985). Root system architectural differences must be related to the growth medium, as the differences were observed repeatedly, but a single 'key factor' underpinning them all has not yet been discovered. It is likely that there are a combination of factors interacting with one another to produce the observed results.

The chemical and physical complexity of natural soil makes it difficult to pinpoint a single physical factor that may heavily influence the outcome of root elongation in barley seedlings (Hinsinger et al., 2009). Therefore the experiment that looked at barley root growth in **TS** of different particle size ranges was useful. It was easier to compare the treatments, because the same substrate was used each time, however the pore size was physically manipulated

by having different particle size ranges of **TS**. Differences were found in root length, and root system width but not in the variables that described the shape of the growth (i.e the curvature and the verticality). This could have been due to real differences in root growth, or it could be that roots in the larger particle size range needed longer to grow in order to respond to gravity (Barlow, 2002) and reach the same verticality as root in the small particle size range. Despite the difficulty in obtaining OPT data, it was still evident that roots grown in the smallest particle size range were more successful in exploring their surrounding environment, which could be due to improved water holding capacity, enabling roots to locate water more easily and exchange ions with the surfaces of **TS** particles (Saxton and Rawls, 2006). Data from this chapter show that root/soil contact was significantly different between the growth mediums, however more detailed analysis of pore geometry is required to fully understand how this impacts on root growth.

3.7 Conclusion

Root system architecture (i.e. the length and shape of root systems) does differ between root systems of barley grown in different growth mediums, potentially because they differ in their physical properties. This was observed clearly in E.i when root growth was compared between seedlings grown in soil and those grown in transparent soil (**TS**), with those growing in soil being longer and more spread out than those grown in **TS**. However, some barley varieties are able to grow in the **TS** medium more successfully than others, which was demonstrated by Troon.

When sieved into different particle size ranges (E.iv), differences in root length were observed once again using the 2-D flatbed method, but not the 3-D OPT method, however this could be due to the need for further development of the OPT system in order to make it more successful in identifying individual roots. The OPT data followed a similar pattern to that of the flatbed data, indicating that significant differences could have been detected if the method had been more sensitive.

Currently the data indicate that by manipulating the **TS** growth medium, it is possible to induce a response by barley roots, whereby those grown in larger particle size ranges of **TS** are significantly shorter than those that grow more successfully in the smaller particle size ranges. This will be investigated further in Chapter 4 by using vertically-stratified split pots containing one particle size range in each side of the pot.

4 Autonomous vs. systemic responses of barley roots grown in different soil structures, visualised using 3-Dimensional images

4.1 Introduction

In chapter 3, barley root growth in different physical structures was investigated. The growth of barley roots in **TS** could be changed by changing the physical structure of the **TS**. The particles were sieved into different size ranges and the longest roots and widest root systems were observed in particles of 850-1250 µm. The smallest roots were observed in the >1676 µm size range which was possibly due to a lack of contact between the roots and TS particles as roots attempted to locate nutrients and water whilst being lost inside very large pores (Carminati et al., 2009). This chapter aims to investigate the effects of physical structures on root growth in greater detail, in order to understand whether the effects seen on barley roots are as a result of events occurring at the root tip of individual roots (i.e. autonomous response) or whether root growth is dependent on events happening across the entire root system (i.e. systemic response). Autonomous vs systemic root responses were discussed briefly in a paper by Davies and Zhang (1991) , who suggested that a systemic response, including communication between roots, would be of great benefit to root systems that were experiencing stress at certain regions of the root system.

4.1.1 Soil pore structure and root growth

Studies assessing response of roots to soil stressors such as strength, compaction or drought often focus on well-established root systems that have been extracted from the soil, washed

and measured using programmes such as WhinRhizo (Arsenault et al., 1995), or alternatively, they focus on detailed observation of events at the root tip (e.g. Brooks et al. (2010), using high-resolution imaging techniques, both 2-D and 3-D.

In a recent study by Valentine et al. (2012b) it was found that physical soil properties had a greater influence on root growth than chemical soil properties, with pore sizes of 60 µm – 300 µm accounting for 65.7% of variation seen in barley root growth. The effects of these pore size thresholds are not well documented across plants and may vary between cultivars, but it demonstrates how important these parameters can be and how further investigation into these processes needs to be conducted in order to understand how the shape as well as the size of pores within a soil structure influence the way that roots grow.

It is known that compacted soils reduce root elongation due to the decrease in pore size, and reduction of air availability (Tracy et al., 2011). Strong soils have the same effects on roots due to the additional effort needed in order for root tips to push apart soil particles (Clark et al., 2003). Dry soils also reduce root elongation, due to roots being unable to absorb water and nutrients, as well as dry soils generally having a higher mechanical strength (Whiteley and Dexter, 1982).

4.1.2 Split pot experiments

Vertically stratified split pots that contain different treatments on different sides of the pot have been used to investigate differential exposure of root systems to various soil properties. Split pots have been used to look at plant responses to water differences in vertically-stratified soil profiles (Gowing et al., 1990), whereby it was found that as long as half of the root system in apple trees was receiving adequate water, the shoot would continue to grow. Mingo et al. (2004) found that root biomass increased in plants whose root systems were in

half wet and half dry soil conditions, as long as the two sections were alternated, so that the previously dry section of soil was watered in the next treatment cycle and the previously watered region of soil was allowed to dry.

Split pot experiments have also been used to further understand the response of root systems to differential nutrient availability. Brouder and Cassman (1994) found that cotton roots preferentially grew in areas containing higher levels of NO^{3-} or higher levels of PO^{4-}. Increased levels of K in one half of the soil did not affect root distribution. Anghinoni and Barber (1980) also found that exposing 50% of a corn root system to higher levels of phosphorous resulted in 25% extra root mass in the section of the root system that had been exposed to increased nutrient layers.

Split pot methods were used to observe the influence of arbuscular mycorrhizal fungi and roots on soil structure (Hallett et al., 2009). This was done by splitting a pot vertically down the middle with a fine mesh and having a tomato plant in one side of the pot and arbuscular mycorrhizal fungi throughout the soil on both sides of the pot. Hallett et al. (2009) found that arbuscular mycorrhizal fungi helped to form aggregates and increased soil stability, however the plant roots were found to have the greatest impact on soil stability, showing statistically significantly more water-stable aggregates than the side with no plant present ($p < 0.001$).

Few studies have observed the effects of soil structure and compaction on root growth in split pot trials, however one such study found that compensatory root growth occurred in roots that were in the side of the pot containing loose soil, versus roots from the same plant that were unable to grow (Montagu et al., 2001). In another study, genotypic variation was seen between two different varieties of tomato plants, when exposed to 1.1/1.5-g cm^{-3} split pot treatments. The wild-type variety showed significantly less plant growth, whereas a

transgenic tomato plant which had been modified to have a reduced capacity to produce ethylene showed shoot growth that was comparable with uncompacted tomato plants (Hussain et al., 1999). Root growth in this experiment was significantly reduced in regions of soil that were packed at 1.5-g.cm^{-3}, but roots were longer in the 1.1-g.cm^{-3} regions of soil.

TS offers a novel way to observe the impact of soil structure on root systems using a split pot method because it allows us to keep certain structural factors in the **TS** constant, for example surface properties and internal aggregate structures. The particles are easily separated into different particle size ranges, which alters the sizes of the pores that the roots have to explore (chapter 3). Using µCT imaging, we can observe their growth using time-lapse methods, to see how different roots belonging to the same plant respond to the different soil structures, and the images are easier to process, because the particles and pore systems are more easily identifiable in **TS** than they are in a natural soil system (section 2.4.3.2.1).

4.1.3 Time-lapse observation of root growth

Adding the dimension of time to barley root system images will help to understand the time-dependent behaviour of barley roots, in order to explore the possibility of whole-plant communication during early growth. Imaging techniques are ideally suited to capturing root responses; providing high quality, permanent records of root growth at a range of time intervals (Jenneson et al., 2003).

Many time-lapse experiments have been conducted on root systems using different imaging techniques. Some earlier examples were as simple as using cameras (IIijima et al., 1998), which were compatible with established rhizotron instruments (Busch et al., 2006). However, over time there has been a push towards setting up and optimising large-scale phenotyping experiments. One such example was recently published by Adu et al. (2014), who placed pre-

germinated *Brassica rapa L.* seedlings on a piece of filter paper, in between two Perspex plates, inside a high-resolution 2-D scanner. This method allowed the acquisition of high-resolution 2-D images of roots at time-intervals specified by customised software. In recent times, there has been a move towards the development of 3-D imaging techniques for roots, with researchers recognising the need to understand how roots explore soils both spatially and temporally (Fraas and Lüthen, 2015).

Understanding how root systems explore soils is done most effectively by using non-destructive 3-D imaging techniques (Dhondt et al., 2010). Tracy et al. (2010) published a time-lapse experiment observing tomato plant root growth in two different compaction treatments. The plants were imaged using X-ray µCT every 24 hours for 10 days and plants grown in the compacted treatment had shorter roots ($p < 0.05$), smaller root systems ($p < 0.05$) and lateral roots formed later than in the uncompacted control ($p < 0.01$). Observing roots growing in a split pot treatment over time can help us to better understand the behaviour of roots in physically heterogeneous substrates.

4.2 Aims

The overall aim of this experiment was to image and quantify root elongation over time in 3-D using µCT for three treatments; **TS** cores containing particles of 850 – 1250 µm (S), particles of 1676 µm (L) or vertically stratified pots, containing one of the aforementioned particle size ranges on each side of the pot (split pot). This was done in order to understand whether root elongation is a systemic process that involves whole plant communication, or an autonomous process, wholly dependent on the local environment surrounding the root tip. To quantify the root system responses the following objectives were defined:

- To observe and quantify, at 24 hour time intervals, root system architecture as roots elongate through **TS**, using µCT images.
- To observe the behaviour exhibited by individual roots from the same plant when confronted with different physical soil conditions.
- To understand in detail the structure of **TS** between different particle sizes and in split pot treatments, with increasing depth.
- To understand how the different physical structures between **TS** treatments affect the way that barley roots grow.
- To understand whether barley root behaviour is individual, or whether it is systemic.

4.3 Questions

The following questions were the focus of this chapter:

1. Are there differences in root growth over time between large particle, small particle and split pot treatments?
2. What are the physical differences between particle size ranges of **TS**?
3. What are the spatial differences in the physical composition of **TS** cores for each treatment?
4. What is the relationship between root system architecture and **TS** over time within different treatments?
5. What are the patterns of barley root exploration over time in different treatments?

4.4 Methods

An experiment was designed, which enabled imaging of root growth of barley seedlings inside transparent soil (**TS**) at 24-hour intervals. µCT was used as the imaging technique of choice, because a study looking at root growth in situ, within the **TS** medium over time has not been conducted before. µCT was also chosen because it was not necessary to flood the **TS** samples before imaging, thus allowing the assessment of **TS** physical conditions. The methodologies employed for this experiment are described in the following section.

4.4.1 Soil and transparent soil core preparation

To observe root growth in **TS** of different particle size ranges, 18 cylindrical cores were prepared, measuring 3.2 x 4.5 cm (diameter x length). The cores were transparent specimen pots (http://www.medfor.co.uk/product/707/110/clear-ps-jar-with-white-pe-screw-cap/709bbca2f05a03b04aadf9542e0d975b) with 6 containing **TS** sieved to the particle size range of 850-1250 µm, 6 containing **TS** sieved to >1676 µm, and 6 vertically split pots that contained the **TS** particle size 850-1250 µm in one side of the pot and TS particles that were >1676 µm particles in the other side of the pot (section 2.4.1.3.1). The experiment was conducted in blocks, with 6 cores (2 x 850-1250 µm; 2 x >1676 µm; 2 x split pots) being prepared and randomised each week for three weeks, so that cores were not prepared and imaged in the same order during each rep. This was due to insufficient amounts of **TS** being available to plant all cores in the same week. **TS** was fully cleaned in between each week, following the **TS** processing protocol (section 2.4.1.2.2). **TS** was packed into the specimen pots using the same method as described previously (section 2.4.1.3.1). All cores contained a single Westminster barley seedling.

4.4.2 Seedling selection, preparation and core incubation

Barley cv. Westminster was selected for this due to reasons specified in section 2.4.1.1. Seeds were selected and prepared according to methods outlined in section 2.4.1.2.1. At 24 hour intervals, the cores were removed from the incubator, imaged using the μCT scanner and returned to the incubator. 5 images were taken of each sample, the first at 0 hours (i.e. time of sowing) and the last at 96 hours of seedling growth. Each scan lasted approximately 55 minutes.

4.4.3 Imaging of samples

The cores were scanned at Abertay University at 24 hour intervals using the HMX 225 X-ray μCT scanner and settings specified in section 2.4.2.1. After the final scan was complete, the incubator temperature was reduced to 0° in order to halt root elongation, the samples were placed inside it and left there for 72 hours before imaging using OPT. Due to unavailability of the μCT scanner, three time points were missed. In these circumstances, the seedlings remained in the incubator untouched until the next time point. The time points that were missed are shown in Table 4-1.

Core I.D	Week	Treatment	0 hours	24 hours	48 hours	72 hours	96 hours
1	1	Split pot	✓	✓	✓	×	✓
2	1	Large	✓	✓	✓	×	✓
3	1	Small	✓	✓	✓	×	✓
4	1	Large	✓	✓	✓	×	✓
5	1	Small	✓	✓	×	×	✓
6	1	Split pot	✓	✓	×	×	✓
7	2	Small	✓	✓	✓	✓	✓
8	2	Split pot	✓	✓	✓	✓	✓
9	2	Large	✓	✓	✓	✓	✓
10	2	Split pot	✓	✓	✓	✓	✓
11	2	Large	✓	✓	✓	✓	✓
12	2	Small	✓	✓	✓	✓	✓
13	3	Small	✓	✓	✓	×	✓
14	3	Large	✓	✓	✓	×	✓
15	3	Split pot	✓	✓	✓	×	✓
16	3	Split pot	✓	✓	✓	×	✓
17	3	Small	✓	✓	✓	×	✓
18	3	Large	✓	✓	✓	×	✓

Table 4-1: Summary of seedlings that were imaged and those that were missed due to the µCT scanner being unavailable for imaging

After imaging was complete, seedlings were extracted from the transparent soil, cleaned with sterilised distilled water, placed in a petri dish containing water and a scale bar, and scanned using the Epson flatbed scanner at the James Hutton Institute (section 2.4.2.3). Seedlings were then stored in specimen pots, in 50% ethanol.

4.4.4 Image analysis

4.4.4.1 Seedling segmentation

Examples of images before and after segmentation are shown in Figure 4-1. µCT images were 51 µm in resolution. The seedling was segmented from the **TS** as described in section 2.4.3.1.1. A region grower tolerance of 500 was used for all images. Roots were then opened by a voxel radius of 1 or 2 in order to remove holes in the region of interest. A .bmp z stack of images visualising the segmented seedling was also exported for future analysis using Fiji (Schindelin et al., 2012).

Figure 4-1: Image of µCT image of TS volume and segmented seedling after region grower applied (resolution, 51µm).

Images of all split-pot seedlings are shown in Figure 4-2.

Figure 4-2: 3-D µCT images of all split pot seedlings grown in during E.v (resolution, 51µm).

4.4.4.2 TS volume segmentation

Transparent soil segmentation was undertaken in all µCT images and the same method was used each time. In VG StudioMax2.2 a median filter of 3 voxels was applied to the **TS** volumes in order to remove noise from the images, whilst retaining the edges of the individual particles. A clearly visible particle was then selected manually and the region grower tool was used to detect the rest of the **TS** volume, with the tolerance level set to 11000.

4.4.4.3 Root system architecture measurements

Root system architecture (RSA) measurements were taken for all µCT images of seedlings using the method described in section 2.4.3. Individual root measurements included; number of roots, length, curvature, horizontal curvature and verticality. Whole root system measurements included root system width and convex hull volume.

In order to compare the roots at different time points directly, scans taken of the same seedling at 24 hour intervals were aligned manually using Fiji according to the method described in section 2.4.3.1.2. Skeletonisation was carried out according to the method described in section 2.4.3.1.3.

4.4.4.4 Root/soil contact measurements

Root/ soil contact was carried out according to the measurements described in section 2.4.3.2.2.

4.4.4.5 Soil and transparent soil measurements

Figure 4-3 shows the process involved in phase distribution analysis (i.e. the relative proportions between air, water and **TS**). This was carried out by importing the **TS** .bmp stacks into Fiji and then extracting a series of cubes of 5.1 mm^3 at adjacent depths down the **TS** profile. A median filter of 2 pixels was applied throughout the image stack. Thresholding for particles, water and air was carried out according to the methods described in section 2.4.3.2.

The soil property measurements porosity and connectivity of **TS** were taken from all µCT images. For total porosity and connectivity analysis, **TS** bmp stacks were imported into Fiji. A 3-D block, measuring 10.2 mm^3 and devoid of roots was extracted from the volume. The images were thresholded using software written specifically for soil analysis (Houston et al., 2013a). Connectivity and porosity measurements were then taken using the thresholded images which were analysed using another piece of software, which used Minkowski functional measures (Houston et al., 2013b).

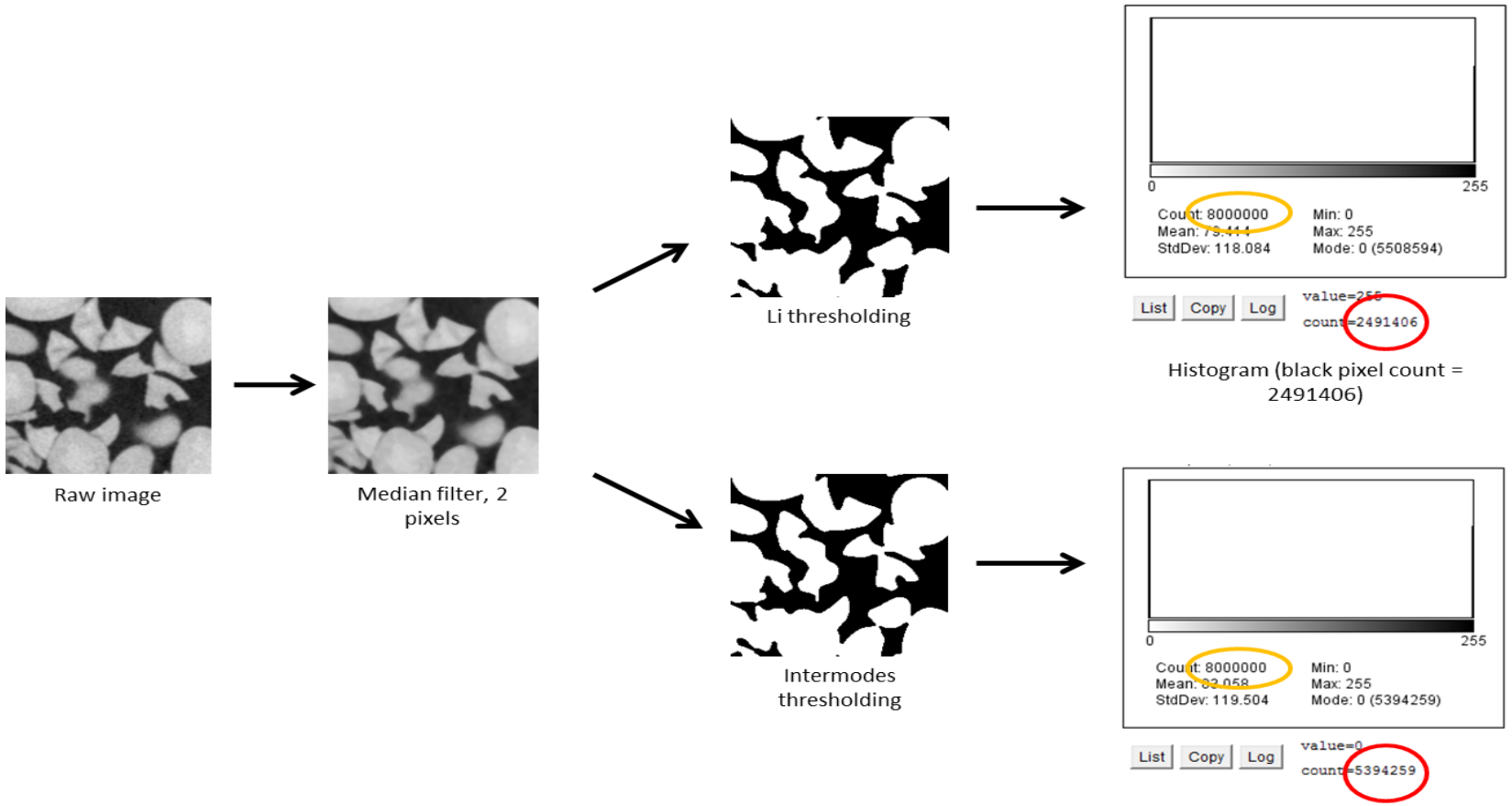

Total no. pixels – air count – particle count = water count
8000000 – 2491406 – 5394259 = 114335

Figure 4-3: The process involved in obtaining percentage particle, air and water by volume from µCT images of TS

4.4.5 Statistical analysis

Statistical methods for μCT images of roots, μCT images of TS and flatbed images of roots are described in sections 2.4.3.1.4, 2.4.3.2.3 and 2.4.3.4.2 respectively.

Data subsets were created according to the age of the roots in order to better understand differences in RSA between different **TS** particle size ranges at the time of seedling observation.

The soil variables were sorted into data subsets according to the particle size distribution present within each **TS** core. REML analysis was carried out on the **TS** variables with the week of sowing, the day of observation and the depth along the **TS** profile being included as random effects. Data subsets were also created according to the day of observation so that a broad understanding of any changes in the physical composition of the soil that occurred during the course of the week could be measured and understood. **TS** data sets were also stratified into data subsets according to the depth along the **TS** profile (0.51 cm sections, 7 sections descending from the top of the **TS** surface), so that comparisons could be made between different depths, to understand how this may change as the roots elongate down the soil profile.

TS subsets were created according to the age of the root at the time of imaging, so that the soil measurements could be directly compared with measured root variables.

4.5 Results

There were 76 roots present at the time of sowing the seedlings and 124 roots by the end of the time course. Root and soil measurements were taken at 24 hour intervals from the 3-D images obtained through µCT scanning.

4.5.1 Barley seedling root growth over time

Root data from the µCT images were split into subsets and mean values of all root variables were recorded. Figure 4-4 shows typical examples images of small, split pot and large seedlings imaged on days 1 – 5.

Figure 4-5 shows that root length increased the most in the small treatment, followed by roots in the split pot - small treatment, followed by those in the split pot - large treatment, followed by those in the large treatment, which did not grow during the time course. The convex hull volume also increased by far the most in the small treatment, followed by those in the split pot treatment, and finally those in the large treatment which did not increase during the time course. The same pattern was seen for root system width, however the roots in the small treatment spread the most between 48 and 72 hours, to a root system width of 27 mm, after which they did not increase dramatically between time points. This was because after reaching the edges of the specimen pots, the root systems could not spread any further, thus causing this measurement to level off much quicker than may be observed in a natural habitat, with unlimited space for root growth.

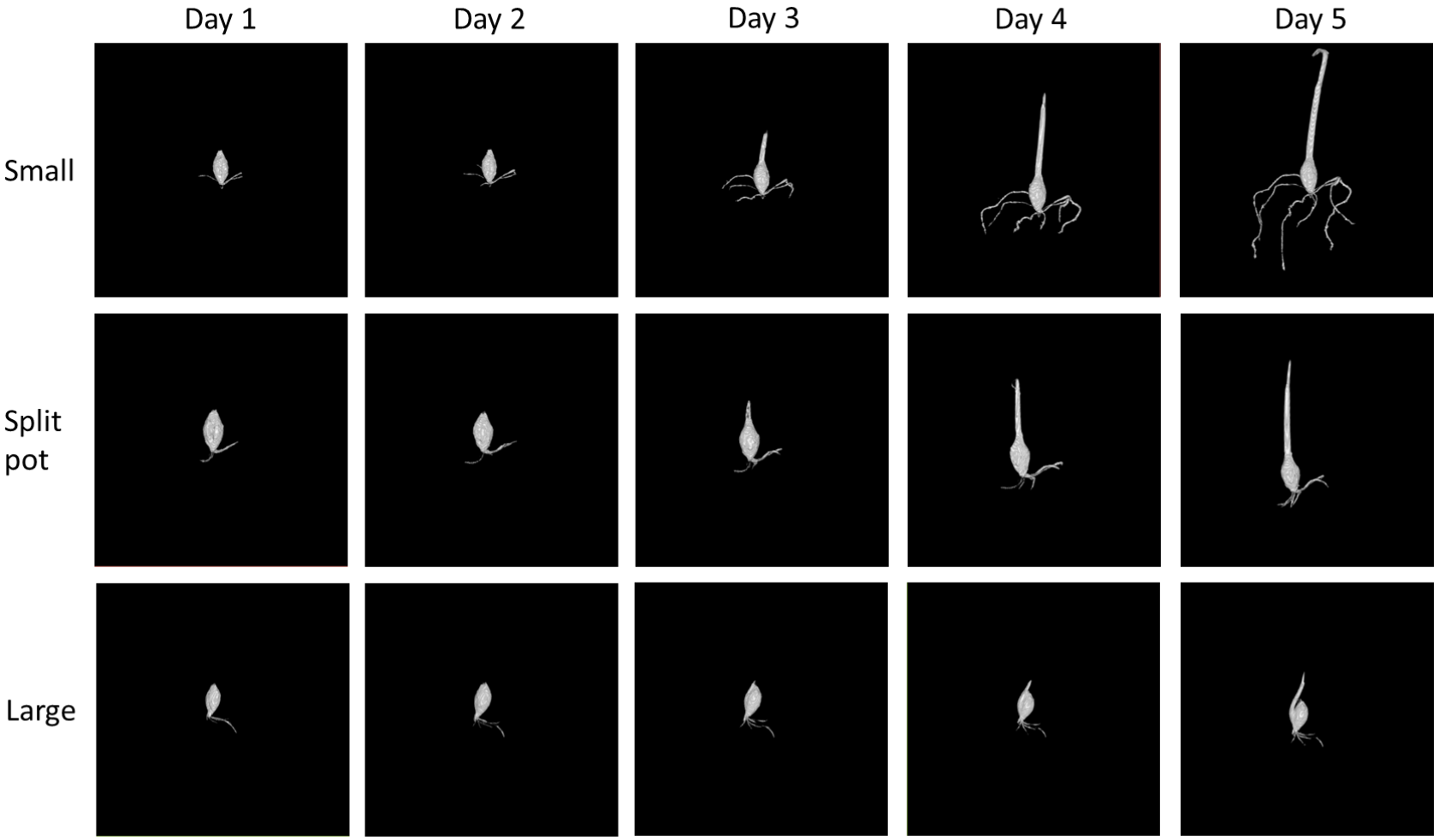

Figure 4-4: Typical examples of seedlings grown in small (top), split pot (middle) and large (bottom) TS cores on Days 1 - 5.

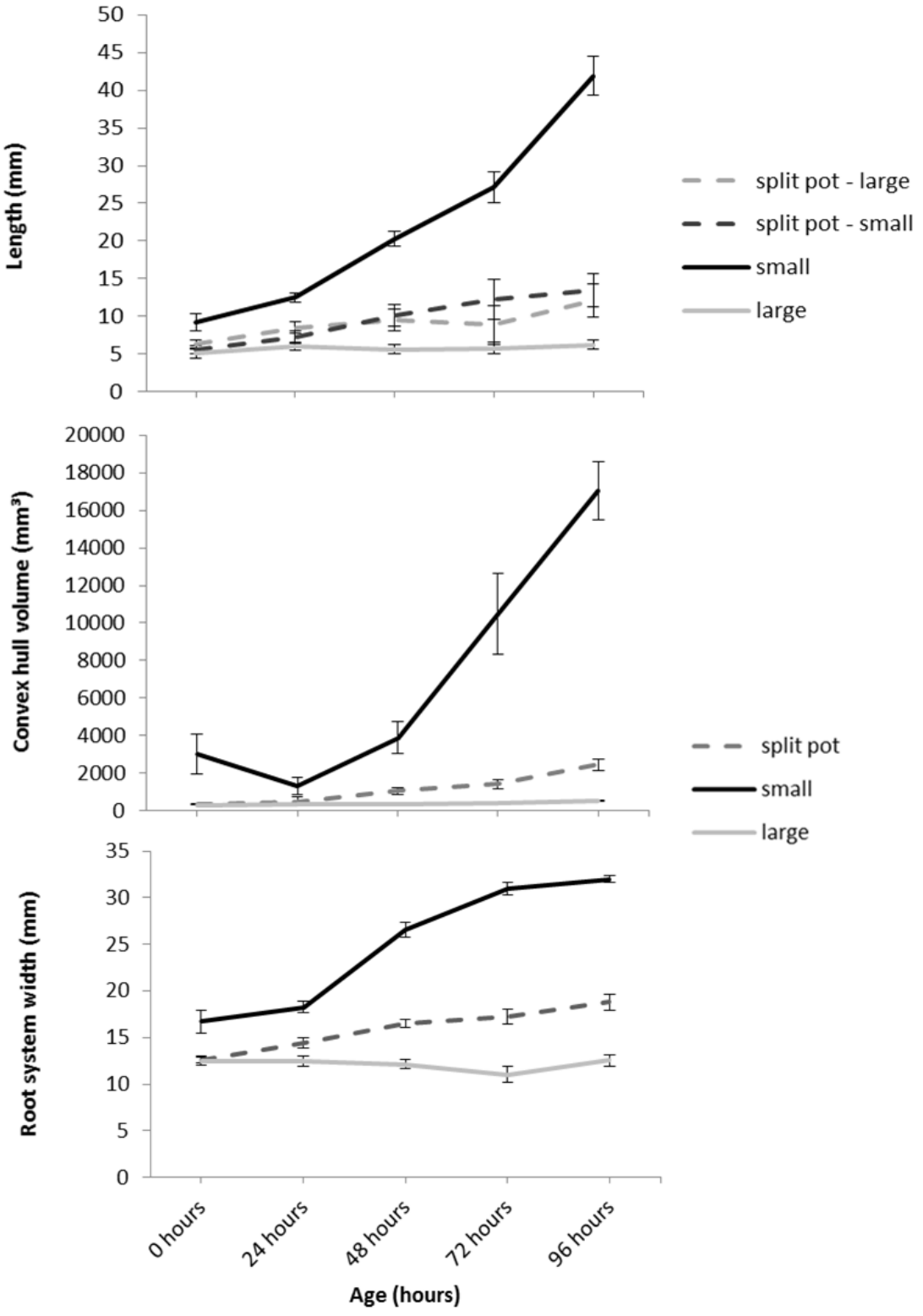

Figure 4-5: Average root length, convex hull volume and root system width with increasing root age, according to the position of the root tip at the time of imaging.

Statistically significant differences were seen between time points for root length ($p < 0.001$; $F = 52.26$), convex hull volume, ($p < 0.001$; $F = 32.15$) and root system width ($p < 0.001$; $F = 52.36$.

After transformation of the data, variables were tested for differences between treatments at each time point, the results of which are recorded in Table 4-2. At the beginning of the time course, no significant differences in root variables (length, curvature, verticality, convex hull volume, root system width) were observed between roots whose tips were present in different particle sizes at the time of imaging. The four particle sizes that seedlings could be present in were defined as split pot-small (**SS**), split pot-large (**SL**), small (**S**) and large (**L**) for the purposes of analysis. This changed later on, as is demonstrated in Table 4-2 and Figure 4-5.

As root growth progressed over the time course, the physical conditions surrounding the seedling influenced root growth greatly. Seventy-two hours after sowing, the effects were already visible and by the end of the time course, it was clear that the **L** treatment had an inhibitory effect on root growth. Seeds sown in the **S** treatment had longer roots ($p = 0.052$; $F = 2.72$) and greater convex hull volumes ($p = 0.001$; $F = 9.90$) and root system widths ($p = 0.021$; $F = 4.64$), demonstrating their abilities to better explore their surrounding soil volumes. Those in the split pots showed root growth inhibition also, however there were no differences between individual roots from the same seedlings growing in the **SS** or **SL** particle sizes.

Age (hours)	0		24		48		72		96	
Value	**P**	**F**	**P**	**F**	**P**	**F**	**P**	**F**	**P**	**F**
Length	0.689	0.49	0.682	0.5	**0.047**	**2.81**	**0.041**	**3.39**	0.052	2.72
Curvature (μm^{-1})	N/A	N/A	0.939	0.13	N/A	N/A	0.506	0.81	0.998	0.01
Verticality (˚)	N/A	N/A	1.000	0.00	0.797	0.34	0.300	1.31	0.826	0.30
Root system width (mm)*	0.863	0.25	0.441	1.02	0.090	2.86	0.092	10.07	**0.021**	**4.64**
Convex Hull Volume (mm^3)*	0.860	0.25	0.132	2.26	**0.043**	**3.93**	**0.002**	**5.07**	**0.001**	**9.90**

Table 4-2: Results of REML tests on transformed variables, according to age of roots. Significant values highlighted in bold. For each variable, the week of sowing, plant ID (for individual root measurements, not whole plant measurements) and age were treated as random effects. The treatment was included as a fixed effect.

Table 4-3 shows how roots were longest from early on when in the **S** treatment. At 0 hours of growth, roots in the **S** treatment were the longest (11.02 mm ± 1.2), being approximately double that of the next longest subgroup of roots; those in the **SL** treatment (7.64 mm ± 0.75). The next shortest subgroup of roots at 0 hours were those in the **SS** treatment (5.91 mm ± 0.69) and the shortest were those in the **L** treatment (5.38 mm ± 0.59). All of the treatments saw an increase in root length between 0 and 24 hours, with the **S** showing the greatest increase in length, followed by **SS**, followed by the **SL** treatment, and finally the **L** treatment. Between 48 and 72 hours, the same pattern between treatments was observed as at the beginning of the time course, with the **S** particle size roots being the longest, followed by the **SL** treatment, the **SS** treatment, and finally the **L** particle treatment which began to decrease in length. At 96 hours, the **S** roots were by far the longest (42.28 mm ± 2.67), followed by the **SS** (13.50 mm ± 2.17), followed by the **SL** roots (12.13 mm ± 1.02), followed by the **L** roots (6.16 mm ± 0.59), which at the final time point were continuing to decrease in length.

Sub-group	0 hours	24 hours	48 hours	72 hours	96 hours
Small	**11.02 ± 1.2**	**16.09 ± 1.5**	**20.24 ± 1.07**	**26.25 ± 2.22**	**42.28 ± 2.67**
Split pot – small	**5.91 ± 0.69**	**9.38 ± 1.51**	**10.39 ± 1.64**	**8.68 ± 2.06**	**13.50 ± 2.17**
Large	**5.38 ± 0.59**	**6.53 ± 0.58**	**6.63 ± 0.68**	**6.34 ± 0.69**	**6.16 ± 0.59**
Split pot – large	**7.64 ± 0.75**	**8.91 ± 0.78**	**10.21 ± 1.00**	**10.57 ± 0.67**	**12.13 ± 1.02**

Table 4-3: Mean values of root length (mm) according to the roots' ages and TS treatments. Green values show an increase since the previous time point; red values show a decrease since the previous time point.

Table 4-4 shows that the curvature varied more over the course of the week in roots growing in the **L** treatment, ranging between 0.027 (least curved) and 0.013 μm^{-1} (most curved). The other treatments maintained a curvature of between 0.012 μm^{-1} and 0.017 μm^{-1}.

Sub-group	0 hours	24 hours	48 hours	72 hours	96 hours
Small	**0.015 ± 0.001**	**0.012 ± 0.000**	0.012 ± 0.001	**0.015 ± 0.003**	**0.011 ± 0.000**
Split pot – small	**0.017 ± 0.002**	**0.015 ± 0.002**	**0.014 ± 0.001**	**0.017 ± 0.003**	**0.014 ± 0.002**
Large	**0.015 ± 0.001**	0.015 ± 0.002	**0.027 ± 0.01**	**0.013 ± 0.003**	0.013 ± 0.001
Split pot – large	**0.016 ± 0.003**	**0.014 ± 0.002**	**0.012 ± 0.002**	**0.013 ± 0.001**	0.013 ± 0.001

Table 4-4: Mean values of root curvature (μm^{-1}) according to the roots' ages and TS treatments. Green values show an increase since the previous time point whereby the root is straightening out along the vertical plane, red values show a decrease since the previous time point, whereby the root is curving along the vertical plane.

Table 4-5 shows mean values of verticality over time. Although significant differences for verticality were not detected between treatments, trends were identified which are outlined below. In the **S** treatment, root verticality was 73.44˚ ± 4.15 at 0 hours of growth. **S** verticality remained above 70˚ until 72 hours growth, after which, the roots started to show a steady decline in verticality, finishing at 59.94˚ ± 2.1. Roots in the **S** treatment were the most vertical of the four treatments by the end of the time course. The **L** treatment began at 0 hours with a higher average verticality (77.68˚ ± 4.71) than the **S** treatment, which gradually increased over the time course. At 96 hours, the average verticality of **L** roots was 87.84˚ ± 5.08; almost 30˚ further away from the vertical vector than roots in the **S** treatment. The split pot treatments behaved more erratically, ranging between 67.83˚ ± 6.13 and 91.9˚ ± 7.85, however at 96 hours they were approximately halfway between the **S** treatment and the **L** treatment.

Sub-group	0 hours	24 hours	48 hours	72 hours	96 hours
Small	73.44 ± 4.15	75.63 ± 0.007	73.74 ± 4.16	66.47 ± 4.7	59.94 ± 2.1
Split pot - small	70.31 ± 6.86	77.24 ± 5.07	70.60 ± 5.56	67.83 ± 6.13	71.83 ± 4.3
Large	77.68 ± 4.71	82.53 ± 4.16	79.63 ± 3.09	89.88 ± 4.96	87.84 ± 5.08
Split pot - large	77.56 ± 5.82	76.3 ± 6.61	78.52 ± 5.31	81.67 ± 6.58	74.12 ± 5.47

Table 4-5: Mean values of verticality (°) according to the roots' ages and TS treatments. Green values show an increase since the previous time point whereby the root is deviating away from the vertical plane, red values show a decrease since the previous time point, whereby the root is closer to the vertical plane.

4.5.2 The differences in physical composition between particle size ranges of TS

Figure 4-6 shows typical images of the air, water and particles contained within TS cores segmented and reconstructed in 3-D.

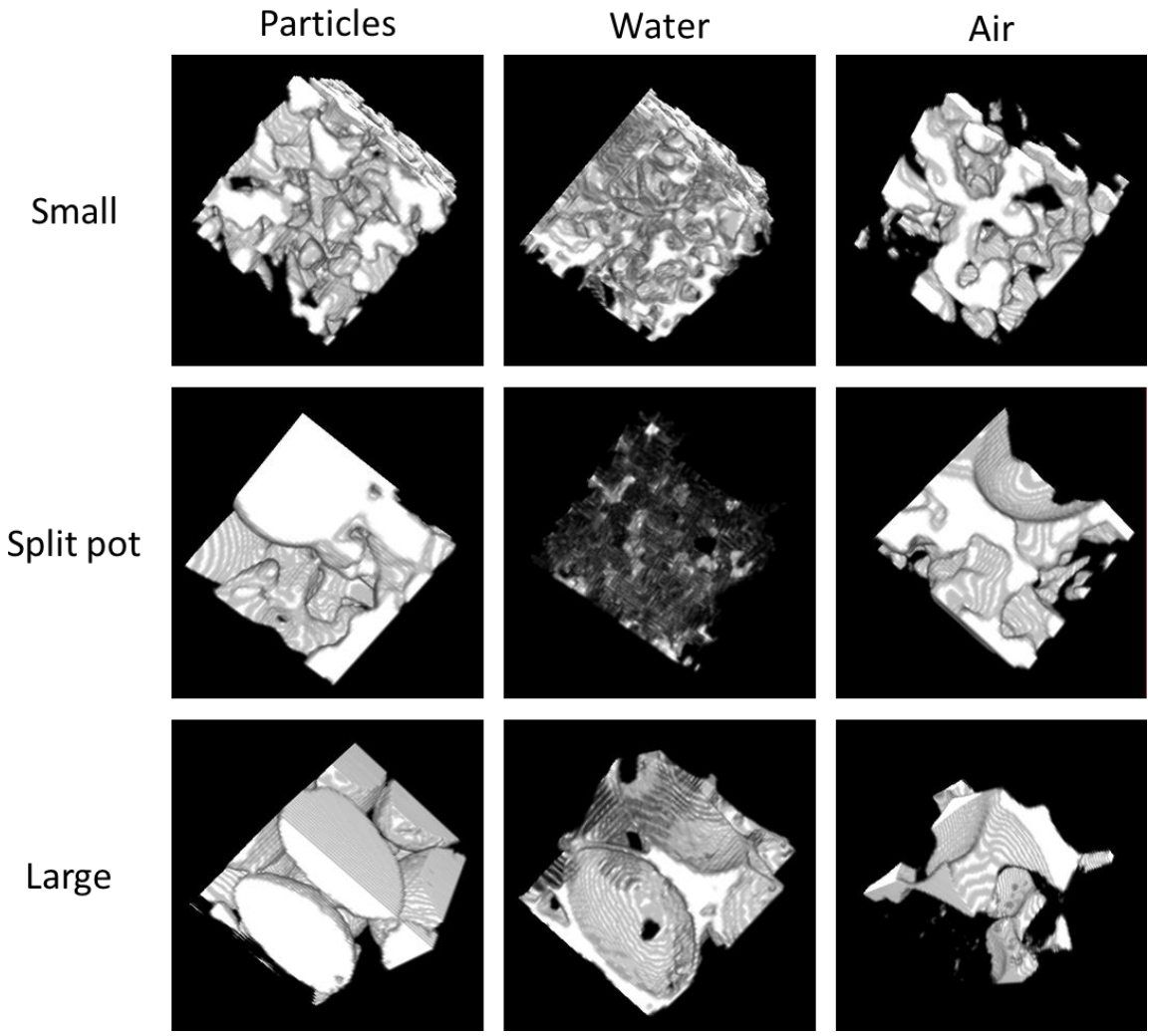

Figure 4-6: Typical examples of particles (left), water (centre) and air (right) of TS cores containing small (top), split pot (middle) and large (bottom) particles. Resolution, 51µm.

Figure 4-7 summarises the average values for percentage air, water and particle by volume of the three different treatments. The average air percentage by volume was 34.30% ± 0.85 for the **S** treatment, 31.31% ± 0.58 for the **L** treatment and 33.49% ± 0.54 for the split pot treatment. The average water percentage by volume was 12.47% ± 1.15 for the **S** treatment,

9.5% ± 0.77 for the **L** treatment and 9.8% ± 0.54 for the split pot treatment. The average particle percentage by volume was 53.19% ± 0.77 for the **S** treatment, 59.54% ± 0.76 for the **L** treatment and 56.66% ± 0.40 for the split pot treatment.

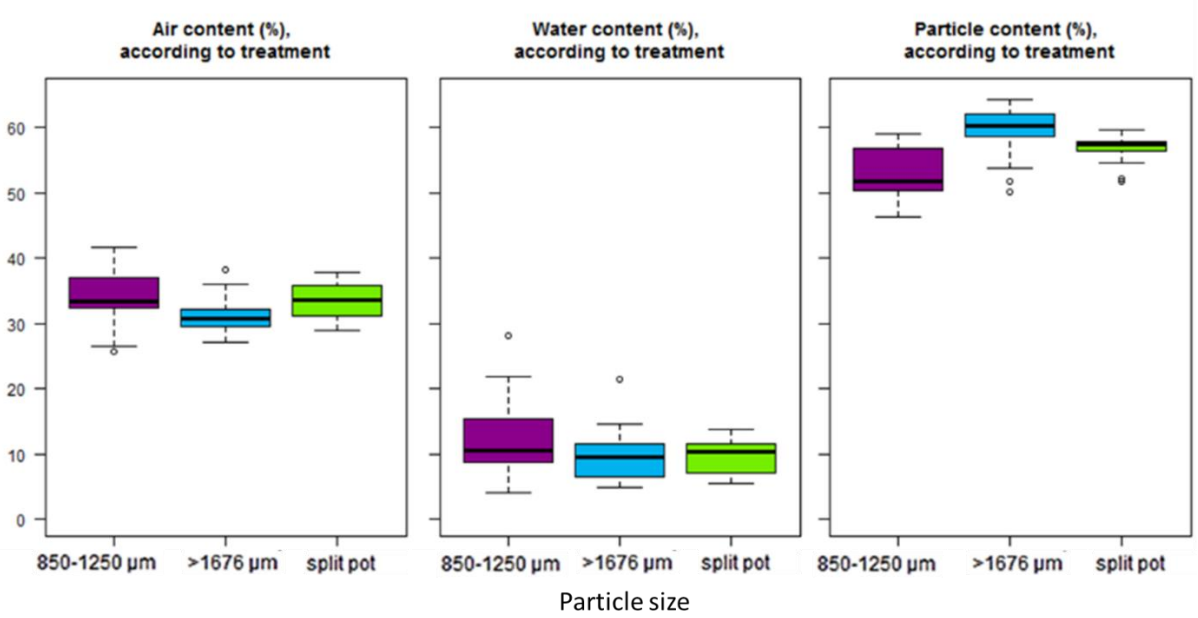

Figure 4-7: Average percentage air, water and particle by volume of the small, large and split pot TS treatments.

Table 4-6 shows statistically significant differences between treatments for air content, water content and particle content.

	Air content (%)	Water content (%)	Particle content (%)
p value	**0.001**	**0.023**	**<0.001**
F value	7.64	4.0	22.08

Table 4-6: REML results for percentage air, water and particle by volume, when separated by treatment. Week, Core ID and Day of imaging were included as random effects, treatment was included as the fixed effect. Significant figures highlighted in bold.

Figure 4-8 shows connectivity and total porosity values for the three different TS treatments. Porosity was 31.99 % ± 1.06 for the S treatment, 32.88% ±0.58 for the L treatment and 29.89% ± 0.78 for the split pot treatment.

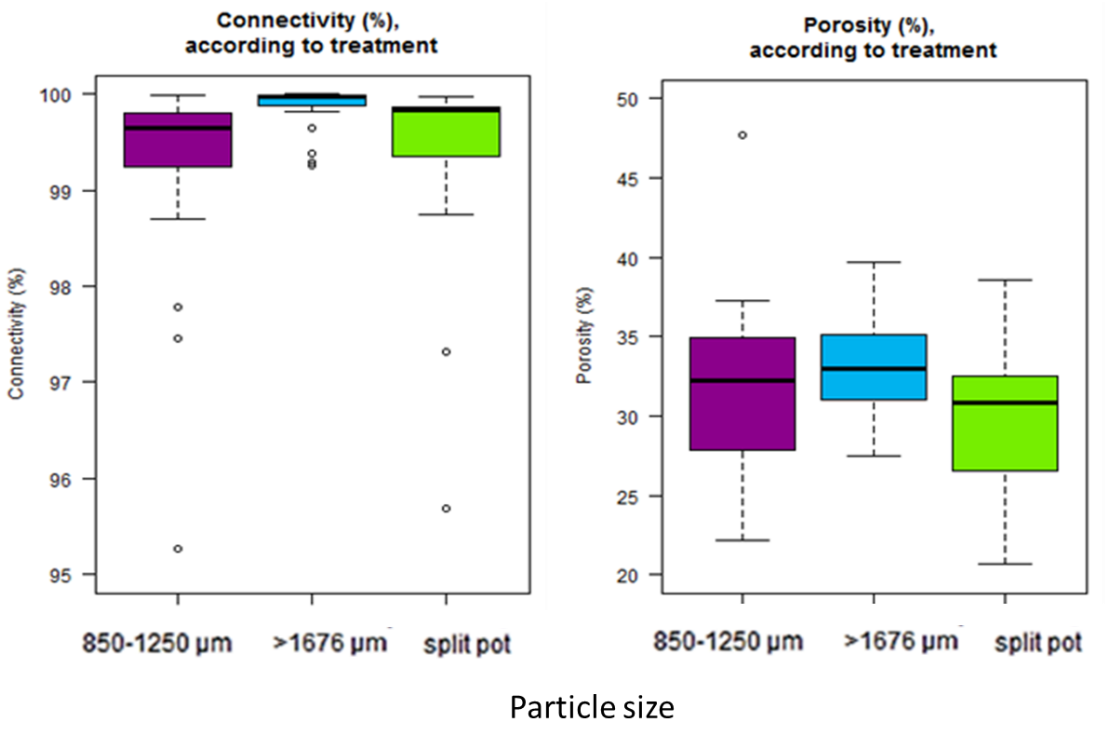

Figure 4-8: Average connectivity and porosity (%) of the small, large and split pot TS treatments.

Table 4-7 shows the statistical results for differences between the treatments in connectivity and total porosity. No significant differences were recorded between treatments for connectivity, which was 99.37% ± 0.15 for the entire dataset.

	Connectivity (%)	**Porosity (%)**
p value	0.061	**0.030**
F value	2.93	3.69

Table 4-7: REML results for connectivity and porosity of TS (%), when separated by treatment. The Week, Core ID and Day of imaging were included as random effects. Treatment was included as a fixed effect. Significant figures highlighted in bold.

Figure 4-9 shows boxplot summaries of largest pore surface area and largest pore volume, according to **TS** treatment. The mean average largest pore surface area was 41171 mm^2 ± 1853 for the **S** treatment, 28442 mm^2 ± 1337 for the **L** treatment and 35815 mm^2 ± 1004 for the split pot treatment. The mean average largest pore volume was 126185.5 mm^3 ± 3871.847 for the **S** treatment, 132828.1 mm^3 ± 2052.601 for the **L** treatment and 121465.4 mm^3 ± 2999.84 for the split pot treatment.

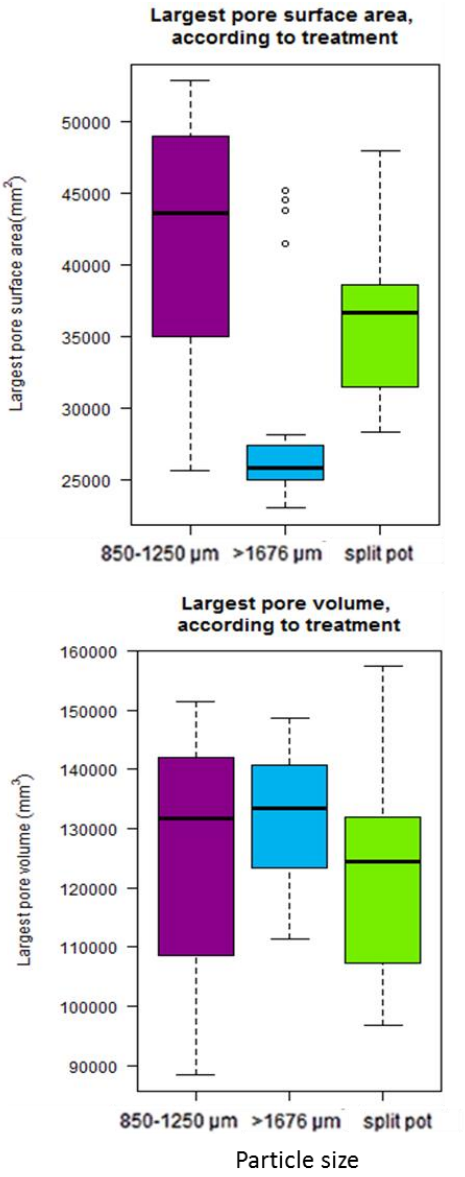

Figure 4-9: Largest pore surface area (mm^2) and largest pore volume (mm^3) of all small, large and split pot TS cores.

Table 4-8 summarises the REML test results for largest pore surface area and largest pore volume area when separated by treatment, both of which were statistically significant.

	Largest pore surface area (mm^2)	**Largest pore volume (mm^3)**
p value	**<0.001**	**0.025**
F value	23.40	3.90

Table 4-8: REML results for largest pore surface area and largest pore volume, by treatment. Week, Core ID and Day of imaging were included as random effects. Treatment was included as a fixed effect. Significant figures highlighted in bold.

In summary, the **S** treatment contained the most air, the most water and the lowest particle volume, compared to the other treatments. Its porosity was between that of the **L** and split pot treatments. It also had largest pore surface areas with the highest values compared to the other treatments and its largest pore volume on average was in between that of the **L** and the split pot treatments. The **L** treatment contained the least air and water but the most particle volume. It had the highest total porosity of the three treatments and its largest pore surface area was the smallest of the treatments. The largest single pore volumes of the **TS** cores containing the **L** treatment were the largest of the three treatments. The percentage air, water and particle by volume of the split pot treatments were between those of the **S** and the **L** treatments. Porosity of the split pot cores was the lowest of the three treatments. The largest pore surface areas of the split pot cores were in between those of the **S** and **L** treatments. The largest pore volumes of the split pot cores were the smallest of the three treatments.

4.5.3 Spatial differences in the physical composition of TS

Figure 4-10 shows the differences in percentage particle by volume between the three treatments. The **S** treatment contained approximately 50% of solid particles, being the

smallest solid proportion of the three treatments. Solid particles made up approximately 60% of the **L** treatment and around 55% of the split pot treatment. Percentage air by volume generally decreased with depth for all three treatments and showed the greatest decrease between 1.3 cm and 1.82 cm of depth. The **L** treatment contained the lowest percentage air by volume, beginning at approximately 35% at the top of the TS core and ending at approximately 20% at a depth of 1.82 cm. The **S** treatment had the greatest percentage air by volume, containing approximately 45% air at the top of the profile and ending with around 30% at 1.82 cm depth. The split treatment was in between the two treatments at the top of the profile, containing approximately 40% air, but showed a lesser decrease along the profile, ending with around 35% air by volume at 1.82 cm depth. Percentage water by volume generally increased with depth along the **TS** profile, with the greatest increase being seen between 1.3 and 1.82 cm of depth. The **L** treatment showed the lowest water concentration for most of the depth, beginning at approximately 5% at the top of the profile and ending with around 20% water concentration at 1.82 cm depth. The **S** treatment generally contained a higher volume of water throughout the profile compared to the other two treatments. The split pot treatment was the most consistent with depth, containing approximately 5% water at the top of the **TS** profile and ending with around 10% water at 1.82 cm depth. Throughout much of the profile, this treatment was somewhere between the other two.

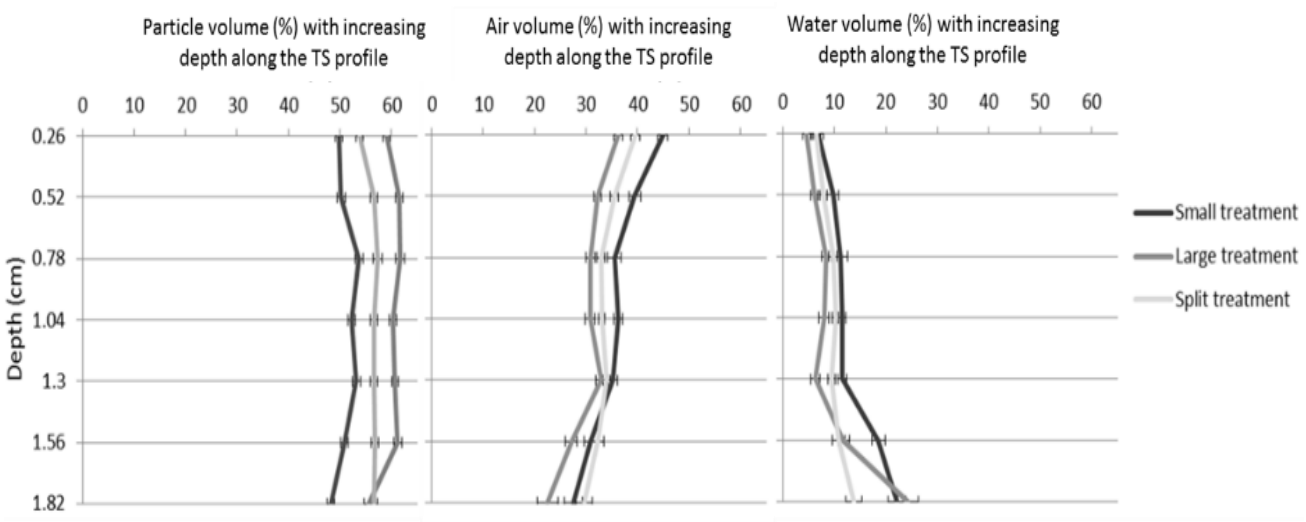

Figure 4-10: Changes in percentage particle, air and water by volume with increasing depth along the TS profile.

The findings described in Figure 4-10 are further supported by Table 4-9, which shows the statistically significant differences between treatments for particle, air and water content with increasing depth down the **TS** profile. Significant differences were present along the entire depth profile for percentage particle by volume. For percentage air by volume, the differences were also largely significant for much of the profile, but began to become less significant towards increasing depth. Differences in percentage water by volume were not significant between treatments at the top of the **TS** profile, but significant differences were seen as depth along the profile increased.

Depth (cm)	Particles	Air	Water
0.26	**< 0.001**	**<0.001**	0.247
0.52	**<0.001**	**<0.001**	**0.005**
0.78	**<0.001**	**0.010**	0.183
1.04	**<0.001**	**<0.001**	**0.025**
1.30	**<0.001**	0.170	**<0.001**
1.56	**<0.001**	**0.012**	**<0.001**
1.82	**0.003**	**0.022**	**0.007**

Table 4-9: One-way ANOVA results testing significant differences between treatments at different depths along the TS profile for particles, air and water. Week, core ID and hour of imaging were random effects. The treatment was a fixed effect. Significant figures highlighted in bold.

4.5.4 The relationship between root system architecture and TS over time

Following detailed separate analysis of soil and root properties, properties were combined to try and understand the physical relationship between the two.

Figure 4-11 (a) shows root length vs. the particle volume within TS cores and Figure 4-11 (b) shows root length vs. root/soil contact. All roots that achieved elongation of greater than 20 mm within 96 hours were of the **S** treatment or the **SS** treatment. These **TS** cores all contained 45 – 55% particle volume and had 20 - 80% contact with the root systems. Root elongation was most successful at approximately 50% particle volume and 50% root/soil contact. Although the large and split pot large **TS** cores contained greater particle volumes of 58 – 68%, they had much lower levels of root/soil contact; between 2 and 20%.

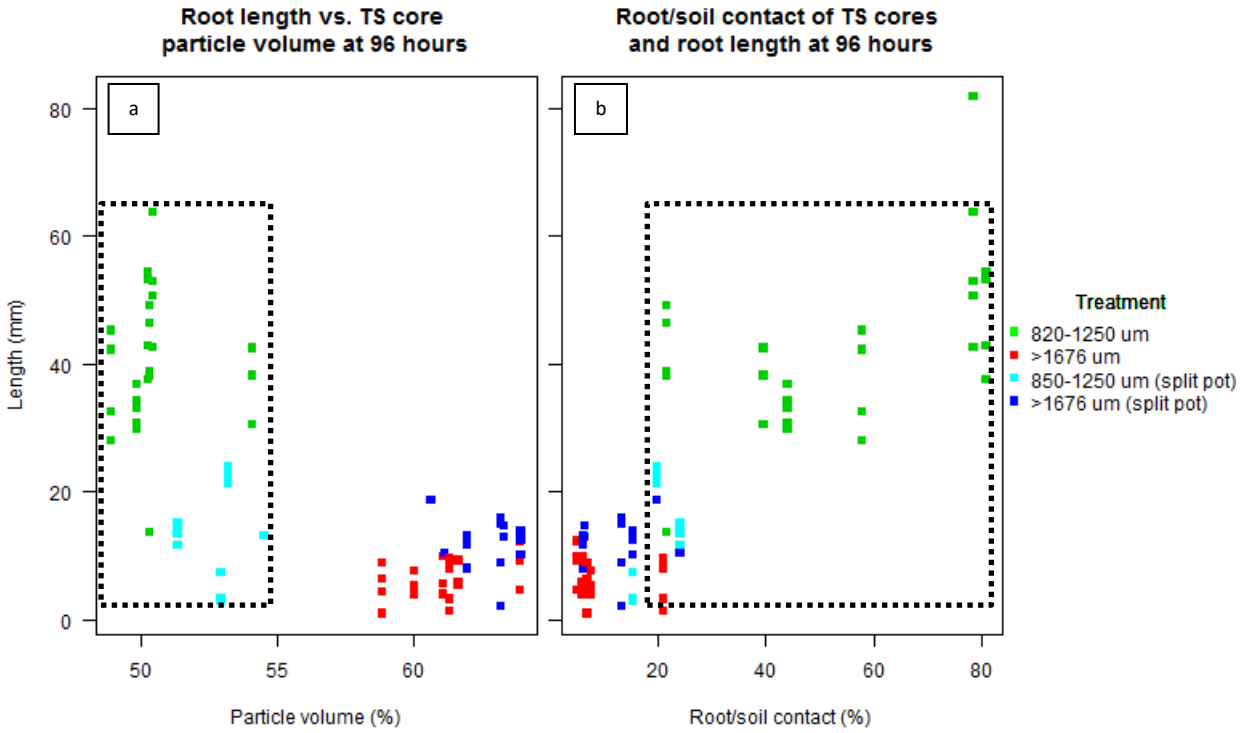

Figure 4-11: Root length at 96 hours of growth vs. particle volume (a) and root/soil contact (b). The region within the dotted squares shows the area whereby roots elongated above 20 mm.

The final measurements taken at the end of the time course were used in order to obtain correlation coefficients for the root/soil relationship. Root/soil contact was identified as being highly important, showing significant relationships with a number of root system architecture variables. There was a strong negative correlation between the percentage particle by volume of TS cores and root length (-0.87, $p < 0.001$). The correlation between root length and percentage particle by volume was stronger than that of length x percentage air by volume (0.64, $p < 0.005$) and length x percentage water by volume (0.37, $p = 0.127$). The correlation coefficient for length x root/soil contact was 0.85, $p < 0.001$. Verticality showed a strong correlation with percentage particle by volume (0.77, $p < 0.001$) and slightly weaker correlations were seen with percentage air by volume (-0.69, $p < 0.005$) and root/soil contact (-0.64, $p < 0.005$). Root system width was also strongly correlated to percentage particle by volume (-0.82, $p < 0.001$) and root/soil contact (0.78, $p < 0.001$). Convex hull volume showed a strong correlation with percentage particle by volume (-0.79, $p < 0.001$) and root/soil contact (0.91, $p < 0.001$).

Figure 4-12 shows examples of typical root systems inside the small, large and split-pot particle size treatments at the end of the time course in E.v.

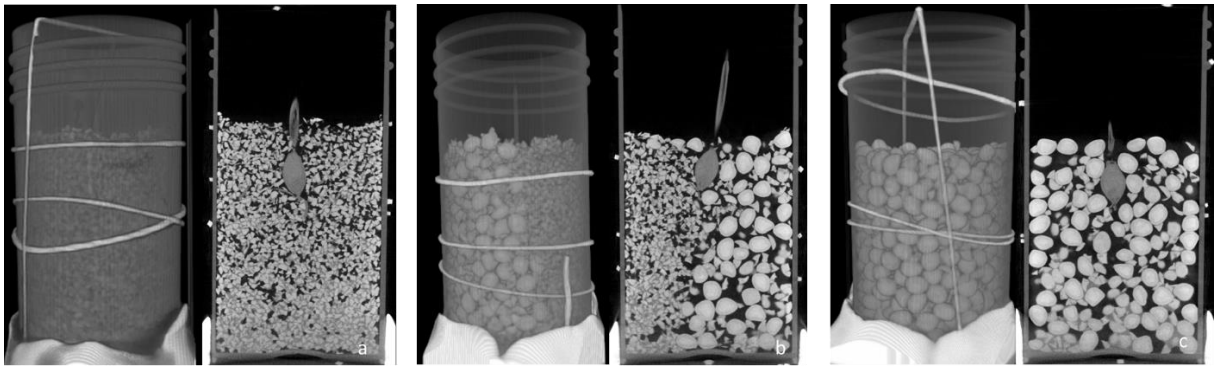

Figure 4-12: Typical examples of 3-D μCT images of TS cores and 2-D cross-sections of root systems grown in small (a) large (b) and split pot (c) treatments. Images taken on day 5 of time course. Resolution, 51μm.

As can be seen in Figure 4-13, root/soil contact was highest for the roots in the **S** treatment from Day 1 of the time course, being between 10.55 and 40.59%. For the split pot treatment, root/soil contact was between 4.79 and 16.24% and for the **L** treatment, root/soil contact was between 4.00 and 16.96%. By day five, root/soil contact was between 21.71 and 80.84% for the **S** treatment, so had increased by 100% over the course of the week. Root-soil contact for the split pot treatment was between 6.28 and 24.26% on day five, so had increased by between 30 and 50%. Root-soil contact for the **L** particle size treatment was between 5.18 and 21.03%, so had increased by around 20 - 30%.

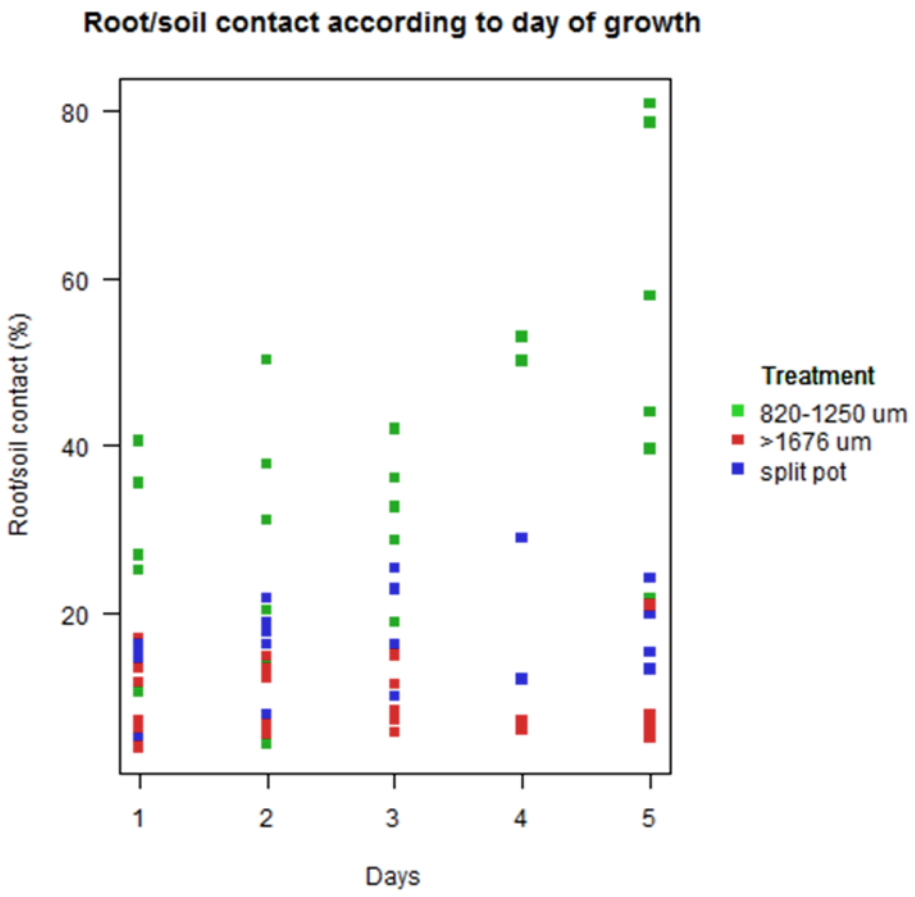

Figure 4-13: Root/soil contact of whole root systems for each day of growth.

.

4.5.5 Patterns of barley root exploration over time

Figure 4-14 compares the number of root tips present in each region of the split pot cores with increasing root age. At 0 hours, there were 13 root tips present in the large particle region of the split pot cores and 13 in the small region. At 24 hours there were 17 present in the large particle region and 18 in the small particle treatment. At 48 hours, roots began to show a preference for the large region of the cores, where there were 19 root tips present and only 14 in the small particle region. At 72 hours there was a lower count of roots due to technical problems with the µCT scanner resulting in some cores not being imaged, however of those that were imaged, 9 root tips were present in the large section of the split pots and 7 were present in the small section. At the end of the week there were 23 root tips in the large particle region and 19 in the small particle region.

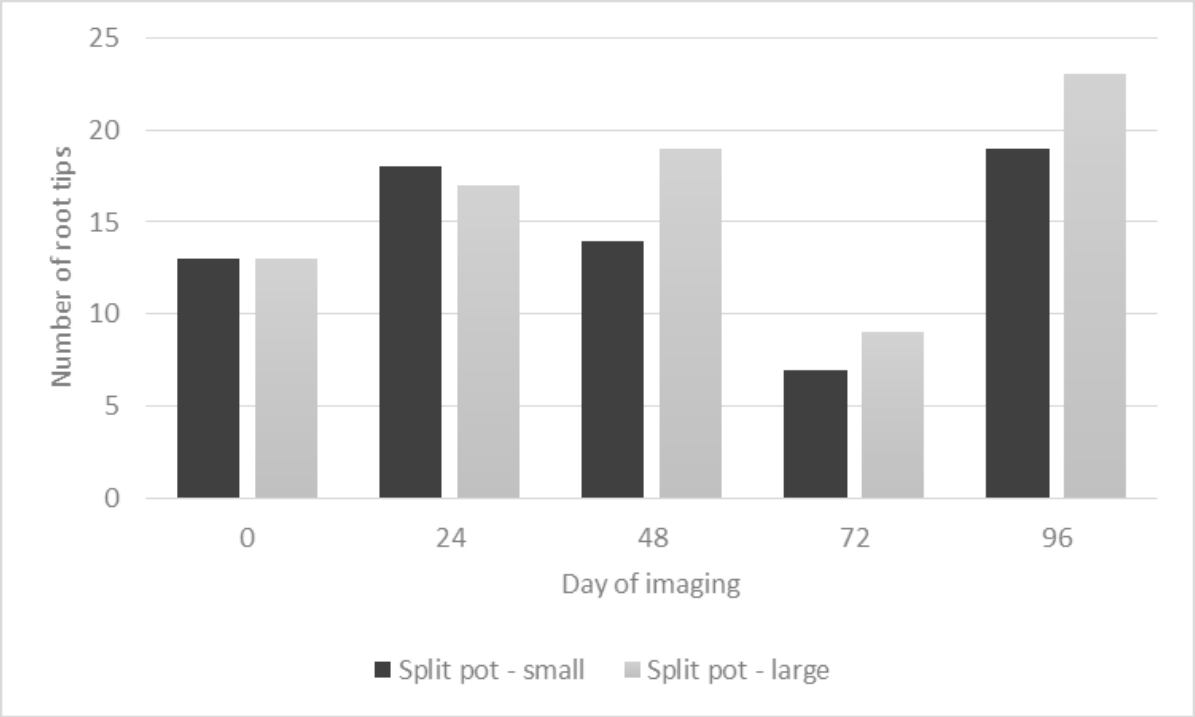

Figure 4-14: Number of root tips present in each region of the split pots with increasing root age.

Figure 4-15 shows the verticality measurements of roots along the depth profile. The trend lines show that roots on average began at approximately 80˚ and then decreased in verticality (i.e. showed more positive gravitropism), when they initially emerged from the seed. The **S** treatment showed a steady decrease in verticality values up until roots reached an average of around 50˚, which occurred approximately 20 mm along the depth profile from where the seed ended and the root began. At this point a steady increase was then seen (i.e. less positive gravitropism), up until measurements ended at approximately 45 mm, with the roots showing an average verticality of approximately 70˚. A similar pattern was seen with the other treatments, however the point at which the roots reached an average verticality of around 45-50˚ and then began to increase in verticality occurred sooner. In the **L** treatment, this was seen at around 6 mm of distance from the seedling; in the **SL** treatment it was seen at approximately 10 mm and for the **SS** treatment it was seen at around 8 mm. In the **L** and the **SS** treatments the verticality rose until it reached around 70˚ and then began to decrease again until measurements ceased to be taken at around 7 mm for the **L** treatment and 13 mm for the **SS** treatment. The verticality of **SL** roots continued to rise until the end of the time course, reaching around 85˚. The longest roots from this treatment were around 13 mm.

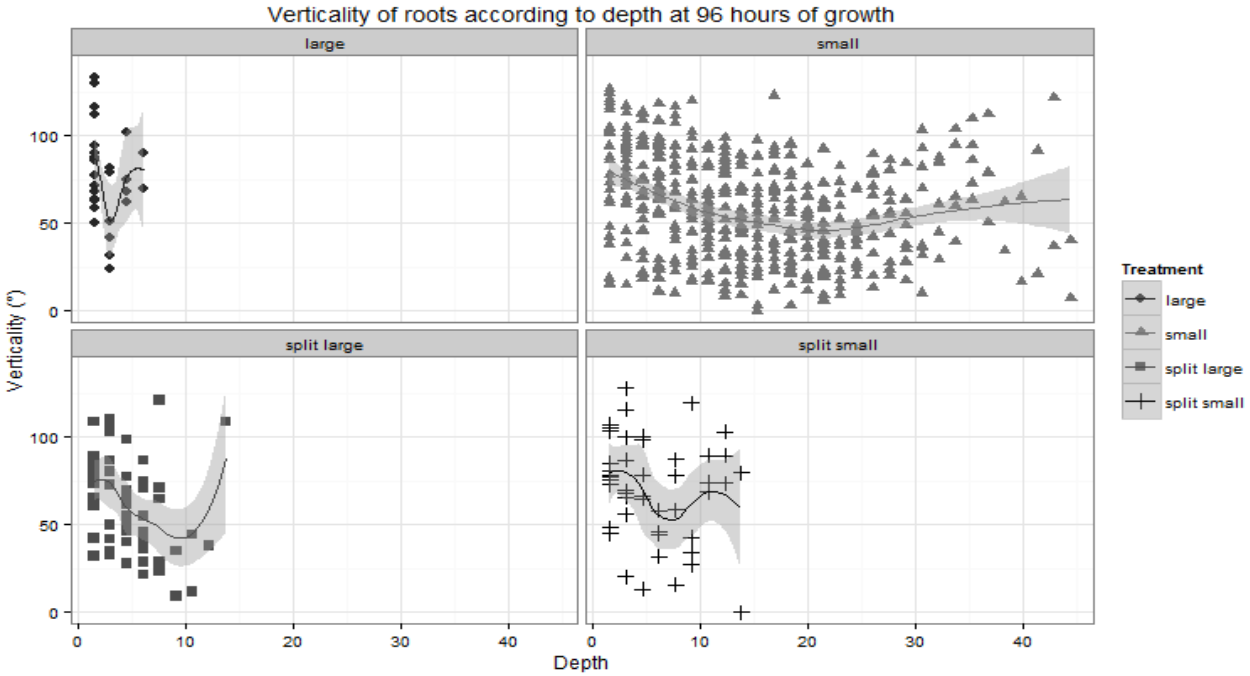

Figure 4-15: Verticality measurements of roots along the depth (mm) of the soil profile. 0 represents the junction at which the seed ends and the root begins. Each plot shows a different treatment and contains a trend line; grey areas show 95% confidence interval, points show average root verticality values.

Figure 4-16 shows curvature measurements along the depth of the **TS** profile. In the **S** treatment, curvature was approximately 0.01 μm^{-1} for the duration of the time course. For the other three treatments average curvature began at approximately 0.01 μm^{-1} as well; however it increased initially in the **L** particle treatment, reaching 0.025 μm^{-1} at approximately 4 mm of depth before showing a steep decrease to almost 0.00 μm^{-1} at around 6 mm. The **SL** treatment showed a gradual increase in curvature to approximately 0.0125 μm^{-1} at 8 mm depth and then decreased to around 0.010 μm^{-1} at around 13 mm depth. The **SS** treatment showed minor decreases and increases in curvature until approximately 10 mm depth, at which point it began to increase substantially to reach almost 0.025 μm^{-1} at around 13 mm depth.

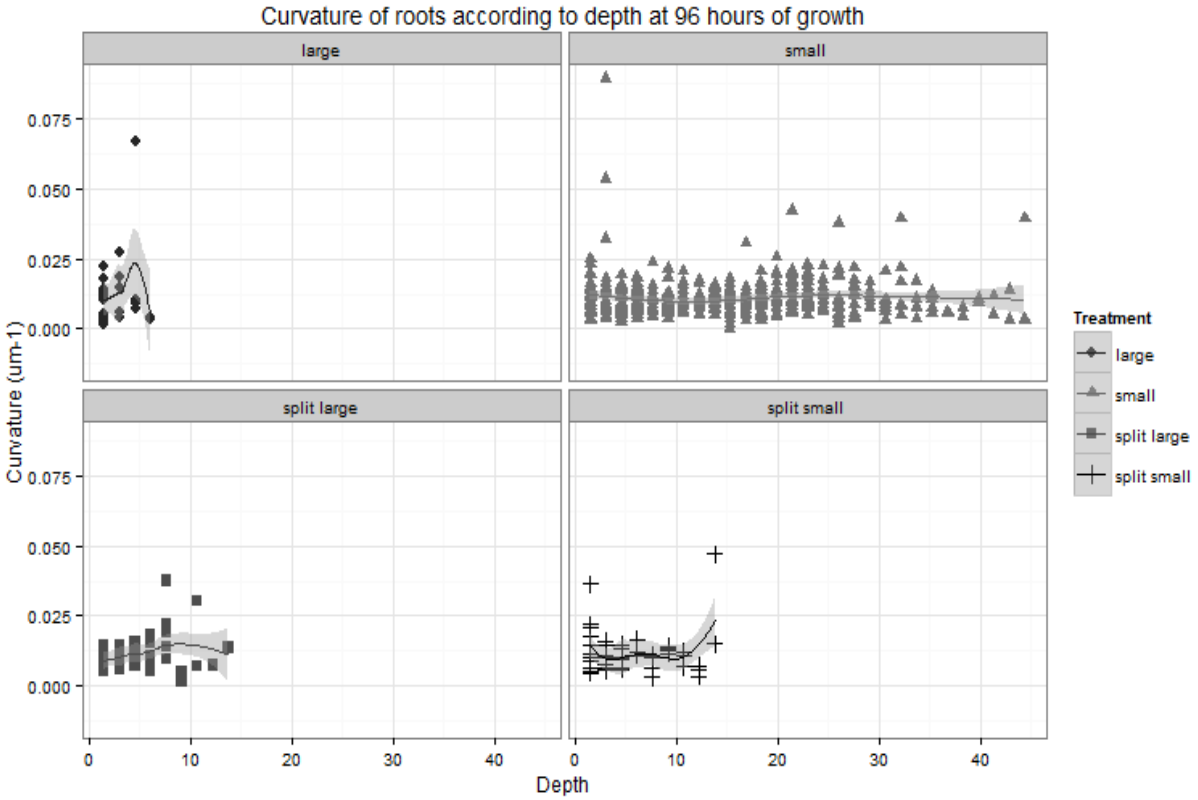

Figure 4-16: Curvature measurements of roots along the depth (mm) of the soil profile after 96 hours of growth. 0 represents the junction at which the seed ends and the root begins. Each plot shows a different treatment and contains a trend line; grey areas show 95% confidence interval, points show average root curvature values.

4.6 Discussion

4.6.1 Discussion of methods

Due to a lack of published methodology and experience of using **TS** as a growth medium, each chapter has resulted in adjustment and further development of the methods used. Aspects of the methodology used in this experiment are discussed in this section.

At 24 hour intervals, the cores were removed from the incubator, imaged using the µCT scanner and returned to the incubator. This was done while the light in the incubator was switched on and the seedling was only removed for one hour each day for the purposes of imaging. Due to the small size of the **TS** cores and the length of time that they were removed, it is possible that the temperature within cores increased from 15˚C to room temperature during that hour each day. The change in light between the incubator and the µCT scanner for 1 hour everyday may have also had an effect, as fluctuating light intensities have been shown to affect the direction of root growth (Galen et al., 2007). There was no way of avoiding this process and it was necessary in order to observe root growth in situ at regular time intervals over a time course. There is a paucity of literature with regards to regular removal of plant seedlings from an incubator for the purposes of obtaining measurements using µCT during time-lapse experiments; however it is known that changes in temperature and light can affect seedling growth and root system development (Al-Karaki et al., 2007, Kiss et al., 2007, Al-Ani and Hay, 1983).

There is a possibility that repeated µCT scanning could influence the way that barley seedling roots grow, as it has been observed that plant species are affected by repeated radiation in different ways (Zappala et al., 2013). Dhondt et al. (2010) observed reduced root growth in

arabidopsis seedlings that were repeatedly scanned. Johnson (1936) also observed that high levels of radiation (33 Gy) had a negative impact on root growth. Most modern CT scanners use much lower levels of radiation (<1.5 Gy).and therefore the effects of repeated radiation exposure on germinated plant seedlings are likely to be minimal (Zappala et al., 2013).

In a recent study, it was found that high flux X-ray imaging in a synchrotron reduced chlorophyll activity in plants, therefore possibly having an effect on root growth. When samples were exposed for one hour they observed condensation on the inside of the tube (Karunakaran et al., 2015). The presence of condensation occurs due to heating of the sample during long exposure imaging in a synchotron (Vijayan et al., 2015). No condensation was seen during this experiment. In older experiments µCT scanning of roots at regular intervals was not found to affect growth of wheat plants (Flavel et al., 2012), however during that experiment the plants were exposed to a maximum of 20 minutes, 50 seconds of µCT radiation over a period of 18 days. The seedlings in this experiment were much younger and in order to obtain high quality images, they were exposed to an hour of µCT scanning every day for 5 days. The results from this experiment were not noticeably unusual or unexpected when compared with other µCT experiments that were carried out during this project, therefore indicating that repeated exposure to radiation for one hour per day did not noticeably affect root growth. It should also be noted that due to problems with the µCT scanner, a number of measurements was missed at the 72 hour time point. Whilst little could be done about this, and the general trends in the data are maintained even with the missing data from weeks 1 and 3, a full data set would have been preferable for the purposes of statistical analysis.

Root/soil contact is an important parameter for root growth at the seedling stage (Schmidt et al., 2012). In this study, the root/soil contact measurements were obtained using the whole root system of the plant, rather than individual roots. The whole root system was used because limitations existed due to data size and the length of time taken to process images containing multiple primary roots. Computers at present are too slow to compute this kind of information in a timely manner and the algorithms used for segmentation tools such as Region Grower in VGStudioMax2.2 are not yet sophisticated enough to identify individual roots. Ideally, image analysis would focus on the individual roots to confirm the interaction between the roots and their local environments.

4.6.2 Discussion of results

The development of the **TS** system and image analysis techniques during this project has enabled us to obtain highly detailed root and soil measurements (e.g. verticality, curvature time-dependent observation of root tip position in 3-D, physically heterogeneous root growth mediums) that were previously unobtainable. This information has allowed us to observe the growth patterns observed as roots grow in different physical **TS** structures over time. It was discovered that growth across the entire root system is affected by physically sub-optimal soil structure and that roots preferentially choose the path of least resistance (larger pores), even if the pores are so large that it is detrimental to root growth.

Hussain et al. (1999) found significant differences in the root mass of tomato plants that had been grown in vertically-stratified split pots containing soils of different strengths and Montagu et al. (2001) observed compensatory growth of roots on the side of the core containing loosely compacted soil. Such extreme differences were not found between roots in different sides of the split pots during this experiment. Here the sub-optimal region of soil

in one side of the pot had an inhibitive effect on all roots, not just those in the side containing large particles. The order of root length from longest to shortest was consistently **S**, **SS**, **SL**, **L** at all time points, except for at 72 hours. This could have been affected by the fact that 72 roots out of 114, and two out of three reps were not measured at the 72 hour time point. Therefore, although measurements taken at 72 hours can help us to confirm observed trends based on what was seen at the other time points, they should also be treated with caution.

Root system width and convex hull volume has been suggested in previous research to be a useful measurement for comparing whole root systems of different plants (Tracy et al., 2012) and in this study it provided a simplistic way of showing patterns within and differences between whole root systems of barley seedlings exposed to different treatments. Root system width and convex hull volume increased between all of the time points on average. The largest root width and convex hull measurements were seen consistently in the **S** treatment, followed by the split pot treatment, followed by the **L** treatment, demonstrating the ability of **S** root systems to better spread throughout their cores and explore the **TS** more successfully.

Verticality was not found to be significantly different between treatments, however when plotted against the depth profile, it was found that patterns of verticality did differ between treatments (Figure 4-15). Verticality occurred in peaks and troughs, with the **S** treatment showing peaks and troughs that occurred over greater distances. The other roots showed peaks and troughs that were much closer together over small differences. In previous research by Digby and Firn (1995), it was pointed out that roots and shoots follow a gravitropic set point angle (GSA), which is defined as “an acceptable gravitropic position for the organ of a particular plant, at a certain developmental stage, in certain environmental conditions”. This

experiment has demonstrated how root GSA can vary due to differences in the physical soil environment. In this experiment, the verticality of roots remained between 80˚ and 45˚ throughout the duration of the time course. Verticality peaks and troughs occurred in healthy roots as well as roots that were under stress in the **L** treatment, due to large pores/particles and a possible lack of water. However, this process happened over a greater distance in the **S** treatment and the peaks and troughs were closer together in the split pot and **L** treatments. **TS** has very little mechanical strength, so this erratic behaviour demonstrated by roots in the **L** treatment could be due to a searching behaviour, whereby roots that find themselves in large pores are searching for contact with the surrounding particles. Furthermore, the data show that the higher average verticality measurements that were seen in the **L** treatment were not due to the roots being short, because in the **S** treatment roots did not exhibit the same patterns in root behaviour even when they were shorter at the beginning of the time series. In the split pot treatment, the presence of 50% suboptimal soil structure also influenced roots growing in optimal sections of the soil core, so that **SS** roots were also showing signs of stress, with peaks and troughs closer together, despite these individual roots experiencing the same local conditions as roots in the small treatment. There is a possibility that roots in the **SS** treatment may have reached similar average verticality values to those seen in the **S** treatment, had they been given more time to grow, however their gravitropic behaviour during this experiment suggests that verticality in these roots was heavily impacted by the presence of suboptimal physical soil conditions, at least during early root elongation. The behaviour of the split pot roots demonstrates that verticality is an RSA characteristic that is at least partly controlled by systemic responses to soil properties, not just events that are happening on an autonomous level at the root tip.

Curvature was also affected by having a region of suboptimal soil structure for **SS** roots. These roots showed unpredictable behaviour, being very different to that of roots in the **S** treatment. The peaks and troughs of curvature measurements for the **SS** treatment were closer together. Again, the conclusion can be drawn that these roots were behaving in this manner because of the soil conditions, not because of a lack of length, because the roots from the **S** treatment did not behave like this early on; their verticality and curvature values remained stable throughout the time course. In the first 10 mm of depth, some higher than expected values were seen for curvature in the small particle treatment, possibly showing an initial branching out behaviour of newly emerging roots or alternatively a measurement error, however these values cannot be considered the norm.

Water content for root/soil studies involving sieved soil cores is often adjusted to between 11% and 20% for experimental purposes (Zarebanadkouki et al., 2013, Valentine et al., 2012b, Stirzaker et al., 1996), which is considered a high enough volume for water to be easily available to the root system whilst reducing the risk of anoxia. In this experiment, water content was difficult to control at the time of sowing the seeds due to the infancy of the method, however it was possible to measure the volumetric water content on each day of imaging for all treatments using the detailed µCT images and a range of 9% - 13% was observed. Water content was lowest in the upper region of the cores, where the seeds were sown, in the **L** treatment. The water content also increased more noticeably with depth in the **L** treatment, due to the inability of large pores to hold water (Saxton and Rawls, 2006). Water levels are always difficult to control along the depth of soil cores, with water often sinking to the bottom during the course of time lapse experiments (Cannavo and Michel, 2013). The water levels in the upper region of the **L** cores where the seeds were sown may have been

too low for the roots to grow, which may help to explain why they did not grow as well as the **S** roots (Bengough et al., 2011). However, particle volume seemed to be a more important factor in this experiment than water or air volume, showing much higher correlation values with root length, root system width and convex hull volume. Particle volume and root/soil contact are also strongly correlated (Schmidt et al., 2012), so it may be useful for future research to consider particle volume as a contributing factor to root development.

Significant differences were seen for total porosity between treatments, with the **L** treatment having the highest average total porosity, followed by the **S** treatment, followed by the split treatment, whose average was lowest, but variation was highest. This is likely due to the method of image analysis used, whereby a segmented block, straddling the intersection of **L** and **S** particles in the split pot treatment was used to determine total porosity for the split pots. Within the segmented block, there may have been slightly more of the **L** particles or **S** particles, which would have increased the variation. Also, the geometry of these pores would have been more variable than those seen in the **L** and **S** treatments, also possibly contributing to the variation observed. Total porosity was always between 20 and 40%. Cannavo and Michel (2013) showed that an air-filled porosity of >10% is essential for healthy root growth, no matter what the growth media. Therefore, it can be assumed that air content was not a limiting factor for this experiment (Cannavo and Michel, 2013).

Root/soil contact is important in root elongation and therefore a series of highly connected soil pores that are large enough to accommodate the growing root, but not so large that roots cannot make contact with the surrounding particles is essential (Carminati et al., 2009). The largest pore surface area and volume may be a useful measurement for understanding the soil pore network, especially as root/soil contact is largely dependent on a combination of

these two factors. This experiment demonstrated that surface area and pore volume do not necessarily correlate. Surface area was highest in the **S** treatment, where there were more tiny particles all highly connected, followed by the split pot treatment, followed by the **L** treatment, which contained fewer large particles with lots of large pores. A schematic diagram of the structure of **TS** in the three different treatment is shown in Figure 4-17. Specific pore geometry must be researched further in order to better understand how it influences root growth in cereals.

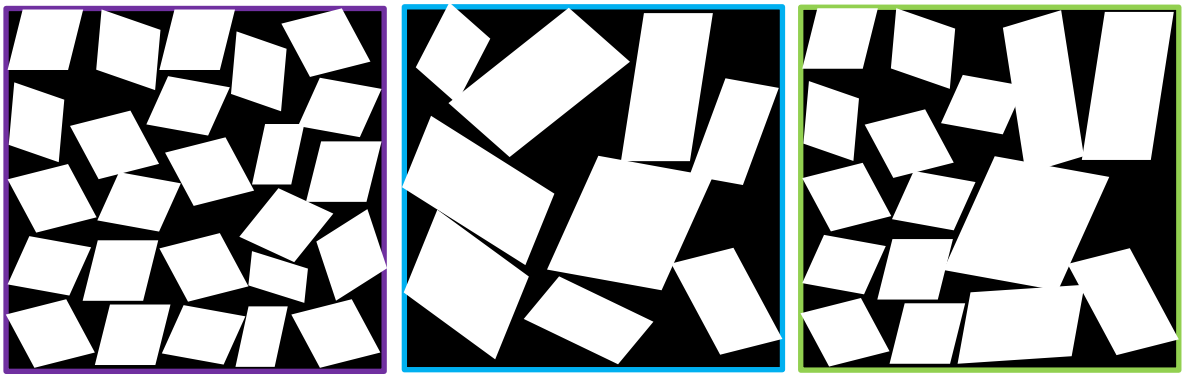

Figure 4-17: Schematic diagram showing the structure of TS pores in the three different treatments. The S treatment contains a high number of small, connected pores. L contains fewer very large pores. Split pot treatment may vary between the two.

µCT technology has made detailed research into root/soil contact easier, and it has been found that it is a strong contributing factor to healthy root growth (Schmidt et al., 2012). During this experiment, it was found that the roots that elongated most successfully increased their contact with the soil during the time course (Figure 4-13). Those that did not increase their contact with the soil did not grow as successfully and therefore this can be interpreted as an essential process in the early stages of seedling establishment. This may be based on an important feedback mechanism, whereby a higher level of root/soil contact upon root emergence helps roots to elongate initially, allowing them to actively increase their level of contact with the soil which causes a further increase in root elongation. The opposite effect

was seen in the **L** treatment and this may be because the lower level of initial root/soil contact inhibited root growth from the start, thereby stopping this process from occurring (Passioura, 2002). Healthy levels of root/soil contact never took place and therefore neither did root elongation. It can be concluded from the measurements that were taken that exposure to a lower level of root/soil contact in a section of the root system has an inhibitory effect on the entire root system. This leads us to question what percentage volume of **TS** needs to be physically sub-optimal before inhibition of root growth begins to take place. If only 20% of the **TS** volume was made up of large particles, would the same inhibitory effect on root/soil contact and root elongation have been observed? This is a question that may have important implications for soil management in agricultural contexts and should be researched further.

Perhaps one of the most interesting findings from this experiment is that root tips preferred the large particle section in the split pot treatment as evidenced by Figure 4-14. This is despite the fact that they grow much more successfully in the small particles. It has long been accepted that roots prefer to follow the path of least resistance during elongation (Bengough and Mullins, 1990), however this study has demonstrated that roots will preferentially choose the path of least resistance, even if it has a lower water holding capacity and results in stunted root growth across the entire root system. This time series was short, so it is difficult to predict what would happen if the split pot seedlings had been given longer to grow. Perhaps the same behaviour would have continued or perhaps the roots in the small particle region may have eventually compensated for those in the large particle region and grown longer, as was the case in Montagu et al. (2001). Perhaps all roots would have moved into the large particle region in the end, in which case it can be hypothesised that their chances of survival would have been greatly decreased. There is also the possibility that if the roots had begun growth

in the small particle section and moved over to the large section later on, that they would have coped better due to the root system being better established. Further research should be carried out in order to understand the behaviour of more mature root systems in split pot treatments.

4.7 Conclusions

Split pot experiments have been used previously in order to understand better how roots behave in heterogeneous soil environments (Montagu et al., 2001) however this is the first time that such an experiment has been carried out using the transparent soil growth medium. Whilst the physical structure of soil can be manipulated in a similar manner to how **TS** was manipulated in E.v, it is difficult to prescribe and manipulate both the structure and nutritional status of soils which may be a benefit of the **TS** growth medium. It is also enabling us to begin collecting new data on root growth in **TS**, which not only contributes to our understanding of root growth in general, but will also become useful in the future as the **TS** system is used to observe fluorescent barley cultivars and root growth changes on a cellular level.

Roots grew longest in the **S** treatment and shortest in the **L** treatment, which was to be expected following the results from E.iv. The roots in the split pot treatment were in between, however no compensatory growth was observed in the section of the split pot that contained **S** particles. This contradicted some of the previous literature, which had observed compensatory growth in split pot cores containing soils packed at different bulk densities (Montagu et al., 2001). This was an interesting discovery, as it suggests that when pore size in split pot cores differs, that the entire root system is affected in a negative way and that early root growth is therefore not dependent on sensing at individual root tips.

Of the three treatments, **S** had the most air, the most water and the least particle percentage by volume. The **L** treatment had the least air, the least water and the most particle percentage by volume. The split pot treatments were in between the other two. It is interesting that **L** had the least air/water and most particles, but the lowest level of root/soil contact of the

three treatments. This indicates that not only is the air: water: particle ratio important, but that pore shape also has a critical role to play in monocotyledonous root growth.

There were differences in spatial distribution of water, air and particles throughout the cores between treatments. In all three treatments, the percentage water by volume increased with depth down the **TS** profile and percentage air by volume decreased. The variable water distribution was most obvious in the **L** treatment, which had less water than the other treatments at shallower depths in the profile, but much more water at the deepest part of the **TS** core. This was to be expected, as it is known that soils with very large pores have a lower water-holding capacity (Saxton and Rawls, 2006). It is possible that the lack of water in the shallower section of the **L** cores, where the seedling was sown, may have contributed to the lack of growth that was then observed in the **L** roots (Bengough et al., 2011).

Root/soil contact was identified as one of the most important parameters for root growth in this experiment, with data suggesting that roots must actively increase their surface area contact with the soil during the first few days of root growth, otherwise severe inhibitory effects on root growth will result. All roots that achieved a length of greater than 20 mm were of the **S** treatment or the **SS** treatment. These **TS** cores all contained 45 – 55% particle volume and had >20% contact with the root systems. The largest root systems had 80% root contact. Root elongation was most successful at approximately 50% particle volume. Air volume was at 30 – 40% and water volume was at 10 – 20%, so these particle: water: air ratios are likely to be the most optimal for root growth in **TS**.

Root verticality and curvature rises and falls with growth, however it occurs over a shorter distance for root systems that are elongating slower due to stress caused by undesirable soil physical conditions. Mechanical stress is very low in **TS** so this was unlikely to be the limiting

factor of root elongation. Instead, these peaks and troughs that were observed close together may have been due to the roots searching for contact with their surrounding particles.

Roots in the split pot treatment preferentially chose the large particle section over the small particle section over the duration of the time course, despite it having a negative effect on overall root system development. This may have been because the large particle section had much larger pores and therefore offered the path of least resistance, but root/soil contact was reduced to a level that had a negative effect on the entire root system. More research must be carried out to determine whether roots continue to gradually move into the larger particle size range, and if so what the effects are on plant development as a whole.

5 Barley root response to soil compaction, using the transparent soil system and 3-dimensional imaging techniques

5.1 Introduction

In Chapter 4, root elongation was observed in **TS** cores that were vertically stratified, containing 50% of the particle size range 850-1250 µm and 50% of the particle size range >1676 µm. The smaller particle size range was found to be conducive to barley root elongation and the larger particle size range was found to be sub-optimal for root growth. The results of this experiment showed that responses of roots to mechanical signals are likely to be a systemic process, with all roots being affected by the presence of the large particles in the core, regardless of whether they were directly in contact with these particles, or growing in the section containing small particles. **TS** has very little mechanical strength, and with the absence of strength, particles can easily be moved by the root to create a more suitable pore space, so the experiment in chapter 4 tested only the effect of pore geometry on root growth. This chapter focuses on the effect of soil mechanical resistance on root growth.

5.1.1 Natural soil compaction and root growth

Soil compaction is defined as ‘‘the process by which the soil grains are rearranged to decrease void space and bring them into close contact with one another, thereby increasing the bulk density” (Soil Science Society of America, 2008). Soil compaction is important because as well as often having a negative effect on root growth and crop yield, it causes soil degradation;

increasing greenhouse gas emissions, and increasing runoff of nitrates from large-scale fertilising processes and pollutants into surface waters (Soane and van Ouwerkerk, 1995).

Compaction makes soil pores smaller, reducing the ability of roots to explore the soil volume (Hamza and Anderson, 2005). Farm animals, heavy machinery, and soil water content at the time of sowing are the biggest causes of soil compaction in an agricultural context (Hamza and Anderson, 2005). Gysi et al. (1999) showed that compaction influences a number of soil characteristics. The application of 160 kPa to moist soil using heavy machinery has been shown to increase the bulk density of sandy loam field soil by 5.8% and decrease air permeability by 27.5% (Gysi et al., 1999). Applying a pressure of 130 kPa to moist soil, and applying 160 and 130 kPa to a dry soil did not result in significant changes in soil structure.

If soil is compacted and large soil aggregates form, roots will have to exert a greater force to push soil particles aside and penetrate pores, reducing root growth and having a negative effect on crop yield (Dürr and Aubertot, 2000). In compacted soils, roots are often shorter and have a decreased rooting depth, often growing in the shallower part of the soil profile (Lipiec and Hatano, 2003).

Soil strength is often used as a measure of compaction, because it represents the soil's resistance to root elongation (Taylor, 1971), and as such offers a reliable predictor of crop yield (Whalley et al., 2008). A number of instruments can be used to measure soil strength (O'Sullivan and Ball, 1982), however the penetrometer is the instrument most commonly used. The amount of force necessary to push the penetrometer's tip into the soil offers a measure of the soil strength (Lowery and Morrison, 2002).

Grzesiak et al. (2013) used a penetrometer to measure impedance in the soil profile from 5 – 35 cm for samples under low compaction (L – 1.10g.cm^{-3}), moderate compaction (M – 1.34 g.cm^{-3}) and severe compaction (S – 1.58 g.cm^{-3}). They found that penetrometer impedance was 0.84, 1.23 and 1.99 MPa respectively in dry soil and 0.73, 1.05 and 1.68 MPa for wet soil. M and S impedance resulted in 38% reduction in root to shoot dry mass ratio compared with L for maize in both treatments after 49 days of growth. For triticale the dry mass of roots was reduced by 29% for M and 41% for S after 49 days growth. The main limitation of using a penetrometer is that it does not dynamically change direction in the same way as roots do, so the amount of force that it needs in order to push particles aside may be greater than that of roots; however it does provide a useful relative measure of soil strength; one that is commonly used by researchers (Bengough and Mullins, 1990).

The rate of soil water infiltration can also be used as an indicator of the level of soil compaction, because water does not penetrate soil as quickly in compacted soils (Hamza and Anderson, 2002).

High resolution imaging techniques allow the non-destructive measurement of properties such as porosity and connectivity. Lipiec et al. (2012) found that total porosity decreased from 50.1% in an uncompacted field soil (U) to 38.1% in a compacted field soil (C). Root length decreased by approximately 50% for barley (from ± 40 cm to ± 20 cm) in the C treatment, however the results were not significant, possibly due to large variation of barley in the U treatment. Compaction increased the vascular cylinder diameter and the cortex area in barley roots. In total, root diameter was increased by 96% in barley under compaction. Mechanical impedance was found to be the main influencing factor on root responses to compaction (Lipiec et al., 2012).

5.1.2 Testing soil compaction in different growth mediums

In order to test the effects of soil compaction on roots, researchers have employed a variety of methods, which usually involve using either soil, ballotini or agarose/gel mediums. When using soil, it is possible to sieve and then re-pack it at different bulk densities in order to achieve different levels of compaction (Bengough and Young, 1993), or they can take undisturbed soil cores from the field and measure their penetrometer resistances in the laboratory (Bengough and Mullins, 1991). Using a sieved, homogenous structure allows accurate packing of soil cores at different bulk densities in a standardised manner, thus allowing the accurate observation of compaction effects on roots.

Due to the complex physical nature of soil, it can be difficult to separate abiotic factors such as strength, compaction, water content and aeration, as these parameters interact and influence root elongation in different ways. Artificial growth mediums offer an alternative option and all have their advantages and limitations for studying various aspects of root growth (Clark et al., 1999). Ballotini beads are hard and round, and therefore cannot be compressed. In order to understand how compaction affects roots growth, pressure must be applied to the ballotini growth medium within a contained cell that has flexible sides (Barley, 1962). During these experiments, root growth resistance was measured as the pressure applied externally to the confined ballotini cells (Bengough and Mullins, 1990). As with penetrometer resistance, this is a relative measure of strength, not a true measure.

Agar and agarose gels have also been tested as a medium to study soil strength, with the great advantage that they are transparent and therefore root growth can be observed directly, without the need for root extraction or µCT imaging. Mixing 5% agarose gels can result in a penetrometer resistance of 1.2 MPa (Clark et al., 1999), but this can vary slightly depending

on the bonding strength of the agar. Clark et al. (1999) found that root elongation was reduced in the agarose growth medium, however during this experiment, the root did not grow long enough to reach the strong layer of agarose, therefore suggesting that mechanical impedance is not the limiting factor in gel mediums; instead the inhibition could be due to the mixture of chemicals that roots were exposed to at high gel concentrations. It was suggested that caution be exercised when interpreting root growth data from roots that had been grown in gel systems (Clark et al., 1999).

TS offers the transparency of agar, and some of the physical heterogeneity of soil (Downie et al., 2012). It also can be compressed in a similar manner to natural soil and the particles can be a variety of shapes; not just round as is the case with ballotini. This chapter develops the system further by using it to observe barley seedling root growth in **TS** under different levels of compaction.

5.1.3 Imaging techniques to observe the effects of soil strength on root growth

There has been little in situ observation of soil compaction and root growth over the years, largely due to the difficulties associated with observing and quantifying such interactions, as well as the time and cost involved in doing so. Thin-slice techniques were traditionally used in order to observe root/soil interactions, up until the development of high-resolution 3-D imaging techniques. Bruand et al. (1996) impregnated soil cores with polyester resin and used a thin-slice technique combined with scanning electron microscopy using the emission of back scattered electrons in order to analyse soil compaction on maize roots. Whilst Bruand found this to be a useful way to measure soil compaction around roots, developments in µCT were already beginning to take place for use in soil research (Hainsworth and Aylmore, 1983). Due

to the non-destructive nature of µCT, it gained popularity for studies on root/soil interactions; including those to do with soil compaction.

Tracy et al. (2012) used X-ray µCT in order to understand how compaction affected root elongation both spatially and temporally. Using this technique, they managed to observe *in situ* the reduction in root length and convex hull volume which occurred when tomato roots were exploring compacted soils, as well as an increase in root diameter.

TS allows the observation of roots inside a physically heterogeneous growth medium (Downie et al., 2012), with a network of pores that can be manipulated manually. It is possible to perform non-destructive, high-resolution, 3-D imaging of seedling roots in situ using µCT which is radiation-based and provides a high level of detail, allowing the observation of particles, liquids and air within the **TS** core (Downie et al., 2015). Another possibility with **TS** is to use light-based OPT, another non-destructive, high-resolution, 3-D imaging technique, which is a quicker and more cost-effective method (section 2.5.3.1), with the potential to use fluorescent dyes and plants to observe root system architecture (Downie et al., 2015). Furthermore, the **TS** growth medium enables better control of nutrients and can be sterile at the time of sowing.

5.2 Aims

The aim of this chapter was to test compaction of barley roots in **TS**. This was done by imaging and quantifying root elongation in **TS** that had different levels of compaction applied to it, with a view to understanding how compaction affects the way that barley roots grow. For this experiment, barley seedlings were sown in 850-1250 µm **TS** and exposed to different levels of compaction. To quantify the root system responses the following objectives were defined:

- To design a soil compaction apparatus, that would allow the application of mechanical pressure to **TS** cores;
- To develop imaging and image analysis techniques that would allow the observation and quantification of root growth in compacted **TS**;
- To observe and quantify how roots responded to pressure in the **TS** system;
- To understand the effect that mechanical pressure has on root/soil contact and how this in turn affects root growth.

5.3 Questions

The following questions were the focus of this chapter:

- Are there differences in root growth between barley seedlings grown under different levels of compaction?
- Do differences in root trajectory occur in different levels of compaction?
- What are the differences in physical composition between transparent soil cores that are compacted to different levels?
- What is the relationship between root system architecture and **TS** within different levels of compaction?

5.4 Methods

By the time this experiment took place, additional method development had also been carried out on the **TS** system, so that more was known about appropriate refractive index matching (Section 2.4.2.2.4) and the types of noise that could be created by the OPT setup (Section 2.4.2.2.2). Therefore, this experiment represents not only an advancement in designing compact soil pressure apparatus that could be used on both **TS** and soil, but it also represents the pinnacle of the **TS** and OPT technique to date.

5.4.1 Seedling selection and sowing

6 seedlings were planted each week in individual **TS** cores, and different levels of compression were applied to them all, using the soil strength apparatus described in Section 2.4.1.4. After imaging, the seedlings were removed and preserved, and the **TS** was cleaned using the protocol described in Section 2.4.1.2.2. This process was repeated 3 times, so that 18 seedlings in total were planted in the **TS** and imaged after having different levels of pressure applied to them.

Westminster seeds were prepared and sown according to the methods described in section 2.4.1.2.1.

5.4.2 TS core preparation and incubation

Core preparation was carried out according to the methods described in section 2.4.1.3. The total volume of **TS** in the cores was 45.4 cm^3.

TS was cleaned and sterilised as described in section 2.4.1.2.2. Before preparing cores, the **TS** was returned to the column and allowed to drain using gravity so that the particles were free from excess fluid. This made it easier to weigh out precise amounts of **TS** and standardise core

preparation. 40 g was weighed out and transferred into the acrylic cast tubes, and then 10 mL water was added to the **TS** volume so that the cores in total contained approximately 20% water. After sowing one seedling in each, the cores were wrapped in tin foil, up to the top level of the **TS** volume. A round, opaque, acrylic disc, 3 mm thick and 32 mm in diameter, with a round hole (to provide a space for the emerging shoot to grow through) in the middle of 5 mm diameter was placed on top of the **TS** volume inside the core. A compression spring with an outside diameter of 30.937 mm, a free length of 31.750 mm and a rate of 18.47 N/mm was then placed on top of the acrylic disc (Lee Spring, object ID: LC125N0M). The entire setup was then placed into a transparent plastic bag in order to retain moisture in the system and the soil strength apparatus, as described in Section 2.4.1.4 was applied to each core.

5.4.3 Imaging of samples

All µCT scans of cores were preformed whilst they were still under pressure, according to the methods described in section 2.4.2.1. After µCT imaging, the cores were placed in an incubator set to 0°C in order to halt seedling growth and the next day cores were imaged using OPT.

The soil pressure apparatus was removed from the **TS** cores before being prepared for OPT scanning. Cores were flooded with 17% sorbitol and OPT imaging was carried out according to the method described in section 2.4.2.2.1.

After OPT imaging, all seedlings were extracted from the TS cores, washed with water and placed in a petri dish lid containing water and a scale bar. They were then imaged using the protocol described for flatbed imaging in section 2.4.2.3.

5.4.4 Image analysis

This section describes the protocols that were used for analysing images of barley roots obtained using µCT, OPT and flatbed scanning. For additional information, the reader is directed to Section 2.4.3.

5.4.4.1 Seedling segmentation of µCT images

Seeding segmentation of µCT images was carried out according to the methods described in section 2.4.3.1.1.

5.4.4.2 Seedling segmentation of OPT images

Seedling segmentation of OPT images was carried out according to the methods described in section 2.4.3.3.

Skeletonisation was performed in the same way as previously described in Section 2.4.3.1.1.

5.4.4.3 TS volume segmentation from µCT images

Reconstructions were imported into VGStudioMax 2.2 (Volume Graphics, 2013), processed and analysed as described in Section 2.4.3.2.1.

5.4.4.4 Root system architecture measurements

Root system architecture measurements were obtained from µCT and OPT images using the method described in section 2.4.3.1.3. Length, curvature, verticality, convex hull volume and root system width were measured using the methods described in section 2.4.3.1.3.

5.4.4.5 Root/soil contact measurements

Root/soil contact measurements were carried out on all µCT images using the methods described in section 2.4.3.2.2.

5.4.4.6 Soil and TS measurements

Soil and TS measurements were carried out according to the methods described in section 2.4.3.2.1.

5.4.5 Statistical analysis

All statistical analysis was carried out in Genstat 16th edition and RStudio (RStudio Team, 2015). Figures were produced using the ggplot2 package in RStudio (Wickham, 2009) and Microsoft Excel (2010).

Three types of measurements were taken from the 3-D µCT and OPT images of roots; individual root co-ordinate measurements (e.g. curvature and verticality), individual root measurements (e.g. length, mean average curvature of a root, total curvature of a root, mean average verticality of a root) and root system measurements (e.g. convex hull volume, root system width, mean average length of roots in a seedling, mean average curvature of roots in a seedling, mean average verticality of roots in a seedling). Summary statistics of all variables were carried out using the statistical programming software, RStudio. After initial inspection of the raw data, subsets were created in order to gain a deeper understanding of the data when separated according to the factors being tested. Data transformation was carried out as detailed in Section 2.4.3.1.4.

To test for differences between roots grown under different compressions, the values measured according to the compression of the springs during incubation were sorted into three levels; no compression (0 kPA), mid compression (1 – 183 kPa) and high compression (184 – 368 kPA). Restricted Maximum Likelihood (REML) tests were carried out on datasets using Genstat 16th edition. REML analysis allowed the inclusion of fixed effects (level of compression) and random effects such as the root I.D., seedling I.D. and the rep number into

the model, therefore allowing roots and root co-ordinates to be treated as individual n-values when necessary. P-values of <0.05 were judged to be statistically significant. For whole root system measurements, such as convex hull volume and root system width, ANOVA tests were carried out in Genstat 16th Edition, taking into account random effects listed previously. P-values of <0.05 were judged to be significant.

The soil variables were sorted into data subsets according to the level of compression applied to the TS core.

Root/soil contact was sorted into data subsets according to the treatment and ANOVA testing was carried out with the treatment being included as a fixed effect and the week of sowing being included as a block within the model. To test for relationships between soil and root variables in all experiments, the statistical dependence of the transformed root measurement data and the soil/**TS** data was measured using the Pearson correlation coefficient in the statistical software programme, R. The Pearson correlation coefficient was also used to test for a relationship between the pressure applied to TS cores and root measurement data. For correlation tests, a p value of < 0.05 was treated as having a significant relationship; a correlation value of > 0.7 or < -0.7 was treated as a significant linear relationship.

5.5 Results

In total, 77 roots from 18 seedlings were identified from flatbed images. 35 roots were identified in the no pressure treatment (**N**), 28 in the mid-pressure treatment (**M**) and 14 in the high pressure treatment (**H**). OPT imaging identified 57 roots out of 77 (74%). From the µCT images 31 roots were identified in the **N** treatment (88%), 21 roots were identified in the **M** treatment (75%) and 9 roots were identified in the **H** treatment. From OPT images, 33 roots were identified from the **N** treatment (94%), 22 were identified and measured in the **M** treatment (78.6%) and 2 were identified and measured in the **H** treatment (14.3%). Figure 5-1 demonstrates typical examples of seedlings from each treatment.

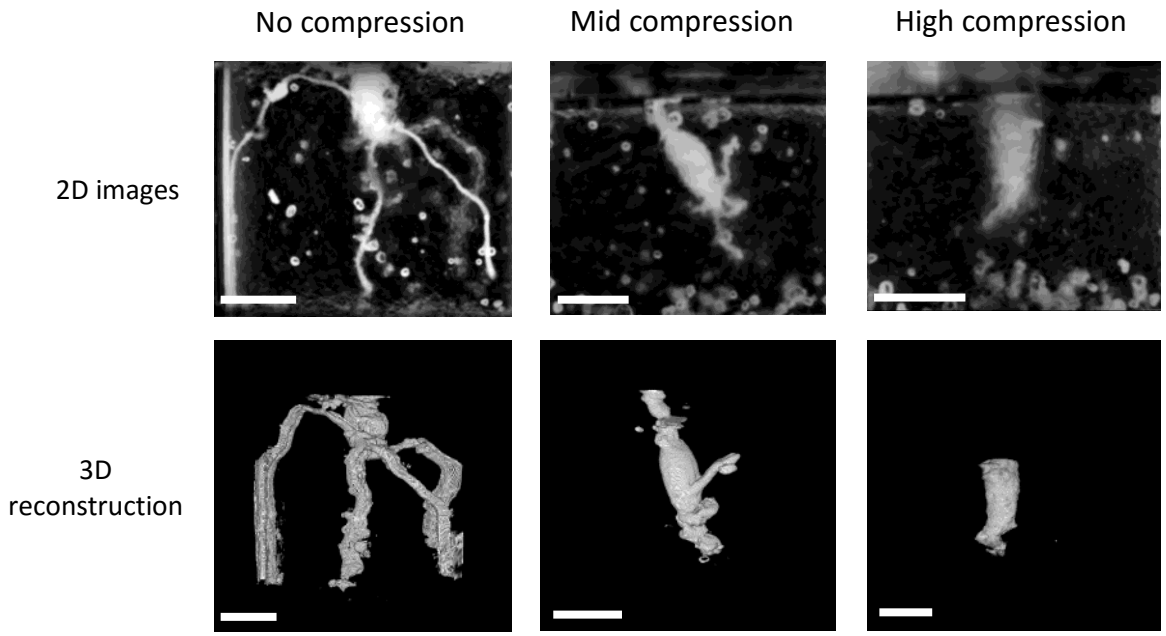

Figure 5-1: Typical OPT images of root systems under the N, M and H treatments. Top row shows raw 2-D images; bottom row shows 3-D reconstructions of the same seedlings (resolution, 41 µm). White bars = 1 cm.

5.5.1 Differences in root growth between barley seedlings grown under different levels of pressure

Figure 5-2 shows typical examples of 3-D µCT images of root systems in the **N**, **M** and **H** compaction treatments.

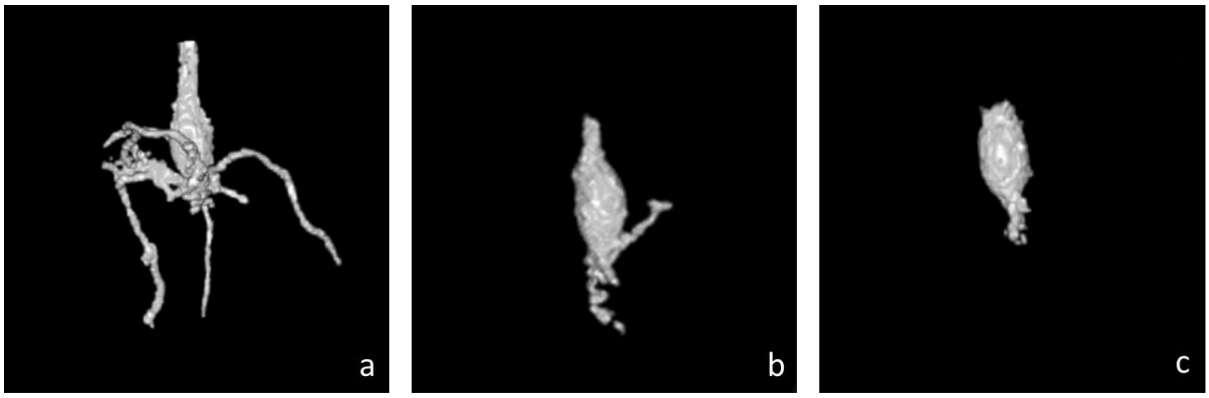

Figure 5-2: Typical examples of seedlings grown in the N (left), M (centre) and H (right) treatments. 3-D µCT imges. Resoultion, 51 µm.

Figure 5-3 shows the range of root length for each treatment with the mean in the **N** treatment being 28.81 mm (±11.23), in the **M** treatment being 12.270 mm (±4.182) and in the **H** treatment being 4.7 mm (±1.022).

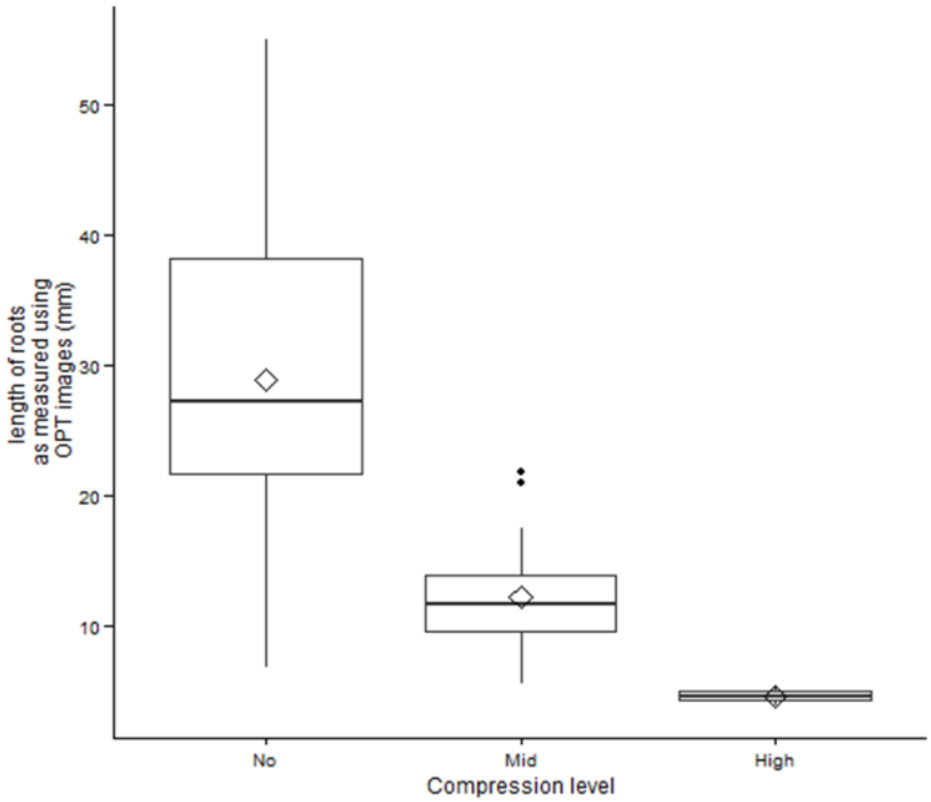

Figure 5-3: Boxplots of root length according to treatment. OPT images used. ◊ indicates the mean average.

Significant differences between treatments were found for root length (REML, p <0.001, F = 20.41; fixed effect = treatment, random effect = week, core ID).

Figure 5-4 shows the range of root curvature for each treatment with the mean in the **N** treatment being 0.017 μm^{-1} (±0.004), in the **M** treatment being 0.018 μm^{-1} (±0.006) and in the **H** treatment being 0.022 μm^{-1} (±0.003).

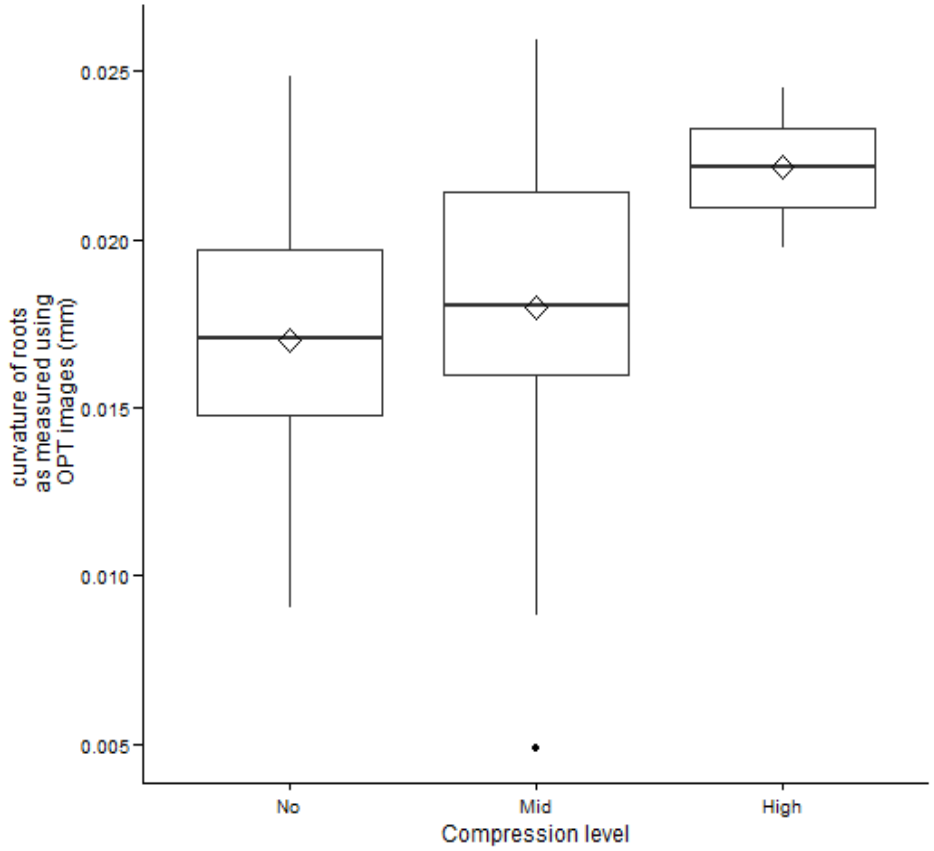

Figure 5-4: Boxplots of root curvature according to treatment. OPT images used. ◊ indicates the mean average.

Significant differences between treatments were not found for root curvature (REML, p = 0.143, F = 2.22; fixed effect = treatment, random effect = week, core ID).

Figure 5-5 shows the range of root verticality for each treatment with the mean in the **N** treatment being 61.76° (±16.17), in the **M** treatment being 81.47° (±22.23) and in the **H** treatment being 23.17° (±32.76).

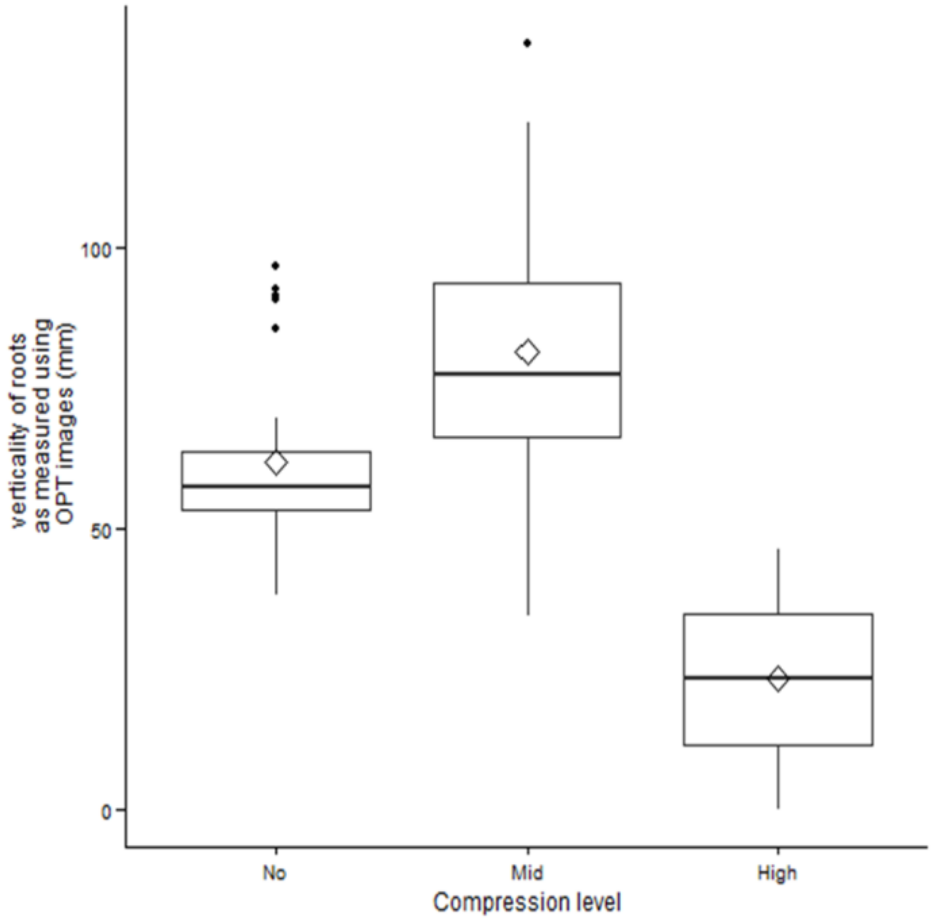

Figure 5-5: Boxplots of root verticality according to treatment. OPT images used. ◊ indicates the mean average.

Significant differences between treatments were found for root verticality (REML, p 0.002, F = 9.12; fixed effect = treatment, random effect = week, core ID).

Figure 5-6 shows the range of convex hull volumes for each treatment with the mean in the **N** treatment being 9130 cm^3 (±4218.09), in the **M** treatment being 1652 cm^3 (±636) and in the **H** treatment being 1185.0 cm^3 (±836).

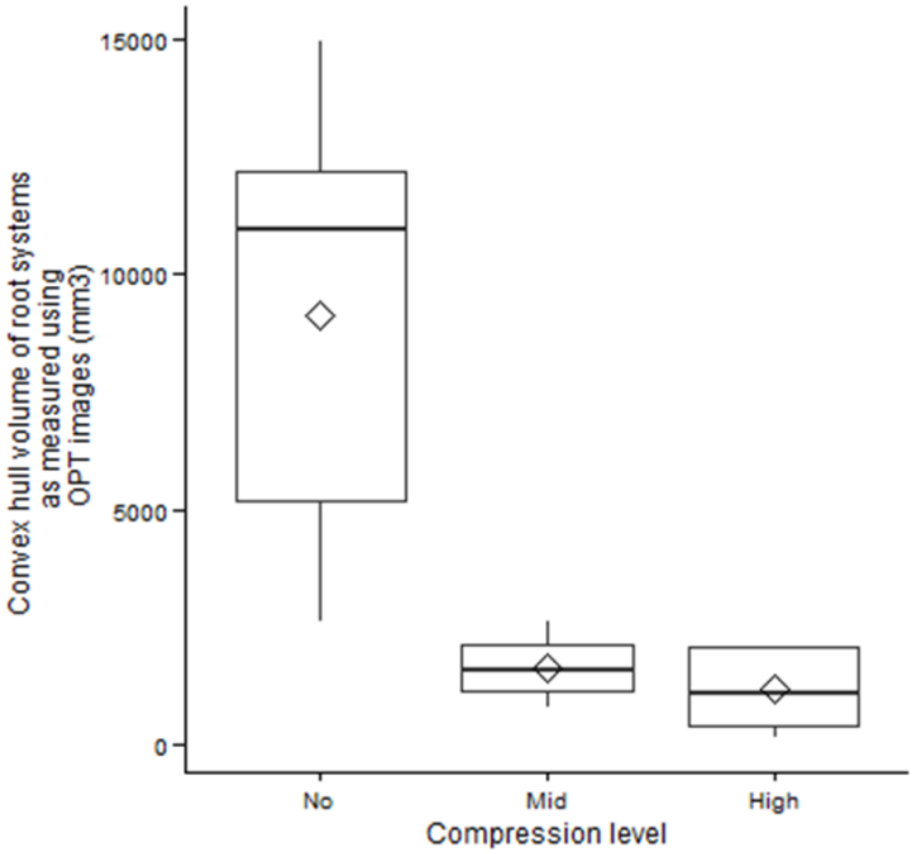

Figure 5-6: Boxplots of root system convex hull volume according to treatment. OPT images used. ◊ indicates the mean average.

Significant differences between treatments were found for convex hull volume (ANOVA, $p < 0.001$; fixed effect = treatment, block = week).

Figure 5-7 shows the range of root system widths for each treatment with the mean in the **N** treatment being 32.17 mm (±3.88), in the **M** treatment being 18.84 mm (±4.23) and in the **H** treatment being 14.170 mm (±4.83).

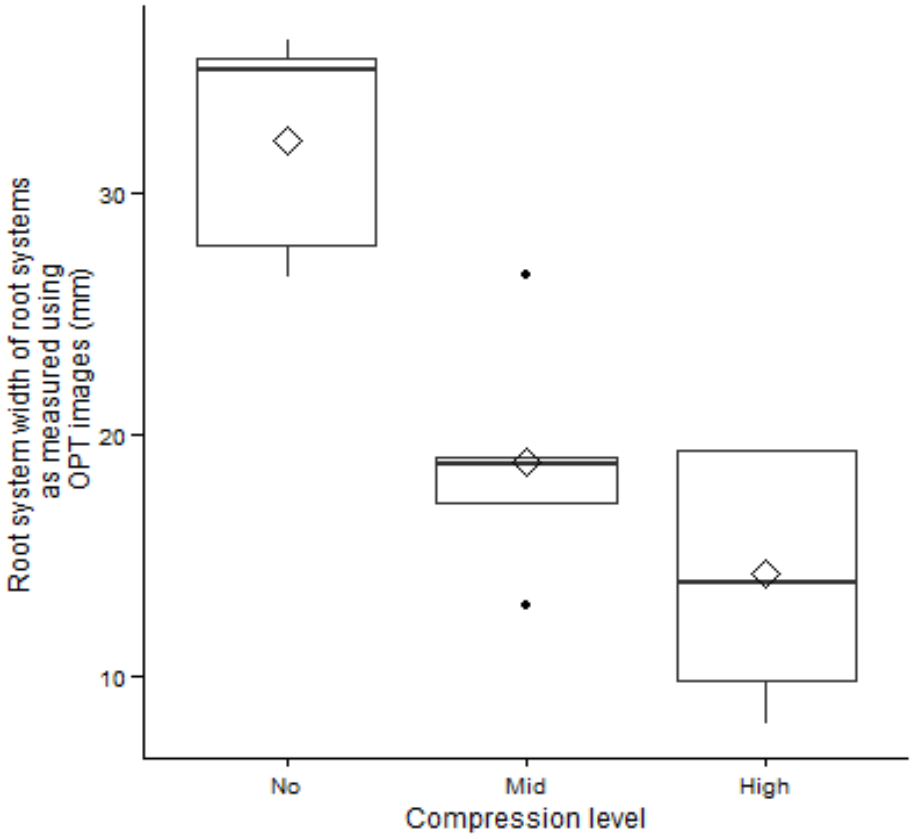

Figure 5-7: Boxplots of root system width, according to treatment. OPT images used. ◊ indicates the mean average.

Significant differences between treatments were found for root system width (ANOVA, $p < 0.001$; fixed effect = treatment, block = week).

By controlling the pressure applied to soil, considerable effects were observed on root growth. These effects are summarised as follows. The roots in the **N** treatment were the longest and had average verticalities in between those of the other treatments. **N** root systems also had the largest convex hull volumes and root system widths. The roots in the **M** treatment had lengths, convex hull volumes and root system widths in between those of the

other two treatments, however they had the least vertical roots. The roots in the **H** treatment were the shortest, and had the smallest convex hull volumes and root system widths. They were also the most vertical.

5.5.2 Root trajectory in different levels of compaction

In the previous section, the average curvature and verticality for each root was used in the analysis, however roots have the potential to behave differently depending on age and environment. Therefore to gain a further understanding of the influence of the pressure on the roots, the μCT images were used to measure the curvature and verticality of roots as a function of distance from the base of the seed.

Histograms showing the frequency of root curvature measurements according to treatment are shown in Figure 5-8. Much higher frequencies were counted for the **N** treatment, because the roots were longer and therefore more curvature measurements were taken than in the **M** and **H** treatments. In all three histograms, there are more measurements close to 0.00 than there are to 0.08, and this is because the smaller the curvature measurement, the wider the angle was at that particular co-ordinate (section 2.4.3.1.3; Figure 2-22). There were fewer measurements in the **H** treatment and Figure 5-8 shows that those that were taken were more widely spread, suggesting a mix of verticality measurements; some of which had more acute angles at the points of measurement, and some of which had wider angles at the point of measurement. Figure 5-9 shows the distribution of curvature measurements according to distance from the seed, with a line of best fit and 95% confidence intervals. Curvature remained quite stable for roots in the **N** treatment, staying close to a mean average of 0.025 μm^{-1} with increasing distance from the base of the seed. For the **M** treatment, curvature values initially decreased slightly (indicating less tortuosity), but then increased again and also

remained around 0.025µm^{-1}. It had wider confidence intervals than the **N** treatment, especially as the distance from the seed increased. The **H** treatment was the only treatment to have a line of best fit that went above 0.025µm^{-1}. This happened initially, as curvature measurements increased to begin with (indicating high levels of tortuosity), but then decreased again to remain below 0.025µm^{-1}.

REML analyses were performed on the individual curvature measurements, with the treatment included as the fixed effect and week, core ID, root ID and depth included as random effects. Significant differences between treatments were found for root curvature ($p < 0.001$; $F = 13.95$).

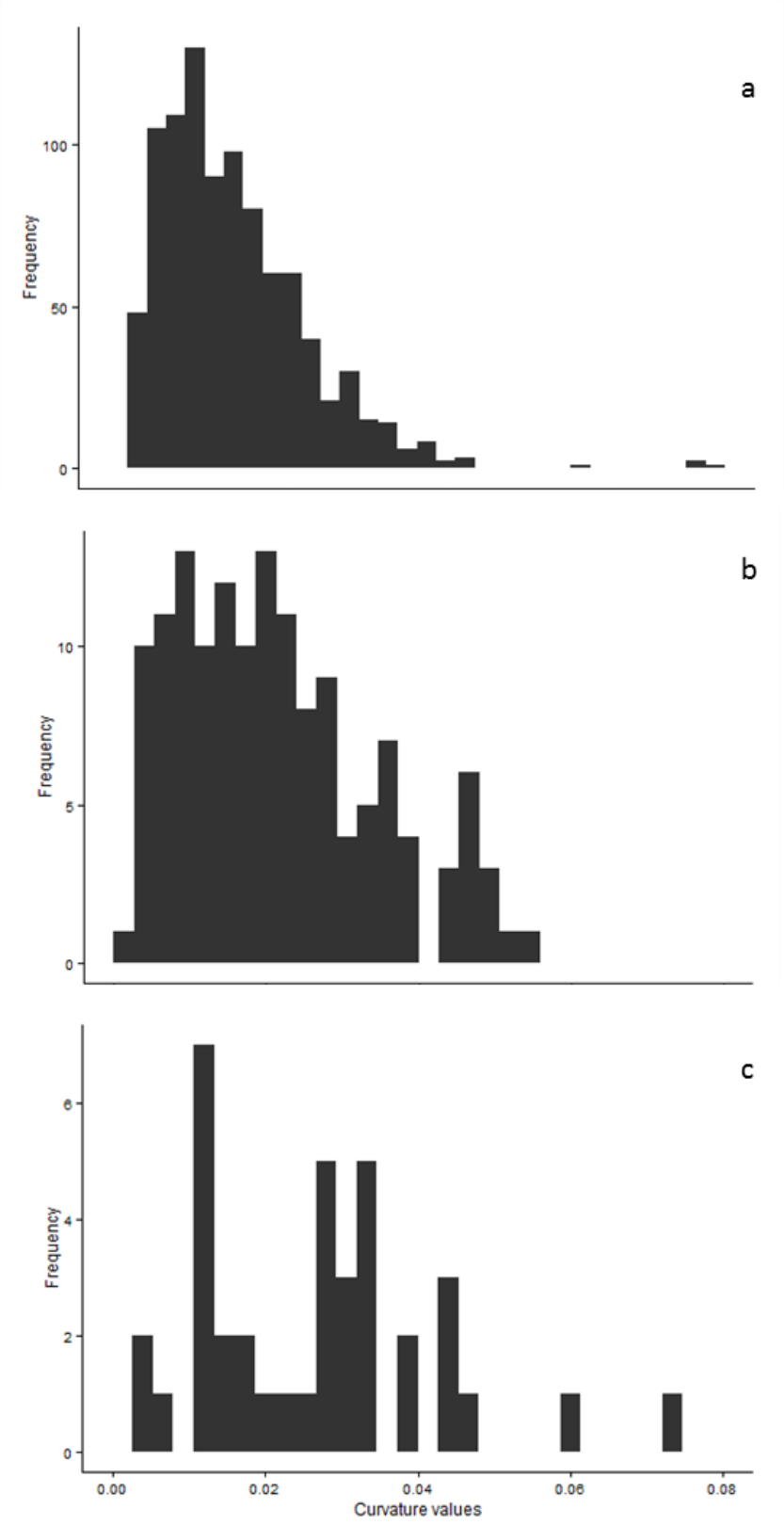

Figure 5-8: Frequency of curvature values for the N (a) - top, M (b) - centre, and H (c) – bottom treatments

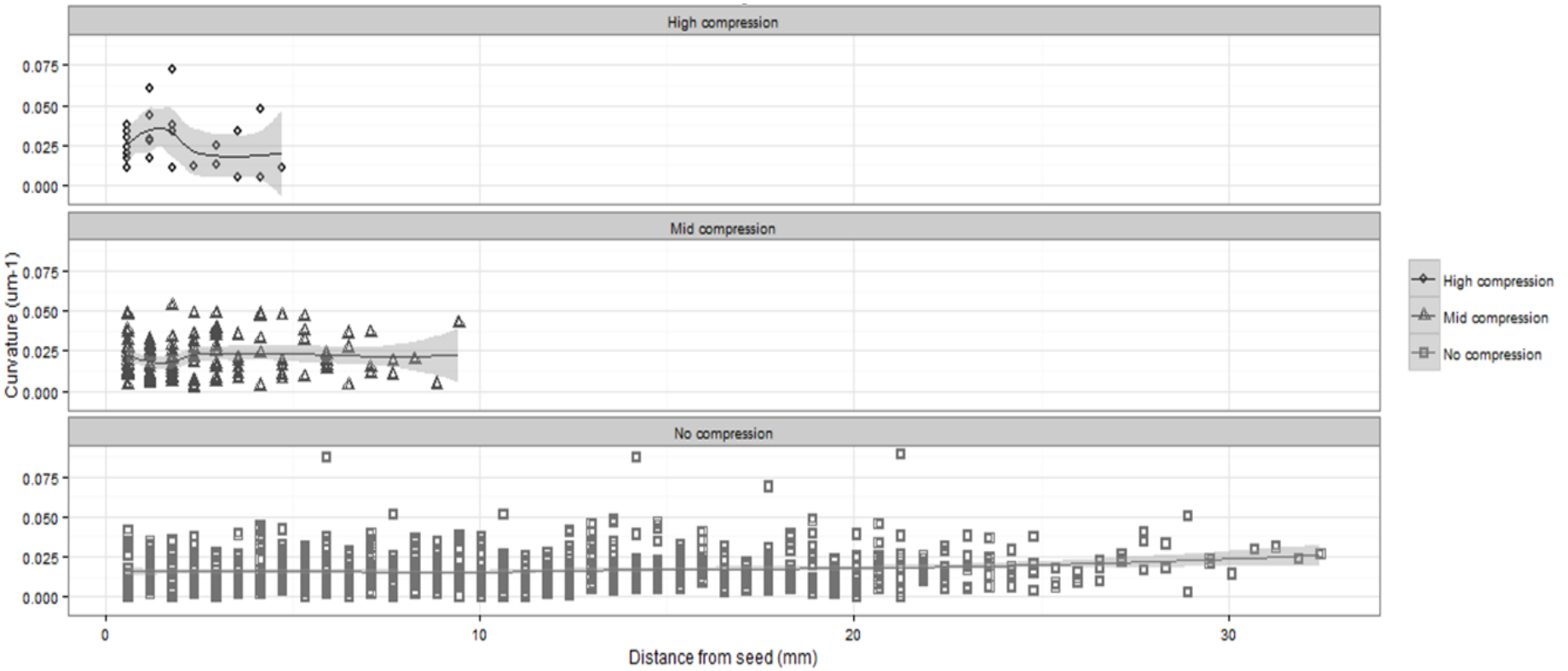

Figure 5-9: Curvature of roots according to distance from the seed. Line shows mean values at each point, grey area surrounding line shows 95% confidence interval

Summary statistics of root data showed that the average verticality of roots in the **N** compaction was 59.59° (±34.34), in the **M** treatment was 78.54° (±31.47) and in the **H** treatment was 69.61° (±31.81). Histograms showing the frequency of root verticality measurements according to treatment are shown in Figure 5-10. Much higher frequencies were counted for the **N** treatment, because the roots were longer and therefore more verticality measurements were taken than in the **M** and **H** treatments. The **H** treatment was the only one that had verticality measurements of above 100°. Figure 5-11 shows the distribution of verticality measurements according to distance from the seed, with a line of best fit and 95% confidence intervals. For the N treatment, verticality began close to 100°, but immediately began to decrease, ending up at approximately 50° at the most distant points from the seed. Roots in the **M** treatment initially increased their verticality, remaining at approximately 75° for some distance, before beginning to show a decrease in root verticality. Roots in the **H** treatment showed an immediate and sharp increase in verticality to begin with, from around 50° to 75°. These roots did begin to show a decrease in verticality by the time the measurements ceased to be taken, however it was much more gradual than the verticality drops seen in the other two treatments. REML analyses were performed on the verticality measurements, with the treatment included as the fixed effect and week, core ID, root ID and depth included as random effects. Statistically significant differences between treatments were not found for root verticality ($p = 0.159$; $F = 1.94$).

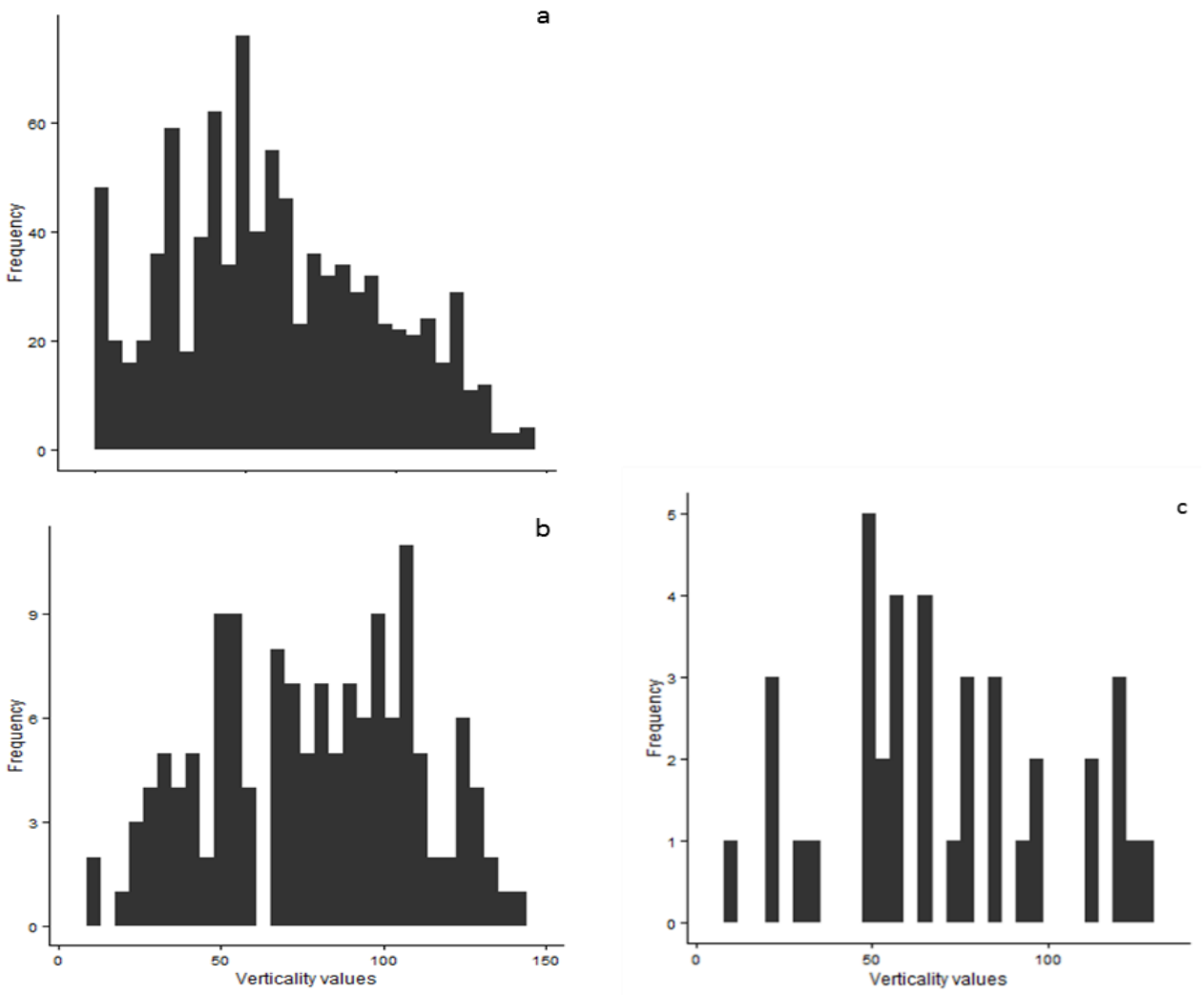

Figure 5-10: Frequency of verticality values for the N (a), M (b), and H (c) treatments

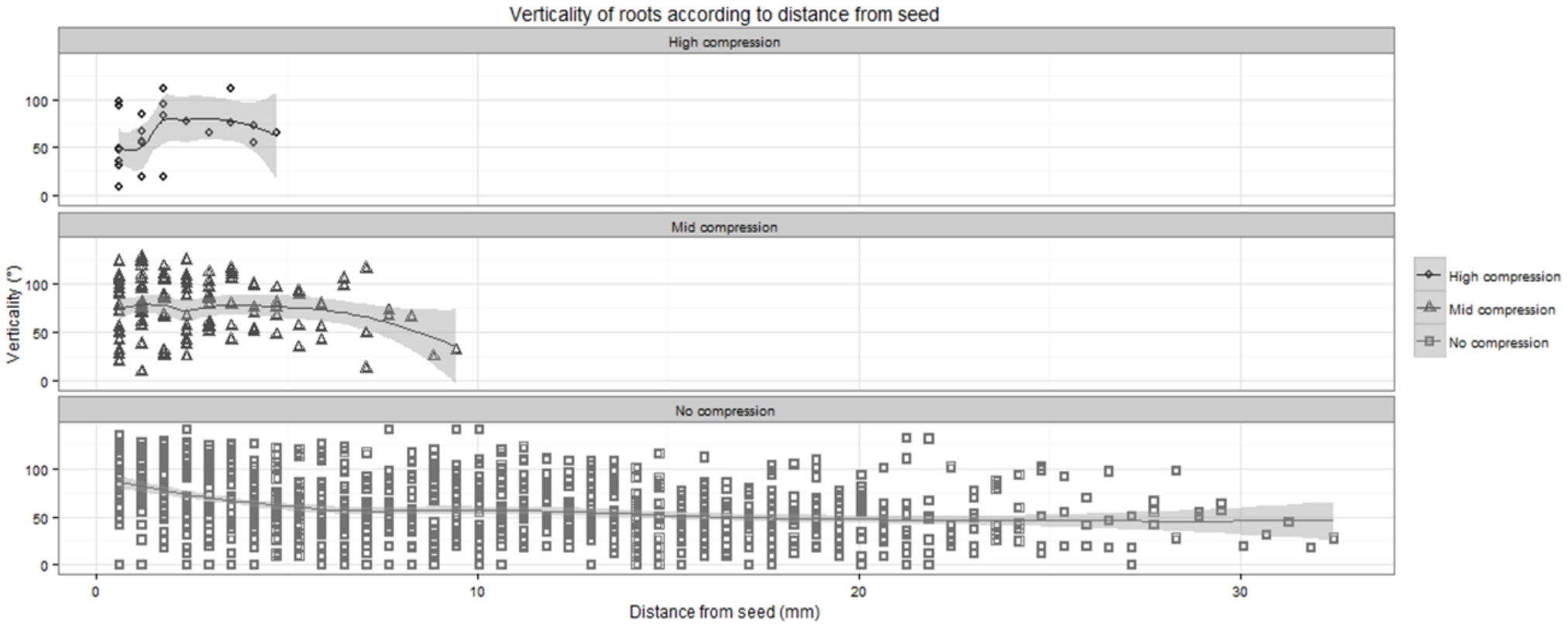

Figure 5-11: Verticality of roots according to distance from the seed. Line shows mean values at each point, grey area surrounding line shows 95% confidence interval

In summary, the **N** roots had a stable level of curvature all the way from the base of the seed, to the tips of the roots. The confidence intervals were narrower than the other treatments, indicating less variation in curvature. The verticality of the **N** roots began high but gradually decreased as the roots grew more in line with the vertical. The **M** roots initially dipped in curvature values, indicative of less curved roots, but then the values increased as the roots began to curve slightly more and find a stable curvature value, similar to that of the **N** roots. The verticality of **M** roots was less linear to begin with; increasing, then decreasing, then increasing slightly once again and then quickly decreasing as the roots began to reach the vertical plane. The **H** roots curvature values were initially high, indicating roots that were highly curved to begin with, but then the curvature values increased, indicative of less curved roots towards the tips. The verticality of the **H** roots was initially lower than the other treatments, with roots being more vertical, but very quickly their verticality increased, growing away from the vertical and ending up much higher than the other treatments. The confidence intervals were also broader (Figure 5-11, grey area surrounding the line) than the other treatments, indicating a greater level of variation in verticality.

5.5.3 Physical composition of transparent soil cores compacted to different levels

Figure 5-12 shows the range of percentage particle by volume for each treatment with the mean in the **N** treatment being 46.94% (±2.96), in the **M** treatment being 55.53% (±5.39) and in the **H** treatment being 62.02% (±5.56).

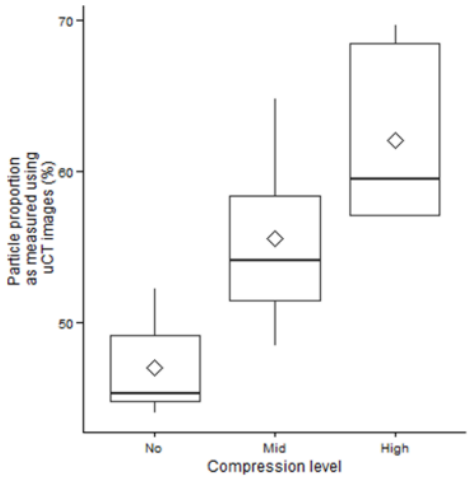

Figure 5-12: Percentage particle by volume in TS cores according to treatment. ◊ indicates the mean average

Significant differences between treatments were found for the percentage particle by volume (ANOVA, p <0.001, fixed effect = treatment, block = week).

Examples of segmented µCT images of TS particles from the **N**, **M** and **H** treatments respectively are shown in Figure 5-13.

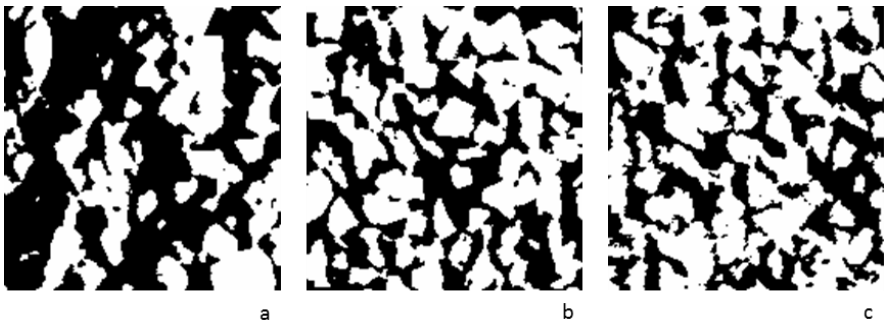

Figure 5-13: Segmented and thresholded cross sections of particles in different treatments (resolution, 51µm). Image a is from a N core, b is from a M core and c is from a H core. White pixels represent TS particles.

Figure 5-14 shows the range of percentage water by volume for each treatment with the mean in the **N** treatment being 20.19% (±1.93), in the **M** treatment being 22.48% (±3.68) and in the **H** treatment being 23.92% (±3.87).

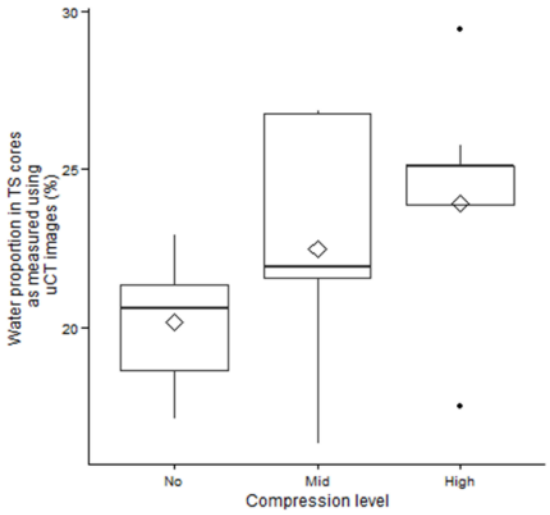

Figure 5-14: Percentage water by volume in TS cores according to treatment. ◊ indicates the mean average

Significant differences between treatments were found for percentage water by volume (ANOVA, p <0.001, fixed effect = treatment, block = week). Examples of segmented µCT images of water from the **N**, **M** and **H** treatments respectively are shown in Figure 5-15.

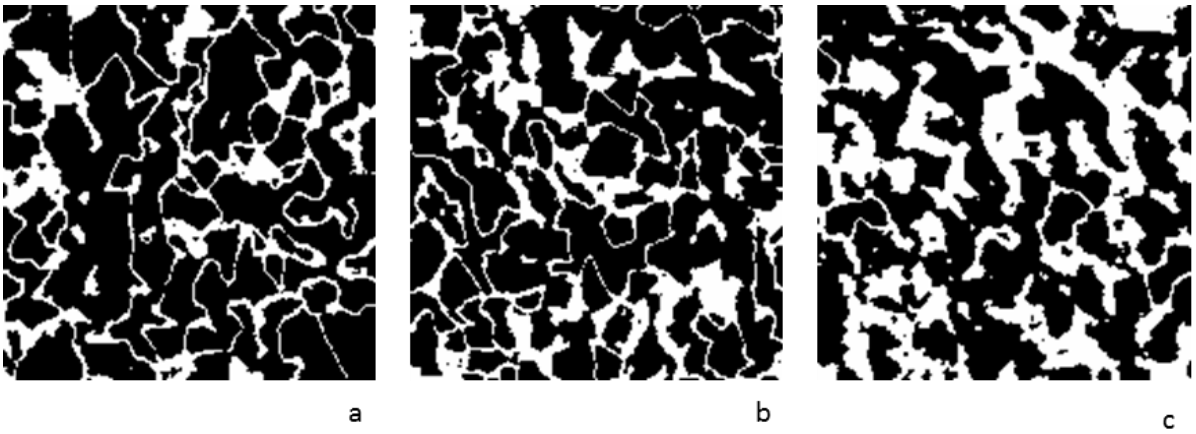

Figure 5-15: Segmented and thresholded cross sections of water in different treatments (Resolution, 51µm). Image a is from a N core, b is from a M core and c is from a H core. White pixels represent water.

Figure 5-16 shows the range of percentage air by volume for each treatment with the mean in the **N** treatment being 32.37% (±2.50), in the **M** treatment being 21.66% (±3.68) and in the **H** treatment being 14.010% (±3.76).

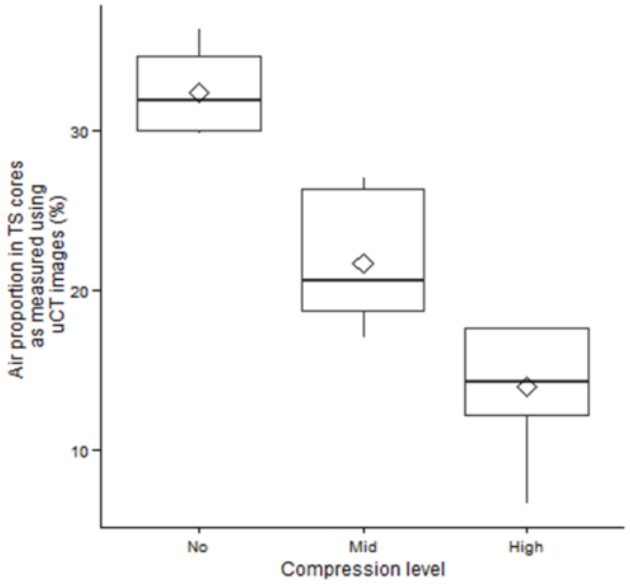

Figure 5-16: Percentage air by volume in TS cores according to treatment. ◊ indicates the mean average

Significant differences between treatments were found for percentage air by volume (ANOVA, p <0.001, fixed effect = treatment, block = week). Examples of segmented µCT images of air from the N, M and H treatments respectively are shown in Figure 5-17.

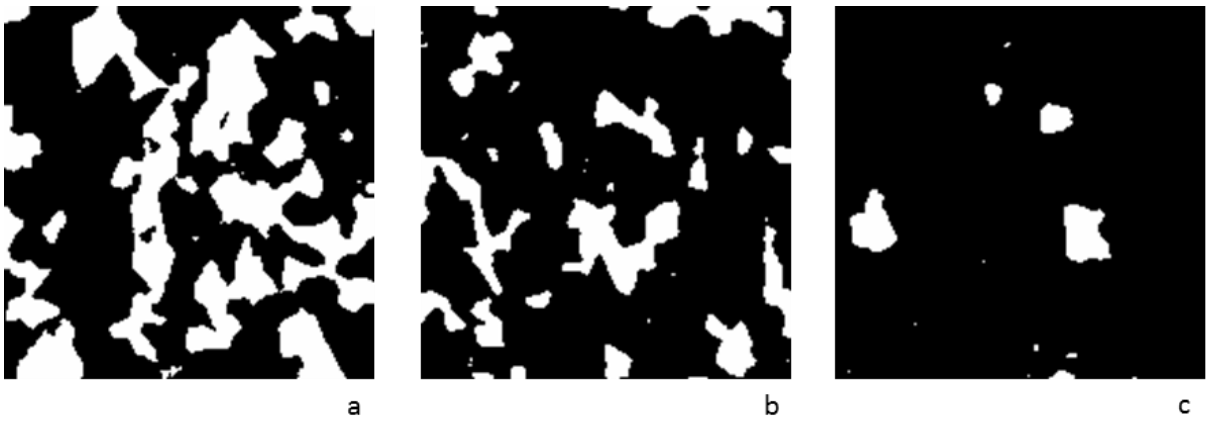

Figure 5-17: Segmented and thresholded cross sections of air in different treatments (Resolution, 51µm). Image a is from a N core, b is from a M core and c is from a H core. White pixels represent air.

Figure 5-18 shows the range of average total connectivity values for each treatment with the mean in the **N** treatment being 99.9% (±0.0), in the **M** treatment being 99.86% (±0.05) and in the **H** treatment being 99.76% (±0.21).

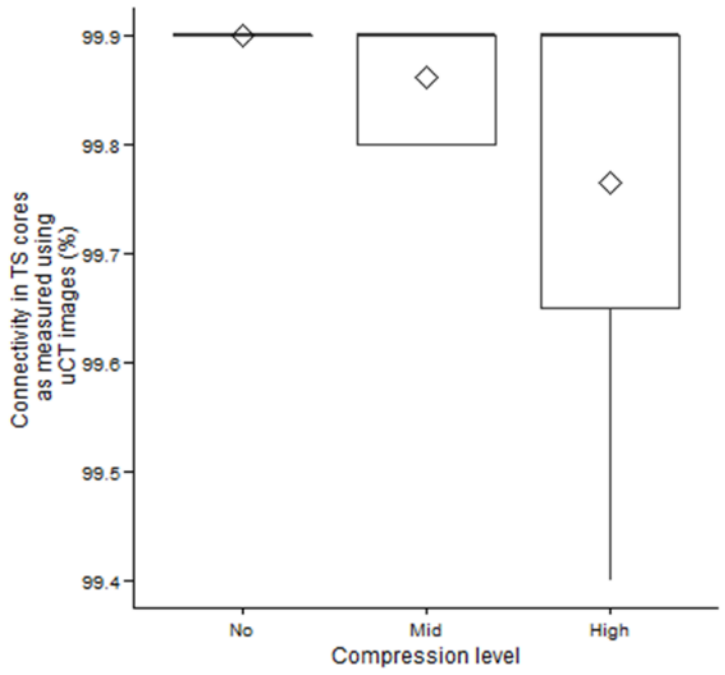

Figure 5-18: Connectivity of air- and water-filled pores in TS cores according to treatment. ◊ indicates the mean average

Significant differences between treatments were found for the average total connectivity (ANOVA, $p < 0.001$, fixed effect = treatment, block = week).

Figure 5-19 shows the range of average total porosity values for each treatment with the mean in the **N** treatment being 51.45% (±2.35), in the **M** treatment being 45.10% (±4.8) and in the **H** treatment being 38.49% (±5.25).

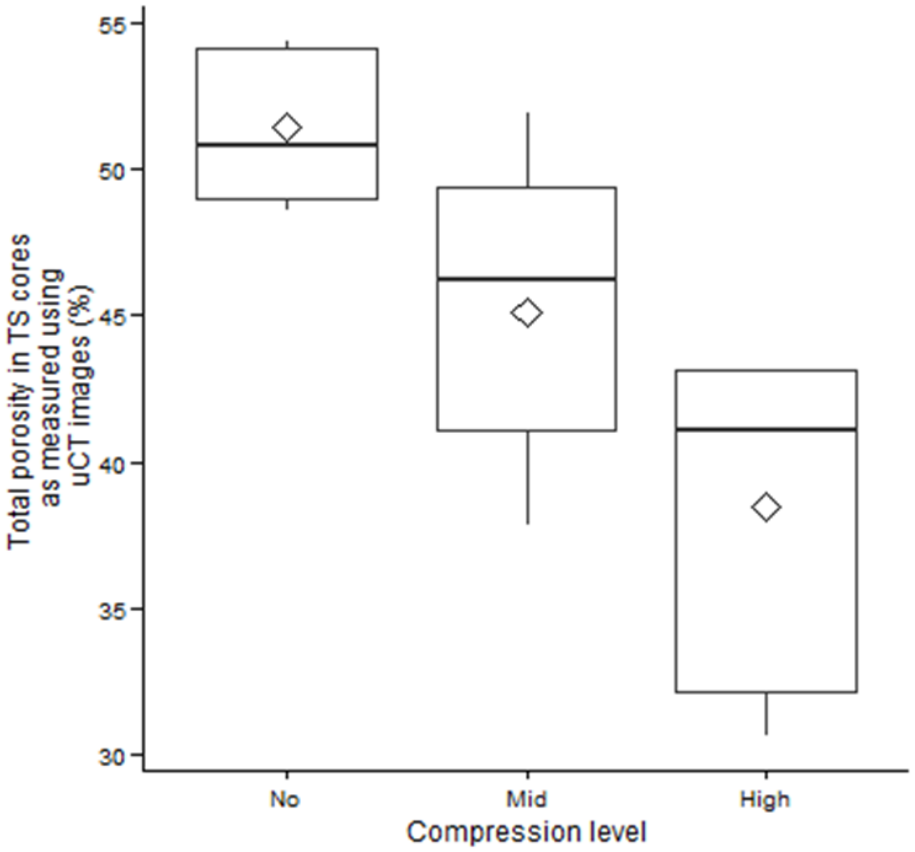

Figure 5-19: Total porosity in TS cores according to treatment. ◊ indicates the mean average

Significant differences between treatments were found for the average total porosity (ANOVA, $p < 0.001$, fixed effect = treatment, block = week).

In summary, significant differences were found between treatments for all of the **TS** variables that were measured. The **N** treatment had the lowest percentage particle by volume, the lowest percentage water by volume and the largest percentage air by volume. The connectivity was also highest in the **N** treatment, as well as the air- and water-filled porosity. The **H** treatment had the highest percentage particle by volume, the highest percentage water

by volume and the lowest percentage air by volume. The connectivity was lowest in the **H** treatment, as was the air- and water-filled porosity. The **M** treatment was in between the **N** and **H** treatments for all measurements.

5.5.4 The relationship between root system architecture and TS compaction

Figure 5-20 shows the range of average root/soil contact values for each treatment with the mean in the **N** treatment being 47.22% (±7.13), in the **M** treatment being 62.69% (±8.13) and in the **H** treatment being 68.74% (±5.1).

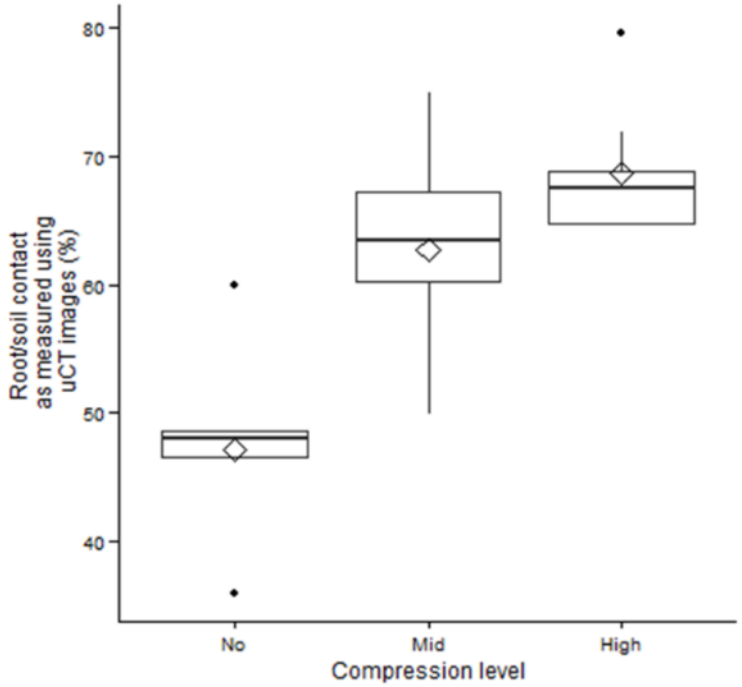

Figure 5-20: Root/soil contact (%) according to treatment. ◊ indicates the mean average

Significant differences between treatments were found for average root/soil contact (ANOVA, $p < 0.001$, fixed effect = treatment, block = week).

Pearson correlations of root and soil variables were carried out in order to better understand any dependent variables. The results of these analyses are shown in Table 5-1. The length of the roots was significantly dependent on all of the soil variables; percentage particle by

volume, percentage water by volume, percentage air by volume, connectivity, total porosity and root/soil contact. A negative correlation was observed between root length and percentage particle by volume (ie. as percentage particle by volume increased, root length decreased) and root length and root/soil contact (increase in contact correlated with a decrease in root length). Root length showed a positive correlation with percentage air by volume (increase in air correlated linearly with increase in root length) and TS total porosity (increase in porosity correlated with an increase in root length).

The curvature of the roots was significantly dependent on all of the **TS** variables, except for **TS** connectivity. A negative correlation was seen between curvature and percentage air by volume, so that as the percentage air by volume increased, curvature decreased. A positive correlation was seen between curvature and root/soil contact, so that as root/soil contact increased, so did the root curvature.

The verticality of roots was significantly dependent on all of the **TS** variables, except for percentage water by volume. The strongest correlations were seen between verticality and percentage particle by volume, and verticality and **TS** connectivity.

Variable	Length		Curvature		Verticality	
	P value	r value	P value	r value	P value	r value
Particle density	<0.001	**-0.626**	<0.005	0.392	<0.005	0.373
Water density	<0.005	-0.372	<0.001	0.49	0.96	-0.006
Air density	<0.001	**0.72**	<0.001	**-0.58**	<0.05	-0.333
TS Connectivity	<0.05	0.264	0.11	-0.2004	<0.005	-0.364
TS total porosity	<0.001	**0.579**	<0.001	-0.415	<0.01	-0.34
Root/soil contact	<0.001	**-0.591**	<0.001	**0.556**	<0.05	0.259

Table 5-1: Pearson test results, showing correlation and r values for root and soil variables. Significant r values are highlighted in bold.

The correlation relationships of length and curvature with **TS** variables are shown in Figure 5-21 and Figure 5-22, whereby it can be seen that root length increased with increasing percentage air by volume and total TS porosity. Root length decreased with increasing percentage particle by volume and root/soil contact. Root curvature values decreased (i.e. roots became less tortuous) with increasing percentage air by volume and increased (i.e. became more tortuous) with increasing root/soil contact.

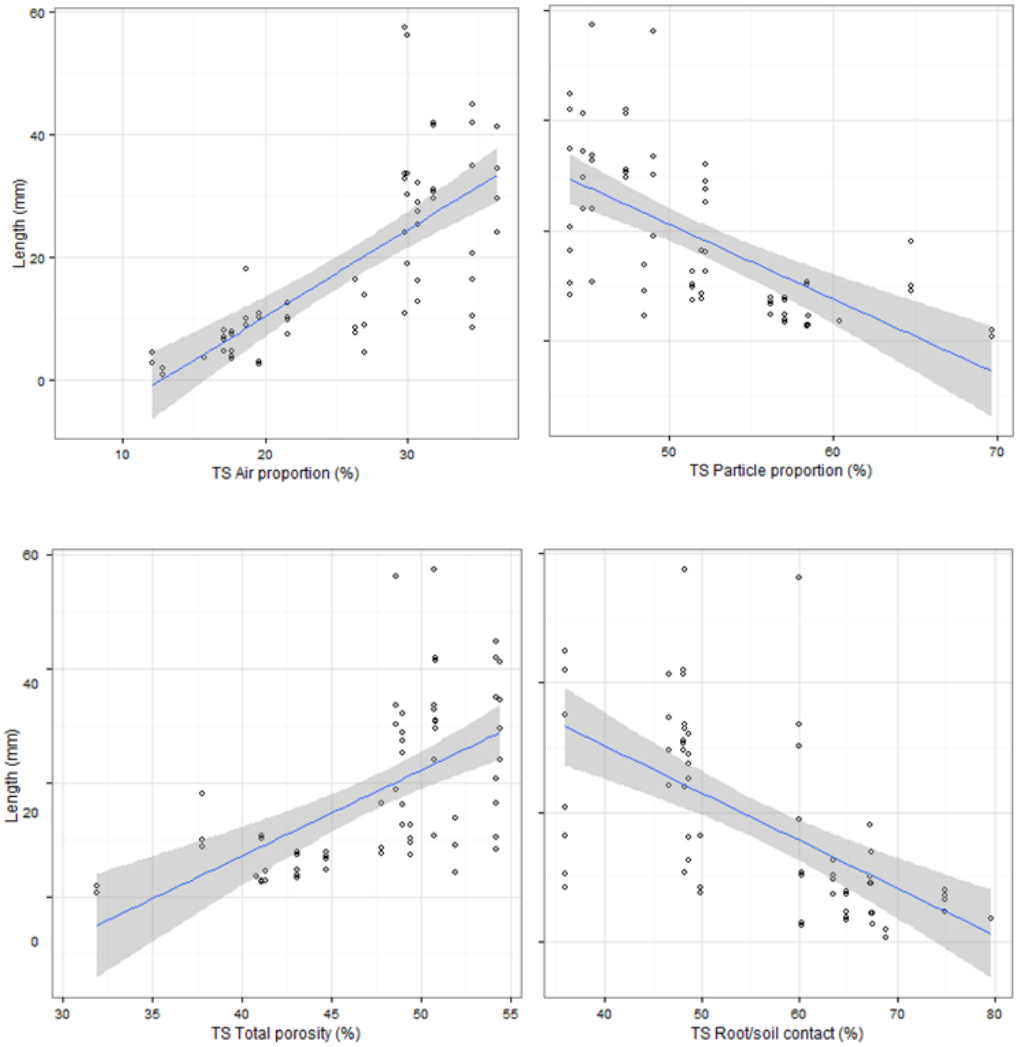

Figure 5-21: Linear regression curves for length as a function of percentage air by volume (r = 0.72), percentage particle by volume (r = -0.626), total porosity (r = 0.579) and root/soil contact (r = -0.591)

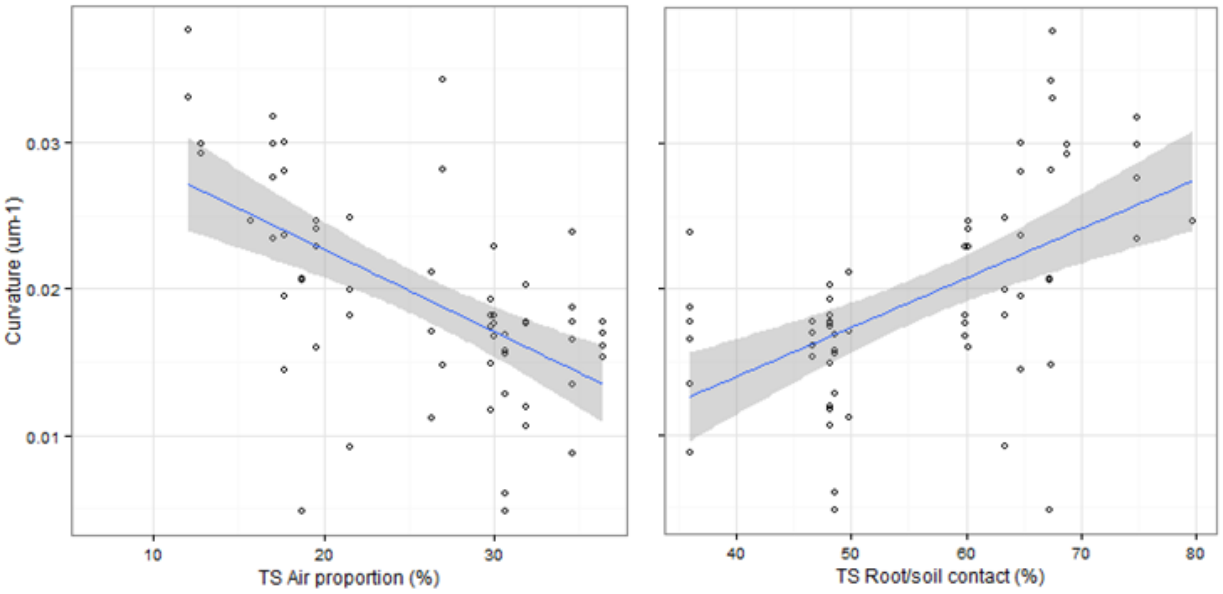

Figure 5-22: Linear regression curves for curvature as a function of percentage air by volume (r =-0.58) and root/soil contact (R^2 = 0.556)

5.6 Discussion

5.6.1 Discussion of methods

The aim of this chapter was to test the effect of compaction on barley root growth in **TS**, using a novel soil strength apparatus. The research for this thesis has involved constant method development, with incremental progression of the **TS** system being made with every experiment performed. The experiment performed for this chapter was the culmination of 3 years of **TS** and OPT method development, and was the best possible methodology that could have been used at the time, given the resources that were available.

The **TS** parameters were better controlled during this experiment than any other. Soil water content of 11 – 20% is often used in soil experiments (Zarebanadkouki et al., 2013, Merotto and Mundstock, 1999), as it offers an adequate amount of easily accessible water for the root system, without saturating the system and reducing air content to anoxic levels. For this experiment, we aimed to have a percentage water by volume of approximately 20%, and this was achieved, with µCT image analysis showing that percentage water by volume in cores ranged from 20-25% on average, depending on the treatment (Figure 5-14). More water was observed in the **H** treatment, because the water was added before the **TS** was compressed. This forced the particles closer together, and removed pore volume from the system (Figure 5-16). The percentage air by volume was between 32% and 15% on average, depending on the treatment. Despite the greater percentage water and lower percentage air by volume in the **H** treatment, these were not extreme enough for them to be considered limiting factors to root growth (Barley, 1962). Therefore, the effects observed are unlikely to have been due to water or air content within the **TS** cores.

The soil compaction apparatus designed for this experiment was another step forward in method development. The compaction level used in the **H** treatment was between 229.67 – 367.47kPa, and this produced a very high level of root growth impedance. Roots from this treatment did not really grow (Figure 5-3) and were very difficult to identify using OPT (Section 5.5). It may be the case that the immature roots were crushed during the application of the **H** compaction level to the system, and this may explain the lack of growth that was observed under this condition. If roots were not crushed and were therefore able to grow, then a significant impact on root growth would likely be observed for this treatment because penetrometer resistance is approximately 2-8 times higher than the axial pressure exerted by roots in order to move soil particles aside (Bengough and Mullins, 1990), which means that if it was possible to measure the penetrometer resistance of these soil cores, the readings may have been up to 3MPa (2-8 times the compression level applied to the **TS** cores). This would result in a significant impact on root growth (Bengough and Mullins, 1991, Bengough et al., 2011). Interestingly, if the **H** treatment had been omitted from this study, the OPT method would have identified a much higher proportion of roots overall (96.6% without H treatment vs.74% with H treatment).

(Valentine et al., 2012b) demonstrated that the 'Optic' cultivar of barley showed inhibited elongation rates in soil pore diameters of <60 µm. Therefore, consideration must be given as to the resolution of the µCT images in E.vii and the pore diameters within the TS cores. Pore size was not measured using the images obtained during this experiment, however the resolution of the images was 51µm and therefore, if it is assumed that the barley roots were unlikely to have penetrated TS pores of <60 µm, then the resolution was high enough to capture the barley roots easily. Whilst root diameters have been shown to differ between

barley varieties (McKenzie et al., 2009), the roots were seen easily in the images obtained during E.vii and segmented with relative ease. Therefore it can be assumed that roots were captured fully along their lengths.

For OPT imaging in E.vii, the concentration of sorbitol was adjusted slightly, from 15% to 17%. This was based on data that indicated 17% was the optimal concentration of sorbitol to use for **TS** that had been sieved to the particle size range of 850 – 1250 µm (Figure 2-18). This minor adjustment aligned the refractive index of the sorbitol and particles more closely, so that the roots were detected by the OPT system more easily. As a result, 74% of the roots across the three treatments were detected and 94% in the **N** treatment; a high enough proportion to rival the µCT imaging system, which detected 79% of roots across the 3 treatments and 88% of the roots in the **N** treatment. As already mentioned, the OPT system did not easily detect the shorter roots; particularly those in the **H** treatment, whereas the µCT imaging system was better able to detect very small roots (64% detected from µCT vs. 18% detected from OPT). This may be an area in which the OPT system can be further improved, however there will always be the limitation of longer roots or the seed blocking the very short roots from view, so although there could still be some further development of the OPT system, it may be the case that it is never suitable for detecting very short roots.

Finally, it is important to note that although detection of barley roots has improved throughout this project and is likely to improve through further research and method development, it will not replace µCT as a tool for observing root/soil interactions. µCT has proved itself to be indispensable for performing detailed analysis of root/soil interactions in 3-D, both during this project (Section 5.4.4.5) and other published experiments (Carminati et al., 2009, Schmidt et al., 2012), and given the importance of root/soil contact in early root

growth (Section 4.5.4), this is an area of research which should be investigated further. Despite OPT's shortcoming in identifying very small roots (< 5 mm), it should also be noted that it is a quick, effective and more economically viable option for studying root growth in **TS** (Section 2.5.3.1), with the potential to carry out large-scale phenotyping studies in the future. It may be a suitable and powerful 3-D imaging technique for institutions that do not have the means to acquire µCT as a resource. It could also be particularly useful for researchers who wish to make use of fluorescent techniques in order to observe root systems in a 3-D, physically heterogeneous transparent substrate (Downie et al., 2012). Currently, it is not possible to image fluorescence with µCT.

5.6.2 Discussion of results

The structure of soil, including particle size and the porous network that roots have to explore has an important effect on the elongation of roots, and this has motivated the development of different ways to visualise and quantify porous networks using µCT images (Taina et al., 2008), however the way that soil images are segmented and analysed can vary substantially between researchers (Baveye et al., 2010). In order to decrease the effects that may occur due to intra-observer error, all images were processed using the same image analysis pipeline and image analysis parameters (section 5.4.4.3). Significant differences were found between treatments for all of the **TS** variables that were measured. The **N** treatment had the lowest percentage particle by volume (Figure 5-12), the lowest percentage water by volume (Figure 5-14) and the largest percentage air by volume (Figure 5-16) within a given space in the core. The connectivity was also highest in the **N** treatment (Figure 5-18), as well as the total porosity (Figure 5-19). The **H** treatment had the highest percentage particle by volume, the highest percentage water by volume and the lowest percentage air by volume. The connectivity was

lowest in the **H** treatment, as was the air- and water-filled porosity. The **M** treatment was in between the **N** and **H** treatments for all measurements. These results are unsurprising, given that all cores began with the same weight of particles and volume of water in the cores, which were then compressed. Therefore, in the **N** treatment, it would be expected that there would be fewer particles, more air and less water per given volume than in the **M** treatment, and the **H** treatment which would have the most particles and water, but the least air, as air would be forced out of the core first due to compression. Due to a higher density of particles in the given volume, it would also make sense that total porosity and connectivity were reduced in the **H** treatment, as particles were forced closer together, blocking the paths of porous networks and shortening them.

This experiment showed that roots in the **N** treatment (0KPa) were the longest, **H** roots (229.67 – 367.47KPa) were by far the shortest and **M** roots (91.87 – 183.7KPa) were in between the other two treatments. Goss (1977) found that the root length of barley decreased by 62% when 25kPa of pressure was applied to roots grown in ballotini and Clark et al. (2001) found that root growth of pea seedlings was reduced by 50% in cores containing sand at a penetrometer resistance of 1.4 MPa. Lipiec et al. (2012) found that barley roots grown in compacted (> 2 MPa), undisturbed soil cores were 50% shorter that barley roots that were grown in uncompacted (0.90 MPa), undisturbed soil cores taken from the field.

In the experiment for this chapter, root growth decreased by 47.4% when 91.87 – 183.7KPa of pressure was applied to the **TS** system. The barley seedlings in Goss' (1977) experiment were grown in narrow ballotini cells for 7 days and were extracted before measuring. Forcing the roots to grow in what was essentially a 2-dimensional plain may have caused the roots to grow and respond to applied pressure differently, or it may have been the case that sections

of the roots were lost during extraction, or that measurements were less accurate than those that can be taken nowadays using modern 3D imaging and image analysis techniques. The soil conditions used in the Clark et al. (2001) experiment were probably most similar to those used in this experiment, whereby cylindrical cores containing sand were used and a 17 kg weight placed on top of them in order to induce compaction, however once again these roots were extracted from the cores before measurement, so similar difficulties in accurate measurement to those in the Goss (1977) experiment may have occurred. The findings from Lipiec et al. (2012) also fit with the results from this experiment (a decrease in length of 50% with > 2MPa soil penetrometer resistance), and so the pattern of 50% shorter roots in the **M** treatment was consistent with findings in the literature, demonstrating that root length is affected by compression in **TS** in the same way as it is in natural soil. It has been shown in previous research that wildtype tomato plants increase their endogenous concentrations of abscisic acid in the roots as they encounter increased soil bulk densities (Tracy et al., 2015). In mutant tomato plants which expressed lower levels of abscisic acid, the ability of their roots to elongate in soils of high bulk density is impaired. If a particular concentration of abscisic acid is required for barley roots to elongate in compacted soils, and the Westminster cultivar was unable to produce high enough endogenous levels of abscisic acid, then this may explain why decreased root length was seen in roots that grew in the **M** and **H** treatments of E.vii.

It is commonly known that the soil penetrometer resistance is considerably greater than the axial pressure that a root can exert during growth (Bengough and Mullins, 1990), which explains why the **M** treatment experienced a decrease of approximately 50% in root growth; the same decrease that would be expected in soil with a penetrometer resistance of 2MPa. It could be assumed that the roots in the **M** treatment were experiencing similar mechanical

resistance to roots that are grown in natural soil of 2MPa in strength. Unfortunately, measuring the strength of **TS** whilst inside the soil compaction apparatus was not possible, due to the free-standing end of the bracket blocking the penetrometer needle. Therefore, conventional soil strength data, obtained using a penetrometer are not available for this experiment and so it is only possible to speculate about the possible soil strength similarities that exist between the **M TS** treatment, and natural soil with a strength of 2MPa.

Convex hull volume and root system width can give an impression of how easily root systems explore soil and was suggested by Tracy et al. (2012) as a useful measurement which can provide quick and easily obtained data using software such as RooTrak (Mairhofer et al., 2012). Often, 'whole root' measurements such as these provide significant results between treatments, as was the case during this experiment (Figure 5-6 and Figure 5-7). **N** root systems had the largest convex hull volumes and root system widths. **H** had the smallest convex hull volumes and root system widths, and **M** root systems were in between the other two treatments. Tracy et al. (2012) found that convex hull volumes and root system widths (termed 'maximum width' in the paper) of tomato plants were significantly smaller in compacted soil than in uncompacted soil in both clay loam and loamy sand soils. These results correspond with the results obtained during this experiment and are likely to be as a direct result of the roots in the uncompacted treatment being longer and better able to explore a greater area of the soil during growth. At least in this way, it would appear that monocotyledonous barley roots and dicotyledenous tomato roots behave in the same manner. It also demonstrates that TS is an appropriate substitute for soil in experiments involving compaction.

Verticality and curvature measurements were taken in order to understand the tortuosity of roots as an active response to different levels of TS compaction. **N** roots had the lowest average curvature values, and so were the least curved. They had average verticalities in between those of the other treatments, but were more vertical than the **M** roots. The roots in the **H** treatment were the most curved and the least vertical. Very few roots were detected by OPT in the **H** treatment and the longest root that was detected was 5.38 mm in length. There was little, if no growth at all in this treatment, and therefore it has to be assumed that any tortuosity seen in these roots was either present before sowing the seeds, or more likely, was forced into such a manner by the surrounding particles during the process of compaction. Therefore, whilst it is important to take note of the results, the curvature and verticality measurements observed for this treatment are unlikely to be a representation of an active root response to mechanical resistance during growth and therefore will be omitted from further discussion.

As stated previously, roots in the **N** treatment were less curved than those in the **M** treatment. Therefore, roots in the **N** treatment showed a lower average level of tortuosity, as indicated by their lower average curvature values. When analysed in further detail (Figure 5-9) it was found that **N** roots had a stable level of curvature all the way from the base of the seed, to the tips of the roots. Curvature started at around 0.0175 μm^{-1} and remained stable at around this value until approximately 27 mm distance from the base of the seed, at which point the average curvature value rose to 0.025 μm^{-1}, so a slight increase in tortuosity was observed at the very tips of the roots. The confidence intervals were narrower than the other treatments, indicating less overall variation in curvature. The **M** roots initially appeared to follow the same curvature pattern as the **N** treatment, dipping in curvature values to approximately 0.0175

μm^{-1}, indicating a similar level of curvature but then values rose at approximately 3 mm distance from the base of the seed, to 0.025 μm^{-1}, indicating a higher level of curvature and tortuosity. It remained at this value until measurements for these roots stopped. Confidence intervals for this treatment were slightly wider than those for the **N** treatment. In summary, the roots from the **M** treatment were on average consistently more curved than those from the **N** treatment, and so demonstrated a higher level of tortuosity.

In an experiment which investigated overall tortuosity of primary tomato roots in different levels of compaction, (Tracy et al., 2012) calculated root tortuosity as the primary root length divided by linear root depth and found that it increased under compaction in loamy sand (1.2 $g.cm^{-1}$ vs. 1.6 $g.cm^{-1}$). Downie (2013) calculated tortuosity of lettuce leaves by dividing the total root length by the greatest distance between the two root extremities and also found that root tortuosity was greater in compacted **TS** on average (0.62 g.cm-^{1} vs. 0.78 $g.cm^{-1}$), however the differences were not found to be significant. Downie (2013) suggested that the differences between their results, and those of Tracy et al. (2012) could be due to the fact that Tracy used a greater difference in compaction between treatments, or because tomato roots behave in a different manner to lettuce roots, or because Tracy used a real soil as opposed to **TS**. The results from this experiment followed a similar pattern to Downie's work, whereby roots became more curved with increasing compression, however the differences were not statistically significant.

Roots in the **N** treatment were more vertical than those in the **M** treatment (Figure 5-5) and this was not unexpected, as an increase in soil compaction causes wider root angles, as they have to take a more tortuous path in order to explore the soil (Andrew, 1987). In this experiment, the verticality of the **N** roots began high but gradually decreased as the roots

grew more in line with the vertical. The verticality of **M** roots was less linear to begin with; increasing, then decreasing, then increasing slightly once again and then quickly decreasing as the roots began to reach the vertical plane (Figure 5-11). This supports the idea that roots in TS under mechanical pressure are less able to grow in a linear fashion and have to take a more tortuous path through the **TS** structure. Goodman and Ennos (1999) found that root angle was increased in sunflower roots that were grown in compacted soil, but that no difference in root angle was observed for maize roots grown in compacted soil. However these measurements were taken after extracting the roots from soil and laying them flat against a protractor. Tracy et al. (2012) took the lateral roots angles from tomato roots using 3-D µCT images and found no significant differences in root angle between compacted and uncompacted treatments, although they did acknowledge the observed trend that lateral roots in compacted treatments were closer to 90˚ than those that had grown in uncompacted soil. Downie (2013) also found that there were no significant differences between lettuce roots grown in uncompacted vs compacted **TS** treatments, although the general trend was that roots in uncompacted soil were less vertical than those in the compacted treatment. This is contrary to the results obtained during this experiment using **TS**, and probably occurred because the level of compaction in Downie et al.'s experiments were not as extreme as in this experiment, or because dicotyledenous roots were tested instead of the monocotyledonous roots that were used during this experiment. Nonetheless, the **TS** system did produce statistically significant differences in verticality during this experiment, which follow the patterns observed previously in the literature. This supports the use of **TS** as a growth medium for conducting studies investigating the effects of compaction on root systems.

Root length decreased linearly with particle proportion within the **TS** cores and root/soil contact (Figure 5-21). It is logical that root/soil contact and particle proportion are closely related and that if one increases so does the other. The importance of root/soil contact was outlined in the previous chapter (section 4.5.4) as well as in the literature (Schmidt et al., 2012, Carminati et al., 2009). In the previous chapter, it was a lack of root/soil contact that caused root growth inhibition in the **L** and split pot treatments (Figure 4-13). Those that achieved healthy elongation had a root/soil contact of >20%. In this experiment, root/soil contact was also correlated with root growth, although shorter roots had a higher level of root/soil contact. **N** roots had an average of 47.22% (±7.13) root contact, **M** roots had 62.69% (±8.13) and **H** roots had 68.74% (Figure 5-20), and so it would seem that root/soil contact of <20% in an uncompacted system or greater than >60% in a compacted system will inhibit root elongation in **TS**. Kooistra et al. (1992) performed root/soil analysis on maize roots grown in loose, intermediate and compacted soil. A thin-section technique was used in order to understand how root/soil contact differed between these treatments. It was found that average root/soil contact was 60% in the loose treatment, 72% in the intermediate treatment and 87% in the compacted treatment. This also corresponded with differences in specific root length of the maize roots. In the centre of the pots, specific root length was between 21.5 and 23.8 $m.g^{-1}$ for the loose treatment, 12.8 – 19.5 $g.m^{-1}$ for the intermediate treatment and 6.43 – 6.8 $g.m^{-1}$ for the compacted treatment. Therefore, specific root length decreased by approximately 75% at a root/soil contact of 87% vs 60%, corresponding with the pattern of root length decreasing once root/soil contact is above 60%. Caution should be applied however, as thin-sectioning and soil was used instead of μCT and **TS** which was used for this experiment. Also, maize was used instead of barley, so different root/soil contact thresholds may apply for different plant species.

Another important relationship appears to be that between root length and percentage air by volume. An increase in air content reflects a higher level of total porosity in the **TS** system, and therefore it is unsurprising that root length increased linearly with percentage air by volume. In an experiment by Merotto and Mundstock (1999), it was found that total root length decreased with decreasing air content and increasing soil bulk density and soil strength. Root length also decreased linearly with decreasing total porosity. All of the plants were grown in soil systems that contained at least 10% air, and it was mentioned that any air content below this level would be a limiting factor to root growth.

Root curvature showed linear relationships with some of the **TS** variables, decreasing (i.e. becoming less tortuous) with increasing percentage air by volume and increasing (i.e. becoming more tortuous) with increasing root/soil contact. Konopka et al. (2009) counted the number of bends observed in 1 cm length of maize roots grown in soils at different compaction levels. They found that as compaction increased, so did the number of bends, i.e. the tortuosity. The air and particle percentage by volume are related, so that if there are fewer particles in a given volume, the air content is likely to increase alongside porosity. The increase in percentage air by volume and total porosity enabled roots in the **N** treatment to grow through the soil system unimpeded. As the particle structure was such that it offered little resistance to the growing root, this means that it was unnecessary for roots to take a tortuous path through the **TS** system, and they were able to grow in a relatively straight manner. In the **H** treatment there was a higher particle proportion and higher levels of root/soil contact. Therefore, mechanical resistance to the roots increased and they were forced to explore a more tortuous route through the **TS** system (Konopka et al., 2009, Andrew, 1987).

5.7 Conclusions

This experiment used a novel compaction system in order to assess the utility of **TS** to mimic soil compaction and explore the effects on root system architecture between roots grown in **N**, **M** and **H** treatments. Those grown in the **N** treatment were the longest, the least curved and the most vertical. This corresponded with a **TS** structure that had the lowest particle density, the highest porosity and the lowest level of root/soil contact. The opposite was true for the **M** treatment roots, which were shorter, more curved and less vertical, and this corresponded with a **TS** structure that had a higher particle density, lower total porosity and a higher level of root/soil contact. The **TS** properties were even more extreme in the **H** treatment, however this treatment was too compacted for roots to grow; therefore it would be interesting to record the compaction threshold at which root growth ceases. In order to investigate this further, the soil compaction apparatus must be developed further so that an accurate, known level of compression can be applied.

Root length decreased by 57.4% in the **M** treatment, compared with the **N** treatment and this corresponds with what has been observed in the literature. Linear relationships were observed between barley root length and percentage air and particle by volume, total porosity and root/soil contact. This supports the idea that these different properties are inter-linked. As pressure increases, percentage particle by volume increases, percentage air by volume decreases, and so does total porosity. This results in a stronger **TS** system. Root/soil contact appears to be extremely important, underpinning all of these properties and providing an overall impression of the roots relationship with the surrounding soil. It was found that root/soil contact of >60% caused a significant decrease in root growth. This, combined with information from the previous experiment indicates that root/soil contact of

>20% but <60% in compacted soil may be the optimum level at which roots can explore the **TS** environment. Significant decreases in length are seen below and above this range.

Curvature was also an important property, yielding significant results between treatments and showing a linear relationship with **TS** percentage air by volume and root/soil contact. As root/soil contact increased, curvature also increased, reflecting the tortuous path that roots had to take in order to penetrate the compacted soil.

The findings from this experiment correspond with those previously found in the literature using a number of physically heterogeneous growth mediums such as soil, sand and ballotini. However, **TS** allows the observation of differences between treatments in a non-destructive manner, using the OPT imaging technique, which produces high resolution 3-D images, but is less expensive and quicker than µCT. This technique can still be developed further; indeed, we are only just beginning to understand what can be done with it. However, it offers a promising new system which may be used in the future for high-resolution phenotyping studies, possibly involving fluorescence technology.

6 General discussion and concluding remarks

This project aimed to develop our understanding of how roots interact with **TS**, with a view to placing it within the context of root growth in natural soil systems. In order to do this, **TS**, initially designed by Downie et al. (2012) was developed further, in order to accommodate the growth of roots which were considerably larger than those that were first grown in **TS**. The project revolved around 3 main areas:

- Root growth in different physically heterogeneous root growth substrates (soil vs. **TS** and **TS** of different particle size ranges);
- Root growth over time in growth mediums that purposely exposed different roots of the same plant to different conditions (vertically stratified 'split pots', observed at set time points as they explored the **TS**);
- Root growth in compacted growth mediums (soil strength apparatus applied to **TS**).

High resolution 3-D images were taken, and a new image analysis technique was developed, in order to better understand the architecture of the roots within these different conditions, and their physical interactions with the particles and pores surrounding them. Comparisons were made between the root growth that was observed in **TS**, vs growth which has been observed in other studies which have used natural soil systems.

Significant development was achieved throughout this project both in terms of what is now known about TS, and what can be done using the OPT imaging technique. The advantages and limitations of both of these methods are summarised in Table 6-1, and further detail regarding both of these points is provided below.

Transparent soil		Optical Projection Tomography	
Advantages	**Limitations**	**Advantages**	**Limitations**
• Transparency of agar, physical heterogeneity of soil. • No risk of hypoxia (compared with other transparent mediums such as agar). • Seeds are sown and left to grow in the same way as soil. • Roots can grow in 3-D, as opposed to being forced into a 2-D growth system. • Can control nutrient variability more effectively than in soil. • Can be physically manipulated with ease by	• Sorbitol required in order for root imaging to be carried out using light-based techniques such as OPT. Induces osmotic shock to plants. • Automated and non-destructive method for removing air bubbles that are trapped in the TS system	• Much less expensive to set up and use than µCT. • Technical expertise does not need to be as high for OPT as it does for µCT as the system is easier to use. • OPT is safe to use as there is no risk of radiation exposure. • Imaging entire root systems is very quick and easy (< 3 muntes).	• OPT is not used widely across institutions yet, so it is difficult to compare findings and validate the technique. • Software to operate the system is not readily available and therefore has to be written by a programmer on-site. • It is not yet operated automatically, so the user has

Transparent soil		Optical Projection Tomography	
Advantages	**Limitations**	**Advantages**	**Limitations**
sieving different particle size ranges. • Fluorescent roots and bacteria can grow in TS. • Segmentation of particles/ water/ air/ roots is easier in µCT images of TS, than µCT images of soil. • TS can be cleaned and recycled indefinitely. Fluorescence is removed during the cleaning.	after flooding with sorbitol has not yet been discovered. • Without a satisfactory method to remove air bubbles, TS cores are still limited in terms of size. • TS is still expensive compared to natural soil. • TS lacks the biological and chemical heterogeneity of soil, so applicability to root growth in field soil is yet to be determined.	• Using the correct concentration of sorbitol enables a high proportion of roots to be captured in 3-D images. • Possibility to image fluorescence which in future experiments will help with root segmentation. • High resolution capabilities will allow fluorescence to be imaged at a cellular scale, enabling relationships	to control the settings of the OPT system manually, and this has the potential to introduce error. • Reconstructing 3-D images currently takes a long time (>3 hours). This needs to be made quicker in order to conduct phenotyping studies.

Transparent soil		Optical Projection Tomography	
Advantages	**Limitations**	**Advantages**	**Limitations**
	• Barley root length is inhibited in TS by approximately 50%, for reasons which are currently unknown.	between roots and bacteria possible. • Imaging fluorescent cells will also enable the measurement of changes in cellular morphology as roots explore TS of different particle size ranges.	

Table 6-1: Summary of the advantages and limitations of the TS growth medium and OPT imaging technique

The first work on **TS** was carried out by Downie et al. (2012) and focused on developing a physically heterogeneous root growth system, with particles and pores, that was transparent enough to use with high-resolution, 3-D, optical imaging techniques (Downie et al., 2012, Downie, 2013). They achieved this, and used it to observe bacteria colonising root systems. They also performed some simple root system architecture experiments on dicotyledonous seedlings (Downie et al., 2012, Downie, 2013). Whilst this revealed information pertaining to root behaviour in **TS**, the dicotyledonous samples were small and the system was not suitable for more applied scientific questions, for example the study of larger root systems of cereals or soil compaction.

Monocotyledonous seedlings have root systems that grow quickly, and have multiple roots very early on as opposed to dicotyledonous seedlings which grow slower and have a single primary root with multiple lateral roots branching from it. Given the differences in growth between the two types of plants, it would be inappropriate to presume that their roots respond to **TS** in the same way.

Using barley roots allowed us to discover current limitations of **TS**, and to design strategies to image larger samples successfully. Transparent soil techniques are still in their infancy and the research has allowed us to advance the technology as well as the scientific knowledge on how barley roots interact with physically heterogeneous substrates. This is becoming ever more important, as agriculture faces growing difficulties due to rising global populations and decreasing areas of arable land (Liu et al., 2014). Overcoming such difficulties will require understanding as much as possible about plant, and root growth, and using it to helps farmers manage their lands in a way that is sustainable, and physically optimal for crop roots to

explore. This thesis marks the discovery of how barley roots grow in TS and respond to physical properties of soil, such as pore size and compaction.

The **TS** system was manipulated in a number of different ways to examine root growth. The scale of the cores was increased substantially compared with Downie et al. (2012), which was possible thanks to the introduction of a column system during the cleaning process. This provided enough **TS** to carry out experiments involving larger, monocotyledonous roots.

The physical structure of the **TS** system was also manipulated by sieving into different particle size ranges, making split pot cores and applying strength using a novel soil compaction apparatus. The barley roots responded to the different particle size ranges by growing longer in the **S** treatment (particle size range 850 – 1250 µm) than in the **L** treatment (>1676 µm), which was expected because the pores in the **L** treatment were very large, resulting in a lack of water availability to the root system. The split pot cores had an interesting effect on the roots, affecting the entire monocotyledonous roots system. This contradicted some of the other split pot experiments in the literature, which observed compensatory root growth in the section of the pot that was optimal (Montagu et al., 2001). In the soil strength experiment, roots were shorter as the pressure on the TS increased. This corresponded with what has been observed previously in the literature (Tracy et al., 2011).

Developments were also made in techniques for 3-D imaging of roots. Refractive index (RI) matching of **TS** and sorbitol was improved and it was found that **TS** of different particle size ranges require different sorbitol concentrations in order to obtain the best possible images using OPT. This may be due to the adsorptions and concentrations of mineral ions surrounding the particles, as well as in the network of micro-capillaries within the **TS** particles, which contain water when saturated (Downie, 2013). It is also not clear whether finer particle sizes

introduce more solid – liquid interface and this may accentuate any mismatch between the RI of the liquid and that of the particles. Once this discovery was made, more roots were detected and measured using the OPT system, and in some treatments the OPT imaging technique detected more roots than the µCT technique, which to this date has been the benchmark for assessing the imaging of root systems non-destructively in 3-D soil systems.

An image analysis technique was developed to extract numerical data from the 3D images that were obtained during this experiment. This method involved the steps outlined in Figure 6-1. The parameters of each step were adjusted slightly, depending on the specific medium being imaged at the time. At present, the steps contained within the yellow and green boxes can be performed using µCT imaging. Steps contained within the green box can be performed using OPT imaging.

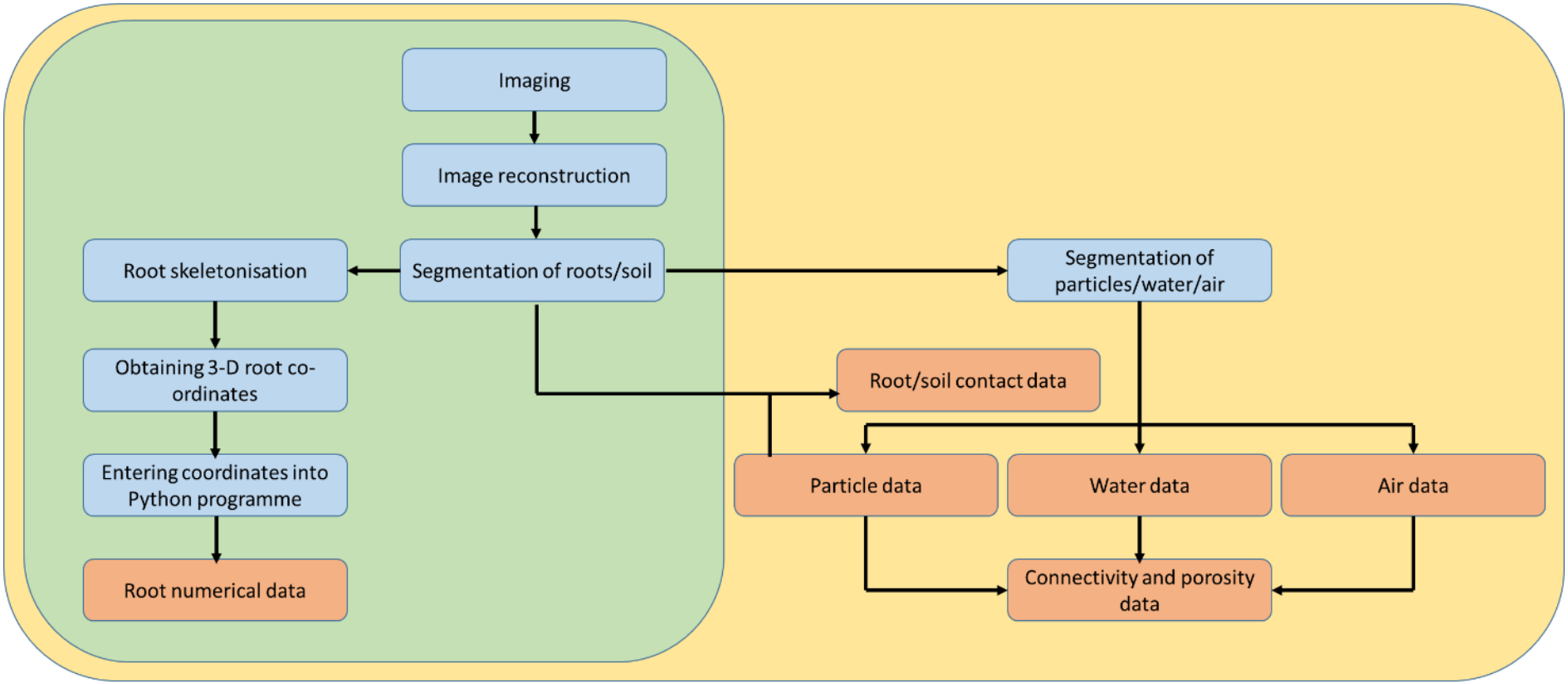

Figure 6-1: The image processing pipeline used throughout this project. Steps contained within the yellow and green boxes can be performed using µCT. Steps contained within the green box can be performed using OPT.

The method for obtaining numerical data from images of roots was initially developed using µCT images, but was later applied to OPT images as well, and was subsequently used throughout the project for all experiments. Roots grown in **TS** were imaged non-destructively in 3-D using both µCT and OPT. Other benefits of using **TS** were discovered, such as ease of **TS** and root segmentation of µCT images. Furthermore, the air, water and particles are also segmented from each other more easily in **TS** images taken using µCT, when compared with images of natural soil which are difficult to segment (Baveye et al., 2010). These advantages possibly offer an alternative growth medium to soil for high-throughput imaging using combined microscopy - µCT techniques in future research.

Root growth was different between the B83 and Troon barley cultivars, but this was largely due to B83's lack of growth. This was the case in both soil and **TS**. B83 was substituted for Westminster, a cultivar that was more similar to Troon in terms of length, but different in terms of root angle (grown in 2-D gel plates; (Valentine et al., 2012a)). There were no statistically significant differences between Troon and Westminster when grown in the **TS** system. There were also no statistical differences between these cultivars and Golden Promise roots grown in **TS**. It is important to note that further testing of a variety of barley cultivars should be carried out, as this experiment showed that phenotypic differences present in 2-D systems may not be the same in 3-D systems. This may be because roots are less constrained within a 3-D system, when compared with 2-D systems such as gel plates, and this should be explored further in larger scale phenotyping studies.

In E.i, two different barley cultivars (B83 and Troon) were found to grow longer in natural soil than in **TS** and this could be due to a number of different reasons, such as nutrient availability (Mengel, 1983), water availability (Manschadi et al., 2006), or the physical structure of **TS**

being different to that of soil (Figure 3-3). It is also important to note that barley roots grow differently in different kinds of soil, so there may be some soils in which root growth is similar to that seen in **TS**. The physical structure is likely to have played a significant role, as there was less total porosity, less connectivity and a higher level of root/soil contact in soil than there was in **TS**. By removing soil from further experiments and focusing more on **TS** by changing its physical structure in a number of ways, we were able to induce changes in the way that roots grew, indicating that the physical structure of soil is highly important and can impact on the morphology of root system architecture in different ways.

E.iv was the first step towards manipulating the physical structure of **TS**. The **TS** was sieved into different particle size ranges which changed the sizes of the pores that were available to the roots and allowed us to identify differences in barley root growth between the different **TS** particle size ranges. It was found that all roots, regardless of cultivar, grew longest in the 850 – 1250 µm treatment and failed to grow in the >1676 µm treatment. Root/soil contact measurements were not taken for all of the particle size ranges during E.iv; however it can be assumed that it was similar to the root/soil contact levels observed in the **S** and **L** treatments during E.v, described in Chapter 4. During E.v, it was found that total porosity was higher in the **S** treatment than in the **L** treatment, as was root/soil contact. Porosity is important for aeration, but it is also an indication of how easily a root tip will be able to exploit the pore space to grow (Marinari et al., 2000). Root/soil contact is important because if the roots have no contact with surrounding particles, they are less able to acquire water and nutrients (Carminati et al., 2009). Therefore, the balance that exists between these two properties is an important one and during this project, we have begun to try and define the optimal thresholds for these properties, using the **TS** system as detailed below.

When roots were observed growing inside vertically stratified split pots (50% 850-1250 µm, 50% >1676 µm), it was found that if 50% of the soil volume was physically sub-optimal (as was the case in the section of the pot containing >1676 µm particles), that this would significantly affect the growth of the entire root system, including the roots present in the physically optimal side of the pot. Interestingly, in this experiment it was found that roots actively grew towards the soil section containing larger particles, presumably because the pores were much larger and offered the path of least resistance for these roots (Bengough and Mullins, 1990). However, these pores were too large to promote healthy root growth, as was demonstrated both in this experiment and in section 3.5.3. Roots were unable to make an adequate level of physical contact with particle surfaces onto which nutrients were adsorbed, or adequately locate water-filled pores. The stress caused to the roots in this section of the **TS** affected the growth of the entire root system, with roots in the layer containing smaller particles also showing a considerable reduction in growth. Whilst the literature has suggested that compensatory root growth can occur when root systems are exposed to different physical conditions, e.g. Montagu et al. (2001) soil compaction experiment, the results from this project also suggest that root growth is not a completely autonomous process, dependent on conditions surrounding individual root tips, but is rather a systemic process, with some form of communication possibly occurring between different roots of the same plant.

E.vii yielded the greatest differences in curvature and verticality between treatments. In this experiment, it was found that roots were shorter, more tortuous and less vertical when compression was applied to them. The roots were shorter due to the mechanical impedance that they had to overcome in order to push particles aside so that they could explore the **TS**

(Bengough and Mullins, 1991). The tortuosity was also increased because roots were forced to change direction and find a path that offered least resistance when the force required to push the particles aside exceeded the critical growth force produced by the root during growth. If the conditions are optimal and roots are not experiencing strong mechanical impedance, orientation towards the vertical plane due to gravitropism is unimpeded and root angles and trajectories are likely to be genetically determined (Digby and Firn, 1995). If there is compaction, then the roots have to respond to this stress and grow along a path that may be further away from the vertical plane (Tracy et al., 2012). This is what occurred in the compacted **TS** treatment, where roots were less vertical than those in the uncompacted treatment. In this respect, roots behaved in the same way as they would have done in soil (Bengough and Mullins, 1991, Digby and Firn, 1995, Tracy et al., 2012),.

As mentioned previously, root/soil contact has been identified as a physical property which determines root growth, with the optimum level of root/soil contact being between 20 and 60%. This relationship is demonstrated in Figure 6-2, whereby it can be seen across all treatments that as root/soil contact increased, so did the elongation rate of the roots observed in that treatment. This trend increased until root/soil contact reached 60%, beyond which root length decreased significantly. Of course, caution should be applied when interpreting this figure as the roots were not all grown for exactly the same amount of time; the roots in the **TS** (>1676 µm), **TS** (split pot) and **TS** (850-1250 µm) were all in the **TS** system for a total of 96 hours, the roots in the **TS** (mixed) and soil (1.1 $g.cm^3$) treatments were in the **TS** system for 48 hours and the roots in the **TS** (no compression), **TS** (mid compression) and **TS** (high compression) treatments were in the TS system for a total of 72 hours. It was for this reason that elongation rate of the roots was presented and not root length. However, the 3

treatments that had the longest roots were each from a different experiment and their levels of root/soil contact were all in between 40 and 60%. It would be interesting to compare root growth in soil vs. **TS** cores containing only the 850-1250 µm particle size range, as it may be the case that these two treatments produce root systems that are very similar to one another and would reduce the negative effect on growth that was seen in the first soil vs. **TS** experiment, where a mixed **TS** treatment was used.

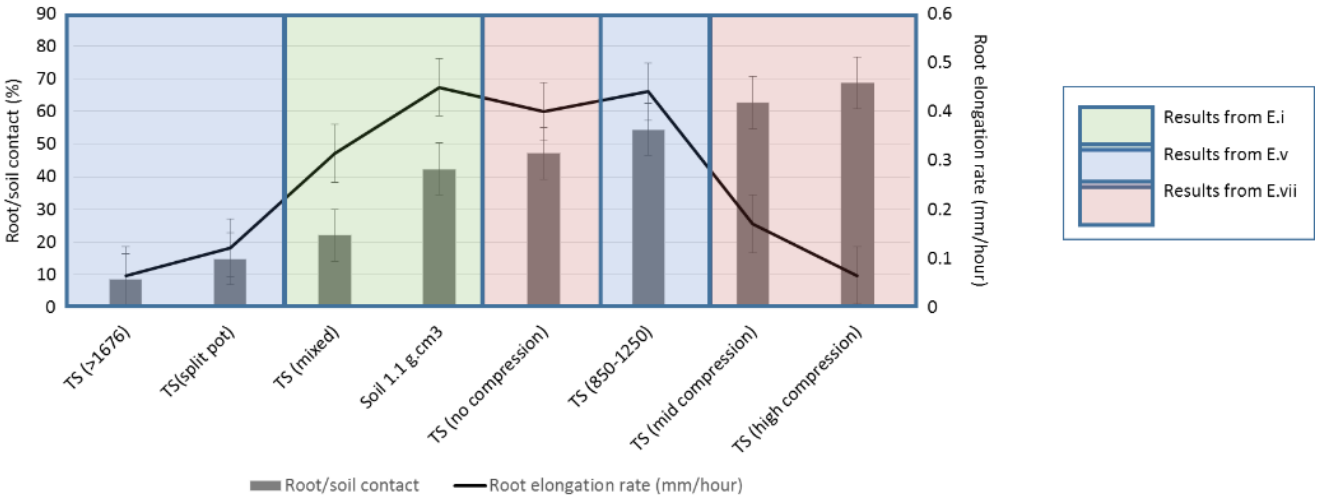

Figure 6-2: Mean average root/soil contact and root elongation rates for all of the treatments used during E.i, E.v and E.vii of this thesis

In E.v (Section 4.5.4), it was demonstrated that 45 – 55% particle volume was optimal for root growth, and that even though there was a higher proportion of particles in the **L** treatment, there was a decrease in root/soil contact. The **S** treatment had the lowest particle volume of the 3 treatments in this experiment, but the highest level of root/soil contact. This was due to the large pores that were created by large particles in the **L** treatment (Nimmo, 2004). There was more solid matter within the **L** cores, but this did not promote healthy root growth, because large pores are not favourable for maintaining root/soil contact (Carminati et al., 2009). In E.vii (Chapter 5), the particle volume per unit area increased along with root/soil contact, and this equally produced an inhospitable environment for healthy root growth, due

to the soil strength that made it more difficult for roots to push the particles aside so that they could explore the porous network (Bengough and Mullins, 1990). Achieving an ideal soil structure therefore involves finding a particle density that maintains contact with up to 60% of the root system at any given time, however the soil structure itself has to be plastic enough for particles to be moved aside easily by the root tip, as it elongates through the soil. This will involve achieving the right balance between air, water and particle content and this balance is likely to differ between growth mediums, depending on carbon content, inherent soil moisture and soil aggregates (Vereecken et al., 1989). This is a research path that warrants further investigation, so that these parameters can be better defined. This is also where **TS** is useful, because **TS** is processed in the same way each time and additional factors such as nutrient gradients, particle size and microbial populations can be more easily controlled, so that only the roots' responses to the physical structure of the system is being tested. By understanding these parameters in more detail, we will be in a better position to advise farmers on soil management practices (e.g. ploughing and watering).

In summary, the following novel findings regarding barley root growth in TS were discovered during this project:

- Barley roots grow in TS. Some varieties are better able to explore TS than others.
- Barley root growth in mixed particle size TS is approximately 50% of that in natural soil sieved to <2 mm.
- Barley roots elongate more successfully in the particle size range 850µm-1250µm, followed by the 1250µm - 1676µm particle size range, followed by the >1676µm particle size range.

- When grown in vertically stratified split pots (one side 850-1250µm, the other side >1676µm), barley root elongation is inhibited across the entire root system, compared with roots grown in pots containing only TS particles of 850-1250µm. Compensatory root growth is not observed in the first 96 hours post-germination.
- Roots appear to preferentially choose the side of the split pot containing particles of >1676µm, despite it being unsuitable for root elongation. This is likely due to it offering larger pores and a path of less resistance.
- Roots respond to compaction in TS in a similar way to how they respond to natural soil compaction; root elongation is inhibited, and root systems are less vertical.

6.1 Possible directions for future research

The versatility of **TS** for testing effects of different physical soil conditions on root growth has been successfully demonstrated during this thesis. **TS** capabilities have also been increased during this project to help answer questions that were previously unanswered about monocotyledonous root growth in **TS**. Particle: air content within cores (Section 5.5.4), root/soil contact (Section4.5.4) and soil strength (Section 5.5.4) have all been identified as important parameters affecting barley root growth and have been discussed in detail in previous sections of this thesis.

There are a number of different possible future research routes, both in method development and in answering biological questions pertaining to the growth of monocotyledonous roots in 3-D heterogeneous substrates. In summary, directions for future work could involve the following areas of research:

- More research should be done to see whether the **TS** system can be modified so that an optically matching solution that is less harmful to the roots growing inside can be applied to the particles. This would allow the observation of root growth under different conditions in real-time using light-based imaging techniques such as OPT.
- The possibility of using 3-D printing to print TS particles should be investigated. This may reduce the cost of TS considerably, and increase the volume of TS that can be produced within a short space of time. Consideration should be given to the material used for printing and its cation exchange capacity, whether it can be loaded with media in the same way as nafion TS can, as well as its refractive index. Consideration could also be given as to the size and shape of particles being printed, and also the printing of particles which can physically replicates soil aggregates within natural systems.
- The development of fluorescent technologies, such as transgenic barley cultivars, fluorescence delivered by a viral delivery system, or the application of fluorescent dyes. This may improve downstream segmentation of OPT images. It would certainly allow researchers to observe at a more detailed level how cell structure is altered by different physical conditions.
- Larger phenotyping studies with a number of different barley varieties, to confirm whether the root system architecture data obtained using 2-D systems is the same as that observed in the 3-D **TS** system. Data from both 2-D and 3-D systems could then be compared with that of field experiments, to calculate any differences and understand further the applicability of data from artificial soil systems, to that obtained using field soil.

- It is important to define the proportion of **TS** that has to be physically suboptimal in vertically stratified **TS** cores before a negative effect is observed on root growth and then to translate it to data obtained from field data. This will help us to better our understanding of soil structure in the field and how it affects barley root growth. It will also help us to inform farm management practices more accurately.
- The precise air, water and particle content in **TS** cores that creates the ideal balance between particle volume and total porosity in **TS** cores, providing optimal root/soil contact and is therefore optimal for growing barley roots. This information can then be translated to field data to understand whether a similar ratio of air: water: particles and root/soil contact is beneficial in the field.

Perhaps one of the greatest challenges will be to bring together the knowledge that can now be acquired from the variety of measurements that are available to us (e.g. verticality, curvature, root/soil contact etc.). By combining different root growth mediums with 3-D imaging techniques, we can acquire detailed information which can be used to develop new theories and models about the laws that underpin root growth. With more knowledge about root growth and soil structure we can improve agricultural practices and make better use of the soil that is available to us.

References

ACHE, B. 2015. *How much does a micro-CT scanner cost? (Costs converted from $US to £GBP)* [Online]. Available: http://blog.microphotonics.com/how-much-does-a-micro-ct-scanner-cost/ [Accessed].

ADU, M. O., CHATOT, A., WIESEL, L., BENNETT, M. J., BROADLEY, M. R., WHITE, P. J. & DUPUY, L. X. 2014. A scanner system for high-resolution quantification of variation in root growth dynamics of Brassica rapa genotypes. *Journal of experimental botany,* 65**,** 2039-2048.

AL-ANI, M. A. & HAY, R. 1983. The influence of growing temperature on the growth and morphology of cereal seedling root systems. *Journal of experimental botany,* 34**,** 1720-1730.

AL-KARAKI, G., AL-AJMI, A. & OTHMAN, Y. 2007. Seed germination and early root growth of three barley cultivars as affected by temperature and water stress. *American-Eurasian Journal of Agriculture and Environment Science,* 2**,** 112-117.

ALIZADEH, V., SHOKRI, V., SOLTANI, A. & YOUSEFI, M. A. 2015. Effects of Climate Change and Drought-Stress on Plant Physiology. *International journal of Advanced Biological and Biomedical Research,* 3**,** 38-42.

ANDERSON, S. H. & HOPMANS, J. 1994. Tomography of soil-water-root processes. *Soil Science Society of America Special Publication,* 36.

ANDREW, S. 1987. A mathematical model of root exploration and of grain fill with particular reference to winter wheat. *Fertilizer research,* 11**,** 267-281.

ANGHINONI, I. & BARBER, S. 1980. Phosphorus influx and growth characteristics of corn roots as influenced by phosphorus supply. *Agronomy Journal,* 72**,** 685-688.

ARSENAULT, J.-L., POULCUR, S., MESSIER, C. & GUAY, R. 1995. WinRHlZO™, a root-measuring system with a unique overlap correction method. *HortScience,* 30**,** 906-906.

ARVIDSSON, J. 1999. Nutrient uptake and growth of barley as affected by soil compaction. *Plant and Soil,* 208**,** 9-19.

ARVIDSSON, J. & HÅKANSSON, I. 2014. Response of different crops to soil compaction—Short-term effects in Swedish field experiments. *Soil and Tillage Research,* 138**,** 56-63.

ATWELL, B., LOUGHMAN, B., GAŠPARÍKOVÁ, O. & KOLEK, J. Physiological responses of lupin roots to soil compaction. Structural and functional aspects of transport in roots. Third international symposium on structure and function of roots. Nitra, Czechoslovakia, 3-7 Aug. 1987., 1989. Kluwer Academic Publishers, 251-255.

BALUŠKA, F., MANCUSO, S., VOLKMANN, D. & BARLOW, P. W. 2010. Root apex transition zone: a signalling–response nexus in the root. *Trends in plant science,* 15**,** 402-408.

BALUŠKA, F., VOLKMANN, D. & BARLOW, P. W. 1996. Specialized zones of development in roots: view from the cellular level. *Plant Physiology,* 112**,** 3.

BARLEY, K. 1962. The effects of mechanical stress on the growth of roots. *Journal of Experimental Botany,* 13**,** 95-110.

BARLOW, P. W. 2002. The root cap: cell dynamics, cell differentiation and cap function. *Journal of Plant Growth Regulation,* 21**,** 261-286.

BARLOW, P. W. 2006. Charles Darwin and the plant root apex: closing a gap in living systems theory as applied to plants. *Communication in Plants.* Springer.

BATEY, T. 2009. Soil compaction and soil management – a review. *Soil Use and Management,* 25**,** 335-345.

BAVER, L. Soil permeability in relation to non-capillary porosity. Soil Science Society of America Journal, 1938. 52-56.

BAVEYE, P. C., LABA, M., OTTEN, W., BOUCKAERT, L., DELLO STERPAIO, P., GOSWAMI, R. R., GRINEV, D., HOUSTON, A., HU, Y., LIU, J., MOONEY, S., PAJOR, R., SLEUTEL, S., TARQUIS, A., WANG, W., WEI, Q. & SEZGIN, M. 2010. Observer-dependent variability of the thresholding step in the quantitative analysis of soil images and X-ray microtomography data. *Geoderma,* 157**,** 51-63.

BENGOUGH, A., GORDON, D., AL-MENAIE, H., ELLIS, R., ALLAN, D., KEITH, R., THOMAS, W. & FORSTER, B. 2004. Gel observation chamber for rapid screening of root traits in cereal seedlings. *Plant and Soil,* 262**,** 63-70.

BENGOUGH, A. & MULLINS, C. 1990. Mechanical impedance to root growth: a review of experimental techniques and root growth responses. *Journal of soil science,* 41**,** 341-358.

BENGOUGH, A. & MULLINS, C. 1991. Penetrometer resistance, root penetration resistance and root elongation rate in two sandy loam soils. *Plant and Soil,* 131**,** 59-66.

BENGOUGH, A. G., MCKENZIE, B., HALLETT, P. & VALENTINE, T. 2011. Root elongation, water stress, and mechanical impedance: a review of limiting stresses and beneficial root tip traits. *Journal of Experimental Botany,* 62**,** 59-68.

BENGOUGH, A. G. & YOUNG, I. M. 1993. Root elongation of seedling peas through layered soil of different penetration resistances. *Plant and Soil,* 149**,** 129-139.

BENGOUGH, G., BRANSBY, F., HANS, J., MCKENNA, S. J., ROBERTS, T. J. & VALENTINE, T. A. 2005. Root responses to soil physical conditions; growth dynamics from field to cell. *Journal of Experimental Botany,* 57**,** 437 - 447.

BIEMELT, S., KEETMAN, U. & ALBRECHT, G. 1998. Re-Aeration following Hypoxia or Anoxia Leads to Activation of the Antioxidative Defense System in Roots of Wheat Seedlings. *Plant Physiology,* 116**,** 651-658.

BINGHAM, I. & BENGOUGH, A. 2003. Morphological plasticity of wheat and barley roots in response to spatial variation in soil strength. *Plant and soil,* 250**,** 273-282.

BÖHM, W. 1979. Techniques of root washing. *Methods of Studying Root Systems.* Springer.

BOONSIRICHAI, K., SEDBROOK, J. C., CHEN, R., GILROY, S. & MASSON, P. H. 2003. ALTERED RESPONSE TO GRAVITY is a peripheral membrane protein that modulates gravity-induced cytoplasmic alkalinization and lateral auxin transport in plant statocytes. *The Plant Cell Online,* 15**,** 2612-2625.

BOUWMAN, L. A. & ARTS, W. B. M. 2000. Effects of soil compaction on the relationships between nematodes, grass production and soil physical properties. *Applied Soil Ecology,* 14**,** 213-222.

BOX, G. E. & COX, D. R. 1964. An analysis of transformations. *Journal of the Royal Statistical Society. Series B (Methodological)*, 211-252.

BRONICK, C. J. & LAL, R. 2004. Soil structure and management: a review. *Geoderma,* 124, 3-24.

BROOKS, T. L. D., MILLER, N. D. & SPALDING, E. P. 2010. Plasticity of Arabidopsis root gravitropism throughout a multidimensional condition space quantified by automated image analysis. *Plant physiology,* 152, 206-216.

BROUDER, S. & CASSMAN, K. 1994. Cotton root and shoot response to localized supply of nitrate, phosphate and potassium: Split-pot studies with nutrient solution and vermiculitic soil. *Plant and Soil,* 161, 179-193.

BRUAND, A., COUSIN, I., NICOULLAUD, B., DUVAL, O. & BEGON, J. C. 1996. Backscattered electron scanning images of soil porosity for analyzing soil compaction around roots. *Soil Science Society of America Journal,* 60, 895-901.

BUSCH, J., MENDELSSOHN, I. A., LORENZEN, B., BRIX, H. & MIAO, S. 2006. A rhizotron to study root growth under flooded conditions tested with two wetland Cyperaceae. *Flora - Morphology, Distribution, Functional Ecology of Plants,* 201, 429-439.

BUSTOS, D., LASCANO, R., VILLASUSO, A. L., MACHADO, E., SENN, M. E., CÓRDOBA, A. & TALEISNIK, E. 2008. Reductions in maize root-tip elongation by salt and osmotic stress do not correlate with apoplastic O2•− levels. *Annals of botany,* 102, 551-559.

CANNAVO, P. & MICHEL, J. C. 2013. Peat particle size effects on spatial root distribution, and changes on hydraulic and aeration properties. *Scientia Horticulturae,* 151, 11-21.

CARMINATI, A., VETTERLEIN, D., WELLER, U., VOGEL, H.-J. & OSWALD, S. E. 2009. When roots lose contact. *Vadose Zone Journal,* 8**,** 805-809.

CHAERLE, L. & VAN DER STRAETEN, D. 2001. Seeing is believing: imaging techniques to monitor plant health. *Biochimica et Biophysica Acta (BBA)-Gene Structure and Expression,* 1519**,** 153-166.

CHENG, Y., LIU, J., LÜ, F. & ZHANG, J. 2012. Three-dimensional reconstruction of soil pore structure and prediction of soil hydraulic properties based on CT images. *Transactions of the Chinese Society of Agricultural Engineering,* 28**,** 115-122.

CLARK, L., WHALLEY, W. & BARRACLOUGH, P. 2001. Partial mechanical impedance can increase the turgor of seedling pea roots. *Journal of experimental botany,* 52**,** 167-171.

CLARK, L., WHALLEY, W. & BARRACLOUGH, P. 2003. How do roots penetrate strong soil? *Plant and Soil,* 255**,** 93-104.

CLARK, L., WHALLEY, W., LEIGH, R., DEXTER, A. & BARRACLOUGH, P. 1999. Evaluation of agar and agarose gels for studying mechanical impedance in rice roots. *Plant and soil,* 207**,** 37-43.

COUDERT, Y., PÉRIN, C., COURTOIS, B., KHONG, N. G. & GANTET, P. 2010. Genetic control of root development in rice, the model cereal. *Trends in Plant Science,* 15**,** 219-226.

DARWIN, C. & DARWIN, F. 1880. The Power of Movement in Plants. London: John Murray.

DAVIES, W. J. & ZHANG, J. 1991. Root signals and the regulation of growth and development of plants in drying soil. *Annual review of plant biology,* 42**,** 55-76.

DEFRA 2015. Farming statistics - 2015 wheat and barley production, UK. *In:* AFFAIRS, D. F. E. F. R. (ed.).

DEN HERDER, G., VAN ISTERDAEL, G., BEECKMAN, T. & DE SMET, I. 2010. The roots of a new green revolution. *Trends in plant science,* 15**,** 600-7.

DHONDT, S., VANHAEREN, H., VAN LOO, D., CNUDDE, V. & INZÉ, D. 2010. Plant structure visualization by high-resolution X-ray computed tomography. *Trends in plant science,* 15**,** 419-422.

DIGBY, J. & FIRN, R. 1995. The gravitropic set-point angle (GSA): the identification of an important developmentally controlled variable governing plant architecture*. *Plant, Cell & Environment,* 18**,** 1434-1440.

DIVISEK, J., EIKERLING, M., MAZIN, V., SCHMITZ, H., STIMMING, U. & VOLFKOVICH, Y. M. 1998. A Study of Capillary Porous Structure and Sorption Properties of Nafion Proton-Exchange Membranes Swollen in Water. *Journal of the Electrochemical Society,* 145**,** 2677-2683.

DOLAN, L. & DAVIES, J. 2004. Cell expansion in roots. *Current Opinion in Plant Biology,* 7**,** 33-39.

DOLAN, L., JANMAAT, K., WILLEMSEN, V., LINSTEAD, P., POETHIG, S., ROBERTS, K. & SCHERES, B. 1993. Cellular organisation of the Arabidopsis thaliana root. *Development,* 119**,** 71-84.

DOWNIE, H., HOLDEN, N., OTTEN, W., SPIERS, A. J., VALENTINE, T. A. & DUPUY, L. X. 2012. Transparent Soil for Imaging the Rhizosphere. *PLoS ONE,* 7**,** e44276.

DOWNIE, H. F. 2013. The development of a transparent soil and its application in imaging root trajectories and root-bacteria interactions - Thesis.

DOWNIE, H. F., ADU, M. O., SCHMIDT, S., OTTEN, W., DUPUY, L. X., WHITE, P. J. & VALENTINE, T. A. 2015. Challenges and opportunities for quantifying roots and rhizosphere interactions through imaging and image analysis? *Plant, Cell & Environment,* 38**,** 1213-1232.

DÜRR, C. & AUBERTOT, J.-N. 2000. Emergence of seedlings of sugar beet (Beta vulgaris L.) as affected by the size, roughness and position of aggregates in the seedbed. *Plant and soil,* 219**,** 211-220.

EAPEN, D., BARROSO, M. A. L., CAMPOS, M. A. E., PONCE, G., CORKIDI, G., DUBROVSKY, J. G. & CASSAB, G. I. 2003. A no hydrotropic response Root Mutant that Responds Positively to Gravitropism in Arabidopsis. *Plant Physiology,* 131**,** 536-546.

ELLIOT, J., JAMES, P., MCMASTER, T., NEWTON, J., ELLIOT, A., HANNA, S. & MILES, M. 2001. Hydrolysis of the Nafion precursor studied by X-ray scattering and in-situ atomic force microscopy. e-Polymer 022.

ESMON, C. A., PEDMALE, U. V. & LISCUM, E. 2005. Plant tropisms: providing the power of movement to a sessile organism. *International Journal of Developmental Biology,* 49**,** 665.

FALIK, O., REIDES, P., GERSANI, M. & NOVOPLANSKY, A. 2005. Root navigation by self inhibition. *Plant, Cell & Environment,* 28**,** 562-569.

FIRN, R. D. & DIGBY, J. 1997. Solving the puzzle of gravitropism—has a lost piece been found? *Planta,* 203**,** S159-S163.

FISHER SCIENTIFIC. 2011. *Filter Papers for the Laboratory and Industry* [Online]. Available: https://static.fishersci.com/cmsassets/downloads/segment/Scientific/pdf/filter_papers.pdf [Accessed].

FLAVEL, R. J., GUPPY, C. N., TIGHE, M., WATT, M., MCNEILL, A. & YOUNG, I. M. 2012. Non-destructive quantification of cereal roots in soil using high-resolution X-ray tomography. *Journal of experimental botany*, err421.

FRAAS, S. & LÜTHEN, H. 2015. Novel imaging-based phenotyping strategies for dissecting crosstalk in plant development. *Journal of experimental botany,* 66**,** 4947-4955.

GALEN, C., RABENOLD, J. J. & LISCUM, E. 2007. Functional ecology of a blue light photoreceptor: effects of phototropin-1 on root growth enhance drought tolerance in Arabidopsis thaliana. *New phytologist,* 173**,** 91-99.

GALES, K. 1983. Yield variation of wheat and barley in Britain in relation to crop growth and soil conditions—a review. *Journal of the Science of Food and Agriculture,* 34**,** 1085-1104.

GOODMAN, A. M. & ENNOS, A. R. 1999. The Effects of Soil Bulk Density on the Morphology and Anchorage Mechanics of the Root Systems of Sunflower and Maize. *Annals of Botany,* 83**,** 293-302.

GOSS, M. J. 1977. Effects of Mechanical Impedance on Root Growth in Barley (Hordeum vulgare L.): I. EFFECTS ON THE ELONGATION AND BRANCHING OF SEMINAL ROOT AXES. *Journal of Experimental Botany,* 28**,** 96-111.

GOWING, D., DAVIES, W. & JONES, H. 1990. A positive root-sourced signal as an indicator of soil drying in apple, Malus x domestica Borkh. *Journal of Experimental Botany,* 41**,** 1535-1540.

GREGORY, P., HUTCHISON, D., READ, D., JENNESON, P., GILBOY, W. & MORTON, E. 2003. Non-invasive imaging of roots with high resolution X-ray micro-tomography. *Plant and Soil,* 255**,** 351-359.

GREGORY, P. J. 2008. *Plant roots: growth, activity and interactions with the soil*, Wiley-Blackwell.

GREGORY, P. J., BENGOUGH, A. G., GRINEV, D., SCHMIDT, S., THOMAS, W. B. T., WOJCIECHOWSKI, T. & YOUNG, I. M. 2009. Root phenomics of crops: opportunities and challenges. *Functional Plant Biology,* 36**,** 922-929.

GROENEVELT, P. H., KAY, B. D. & GRANT, C. D. 1984. Physical assessment of a soil with respect to rooting potential. *Geoderma,* 34**,** 101-114.

GROT, W. F. 1973. *US Patent No. 3,718,627*.

GRZESIAK, S., GRZESIAK, M. T., HURA, T., MARCIŃSKA, I. & RZEPKA, A. 2013. Changes in root system structure, leaf water potential and gas exchange of maize and triticale seedlings affected by soil compaction. *Environmental and Experimental Botany,* 88**,** 2-10.

GYSI, M., OTT, A. & FLÜHLER, H. 1999. Influence of single passes with high wheel load on a structured, unploughed sandy loam soil. *Soil and Tillage Research,* 52**,** 141-151.

HAINSWORTH, J. & AYLMORE, L. 1983. The use of computer assisted tomography to determine spatial distribution of soil water content. *Soil Research,* 21**,** 435-443.

HAJNOS, M., LIPIEC, J., ŚWIEBODA, R., SOKOŁOWSKA, Z. & WITKOWSKA-WALCZAK, B. 2006. Complete characterization of pore size distribution of tilled and orchard soil using water retention curve, mercury porosimetry, nitrogen adsorption, and water desorption methods. *Geoderma,* 135**,** 307-314.

HALLETT, P. D., FEENEY, D. S., BENGOUGH, A. G., RILLIG, M. C., SCRIMGEOUR, C. M. & YOUNG, I. M. 2009. Disentangling the impact of AM fungi versus roots on soil structure and water transport. *Plant and Soil,* 314**,** 183-196.

HAMZA, M. & ANDERSON, W. 2002. Improving soil physical fertility and crop yield on a clay soil in Western Australia. *Crop and Pasture Science,* 53**,** 615-620.

HAMZA, M. A. & ANDERSON, W. K. 2005. Soil compaction in cropping systems: A review of the nature, causes and possible solutions. *Soil and Tillage Research,* 82**,** 121-145.

HARGREAVES, C. E., GREGORY, P. J. & BENGOUGH, A. G. 2009. Measuring root traits in barley (Hordeum vulgare ssp. vulgare and ssp. spontaneum) seedlings using gel chambers, soil sacs and X-ray microtomography. *Plant and Soil,* 316**,** 285-297.

HAWES, M. C., BENGOUGH, G., CASSAB, G. & PONCE, G. 2002. Root caps and rhizosphere. *Journal of Plant Growth Regulation,* 21**,** 352-367.

HEERAMAN, D., HOPMANS, J. & CLAUSNITZER, V. 1997. Three dimensional imaging of plant roots in situ with X-ray computed tomography. *Plant and Soil,* 189**,** 167-179.

HEERAMAN, D. & JUMA, N. 1993. A comparison of minirhizotron, core and monolith methods for quantifying barley (Hordeum vulgare L.) and fababean (Vicia faba L.) root distribution. *Plant and Soil,* 148**,** 29-41.

HELLIWELL, J., STURROCK, C., GRAYLING, K., TRACY, S., FLAVEL, R., YOUNG, I., WHALLEY, W. & MOONEY, S. 2013. Applications of X-ray computed tomography for examining biophysical

interactions and structural development in soil systems: a review. *European Journal of Soil Science,* 64**,** 279-297.

HINSINGER, P., BENGOUGH, A. G., VETTERLEIN, D. & YOUNG, I. M. 2009. Rhizosphere: biophysics, biogeochemistry and ecological relevance. *Plant and soil,* 321**,** 117-152.

HOCHHOLDINGER, F. & ZIMMERMANN, R. 2008. Conserved and diverse mechanisms in root development. *Current Opinion in Plant Biology,* 11**,** 70-74.

HOUSTON, A. N., OTTEN, W., BAVEYE, P. C. & HAPCA, S. 2013a. Adaptive-window indicator kriging: A thresholding method for computed tomography images of porous media. *Computers & Geosciences,* 54**,** 239-248.

HOUSTON, A. N., SCHMIDT, S., TARQUIS, A. M., OTTEN, W., BAVEYE, P. C. & HAPCA, S. M. 2013b. Effect of scanning and image reconstruction settings in X-ray computed microtomography on quality and segmentation of 3D soil images. *Geoderma,* 207–208**,** 154-165.

HUCK, M. G. & TAYLOR, H. M. 1982. The rhizotron as a tool for root research. *Advances in Agronomy,* 35**,** 1-35.

HUSSAIN, A., BLACK, C. R., TAYLOR, I. B. & ROBERTS, J. A. 1999. Soil compaction. A role for ethylene in regulating leaf expansion and shoot growth in tomato? *Plant Physiology,* 121**,** 1227-1237.

IIIJIMA, M., ORIBE, Y., HORIBE, Y. & KONO, Y. 1998. Time Lapse Analysis of Root Elongation Rates of Rice and Sorghum During the Day and Night. *Annals of Botany,* 81**,** 603-607.

IIJIMA, M., HIGUCHI, T., BARLOW, P. W. & BENGOUGH, A. G. 2003. Root cap removal increases root penetration resistance in maize (Zea mays L.). *Journal of Experimental Botany,* 54**,** 2105-2109.

ISHIKAWA, H. & EVANS, M. L. 1995. Specialized zones of development in roots. *Plant Physiology,* 109**,** 725.

IVERSEN, T. H. & LARSEN, P. 1973. Movement of Amyloplasts in the Statocytes of Geotropically Stimulated Roots. The Pre-Inversion Effect. *Physiologia Plantarum,* 28**,** 172-181.

JAFFE, M., TAKAHASHI, H. & BIRO, R. 1985. A pea mutant for the study of hydrotropism in roots. *Science,* 230**,** 445-447.

JAIN, A., POLING, M. D., SMITH, A. P., NAGARAJAN, V. K., LAHNER, B., MEAGHER, R. B. & RAGHOTHAMA, K. G. 2009. Variations in the Composition of Gelling Agents Affect Morphophysiological and Molecular Responses to Deficiencies of Phosphate and Other Nutrients. *Plant Physiology,* 150**,** 1033-1049.

JENNESON, P. M., GILBOY, W. B., MORTON, E. J. & GREGORY, P. J. 2003. An X-ray micro-tomography system optimised for the low-dose study of living organisms. *Applied radiation and isotopes: including data, instumentation and methods for use in agriculture, industry and medicine,* 58**,** 177-81.

JOHNSON, E. L. 1936. Susceptibility of seventy species of flowering plants to X-radiation. *Plant Physiology,* 11**,** 319-342.

JOHNSON, M., TINGEY, D., PHILLIPS, D. & STORM, M. 2001. Advancing fine root research with minirhizotrons. *Environmental and Experimental Botany,* 45**,** 263-289.

KARUNAKARAN, C., LAHLALI, R., ZHU, N., WEBB, A. M., SCHMIDT, M., FRANSISHYN, K., BELEV, G., WYSOKINSKI, T., OLSON, J. & COOPER, D. M. 2015. Factors influencing real time internal structural visualization and dynamic process monitoring in plants using synchrotron-based phase contrast X-ray imaging. *Scientific reports,* 5.

KISS, J. Z., CORRELL, M. J., MULLEN, J. L., HANGARTER, R. P. & EDELMANN, R. E. 2007. Root phototropism: how light and gravity interact in shaping plant form. *Gravitational and Space Biology,* 16.

KONOPKA, B., PAGES, L. & DOUSSAN, C. 2009. Soil compaction modifies morphological characteristics of seminal maize roots. *Plant, Soil and Environment,* 55**,** 1-10.

KOOISTRA, M., SCHOONDERBEEK, D., BOONE, F., VEEN, B. & VAN NOORDWIJK, M. 1992. Root-soil contact of maize, as measured by a thin-section technique. *Plant and soil,* 139**,** 119-129.

KUCHENBUCH, R. O. & INGRAM, K. T. 2002. Image analysis for non-destructive and non-invasive quantification of root growth and soil water content in rhizotrons. *Journal of Plant Nutrition and Soil Science,* 165**,** 573-581.

KUCHENBUCH, R. O. & INGRAM, K. T. 2004. Effects of soil bulk density on seminal and lateral roots of young maize plants (Zea mays L.). *Journal of Plant Nutrition and Soil Science,* 167**,** 229-235.

KUZNETSOV, O. A. & HASENSTEIN, K. H. 1996. Intracellular magnetophoresis of amyloplasts and induction of root curvature. *Planta,* 198**,** 87-94.

LAMBIN, E. F., GIBBS, H. K., FERREIRA, L., GRAU, R., MAYAUX, P., MEYFROIDT, P., MORTON, D. C., RUDEL, T. K., GASPARRI, I. & MUNGER, J. 2013. Estimating the world's potentially available cropland using a bottom-up approach. *Global Environmental Change,* 23**,** 892-901.

LAWRENCE, G. 1978. Stability of soil pores during mercury intrusion porosimetry. *Journal of Soil Science,* 29**,** 299-304.

LETEY, J. 1985. Relationship between soil physical properties and crop production. *Advances in soil science.* Springer.

LIPIEC, J. & HATANO, R. 2003. Quantification of compaction effects on soil physical properties and crop growth. *Geoderma,* 116**,** 107-136.

LIPIEC, J., HORN, R., PIETRUSIEWICZ, J. & SICZEK, A. 2012. Effects of soil compaction on root elongation and anatomy of different cereal plant species. *Soil and Tillage Research,* 121**,** 74-81.

LIU, Y., PAN, X. & LI, J. 2014. Current Agricultural Practices Threaten Future Global Food Production. *Journal of Agricultural and Environmental Ethics,* 28**,** 203-216.

LOBET, G., PAGES, L. & DRAYE, X. 2011. A novel image analysis toolbox enabling quantitative analysis of root system architecture. *Plant Physiology,* 157**,** 29-39.

LOMBI, E., SMITH, E., HANSEN, T. H., PATERSON, D., DE JONGE, M. D., HOWARD, D. L., PERSSON, D. P., HUSTED, S., RYAN, C. & SCHJOERRING, J. K. 2011. Megapixel imaging of (micro) nutrients in mature barley grains. *Journal of experimental botany,* 62**,** 273-282.

LOWERY, B. & MORRISON, J. E. 2002. 2.8 Soil Penetrometers and Penetrability. *Methods of Soil Analysis: Part 4 Physical Methods***,** 363-388.

MACKAY, I., HORWELL, A., GARNER, J., WHITE, J., MCKEE, J. & PHILPOTT, H. 2011. Reanalyses of the historical series of UK variety trials to quantify the contributions of genetic and environmental factors to trends and variability in yield over time. *Theoretical and Applied Genetics,* 122**,** 225-238.

MAIRHOFER, S., ZAPPALA, S., TRACY, S. R., STURROCK, C., BENNETT, M., MOONEY, S. J. & PRIDMORE, T. 2012. RooTrak: Automated Recovery of Three-Dimensional Plant Root Architecture in Soil from X-Ray Microcomputed Tomography Images Using Visual Tracking. *Plant Physiology,* 158**,** 561-569.

MANSCHADI, A. M., CHRISTOPHER, J. & HAMMER, G. L. 2006. The role of root architectural traits in adaptation of wheat to water-limited environments. *Functional Plant Biology,* 33**,** 823-837.

MARINARI, S., MASCIANDARO, G., CECCANTI, B. & GREGO, S. 2000. Influence of organic and mineral fertilisers on soil biological and physical properties. *Bioresource Technology,* 72**,** 9-17.

MARSCHNER, H. 1991. Mechanisms of adaptation of plants to acid soils. *In:* WRIGHT, R. J., BALIGAR, V. C. & MURRMANN, R. P. (eds.) *Plant-Soil Interactions at Low pH.* Springer Netherlands.

MASLE, J. 1992. Genetic Variation in the Effects of Root Impedance on Growth and Transpiration Rates of Wheat and Barley. *Functional Plant Biology,* 19**,** 109-125.

MASSA, G. D. & GILROY, S. 2003. Touch modulates gravity sensing to regulate the growth of primary roots of Arabidopsis thaliana. *The Plant Journal,* 33**,** 435-445.

MATASSA, S., BATSTONE, D. J., HÜLSEN, T., SCHNOOR, J. & VERSTRAETE, W. 2015. Can direct conversion of used nitrogen to new feed and protein help feed the world? *Environmental science & technology,* 49**,** 5247-5254.

MATERECHERA, S., ALSTON, A., KIRBY, J. & DEXTER, A. 1993. Field evaluation of laboratory techniques for predicting the ability of roots to penetrate strong soil and of the influence of roots on water sorptivity. *Plant and Soil,* 149**,** 149-158.

MATERECHERA, S. A., DEXTER, A. R. & ALSTON, A. M. 1991. Penetration of very strong soils by seedling roots of different plant species. *Plant and Soil,* 135**,** 31-41.

MATHIEU, L., LOBET, G., TOCQUIN, P. & PÉRILLEUX, C. 2015. "Rhizoponics": a novel hydroponic rhizotron for root system analyses on mature Arabidopsis thaliana plants. *Plant Methods,* 11**,** 1-8.

MCKENZIE, B., BENGOUGH, A., HALLETT, P., THOMAS, W., FORSTER, B. & MCNICOL, J. 2009. Deep rooting and drought screening of cereal crops: a novel field-based method and its application. *Field Crops Research,* 112**,** 165-171.

MENGEL, K. 1983. Responses of various crop species and cultivars to fertilizer application. *Plant and Soil,* 72**,** 305-319.

MENON, M., ROBINSON, B., OSWALD, S., KAESTNER, A., ABBASPOUR, K., LEHMANN, E. & SCHULIN, R. 2007. Visualization of root growth in heterogeneously contaminated soil using neutron radiography. *European journal of soil science,* 58**,** 802-810.

MEROTTO, A. & MUNDSTOCK, C. 1999. Wheat root growth as affected by soil strength. *Revista Brasileira de Ciência do Solo,* 23**,** 197-202.

MEYEROWITZ, E. 1997. Genetic control of cell division patterns in developing plants. *Cell,* 88**,** 299-308.

MINGO, D. M., THEOBALD, J. C., BACON, M. A., DAVIES, W. J. & DODD, I. C. 2004. Biomass allocation in tomato (Lycopersicon esculentum) plants grown under partial rootzone drying: enhancement of root growth. *Functional Plant Biology,* 31**,** 971-978.

MONTAGU, K. D., CONROY, J. P. & ATWELL, B. J. 2001. The position of localized soil compaction determines root and subsequent shoot growth responses. *Journal of Experimental Botany,* 52**,** 2127-2133.

MONTEITH, J. & GREENWOOD, D. 1986. How Do Crops Manipulate Water Supply and Demand?[and Discussion]. *Philosophical Transactions of the Royal Society of London. Series A, Mathematical and Physical Sciences,* 316**,** 245-259.

MOONEY, S., PRIDMORE, T., HELLIWELL, J. & BENNETT, M. 2012. Developing X-ray Computed Tomography to non-invasively image 3-D root systems architecture in soil. *Plant and Soil,* 352**,** 1-22.

MOONEY, S. J. 2002. Three-dimensional visualization and quantification of soil macroporosity and water flow patterns using computed tomography. *Soil Use and Management,* 18**,** 142-151.

MORAN, C., PIERRET, A. & STEVENSON, A. 2000. X-ray absorption and phase contrast imaging to study the interplay between plant roots and soil structure. *Plant and Soil,* 223**,** 101-117.

MOZAFAR, A. 1991. Contact with ballotini (glass spheres) stimulates exudation of iron reducing and iron chelating substances from barley roots. *Plant and Soil,* 130**,** 105-108.

MULLEN, J. L., ISHIKAWA, H. & EVANS, M. L. 1998. Analysis of changes in relative elemental growth rate patterns in the elongation zone of Arabidopsis roots upon gravistimulation. *Planta,* 206**,** 598-603.

MUSTROPH, A. & ALBRECHT, G. 2003. Tolerance of crop plants to oxygen deficiency stress: fermentative activity and photosynthetic capacity of entire seedlings under hypoxia and anoxia. *Physiologia Plantarum,* 117**,** 508-520.

NEUBERGER, T., SREENIVASULU, N., ROKITTA, M., ROLLETSCHEK, H., GÖBEL, C., RUTTEN, T., RADCHUK, V., FEUSSNER, I., WOBUS, U. & JAKOB, P. 2008. Quantitative imaging of oil storage in developing crop seeds. *Plant Biotechnology Journal,* 6**,** 31-45.

NIKON. 2016. *XT H 225 for all-purpose X-ray and CT inspection* [Online]. Available: http://www.nikonmetrology.com/en_EU/Products/X-ray-and-CT-Inspection/Computed-Tomography/XT-H-225-Industrial-CT-Scanning [Accessed 20/02016 2016].

NIMMO, J. 2004. Porosity and pore size distribution. *Encyclopedia of Soils in the Environment,* 3**,** 295-303.

O'SULLIVAN, M. & BALL, B. 1982. A comparison of five instruments for measuring soil strength in cultivated and uncultivated cereal seedbeds. *Journal of Soil Science,* 33**,** 597-608.

PAEZ-GARCIA, A., MOTES, C. M., SCHEIBLE, W.-R., CHEN, R., BLANCAFLOR, E. B. & MONTEROS, M. J. 2015. Root traits and phenotyping strategies for plant improvement. *Plants,* 4**,** 334-355.

PASSIOURA, J. 2002. Soil conditions and plant growth. *Plant, Cell & Environment,* 25**,** 311-318.

PAYNE, R. W., MURRAY, D. A., HARDING, S. A., BAIRD, D. B. & SOUTAR, D. M. 2011. An Introduction to GenStat for Windows. *In:* INTERNATIONAL, V. (ed.). Hemel Hempstead, UK.

PERRET, J., AL-BELUSHI, M. & DEADMAN, M. 2007. Non-destructive visualization and quantification of roots using computed tomography. *Soil Biology and Biochemistry,* 39**,** 391-399.

PHILLIPS, D. L., JOHNSON, M. G., TINGEY, D. T., BIGGART, C., NOWAK, R. S. & NEWSOM, J. C. 2000. Minirhizotron installation in sandy, rocky soils with minimal soil disturbance. *Soil Science Society of America Journal,* 64**,** 761-764.

PIERRET, A., CAPOWIEZ, Y., BELZUNCES, L. & MORAN, C. 2002. 3D reconstruction and quantification of macropores using X-ray computed tomography and image analysis. *Geoderma,* 106**,** 247-271.

PIERRET, A., DOUSSAN, C., GARRIGUES, E. & MC KIRBY, J. 2003. Observing plant roots in their environment: current imaging options and specific contribution of two-dimensional approaches. *Agronomie,* 23**,** 471-479.

POTTERS-BALLOTINI CO. LTD. 2004-2011. *Potters-Ballotini Co., Ltd.* [Online]. Available: http://www.pqj.co.jp/en/index.html [Accessed].

POURKHEIRANDISH, M. & KOMATSUDA, T. 2007. The Importance of Barley Genetics and Domestication in a Global Perspective. *Annals of Botany,* 100**,** 999-1008.

PRITCHARD, J. 1994. The control of cell expansion in roots. *New Phytologist,* 127**,** 3-26.

PROCHNOW, L. I. & CANTARELLA, H. 2015. Modifying soil to improve crop productivity. *Better Crops with Plant Food,* 99**,** 10-12.

RAHMAN, M. M., LO, S. R. & GNANENDRAN, C. T. 2009. Reply to the discussion by Wanatowski and Chu on "On equivalent granular void ratio and steady state behaviour of loose sand with fines"Appears in the Canadian Geotechnical Journal, 46(4): 482. *Canadian Geotechnical Journal,* 46**,** 483-486.

READ, D., GREGORY, P. & BELL, A. 1999. Physical properties of axenic maize root mucilage. *Plant and Soil,* 211**,** 87-91.

RIGAS, S., DITENGOU, F. A., LJUNG, K., DARAS, G., TIETZ, O., PALME, K. & HATZOPOULOS, P. 2013. Root gravitropism and root hair development constitute coupled developmental responses regulated by auxin homeostasis in the Arabidopsis root apex. *New Phytologist,* 197**,** 1130-1141.

RILLIG, M. C., WRIGHT, S. F., ALLEN, M. F. & FIELD, C. B. 1999. Rise in carbon dioxide changes soil structure. *Nature,* 400**,** 628-628.

RODRIGUEZ-ITURBE, I., D'ODORICO, P., PORPORATO, A. & RIDOLFI, L. 1999. On the spatial and temporal links between vegetation, climate, and soil moisture. *Water Resources Research,* 35**,** 3709-3722.

ROGERS, W. 1969. The East Mailing root-observation laboratories. *Root growth***,** 361-376.

ROYSTON, J. 1982. An extension of Shapiro and Wilk's W test for normality to large samples. *Applied Statistics***,** 115-124.

RSTUDIO TEAM 2015. RStudio: Integrated development for R. RStudio, Inc., Boston, MA.

RYŻAK, M. & BIEGANOWSKI, A. 2011. Methodological aspects of determining soil particle-size distribution using the laser diffraction method. *Journal of Plant Nutrition and Soil Science,* 174**,** 624-633.

SABLOWSKI, R. 2004. Plant and animal stem cells: conceptually similar, molecularly distinct? *Trends in Cell Biology,* 14**,** 605-611.

SAXTON, K. E. & RAWLS, W. J. 2006. Soil Water Characteristic Estimates by Texture and Organic Matter for Hydrologic Solutions. *Soil Science Society of America Journal,* 70**,** 1569-1578.

SCHERES, B., MCKHANN, H. I. & VAN DEN BERG, C. 1996. Roots redefined: Anatomical and genetic analysis of root development. *Plant Physiology,* 111**,** 959-964.

SCHINDELIN, J., ARGANDA-CARRERAS, I., FRISE, E., KAYNIG, V., LONGAIR, M., PIETZSCH, T., PREIBISCH, S., RUEDEN, C., SAALFELD, S. & SCHMID, B. 2012. Fiji: an open-source platform for biological-image analysis. *Nature methods,* 9**,** 676-682.

SCHMIDT, S., BENGOUGH, A., GREGORY, P., GRINEV, D. & OTTEN, W. 2012. Estimating root–soil contact from 3D X-ray microtomographs. *European Journal of Soil Science,* 63**,** 776-786.

SCHMIDT, S., GREGORY, P. J., GRINEV, D. V. & BENGOUGH, A. G. 2013. Root elongation rate is correlated with the length of the bare root apex of maize and lupin roots despite contrasting responses of root growth to compact and dry soils. *Plant and Soil,* 372**,** 609-618.

SCHNEIDER, C. A., RASBAND, W. S. & ELICEIRI, K. W. 2012. NIH Image to ImageJ: 25 years of image analysis. *Nat Methods,* 9**,** 671-675.

SHARP, R. E. 2002. Interaction with ethylene: changing views on the role of abscisic acid in root and shoot growth responses to water stress. *Plant, Cell & Environment,* 25**,** 211-222.

SIEVERS, A., BRAUN, M. & MONSHAUSEN, G. B. 1996. The root cap: structure and function. *Plant roots: The hidden half***,** 53-73.

SIGMA ALDRICH. 2016. *Gelling agents - plant tissue structure protocol* [Online]. Available: http://www.sigmaaldrich.com/technical-documents/protocols/biology/gelling-agents.html [Accessed].

SMITH, S. & DE SMET, I. 2012. Root system architecture: insights from Arabidopsis and cereal crops. *Philosophical Transactions of the Royal Society B: Biological Sciences,* 367**,** 1441-1452.

SMUCKER, A. 1993. Soil environmental modifications of root dynamics and measurement. *Annual Review of Phytopathology,* 31**,** 191-218.

SOANE, B. D. & VAN OUWERKERK, C. 1995. Implications of soil compaction in crop production for the quality of the environment. *Soil and Tillage Research,* 35**,** 5-22.

SOIL SCIENCE SOCIETY OF AMERICA 2008. *Glossary of Soil Science Terms 2008*, ASA-CSSA-SSSA.

STEWART, J., MORAN, C. & WOOD, J. 1999. Macropore sheath: quantification of plant root and soil macropore association. *Plant and Soil,* 211**,** 59-67.

STIRZAKER, R. J., PASSIOURA, J. B. & WILMS, Y. 1996. Soil structure and plant growth: Impact of bulk density and biopores. *Plant and Soil,* 185**,** 151-162.

STUPPY, W. H., MAISANO, J. A., COLBERT, M. W., RUDALL, P. J. & ROWE, T. B. 2003. Three-dimensional analysis of plant structure using high-resolution X-ray computed tomography. *Trends in Plant Science,* 8**,** 2-6.

TAINA, I., HECK, R. & ELLIOT, T. 2008. Application of X-ray computed tomography to soil science: A literature review. *Canadian Journal of Soil Science,* 88**,** 1-19.

TAKAHASHI, H. 1997. Hydrotropism: the current state of our knowledge. *Journal of plant research,* 110**,** 163-169.

TAKAHASHI, H. & SCOTT, T. 1993. Intensity of hydrostimulation for the induction of root hydrotropism and its sensing by the root cap. *Plant, Cell & Environment,* 16**,** 99-103.

TAYLOR, H., UPCHURCH, D., BROWN, J. & ROGERS, H. 1991. Some methods of root investigations. *Developments in agricultural and managed-forest ecology,* 24**,** 553-564.

TAYLOR, H. M. 1971. Effects of soil strength on seedling emergence, root growth and crop yield. *Compaction of agricultural soils.* Am. Soc. Agric. Eng St. Joseph, MI.

THE SCOTTISH GOVERNMENT. 2005. *FSP Farm Soils Plan - Protecting soils and income in Scotland* [Online]. Available: http://www.gov.scot/Publications/2005/12/01130314/03147 [Accessed 24/01/2016 2016].

TO, J. & KAY, B. 2005. Variation in penetrometer resistance with soil properties: the contribution of effective stress and implications for pedotransfer functions. *Geoderma,* 126**,** 261-276.

TRACY, S. R., BLACK, C. R., ROBERTS, J. A., DODD, I. C. & MOONEY, S. J. 2015. Using X-ray computed tomography to explore the role of abscisic acid in moderating the impact of soil compaction on root system architecture. *Environmental and Experimental Botany,* 110**,** 11-18.

TRACY, S. R., BLACK, C. R., ROBERTS, J. A. & MOONEY, S. J. 2011. Soil compaction: a review of past and present techniques for investigating effects on root growth. *Journal of the Science of Food and Agriculture,* 91**,** 1528-1537.

TRACY, S. R., BLACK, C. R., ROBERTS, J. A., STURROCK, C., MAIRHOFER, S., CRAIGON, J. & MOONEY, S. J. 2012. Quantifying the impact of soil compaction on root system architecture in tomato (Solanum lycopersicum) by X-ray micro-computed tomography. *Annals of Botany,* 110**,** 511-519.

TRACY, S. R., ROBERTS, J. A., BLACK, C. R., MCNEILL, A., DAVIDSON, R. & MOONEY, S. J. 2010. The X-factor: visualizing undisturbed root architecture in soils using X-ray computed tomography. *Journal of experimental botany,* 61**,** 311-313.

TUMLINSON, L. G., LIU, H., SILK, W. K. & HOPMANS, J. W. 2008. Thermal neutron computed tomography of soil water and plant roots. *Soil Science Society of America Journal,* 72**,** 1234-1242.

UBEDA-TOMÁS, S., BEEMSTER, G. T. S. & BENNETT, M. J. 2012. Hormonal regulation of root growth: integrating local activities into global behaviour. *Trends in plant science,* 17**,** 326-331.

ULLRICH, S. E. 2010. *Barley: Production, improvement, and uses*, John Wiley & Sons.

USDA 2016. World Agricultural Production. *In:* AGRICULTURE, U. S. D. O. (ed.).

VALENTINE, T. A., BINNIE, K., SQUIRE, G. R., HAWES, C., HALLETT, P. D. & BENGOUGH, A. G. How does variation in root traits affect barley cultivar responses to agriculturally relevant soil physical constraints? International Society of Root Research Conference. Roots to the future - Dundee 2012, 2012a Dundee.

VALENTINE, T. A., HALLETT, P. D., BINNIE, K., YOUNG, M. W., SQUIRE, G. R., HAWES, C. & BENGOUGH, A. G. 2012b. Soil strength and macropore volume limit root elongation rates in many UK agricultural soils. *Annals of Botany,* 110**,** 259-270.

VAN DEN BERG, C., WILLEMSEN, V., HENDRIKS, G., WEISBEEK, P. & SCHERES, B. 1997. Short-range control of cell differentiation in the Arabidopsis root meristem. *Nature,* 390**,** 287-289.

VAN NOORDWIJK, M., SCHOONDERBEEK, D. & KOOISTRA, M. 1993. Root-soil contact of field-grown winter wheat. *Geoderma,* 56**,** 277-286.

VEREECKEN, H., MAES, J., FEYEN, J. & DARIUS, P. 1989. Estimating the soil moisture retention characteristic from texture, bulk density, and cabon content. *Soil Science,* 148**,** 389-403.

VIJAYAN, P., WILLICK, I. R., LAHLALI, R., KARUNAKARAN, C. & TANINO, K. K. 2015. Synchrotron Radiation Sheds Fresh Light on Plant Research: The Use of Powerful Techniques to Probe Structure and Composition of Plants. *Plant and Cell Physiology*.

VOLKMAR, K. M. Pre-germination effects on mechanically impeded root growth of barley (Hordeum vulgare L). *Plant and Soil,* 163**,** 197-202.

VOLUME GRAPHICS 2013. VG Studio MAX 2.2. Heidelberg, Germany.

WALKER, T. S., BAIS, H. P., GROTEWOLD, E. & VIVANCO, J. M. 2003. Root Exudation and Rhizosphere Biology. *Plant Physiology,* 132**,** 44-51.

WATT, M., MCCULLY, M. E. & CANNY, M. J. 1994. Formation and stabilization of rhizosheaths of Zea mays L.(Effect of soil water content). *Plant Physiology,* 106**,** 179-186.

WENT, F. W. & THIMANN, K. V. 1937. Phytohormones. *Phytohormones.*

WESTERN, A. W., GRAYSON, R. B., BLÖSCHL, G., WILLGOOSE, G. R. & MCMAHON, T. A. 1999. Observed spatial organization of soil moisture and its relation to terrain indices. *Water resources research,* 35**,** 797-810.

WHALLEY, W. R., WATTS, C., GREGORY, A., MOONEY, S., CLARK, L. & WHITMORE, A. 2008. The effect of soil strength on the yield of wheat. *Plant and Soil,* 306**,** 237-247.

WHITELEY, G. & DEXTER, A. 1982. Root development and growth of oilseed, wheat and pea crops on tilled and non-tilled soil. *Soil and Tillage Research,* 2**,** 379-393.

WICKHAM, H. 2009. *ggplot2: elegant graphics for data analysis*, Springer Science & Business Media.

WIENGWEERA, A., GREENWAY, H. & THOMSON, C. J. 1997. The use of agar nutrient solution to simulate lack of convection in waterlogged soils. *Annals of Botany,* 80**,** 115-123.

WIERSUM, L. 1962. Uptake of nitrogen and phosphorus in relation to soil structure and nutrient mobility. *Plant and Soil,* 16**,** 62-70.

WILSON, A. J. & ROBARDS, A. W. 1979. Some observations of the effects of mechanical impedance upon the ultrastructure of the root caps of barley. *Protoplasma,* 101**,** 61-72.

WILSON, A. J., ROBARDS, A. W. & GOSS, M. J. 1977. Effects of Mechanical Impedance on Root Growth in Barley, Hordeum vulgare L.: II. EFFECTS ON CELL DEVELOPMENT IN SEMINAL ROOTS. *Journal of Experimental Botany,* 28**,** 1216-1227.

WILSON, M. J. 2004. Weathering of the primary rock-forming minerals: processes, products and rates. *Clay Minerals,* 39**,** 233-266.

YOUNG, I. 1995. Variation in moisture contents between bulk soil and the rhizosheath of wheat (Triticum aestivum L. cv. Wembley). *New Phytologist,* 130**,** 135-139.

ZACARIAS, L. & REID, M. S. 1992. Inhibition of ethylene action prevents root penetration through compressed media in tomato (Lycopersicon esculentum) seedlings. *Physiologia Plantarum,* 86**,** 301-307.

ZAPPALA, S., HELLIWELL, J. R., TRACY, S. R., MAIRHOFER, S., STURROCK, C. J., PRIDMORE, T., BENNETT, M. & MOONEY, S. J. 2013. Effects of X-Ray Dose On Rhizosphere Studies Using X-Ray Computed Tomography. *PLoS ONE,* 8**,** e67250.

ZAREBANADKOUKI, M., KIM, Y. X. & CARMINATI, A. 2013. Where do roots take up water? Neutron radiography of water flow into the roots of transpiring plants growing in soil. *New Phytologist,* 199**,** 1034-1044.

ZHU, J., INGRAM, P. A., BENFEY, P. N. & ELICH, T. 2011. From lab to field, new approaches to phenotyping root system architecture. *Current opinion in plant biology,* 14**,** 310-317.

Appendix A

Protocol - Preparation of Nafion particles for root growth (Downie et al., 2012)

Day 1

Solutions

- 15% KOH / 35% DMSO / 50% dH_2O
- 15% Nitric acid (enough for 2 washes)

Instructions

1. Heat water bath to 80 °C
2. Add KOH solution to particles and place in water bath
3. Heat particles in solution for 5 hours
4. Take off solution and replace with dH_2O. Leave for 30 minutes at room temperature
5. Take off dH_2O and rinse the particles thoroughly with fresh dH_2O
6. Add 15% nitric acid to particles at room temperature and leave for 1 hour
7. Rinse with dH_2O and replace with fresh nitric acid solution and leave overnight

Day 2

Solutions

- 1 M sulphuric acid
- 3 wt % hydrogen peroxide

Instructions

1. Take off nitric acid solution and rinse particles thoroughly with dH_2O.

2. Replace with 1 M sulphuric acid solution at room temperature.
3. Heat the solution to 65 °C and incubate for 1 hour
4. Allow to cool down to room temperature **(sterile from this point onwards)**
5. Remove sulphuric acid, place with deionised water and heat to 65 °C
6. Maintain at this temperature for 1h
7. Allow to cool down to room temperature
8. Wash the membrane with deionised water multiple times
9. Add 3 wt % hydrogen peroxide solution
10. Heat the solution to 65 °C and incubate for 1 hour
11. Allow to cool down to room temperature
12. Rinse with dH_2O multiple times

<u>Day 3</u>

Solutions

- Stock solutions for MSR media – Macroelements, calcium nitrate, NaFe EDTA, microelements (recipes page 16 lab book)

Instructions

1. Combine enough vol of each stock solution in correct proportion (lab book pg 16) in a beaker but do not dilute
2. Mix briefly and add to nafion particles in a duran bottle
3. Put bottle in shaker at 30 °C for 30 minutes
4. Remove concentrated MSR and test pH
5. Repeat this procedure until pH is neutral

6. Rinse nafion thoroughly with dH_2O

It is now ready for use in plant growth media

Appendix B

Python code for obtaining root measurements from image co-ordinates

```
import math     # basic maths

import numpy    # Numerics

import pylab    # plots

from scipy import interpolate

import matplotlib

from mpl_toolkits.mplot3d import Axes3D

import msvcrt as m

def wait():

   m.getch()

# ########################################################

# READ DATA

# ########################################################

#write has many root file as you want, the name doesn't matter... as long as you write it correctly :)

files = ["Root1.txt"]

# 0 - don't show graphs/pop-ups, 1 - show graphs/pop-ups
```

```
showGraph = 1

nbFiles = len(files)

fileRows = []

for i in range(nbFiles):

   fileRows.append(0)

IMPORTED_DATA = []

roots_imported_data = [[] for i in range(nbFiles)]

fileIndex = 0

counter = 0

for file in files:

        counter = 0

        f = open(file,'r')

        for line in f:

                row = line.split('\t')

                if row[0] != "Index":

                        ID = row[1].split("-")

                        IMPORTED_DATA.append([float(row[3]) , float(row[4]), float(ID[0])])
```

```
                        roots_imported_data[fileIndex].append([float(row[3]) , float(row[4]),
float(ID[0])])

                        counter += 1

        f.close()

        fileRows[fileIndex] = counter

        fileIndex += 1

#find the root with the most data

longest = fileRows[0]

for i in range(nbFiles):

   if fileRows[i] > longest:

                longest = fileRows[i]

#treat each file one by one

roots_length = [0 for i in range(nbFiles)]

roots_X = [[] for i in range(nbFiles)]

roots_Y = [[] for i in range(nbFiles)]

roots_Z = [[] for i in range(nbFiles)]

roots_VERTICALITY = [[] for i in range(nbFiles)]

roots_CURVATURE = [[] for i in range(nbFiles)]
```

```
roots_CURVATURE_XY = [[] for i in range(nbFiles)]

roots_LENGTH = [[] for i in range(nbFiles)]



for fileIndex in range(nbFiles):

        n = len(roots_imported_data[fileIndex])

        for i in range(n-2):

                row0 = roots_imported_data[fileIndex][i]

                row1 = roots_imported_data[fileIndex][i+1]

                row2 = roots_imported_data[fileIndex][i+2]

                roots_X[fileIndex].append(row0[0])

                roots_Y[fileIndex].append(row0[1])

                roots_Z[fileIndex].append(row0[2])

                dR0 =  numpy.array([row1[0] - row0[0], row1[1] - row0[1], row1[2] - row0[2]
])

                dR1 =  numpy.array([row2[0] - row1[0], row2[1] - row1[1], row2[2] - row1[2]
])

                dR0_XY =  numpy.array([row1[0] - row0[0], row1[1] - row0[1] ])

                dR1_XY =  numpy.array([row2[0] - row1[0], row2[1] - row1[1] ])
```

```
                dr = math.sqrt(dR0[0]**2 + dR0[1]**2)

                dl = math.sqrt(numpy.dot(dR0,dR0))

                dl1 = math.sqrt(numpy.dot(dR1,dR1))

                dl_XY = math.sqrt(numpy.dot(dR0_XY,dR0_XY))

                dl1_XY = math.sqrt(numpy.dot(dR1_XY,dR1_XY))

                #print "Line: ", i

                #print "0 - ", row0, " / ", row1, " / ", row2

                #print "1 - ",dl_XY , " / ", dR0_XY

                #print "2 - ",dl1_XY , " / ", dR1_XY

                roots_LENGTH[fileIndex].append(roots_length[fileIndex])

                roots_length[fileIndex] += dl

                roots_VERTICALITY[fileIndex].append(abs(math.atan(dr/dR0[2])))

                crossprod                                                    =
math.sqrt(numpy.dot(numpy.cross(dR0/dl,dR1/dl1),numpy.cross(dR0/dl,dR1/dl1)))

                angle = math.asin(crossprod)



                if dr>0:
```

```
                    crossprod_XY =
math.sqrt(numpy.dot(numpy.cross(dR0_XY/dl_XY,dR1_XY/dl1_XY),numpy.cross(dR0_XY/dl_
XY,dR1_XY/dl1_XY)))
                    angle_XY = math.asin(crossprod_XY)

        roots_CURVATURE_XY[fileIndex].append(abs(angle_XY/(dl_XY+dl1_XY)))
            else:
                angle_XY = 0
                roots_CURVATURE_XY[fileIndex].append(0)
            roots_CURVATURE[fileIndex].append(abs(angle/(dl+dl1)))



        roots_length[fileIndex] += dl1
        roots_LENGTH[fileIndex].append(roots_length[fileIndex])
        roots_X[fileIndex].append(row1[0])
        roots_Y[fileIndex].append(row1[1])
        roots_Z[fileIndex].append(row1[2])
        roots_X[fileIndex].append(row2[0])
        roots_Y[fileIndex].append(row2[1])
```

```
            roots_Z[fileIndex].append(row2[2])



#write all data in a single file

f = open("results.csv",'w')



#FILE HEADER

wStr = "";

for i in range(nbFiles):

            wStr += "Root " + str(i) + ", "

wStr += "\n\n"

f.write(wStr);

#WRITE LENGTH

f.write("LENGTH \n")

wStr = ""

for i in range(nbFiles):

            wStr += str(roots_length[i]) + ", "

wStr += "\n\n"

f.write(wStr)
```

```
#WRITE VERTICALITY

f.write("VERTICALITY \n")

for elem in range(longest-2):

        wStr = ""

        for i in range(nbFiles):

                index = 0

                if (elem) < (fileRows[i]-2):

                        wStr += str(roots_VERTICALITY[i][elem]) + ", "

                else:

                        wStr += " , "



        wStr += "\n"

        f.write(wStr)

f.write("\n")

#WRITE CURVATURE

f.write("CURVATURE \n")

for elem in range(longest-2):

        wStr = ""
```

```
        for i in range(nbFiles):
                index = 0
                if (elem) < (fileRows[i]-2):
                        wStr += str(roots_CURVATURE[i][elem]) + ", "
                else:
                        wStr += " , "

        wStr += "\n"
        f.write(wStr)
f.write("\n")
#WRITE CURVATURE_XY
f.write("CURVATURE_XY \n")
for elem in range(longest-2):
        wStr = ""
        for i in range(nbFiles):
                index = 0
                if (elem) < (fileRows[i]-2):
                        wStr += str(roots_CURVATURE_XY[i][elem]) + ", "
```

```
                else:
                        wStr += " , "

        wStr += "\n"
        f.write(wStr)
f.write("\n")
f.close()
if showGraph > 0:
        # ########################################################
        # Plot
        # ########################################################
        fig = pylab.figure(1)

        ax = fig.add_subplot(211)
        # the histogram of the data
        n, bins, patches = ax.hist(numpy.array(roots_CURVATURE[0]), 30, normed=1,
facecolor='green', alpha=0.75)
        bincenters = 0.5*(bins[1:]+bins[:-1])
```

```
        ax.set_xlabel('curvature')

        ax.set_ylabel('P')

        #ax.set_title(r'$\mathrm{Histogram\ of\ IQ:}\ \mu=100,\ \sigma=15$')

        #ax.set_xlim(40, 160)

        #ax.set_ylim(0, 0.03)

        ax.grid(True)

        ax = fig.add_subplot(212)

        # the histogram of the data

        n, bins, patches = ax.hist(numpy.array(roots_VERTICALITY[0]), 30, normed=1,
facecolor='green', alpha=0.75)

        bincenters = 0.5*(bins[1:]+bins[:-1])

        ax.set_xlabel('Verticality (0 = vertical)')

        ax.set_ylabel('P')

        #ax.set_title(r'$\mathrm{Histogram\ of\ IQ:}\ \mu=100,\ \sigma=15$')

        #ax.set_xlim(40, 160)

        #ax.set_ylim(0, 0.03)

        ax.grid(True)

        ################################
```

```
# Trajectory

##############################

# 2D

fig = pylab.figure(2)

for i in range(nbFiles):

        pylab.plot(roots_LENGTH[i][0:-1],numpy.array(roots_VERTICALITY[i]))

#pylab.axis('equal')

pylab.xlabel("distance from the base")

pylab.ylabel("Verticality")

fig = pylab.figure(3)

for i in range(nbFiles):

        pylab.plot(roots_LENGTH[i][0:-1],numpy.array(roots_CURVATURE[i]))

#pylab.axis('equal')

pylab.xlabel("distance from the base")

pylab.ylabel("Curvature")



# 3D

fig = pylab.figure(4)
```

```
ax = Axes3D(fig)

for i in range(nbFiles):

        ax.plot(roots_X[i],roots_Y[i],zs=roots_Z[i])

ax.auto_scale_xyz([0, 1000], [0, 1000], [0, 1000])

pylab.show
```